

Distribution Agreement

In presenting this thesis or dissertation as a partial fulfillment of the requirements for an advanced degree from Emory University, I hereby grant to Emory University and its agents the non-exclusive license to archive, make accessible, and display my thesis or dissertation in whole or in part in all forms of media, now or hereafter known, including display on the world wide web. I understand that I may select some access restrictions as part of the online submission of this thesis or dissertation. I retain all ownership rights to the copyright of the thesis or dissertation. I also retain the right to use in future works (such as articles or books) all or part of this thesis or dissertation.

Signature:

Jie Song

Date

Exploring Catalytic Properties of Polyoxometalates in Aerobic
Decontamination and Water Oxidation

By

Jie Song
Doctor of Philosophy

Chemistry

Craig L. Hill
Advisor

Fredric M. Menger
Committee Member

Cora E. MacBeth
Committee Member

Accepted:

Lisa A. Tedesco, Ph. D.
Dean of the James T. Laney School of Graduate Studies

Date

Exploring Catalytic Properties of Polyoxometalates in Aerobic Oxidation
and Water Oxidation

By

Jie Song

B.S., Shandong University, China, 1997

M.S., Lanzhou University, China, 2001

Advisor: Craig L. Hill, Ph. D.

An Abstract of
A dissertation submitted to the Faculty of the
James T. Laney School of Graduate Studies of Emory University
in partial fulfillment of the requirements for the degree of
Doctor of Philosophy in Chemistry

2011

Abstract

Exploring Catalytic Properties of Polyoxometalates in Aerobic Oxidation and Water Oxidation

By Jie Song

The focus of this thesis is to explore the catalytic properties of POMs either in degradation of toxic industrial chemicals *via* aerobic oxidation or splitting water *via* water oxidation.

In chapter 2, new types of covalently-linked organic-hexavanadate hybrids are synthesized through solvothermal method or postsynthesis techniques and demonstrate their catalytic capability in aerobic oxidation of toxic organic chemicals such as propanethiol, hydrogen sulfide, and aldehyde, under ambient condition.

In chapter 3, two novel inorganic-organic hybrid clusters with one or two covalently linked pyrene fluorescent probes are employed as synthons for the controlled assembly of large vesicle nanostructure in solution and exhibit interesting pH-dependent fluorescence and interactions between hybrid clusters and their counterions.

In chapter 4, a polyoxometalate-metal organic framework material was documented as a new type of catalyst that exhibits the attractive features of both its components (POM and MOF) and mutual enhancement of stability by each unit. This catalyst can effectively catalyze detoxification of various sulfur-containing compounds including H₂S using only ambient air.

In chapter 5, two photosensitizer-POM hybrids were studied by both spectroscopic techniques and computational methods. This research provides detailed structural information in understanding the electron transfer character between cationic photosensitizers commonly-employed in dye-sensitized solar cells and catalytic polyanions studied in the water splitting process.

In chapter 6, a multicobalt substituted polyoxometalate was discovered to be a new efficient all-inorganic molecular water oxidation catalyst. The extremely high turnover number (TON ≈ 1500) and turnover frequency (TOF $> 10 \text{ s}^{-1}$) under the optimal conditions set a new record in this area to date. Multiple physicochemical techniques and catalytic kinetics studies provide the evidences that the POM-based catalysts remain intact during turnovers.

Exploring Catalytic Properties of Polyoxometalates in Aerobic Oxidation
and Water Oxidation

By

Jie Song

B.S., Shandong University, China, 1997

M.S., Lanzhou University, China, 2001

Advisor: Craig L. Hill, p.H. D.

A dissertation submitted to the Faculty of the
James T. Laney School of Graduate Studies of Emory University
in partial fulfillment of the requirements for the degree of
Doctor of Philosophy in Chemistry

2011

Acknowledgments

I would like to acknowledge many people for helping me during my doctoral work. My deepest gratitude goes first and foremost to my advisor, Professor Craig L. Hill, for his constant encouragement, patient guidance, invaluable advice and unconditional support. Working with him is a great experience in my whole life.

Secondly, my special thanks go to the exceptional research committee, Professor Fred Menger and Professor Cora MacBeth for their continual support and encouragement, rigorous but precious comments and advice for my research and career development.

I also thank Professor Tianbo Liu and his graduate students, Dong Li and Panchao Yin, for initiating of our interdisciplinary collaboration work on POM-based hybrid materials between Lehigh and Emory.

I am also indebted to Dr. Yurii V. Geletii for his generous guidance in research. Dr. Geletii is the person who always gives us instructive suggestions in the trivial research and the one that we can always count on to discuss the tiniest details of a problem.

I am very grateful for the help from Dr. Kenneth I. Hardcastle, Director of the X-ray Center at Emory, and the service instructors, Chongchao Zhao, Dr. Sheri Lense, and Dr. Rui Cao for solving the crystal structures. Special thanks also go to Professor Karl S. Hagen for his academic help and Dr. Bing Wang and Dr. Shaoxiong Wu for their help in collecting NMR data. Thanks Yi Hong and Jennet for mentoring me when I was working in Robert P. Apkarian Integrated Electron Microscopy Core at Emory. I really appreciate with the kind and warmhearted help from Mr. Steve Krebs and Ms. Patti Barnett, who put

great time and efforts to accelerate my research and solve any kinds of questions and problems I may have including improving my speaking English.

I thank Dr. Xikui Fang for his friendly help not only in our research on POM-based single molecular magnet but also in my career development.

I extend many thanks to the previous and current members of the Hill group. Dr. Zhen Luo, Dr. Yu Hou, Hongjin Lv, Guibo Zhu, and James Wesley Vickers provide tremendous help in my research. Especially, I am indebted to Dr. Kevin O'Halloran for reviewing my thesis and recovering me from depressing situations. I would also like to thank Leslie Chauvin for being so organized and helpful to the group. Furthermore, I give my great appreciation to Ms. Ann Dasher for her nice personality and beautiful smile to unconditional support me all the time when I am working at Emory.

My thanks would also go to all my beloved family members, especially my mother, Yumin Song and my twin brother, Liang Song, for their boundless love and whole-hearted support over all these past thirty-six years. I really miss the past time when we were together no matter of happiness or misery. However, I know and believe that our family will definitely have a brand new start to enjoy a healthier, happier, and better life from now.

Most importantly, I wish to express my deepest gratitude to my wife, Linlin Chai, for her selfless love, patience and support through all these years. Additionally, I wish to extend my deepest respect and appreciation to my mother-in-law and father-in-law to bring the most beautiful color to my life. I love you all family members forever!

Another special thank goes to Ms. Weihua Jiang, the turn point of my life. Thousands of words could not express my gratitude to her but in my heart.

I also thank Shangdong Qilu Association, especially Chairman Guohua Lian in helping me adapt to the life in Atlanta. My special thanks go to Professor James Lu and Li Xiong at Emory for their considerate support for my family. In addition, I thank Professor Gang Bao, Zhonglin Wang at Georgia Institute of Technology, Professor Binghe Wang at Georgia State University, Professors Gongli Tan, Wen Liu, Yixiang Ding at Shanghai Institute of Organic Chemistry, Professor Yong Wang at Shanghai Institute for Biological Sciences, Professors Weisheng Liu, Ning Tang, Minyu Tan at Lanzhou University, Professors Wenhua Sun at Beijing Institute of Chemistry, Professors Jingtian Hu, Yudao Ma, Qilong Wang, Qijun Lin at Shandong University, Professors Chengyong Su and Tongbu Lu at Sun Yat-sen University for mentoring me in my research. Last but not the least, I would like to give my appreciation to all the people who helped and are helping me.

All these delightful things during my Ph. D study in Atlanta will be in my memory forever, which will unequivocally inspire me with the boundless perseverance and adamancy, imperishable courage and optimism, endless love and pursuit of truth of science, benevolence of moral, and beauty of life in the everlasting cosmos.

Table of Contents

Chapter One: Introduction: Structures and Features of Isopolyanions and Heteropolyanions	1
Chapter Two: Covalently-linked organic-POM hybrids: synthesis, characterization, and catalytic removal of toxic chemicals	42
Chapter Three: Inorganic-Organic Hybrid Vesicles with Counterion- and pH-Controlled Fluorescent Properties	86
Chapter Four: A Multi-unit Catalyst with Synergistic Stability and Reactivity: A Polyoxometalate-Metal Organic Framework for Aerobic Decontamination	124
Chapter Five: Synthesis, structure, and characterization of two polyoxometalate-photosensitizer hybrid materials	155
Chapter Six: An Efficient Homogeneous Carbon-free Multi-cobalt Water Oxidation Catalyst: New Structure and High Activity	182

List of Figures

Chapter 1

- Figure 1-1.** Polyhedral representation of isopolyanions, A and B, and hetero polyanions, C and D. A), $[M_6O_{19}]^{2-}$ (M=Mo, V, W); B), $[M_{10}O_{28}]^{6-}$ (M=V); C), $[\alpha XM_{12}O_{40}]^{4-}$; D), $[\alpha-X_2M_{18}O_{62}]^{6-}$ (X=P, As, Si, Ge, etc; M=Mo, W, etc). **3**
- Figure 1-2.** Baker-Figgis isomers of Keggin structures: α , β , γ , δ , ϵ (the rotated M_3O_{13} group(s) are in yellowish green). **5**
- Figure 1-3.** IUPAC numbering scheme of Wells-Dawson $[\alpha-M_2W_{18}O_{62}]^{n-}$. **6**
- Figure 1-4.** Isomerization process of dodecatungstosilicate in aqueous solutions **8**
- Figure 1-5.** Transformations of different polytungstodiphosphate species. **9**
- Figure 1-6.** Polyhedral representations of TMSPPs: a). $[(\alpha-Cu(H_2O)PW_{11}O_{39})]^{5-}$, b) $[\alpha-Cr_2(H_2O)_2SiW_{10}O_{36}]^{2-}$ c) $[Co_4(H_2O)_2(PW_9O_{34})_2]^{10-}$, d) $[\alpha_1 Cu(H_2O)PW_{17}O_{61}]^{10-}$ e) $[\alpha_2-Cu(H_2O)P_2W_{17}O_{61}]^{10-}$, f) $[Mn_4(H_2O)(P_2W_{15}O_{56})_2]^{16-}$, g) $[\{Co_9Cl_2(OH)_3(H_2O)_9\}_3(B-\beta-SiW_8O_{31})_3]^{17-}$. **12**
- Figure 1-7.** Type I organic-inorganic POM hybrids. $[Ru(bpy)_3][H_4V_{10}O_{28}]$ (left) and $\{[5,6-(15-crown-5)-1,10-phenanthroline]-Na-[HPW_{12}O_{40}]\}$ **14**
- Figure 1-8.** Type II organic-inorganic POM hybrids. a). Linqvist $[V_6O_{13}\{(OCH_2)_3CNH_2\}_2]^{2-}$ $[[H_4V_{10}O_{28}]$; b). Wells-Dawson $[H_2NC(CH_2O)_3P_2V_3W_{15}O_{59}]^{6-}$; b). Anderson $[MnMo_6O_{18}\{(OCH_2)_3CNH_2\}\{(OCH_2)_3CNHCH_2C_5H_4N\}]^{3-}$; c). molecular cage $[\{Ni_6(Tris)(ethylenediamine)_3(1,3,5-benzenetricarboxylate)_{1.5}(B-\alpha-PW_9O_{34})\}_8]^{6-}$ **16**
- Figure 1-9.** Type II organic-inorganic POM hybrids. $[\alpha_2-P_2W_{17}O_{61}\{OR\}_2]^{6-}$ a). R = $Si(CH_2)_3SH$; b). R = SiPh; c). R = $Si(CH_2)_3SCN$; d). $[(^tBuSiO)_3(Si-CH_2-CH=CH_2)]$

$(A-\beta\text{-PW}_9\text{O}_{34})_8]^{3-}$ **18**

Figure 1-10. Type II organic-inorganic POM hybrids. $[\text{WZn}(\text{RSn})_2(\text{ZnW}_9\text{O}_{34})_2]^{10-}$ a).

R = CH₃; b). R = n-C₄H₉. c). $[(\text{SnPh})_4(\alpha\text{-AsW}_9\text{O}_{34})_2]^{10-}$ **20**

Figure 1-11. Type II organic-inorganic POM hybrids. a). *trans*- $[\text{Mo}_6\text{O}_{17}\{\text{N}(2,6\text{-dimethylphenyl})_2\}]^{2-}$; b). *cis*- $[\text{Mo}_6\text{O}_{14}\{\text{N}(2,6\text{-diisopropylphenyl})_5\}]^{2-}$; c). $[\text{Mo}_6\text{O}_{18}(\text{N}=\text{C}(\text{C}_6\text{H}_4\text{OCH}_3)\text{CH}_3)]^{2-}$ **22**

Figure 1-12. Type II organic-inorganic POM hybrids. a).

$[\text{H}_2\text{V}_{10}\text{O}_{18}(\text{O}_3\text{PC}_6\text{H}_4\text{PO}_3)_4]^{8-}$; b). $[\text{V}_5\text{O}_9(\text{O}_3\text{AsC}_6\text{H}_4\text{-4-NH}_2)_4]^{5-}$; c).

$[\text{V}_{12}\text{O}_{12}(\text{OH})_4(\text{O}_3\text{AsC}_6\text{H}_4\text{-4-NH}_2)_{10}]^{4-}$; d). $[\{\text{PhSbOH}\}_3(\text{A}-\alpha\text{-PW}_9\text{O}_{34})_2]^{9-}$ **24**

Figure 1-13. $[\gamma\text{-H}_2\text{PV}_2\text{W}_{10}\text{O}_{40}]^{3-}$ (left) and $[\text{PMo}_{11}\text{VO}_{40}]^{4-}$ (right). **26**

Figure 1-14. X-Ray structure of $\text{Ru}_2\text{Zn}_2(\text{H}_2\text{O})_2(\text{ZnW}_9\text{O}_{34})_2]^{11-}$ (left) and $[\text{Ru}^{\text{IV}}_4\text{O}_4(\text{OH})_2(\text{H}_2\text{O})_4(\gamma\text{-SiW}_{10}\text{O}_{36})_2]^{10-}$ (right) in combined polyhedral (polytungstate ligands) and ball-and-stick notation. Ru: purple, O: red; WO₆ octahedra: gray, SiO₄ tetrahedra: blue. ZnO₄ tetrahedra: pale white. **28**

Figure 1-15. X-ray structure of $[\text{Co}_4(\text{H}_2\text{O})_2(\alpha\text{-PW}_9\text{O}_{34})_2]^{10-}$ in combined polyhedral (polytungstate ligands) and ball-and-stick notation. Co: blue, O: red; WO₆ octahedra: gray, PO₄ tetrahedra: yellow. **29**

Chapter 2

Figure 2-1. X-ray single crystal structure of **1**. Yellow: V; red: O; Black: C. (H atoms and counterions omitted for clarity) **63**

Figure 2-2. ³¹P and ¹H NMR of POM-dumbbell. **65**

Figure 2-3. Dioxygen oxidation of PrSH catalyzed by **1**. The upper lines show the consumption of PrSH; the bottom lines show the formation of PrSSPr. Triangle:

control; dot:1. 67

Figure 2-4. Aerobic oxidation of acetaldehyde (blue) to acetic acid (red) at room temperature. Crosses (control); squares (**1**). 68

Figure 2-5. Single crystal structure of **2-e**. Cations and solvent molecules omitted for clarity. 77

Figure 2-6. 1-D chain assembly of **2-e** via p- π stacking and H-bonding ($H_{org} \cdots O_{POM}$). 78

Figure 2-7. 2-D grandstand network of **2-e**. 78

Figure 2-8. 3-D framework assembly of **2-e**. C-H \cdots O-POMs interaction and ionic attraction between POMs and TBA salts. 79

Figure 2-9. Space-filled 3-D framework of **2-e** showing its channels along *a* direction. 80

Chapter 3

Figure 3-1. Three-dimensional packing of TBA-NH₂V₆ (**top**) and TBA-**2** (**bottom**) (views along *a*-axis) showing the arrangement of TBA cations around associated POMs (bottom). 102

Figure 3-2. Weak intermolecular interactions between the hybrid cluster **2**. Top: π - π stacking between two adjacent pyrene groups (distance between two aromatic planes are less than 3.351 Å and the green dot line shows the most adjacent two carbon atoms on two pyrenes). Bottom: H-bonding between the hydrogen atoms on amide groups in one POM and one of the terminal oxygens on another. 103

Figure 3-3. (A) The total scattered intensity recorded by SLS for hybrid cluster **1** with different counterions in H₂O/DMSO mixed solvents. (B) CONTIN plot of the size distribution of vesicular structures formed by hybrid cluster **1** with different

counterions in 80:20 v/v H₂O/DMSO mixed solvents. (C) A TEM image of the vesicular structure formed in 80:20 v/v H₂O/DMSO mixed solvents (bar = 0.2 μm). (D) An enlarged region of (C) in order to show the structural details of the hollow spherical vesicular structures. **106**

Figure 3-4. The size distribution plot of hybrid **1** in 80:20 v/v H₂O:DMSO solution under different scattering angles shows no obvious angular dependence. **108**

Figure 3-5. The Berry plot of hybrid **1** in 80:20 v/v H₂O:DMSO solution from which the R_g is determined to be 48 nm. **108**

Figure 3-6. The average R_h of vesicles formed by hybrid **1** and **2** in different mixed solvents. **109**

Figure 3-7. (A) ¹H NMR spectra of hybrid **1** with TBA (top) and H (bottom) as counterions in DMSO-*d*₆ (B) ¹H NMR spectra of hybrid **2** with TBA (top) and H (bottom) as counterions in DMSO-*d*₆. **110**

Figure 3-8. (A) Fluorescence spectra of hybrid clusters **1** and **2** with different counterions. (For the TBA, TEA and TMA salts, the solvent is 80:20 v/v H₂O:DMSO; for the H salt, the solvent is H₂O). (B) Plot of the pyrene monomer fluorescence peak I (375nm)/I(395nm) versus the counterion size for hybrid clusters **1** and **2** with different counterions. **113**

Figure 3-9. (A) 2D NOESY spectrum of TBAI in DMSO-*d*₆. (B) 2D NOESY spectrum of (TBA⁺)₂**1** in DMSO-*d*₆. (C) An enlarged region of **B** showing the TBA cross peaks. (D) An enlarged region of **E** showing the TBA-pyrene cross peaks. (E) 2D NOESY spectrum of (TBA⁺)₂**1** in 90:10 v/v D₂O:DMSO-*d*₆ mixed solvent. (F) An enlarged region of **E** show the TBA cross peaks. (Positive NOE peaks are in dark

green color while negative NOE peaks are in light green color.)	114
Figure 3-10. The calibration curve of hybrid 2 to determine the concentration of $(H^+)_{22}$ in water.	116
Figure 3-11. pH effect on the vesicular structure determined by total scattered intensity recorded by SLS for hybrid H_{22} in different solution pH values.	116
Figure 3-12. (A) Fluorescence spectra of hybrid clusters $(H^+)_{22}$ in water at different pH values (the fluorescence intensity has been normalized). (B) Plot of pyrene excimer/monomer intensity ratio versus solution pH for hybrid clusters $(H^+)_{22}$. (C) Change in the vesicular structure size with solution pH for $(H^+)_{22}$. (D) Zeta potential of the vesicular structure with solution pH for $(H^+)_{22}$.	118

Chapter 4

Figure 4-1. FT-IR spectra of MOF-199 alone (blue), $K_5[CuPW_{11}O_{39}]$ alone (red), and 1 (black).	133
Figure 4-2. N_2 gas adsorption isotherms of 1 (left) and MOF-199 (right) measured at 77K. Filled symbols, adsorption; open symbols, desorption. The BET surface areas of 1 and MOF-199 alone are 462 and 1,264 m^2/g , respectively.	134
Figure 4-3. Thermogravimetric analysis of 1 . The calculated weight percentages of water + tetramethylammonium cations and the MOF framework are 16.46% and 26.82%, respectively, based on the molecular formula of 1 .	135
Figure 4-4. Powder X-ray diffraction patterns of 1 and MOF-199.	136
Figure 4-5. X-ray crystal structure of 1 . The POM, represented as off-white polyhedra, is orientationally disordered in the pores. The MOF-199 framework is	

represented in ball and stick form wherein C atoms are represented in gray, O in red, and Cu in blue. Yellow squares denote the geometry of the copper(II) acetate clusters. Tetramethylammonium (TMA) cations, which are disordered in the pores, and hydrogen atoms are omitted for clarity. 137

Figure 4-6. Aerobic oxidation of H₂S to S₈ catalyzed by the POM-MOF, **1**, in water. An aqueous solution of H₂S (0.1 mol/L, pH=4.8, 75 mL) containing **1** (10.0 mg) was flushed with oxygen (black triangles) or air (open squares) and stirred at room temperature for the duration of the reaction (20 hours). Parallel reactions were conducted and stopped at specific reaction times for product separation and measurement. Control experiments for POM only (10.0 mg) and MOF-199 (10.0 mg) only under identical conditions showed no catalytic activity (no production of S₈). 139

Figure 4-7. FT-IR spectra of **1** before and after the catalytic oxidation of H₂S using O₂ or air (approximately 4,000 turnovers). 141

Figure 4-8. Aerobic oxidation of PrSH to PrSSPr catalyzed by **1**. PrSH (0.662 mmol) and the catalyst, **1** (10 mg, ~0.025 mmol), were stirred in chlorobenzene (2.9 mL) with decane (internal standard, 0.092 mmol) in a pressure tube fitted with a PTFE plug under 100% O₂ at 50 °C. Consumption of PrSH (red diamonds, ◆) and formation of PrSSPr (blue diamonds, ◆) catalyzed by **1**; PrSSPr concentration in presence of PW₁₂-MOF (orange circle, ●); PrSSPr concentration in presence of MOF-199 alone (green triangle, ▲); PrSSPr concentration in presence of TBA₅[CuPW₁₁O₃₉] alone (purple crosses, ×); and PrSSPr concentration in absence of any additives (black squares, ■). 143

Figure 4-9. Reflect-IR of **1** before and after treatment in pH 11.0 aqueous solution for 12 hours. 147

Figure 4-10. IR spectra of MOF-199, $K_5[CuPW_{11}O_{39}]$, and **1** before and after the catalytic oxidation of propanethiol. **148**

Figure 4-11. The powder X-ray diffraction patterns of MOF-199, **1**, and **1** after catalytic oxidation of propanethiol. **148**

Chapter 5

Figure 5-1. ORTEP diagram of the asymmetric unit of complex **2** with the atomic numbering scheme (30% thermal ellipsoids). Potassium (green), ruthenium (pink), carbon (green), tungsten (black), nitrogen (blue), and oxygen (red) phosphor (yellow). H atoms are omitted for clarity. **164**

Figure 5-2. Three-dimensional structure of **2**: view of the ion channel of potassium in plane (001) or the z-axis. **168**

Figure 5-3. UV/vis spectra of **1** in CH_3CN (solid black line), **2** in $CH_3CN/DMSO$ (9:1 in volume, dashed red line), **2** in DMSO (dotted blue curve), $[Ru(bpy)_3]^{2+}$ in $CH_3CN/DMSO$ (9:1 in volume, pink dash-dot-dash line), and $[H_3PW_{12}O_{40}]$ in DMSO (green dash-dot-dot-dash line). The inset shows the enlarged spectra. **169**

Figure 5-4. Emission spectra of the POM-Dye complexes in DMSO **170**

Figure 5-5. Emission spectra of the POM-Dye complexes in MeCN; fluorescence quenching were observed in MeCN solution **171**

Figure 5-6. Stern-Volmer plots for samples in DMSO solutions containing 0% (green squares), 50% (red triangles) and 75% (purple diamonds) of CH_3CN in volume as indicated in the figure. All solutions contained $5 \mu M [Ru(bpy)_3]^{2+}$ and were purged with N_2 . The emission intensities of $[Ru(bpy)_3]^{2+}$ with (I) and without (I_0)

[H₃PW₁₂O₄₀] were collected, averaged at 615 nm ~ 620 nm after 450 nm excitation. **172**

Figure 5-7. FT-IR spectra of the dye and the hybrid complexes. **174**

Figure 5-8. Calculated structure and important geometry parameters (in Å) of the { [Ru(bpy)₃]²⁺ ... [PW₁₂O₄₀]³⁻ } complex. **177**

Chapter 6

Figure 6-1. Ellipsoid and Ball-and-stick representations of X-ray single crystal structure of **1**. W (green), O (red), Co (blue). **191**

Figure 6-2. Coordination environment of tetrahedral (Co1) and octahedral cobalt (Co2). Each belt atom reveals distorted octahedral coordination site in a close-packed arrangement. The W(10) – O bond lengths of the belt tungsten range from 1.954(8) to 2.041(7) Å and the Co (2) – O bond lengths of the belt cobalt from 2.083(7) to 2.210(10) Å. **193**

Figure 6-3. XPS diagram of **1** for W 4f (Left) and Co 3p (Right). Blue line represents raw data, red line represents simulated data. **199**

Figure 6-4. Thermogravimetric Analysis (TGA) of crystalline **1**. The total weight loss observed (14%) is attributed to hydration water, the calculation shows that there are approximately 46 hydration water molecules. **200**

Figure 6-5. UV-Visible spectroscopy of 1 mM **1** in borate buffer (0.2M, pH = 9.0). The calculated extinction coefficient at λ_{max} (609 nm) is ε₆₀₉ = 622 M⁻¹ cm⁻¹. **200**

Figure 6-6. FT-IR spectrum of **1**. The FT-IR spectroscopy were performed using 1 wt% sample in KBr pellet. **201**

Figure 6-7. Cyclic voltammetry spectrum of **1** (0.16 mM) in sodium borate buffer (20 mM, pH=9). **201**

Figure 6-8. Kinetics of $[\text{Ru}(\text{bpy})_3]^{3+}$ reduction to $[\text{Ru}(\text{bpy})_3]^{2+}$ over different catalysts (Left), and different concentrations of **1**. The absorbance was measured at 670 nm.

Conditions: Left: **Buffer** (black solid line), **Co4** (blue dot line; 0.5 μM (final)), **1** (red solid line; 0.5 μM (final)); Right: **1** (0.1 μM ~ 4 μM); 1 mM $[\text{Ru}(\text{bpy})_3]^{3+}$ (final), 40 mM sodium borate buffer (final), pH 9.0, 298 K

203

Figure 6-9. Kinetics of O_2 evolution over different POM catalysts in the photocatalytic system. **1** (green triangles), **Co4** ($\text{Na}_{10}[\text{Co}_4(\text{H}_2\text{O})_2(\text{PW}_9\text{O}_{34})_2]$, green crosses), and buffer control (blue squares). Conditions: LED-lamp, 455 nm, 17 mW light beam with a diameter of ~0.4 cm focused on the reaction solution, 1.0 mM $[\text{Ru}(\text{bpy})_3]^{2+}$, 5.0 mM $\text{Na}_2\text{S}_2\text{O}_8$, 40 mM sodium borate buffer (initial pH 9.0), total reaction volume 2.0 mL, vigorous stirring (4×10^3 RPM). Concentrations of catalyst: 2 μM .

204

Figure 6-10. Kinetics of O_2 formation at different concentrations of **1** (0.2 ~ 6.0 μM). Condition: see Figure 6-9.

204

Figure 6-11. O_2 yield and turn-over number vs. concentration of **1** at 11 minutes of illumination. Red line: **Co4**; blue line: **1**. Condition: see Figure 6-1.

207

Figure 6-12. Kinetics of O_2 formation in the photo-catalytic system. Freshly prepared solution **1** in the presence of 2,2'-bipyridine. Condition: see Figure 6-1. Blue squares: 2 μM **1**; Red squares: 2 μM **1** + 24 μM bpy; Green triangles: 2 μM **1** 60 μM bpy.

208

Figure 6-13. FT-IR spectra for **1** under photo driven water oxidation before (a) the dark-yellow precipitate obtained from mixing two concentrated solutions of **Na10-1** and $[\text{Ru}(\text{bpy})_3]^{2+}$, and after reaction (b) the light-yellow precipitate re-isolated from a

“post-chemical reaction” solution. All FT-IR spectroscopy were performed using 1 wt% sample in KBr pellet.

List of Schemes

Chapter 1

Scheme 1-1. Crystallographic Data and Structure Refinement for **1**. **28**

Scheme 1-2. Thermal oxidation of water catalyzed by $[\text{Co}_4(\text{H}_2\text{O})_2(\alpha\text{-PW}_9\text{O}_{34})_2]^{10-}$ using $[\text{Ru}(\text{bpy})_3]^{3+}$ as an oxidant. **29**

Chapter 2

Scheme 2-1. Hydrothermal synthesis of hybrid dendrimer **1**. Yellow: V; red: O. **62**

Scheme 2-2. Linqvist and Wells-Dawson hybrid POM-dumbbell. **65**

Scheme 2-3. Functionalization of hexavanadate **2** triesters by amidation reaction. Yellow, V; red, O. **70**

Chapter 3

Scheme 3-1. The construction of hybrids **1** and **2**. **100**

Scheme 3-3. An illustration of possible vesicular structures formed by hybrid clusters, **2**, in polar solvents, and how the TBA counterions may be arranged in the packing of individual clusters. The hexagons, parallelograms and four-legged stars represent the POM, pyrene, and TBA cations, respectively. **104**

Chapter 5

Scheme 5-1. Synthesis of photosensitizer-POMs adducts. **163**

List of Tables

Chapter 2

Table 2-1. Crystallographic Data and Structure Refinement for 1 .	64
Table 2-2. Reaction of 2 with acyl chlorides, carboxylic acids, and esters.	71
Table 2-3. Amidation of cyclic anhydrides with 1 .	75
Table 2-4. Amidation of acyclic anhydrides with 1 .	76

Chapter 3

Table 3-1. Crystallographic Data for NH_3V_6 , $\text{TBA-NH}_2\text{V}_6$ and TBA-2	101
--	------------

Chapter 4

Table 4-1. Crystallographic Data and Structure Refinement for 1 .	130
Table 4-2. The quantity of sulfur, produced via eq 1 in aqueous solution, catalyzed by 10 mg of the POM-MOF, 1 .	140
Table 4-3. The quantity of sulfur, produced via eq 1 in gas phase under ambient conditions, catalyzed by 1 , $\text{PW}_{12}\text{-MOF}$, MOF 199 , and $\{\text{CuPW}_{11}\}$.	140
Table 4-4. The aerobic oxidation of thiols to disulfides catalyzed by 1 .	146

Chapter 5

Table 5-1. Crystallographic parameters and refinement details for complex 2 .	161
Table 5-2. Atomic distances (\AA) and angles ($^\circ$) of $\text{O}_{\text{POM}} \cdots \text{H}_{\text{pyr}}$ interactions in the crystal structure of complex 2 .	165
Table 5-3. Selected bond lengths (\AA) and angles ($^\circ$) for 2 . The bpy unit on the	

[Ru(bpy)₃]²⁺ has disorder that could not be modeled well because the molecule sits on a symmetry site. 165

Table 5-4. Major FT-IR peaks for K₇PW₁₁O₃₉, H₃PW₁₂O₄₀, [Ru(bpy)₃]²⁺, and the two hydrid complexes, **1** and **2** (cm⁻¹). 175

Table 5-5. ³¹P and ¹H NMR for K₇PW₁₁O₃₉, H₃PW₁₂O₄₀, [Ru(bpy)₃]²⁺, and the two hydrid complexes, **1** and **2** in *d*-DMSO (ppm). 176

Chapter 6

Table 6-1. Crystallographic Data and Structure Refinement for **1**. 190

Table 6-2. Selected bond lengths [Å] and angles [°] for **1**. 192

Table 6-3. The Bond valence sums of cobalt atoms and belt tungsten atom. 198

Table 6-4. Turnover numbers (TON), chemical yields, and initial turnover frequency (TOF) for homogeneous visible-light-driven water oxidation catalyzed by different POM catalysts^a. 205

List of Abbreviations

Å	Angstrom
<i>a, b, c</i>	unit cell axial lengths
<i>n</i> -Bu	<i>n</i> -butyl
Br	bromine
°C	degrees Celsius
calcd.	Calculated
CEES	2-chloroethyl ethyl sulfide
CIF	crystallographic information file
cm ⁻¹	reciprocal centimeter
DMS	dimethyl sulfide
DMSO	dimethyl sulfoxide
DSC	differential scanning calorimetry
equiv.	equivalent
EXAFS	extended X-ray absorption fine structure method
Fe	iron
F.W.	formula weight
<i>F</i> (000)	structure factor for the unit cell; it is equal to the total number of electrons in the unit cell
FT-IR	Fourier transform infrared spectroscopy
g	grams(s)
h	hour(s)
IS	internal standard
Hz	Hertz
K	kelvin
L	ligand
m	medium (FT-IR)
M	molarity
Me	methyl
mg	milligram(s)
MHz	megahertz
min	minutes(s)
mL	milliliters(s)
Mn	manganese
mmol	millimole
mol	mole
nm	nanometer
NMR	nuclear magnetic resonance spectroscopy
OAc	acetate
pH	potential of hydrogen, a measure of the acidity or alkalinity of a solution
Ph	phenyl
POM	polyoxometalate
ppm	part per million
Pt	platinum
<i>R</i>	discrepancy index for crystal structure refinement

s	strong (FT-IR)
sec	second(s)
sh	shoulder (FT-IR)
TBA	tetrabutylammonium
THpA	tetraheptylammonium
TMSP	transition-metal-substituted Polyoxometalate
TGA	thermogravimetric analysis
UV	ultraviolet
V	volume of the unit cell
vs	very strong (FT-IR)
w	weak (FT-IR)
Z	number of molecules per unit cell
α, β, γ	interaxial angles between unit cell vector b and c , a and c , and a and b , respectively
δ	chemical shift (expressed in ppm for NMR)
ϵ	molar extinction (or absorption) coefficient
θ	the glancing angle of the X-ray beam to the “reflecting plane”
λ	wavelength
μ	the total linear absorption coefficient (with unit of cm^{-1})

———— CHAPTER ————

1

**Introduction: Structures and Features of
Isopolyanions and Heteropolyanions**

1-1. Overview of polyoxometalates

Polyoxometalates (POMs) comprise a large of class of early-transition-metal-oxide clusters. These clusters are formed by covalently linking metal ions in their highest oxidation state (d^0), such as V(V), Nb(V), Ta(V), Mo(VI), and W(VI) in groups VB and VIB, with oxo anions through self-assembly processes in solution.¹

Berzelius discovered the first heteropolyanion, $(\text{NH}_4)_3\text{PMo}_{12}\text{O}_{40}$, in 1826, thus the history of POM dates back 185 years.² With the development of modern physicochemical techniques, especially the introduction of single crystal X-ray diffraction and nuclear magnetic resonance techniques, thousands of new POMs with different structural features have been discovered.³⁻⁵ POMs can be classified into two main types.⁶⁻¹³ Complexes formed exclusively from addenda (i.e. W(VI) or Mo (VI)) and oxygen atoms are named *isopolyanions* (Figure 1-1). This type of POMs is limited to Linqvist-type $[\text{M}_6\text{O}_{19}]$ (M=V, Nb, Ta, Mo, W) structures, polymolybdates (such as $[\text{Mo}_8\text{O}_{26}]^{4-}$ and $[\text{Mo}_2\text{O}_{24}]^{6-}$), polytungstates (such as $[\text{W}_{10}\text{O}_{32}]^{4-}$ and $[\text{W}_{12}\text{O}_{42}\text{H}_2]^{10-}$), and polyvanadates (such as $[\text{V}_{10}\text{O}_{28}]^{6-}$ and $[\text{V}_4\text{O}_{12}]^{4-}$). POMs that contain one or more elements in addition to the above metals and oxygen are named *heteropolyanions*. The latter have more diverse structure features and richer chemistry than isopolyanions.

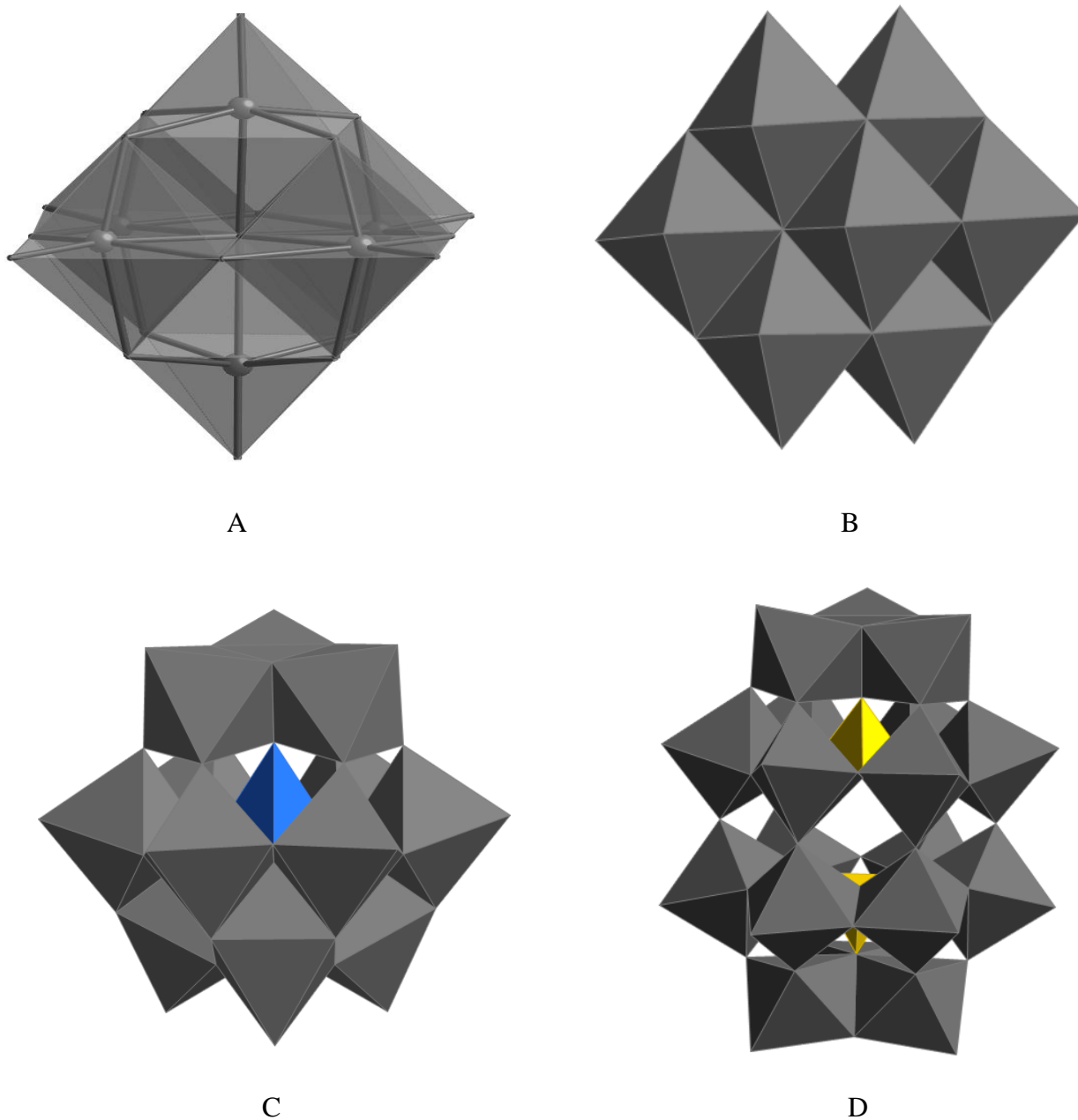


Figure 1-1. Polyhedral representation of isopolyanions, A and B, and heteropolyanions, C and D. A), $[M_6O_{19}]^{2-}$ (M=Mo, V, W); B), $[M_{10}O_{28}]^{6-}$ (M =V, Nb); C), $[\alpha\text{-}XM_{12}O_{40}]^{4-}$; D), $[\alpha\text{-}X_2M_{18}O_{62}]^{6-}$ (X=P, As, Si, Ge, etc; M=Mo, W, etc).

Among all the known heteropolyanions, Keggin- and Wells-Dawson- types are the two most common ones. The Keggin POMs consist of a central $[\text{XO}_4]^{n-}$ tetrahedron and four corner-sharing $[\text{M}_3\text{O}_{13}]^{m-}$ triads, which are connected together via each of the four oxygen atoms in $[\text{XO}_4]^{n-}$. Generally, there are five isomers that are related by successive 60° rotation of the M_3O_{13} groups (Figure 1-2). The α -Keggin structure with T_d symmetry is the most thermodynamically stable one among these five isomers.¹⁴⁻¹⁶

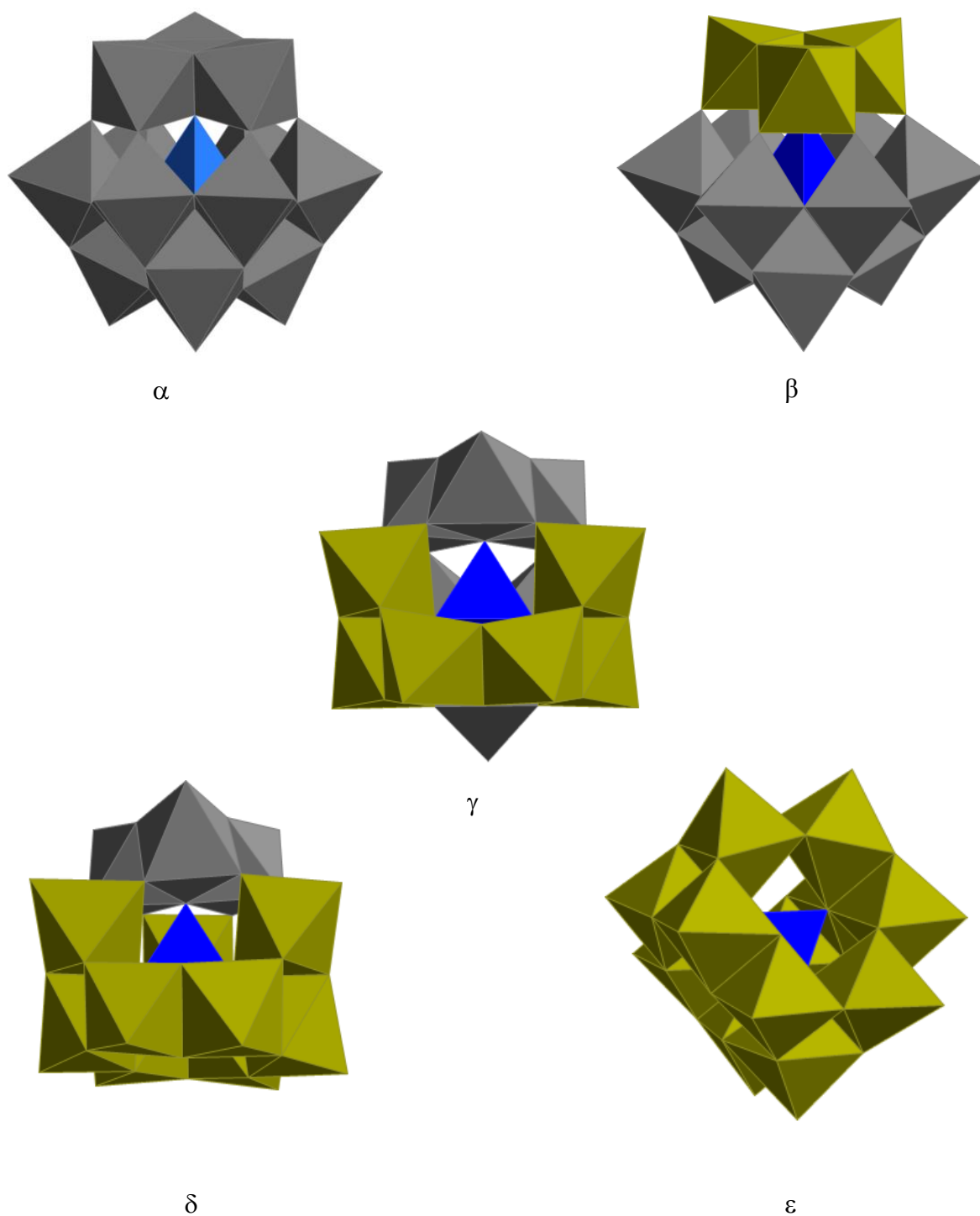


Figure 1-2. Baker-Figgis isomers of Keggin structure: α , β , γ , δ , ϵ (the rotated M_3O_{13} group(s) are in yellowish green).

The Wells-Dawson structure with a general formula $[X_2M_{18}O_{62}]^{x-}$ ($X = P, As, etc$) is built from two tetrahedral $[XO_4]^{n-}$ units each coordinating one $[M_3O_{13}]^{m-}$ triad cap on the opposite side and one $[M_6O_{14}]$ unit in the belt position. The two $[M_6O_{14}]$ units are further connected by corner-sharing oxygen atoms (Figure 1-3). Among the six isomers suggested by Baker and Figgis^{16,17}, the α and β isomers of Dawson structures are the most common ones.

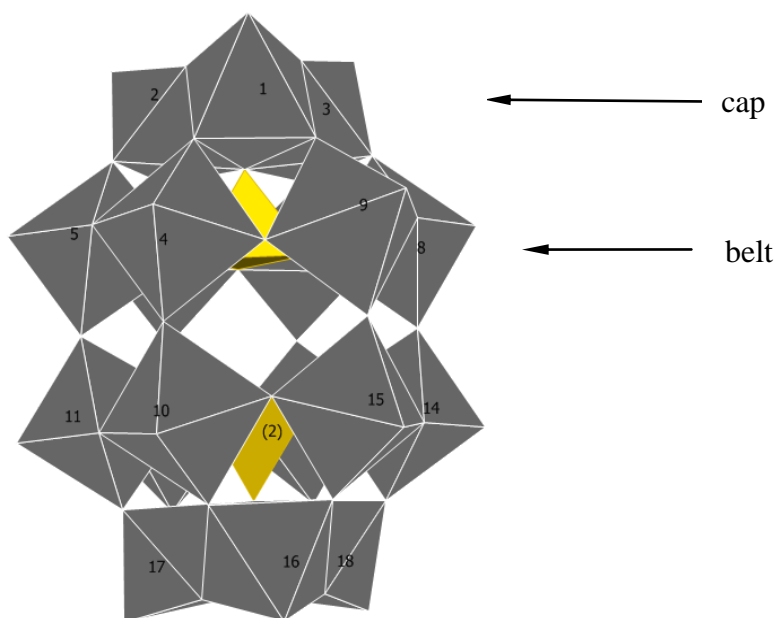


Figure 1-3. IUPAC numbering scheme of Wells-Dawson $[\alpha-M_2W_{18}O_{62}]^{x-}$.

In general, the parent Keggin and Wells-Dawson POMs with “complete” structures (referred to plenary) are normally stable in a specific pH range which depends on the POM structure and metal composition. Outside this range hydrolysis reactions will occur to form defect (referred to lacunary) POMs by the removal of one or more MO_x units from the plenary structure.

Keggin-type POMs can form mono-,bi- and tri-lacunary species under different hydrolysis conditions. Isomerizations of the Keggin monolacunary polytungstosilicate are shown in Figure 1-4.¹⁷ The β isomers are only meta-stable and slowly convert to α isomers in solution. In the Keggin type polytungstophosphates, only the α isomer is observed. The species $[\gamma\text{-SiW}_{10}\text{O}_{36}]^{8-}$ is the only stable di-lacunary (di-defect) POM isolated from the hydrolysis of $[\beta_2\text{-SiW}_{11}\text{O}_{39}]^{8-}$. Tri-lacunary POMs species usually come in two structural isomers, A type, which is formed by removing three corner-sharing WO_6 octahedron from three neighboring $[\text{W}_3\text{O}_{13}]^{8-}$ triads in the POM, and B type, which is formed by removing an edge-sharing $[\text{W}_3\text{O}_6]$ cap.

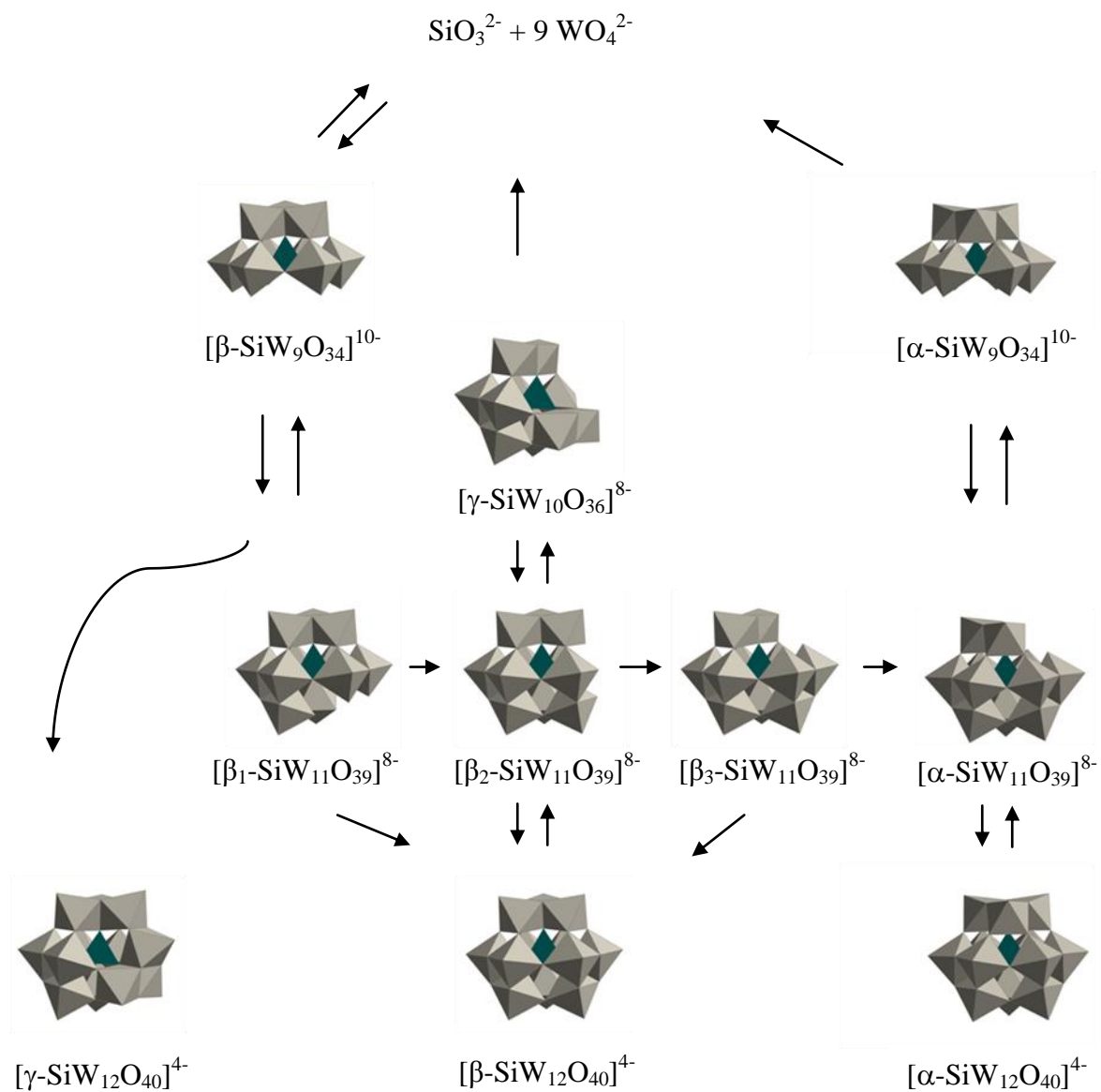


Figure 1-4. Dodecatungstosilicate isomerization processes in aqueous solution.

For the Wells-Dawson structures, multi-lacunary derivatives can also be synthesized *via* controlled hydrolysis. The hexavacant $[\text{P}_2\text{W}_{12}\text{O}_{48}]^{14-}$ is obtained by removing six WO_x units along the C_3 axis of the parent $[\alpha\text{-P}_2\text{W}_{18}\text{O}_{62}]^{6-}$. The most common tri-lacunary species is $[\text{P}_2\text{W}_{15}\text{O}_{56}]^{12-}$, which is formed from the “saturated” structure by removal of one of the capping $[\text{M}_3\text{O}_{13}]^n$ triads. From the hydrolysis of the parent α -Wells-Dawson structure, α_1 and α_2 isomers of monolacunary species can be

isolated. The $[\alpha_1\text{-P}_2\text{W}_{17}\text{O}_{61}]^{10-}$ isomer has the vacant site on its belt position and is synthesized from $[\text{P}_2\text{W}_{12}\text{O}_{48}]^{14-}$ with additional WO_x species. The $[\alpha_2\text{-P}_2\text{W}_{17}\text{O}_{61}]^{10-}$ isomer can be directly prepared by removing one WO_x octahedron from one of the capping $[\text{W}_3\text{O}_{13}]^{8-}$ triads in the parent structure (Figure 1-5).

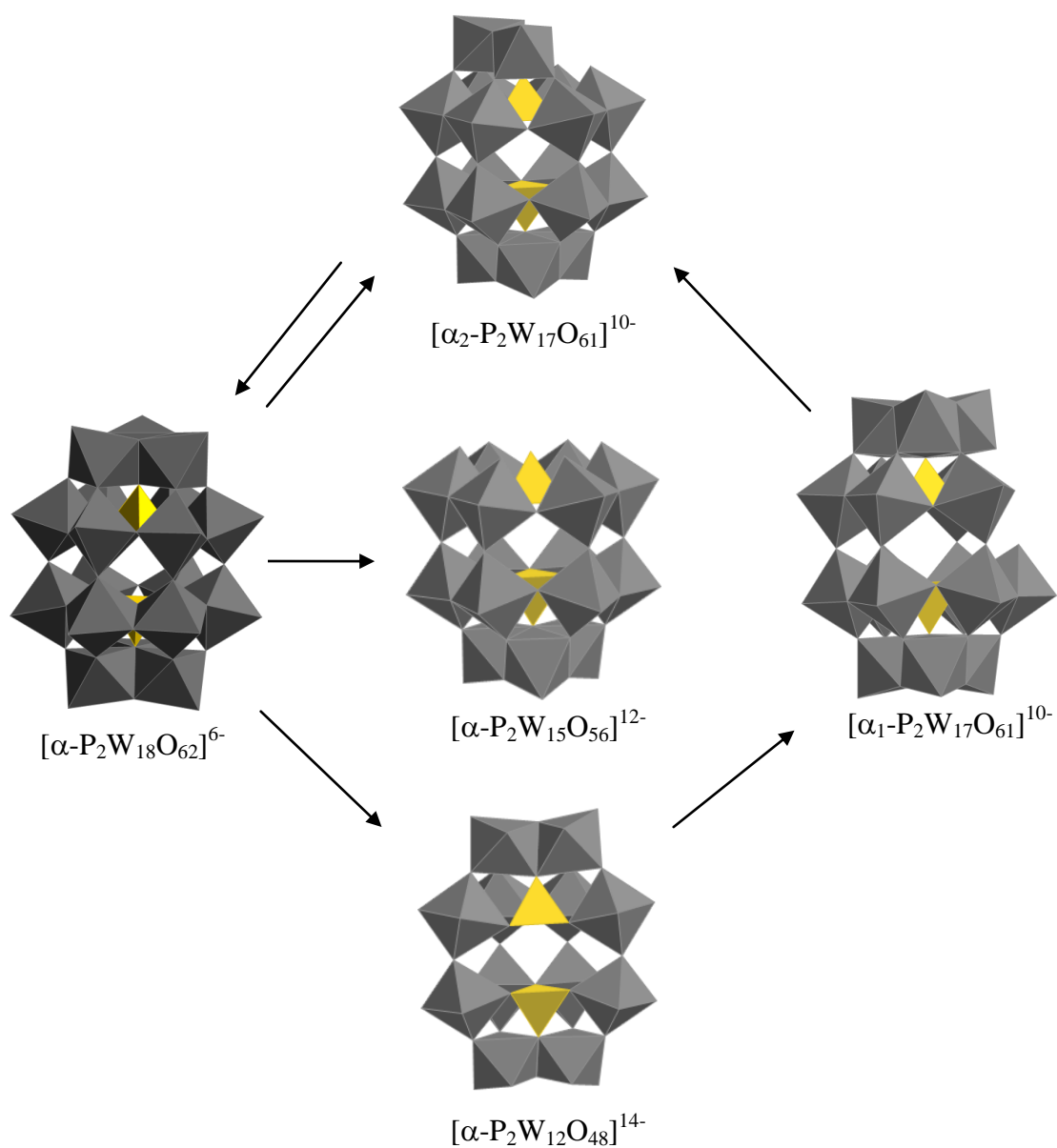


Figure 1-5. Transformations of different polytungstodiphosphate species.

The transition metal-substituted POMs (TMSPs) are an attractive and large subclass of heteropolyoxometalates which exhibit many interesting properties and have found application in molecular assembly, catalysis, and magnetic materials. The general synthetic strategy used in forming TMSPs is to react one type of d-electron transition metal with a preformed lacunary POM in a one-pot procedure to produce one or multiple d-electron centers coordinated in the vacant sites. Many new TMSP structures are obtained based on the specific reactivity and stability of one lacunary species under certain synthetic conditions (Figure 1-6). For example, modifications in cation type, buffer capacity, ionic strength, pH and temperature can all substantially affect the association/disassociation of polyanion equilibria and final product identity and formation.

Monosubstituted TMSPs can be synthesized using monovacant POMs as a pentadentate ligand by inserting a transition metal in the vacant addenda position. However, these monosubstituted α -Keggin derivatives always exhibit twelve-fold crystallographic disorder which prevents the X-ray diffraction from accurately locating the metal center and identifying the terminal ligand on the d-electron metal.¹⁸

The reaction of di or trivacant POMs, which can be derived from either the Keggin or Wells-Dawson structural families, with multi-d-electron transition metal ions can lead to complicated and structurally-novel TMSPs and complex assemblies. The divacant POM, $[\gamma\text{-SiW}_{10}\text{O}_{36}]^{8-}$, shows a pH-dependent stability in aqueous media and its structural transformations are observed at both low and high pH in the presence of additional transition metal ions. The coordination between the divacant POM and transition metals under different conditions can lead to saturated disubstituted POMs,^{19,20}

disubstituted dimers,²¹ and many other complexes.²²⁻²⁵ Trivacant POMs are also the commonligands used to construct two types sandwich structures.^{26,27} The A-type sandwich POMs contain three corner-sharing transition metal $[\text{MO}_6]^{n-}$ octahedra between two $[\text{A-}\alpha\text{-XW}_9\text{O}_{34}]^{n-}$ units, while the B-type sandwich POMs contain four edge-sharing metal octahedra between two B- α -trivacant units.

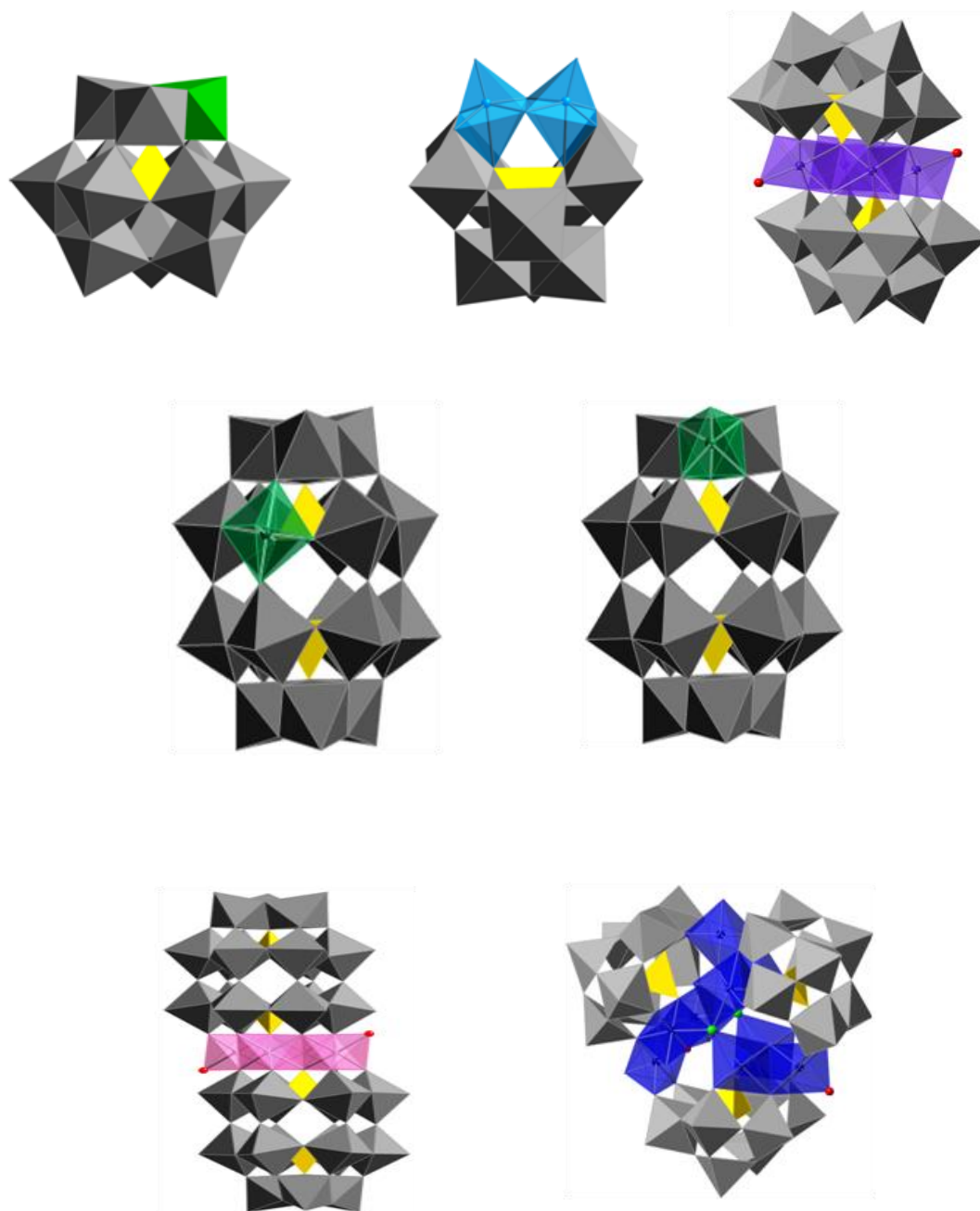


Figure 1-6. Polyhedral representations of TMSPs: a). $[(\alpha\text{-Cu}(\text{H}_2\text{O})\text{PW}_{11}\text{O}_{39})]^{5-}$, b) $[\gamma\text{-Cr}_2(\text{H}_2\text{O})_2\text{SiW}_{10}\text{O}_{36}]^{2-}$ c) $[\text{Co}_4(\text{H}_2\text{O})_2(\text{PW}_9\text{O}_{34})_2]^{10-}$, d) $[\alpha_1\text{-Cu}(\text{H}_2\text{O})\text{PW}_{17}\text{O}_{61}]^{10-}$ e) $[\alpha_2\text{-Cu}(\text{H}_2\text{O})\text{P}_2\text{W}_{17}\text{O}_{61}]^{10-}$, f) $[\text{Mn}_4(\text{H}_2\text{O})(\text{P}_2\text{W}_{15}\text{O}_{56})_2]^{16-}$, g) $\{[\text{Co}_9\text{Cl}_2(\text{OH})_3(\text{H}_2\text{O})_9]_3(\text{B-}\beta\text{-SiW}_8\text{O}_{31})_3\}^{17-}$.

1-2. Overview of organic-polyoxometalate hybrids

Giant polyoxometalate metal-oxide molecular clusters represent a large group of functional inorganic materials with important applications in catalysis, materials science (electronic, magnetic, optical) and anti-tumoral chemotherapy.^{3,28,29} Most of the POM clusters have hydrophilic surfaces that limit their compatibility with organic media. In order to solve this problem and extend the applications of POMs, one can chemically incorporate organic components (building blocks) onto the POMs. Such organic-POM composite units have been proved to be powerful and novel synthons for construction of extended architectures exhibiting complementary inorganic and organic functionalities.³⁰ In particular, this approach is very promising for the controlled and programmed assembly of large nanostructure and framework materials containing POMs. This POM-surface modification chemistry renders the POM units amphiphilic in nature and therefore is expected to trigger self-organization in a range of media. For example, such inorganic-organic hybrids can be treated as novel “surfactants” with functional, bulky polar head groups. Furthermore, the modified POM clusters with reactive end groups can be further modified *via* post-synthesis chemical modifications. A significant and engaging aspect of such organic-inorganic hybrid materials is that they possess the important features of soft materials such as good processibility, controllable and reconfigurable supramolecular structures (micelles, vesicles, emulsions, liquid crystalline structures, gel-like cubic, hexagonal and lamellar structures, to name a few) and simultaneously retain the important physicochemical properties of the POM units themselves.³¹⁻³⁶ All the organic-POM hybrid materials to date can be classified into two types based on the nature of the interactions between the organic moiety and

inorganic polyanions.³⁷ In Type I organic-POM hybrids, the organic and inorganic parts associate *via* non-covalent bonds. These inter-moiety interactions normally involve electrostatic attraction between organic cations and polyanions, hydrogen-bonding, or van der Waals forces.³⁸⁻⁴¹ Two examples are shown in Figure 1-7.

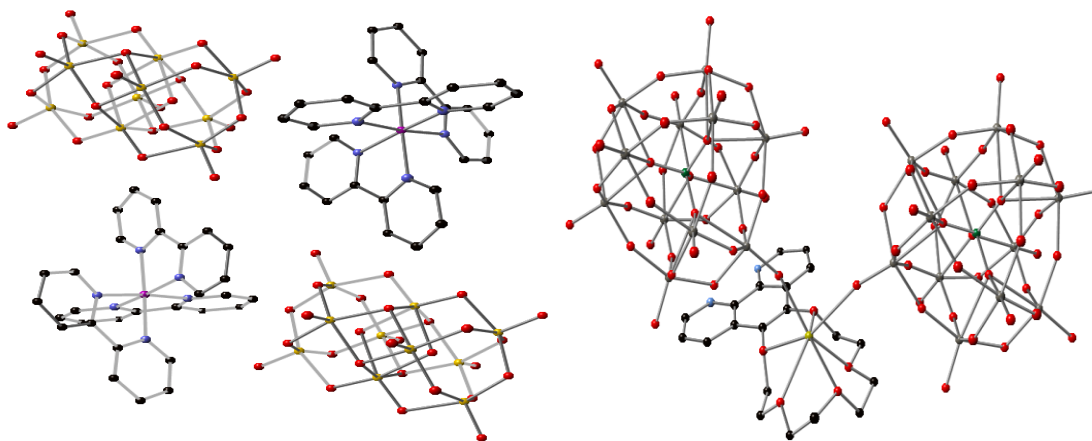


Figure 1-7. Type I organic-inorganic POM hybrids. $[\text{Ru}(\text{bpy})_3][\text{H}_4\text{V}_{10}\text{O}_{28}]$ (left) and $\{[5,6-(15\text{-crown-5})-1,10\text{-phenanthroline}]\text{-Na-}[\text{HPW}_{12}\text{O}_{40}]\}$ (right).

The second type (Type II) of organic-POM hybrid molecule involves inter-unit covalent bonding.⁴²⁻⁴⁶ In these species, the organic and inorganic parts are generally linked through one or more oxo groups on the POM surface or they are connected by N- M_{POM} multiple bonds. However, covalent organic functionalization of POMs is frequently not straightforward, but this depends critically on the building blocks chosen. A brief overview is given here summarizes the commonly employed synthesis methods for covalently-linked organic-POM hybrids. These exhibit one or more main group elements (Group 14 and Group 15) as inter-unit connectors.

Organic groups covalently linked to POM via C-O bonds

This type of organic-POM hybrid is usually formed in the reaction of polyvanadate and polymolybdate with tri-alcohol ligands via transesterification in anhydrous, polar aprotic solvents (Figure 1- 8). To date, Linqvist,^{43,47} Anderson,^{43,44,48-56} and Wells-Dawson^{33,57,58} type POM hybrids have been successfully synthesized using this approach. They are covalently tethered with either one or two tripodal-like ligands, such as *tris*(hydroxymethyl)aminomethane (Tris), on their surfaces.⁵⁹⁻⁶² Recently, a {Ni₆PW₉} unit was also covalently linked with Tris ligands to form a cubic organic-POM molecular cage with high thermal and hydrolytic stability that displays a superlarge inner spherical cavity (diameter *ca.* 1.7 nm).⁶³ The reactive organic termini, such as primary amine groups in Tris derivatives, can be further functionalized *via* appropriate postsynthesis chemical modification when taking into account the stability and reactivity of POMs with different negative charges towards the organic substrates.

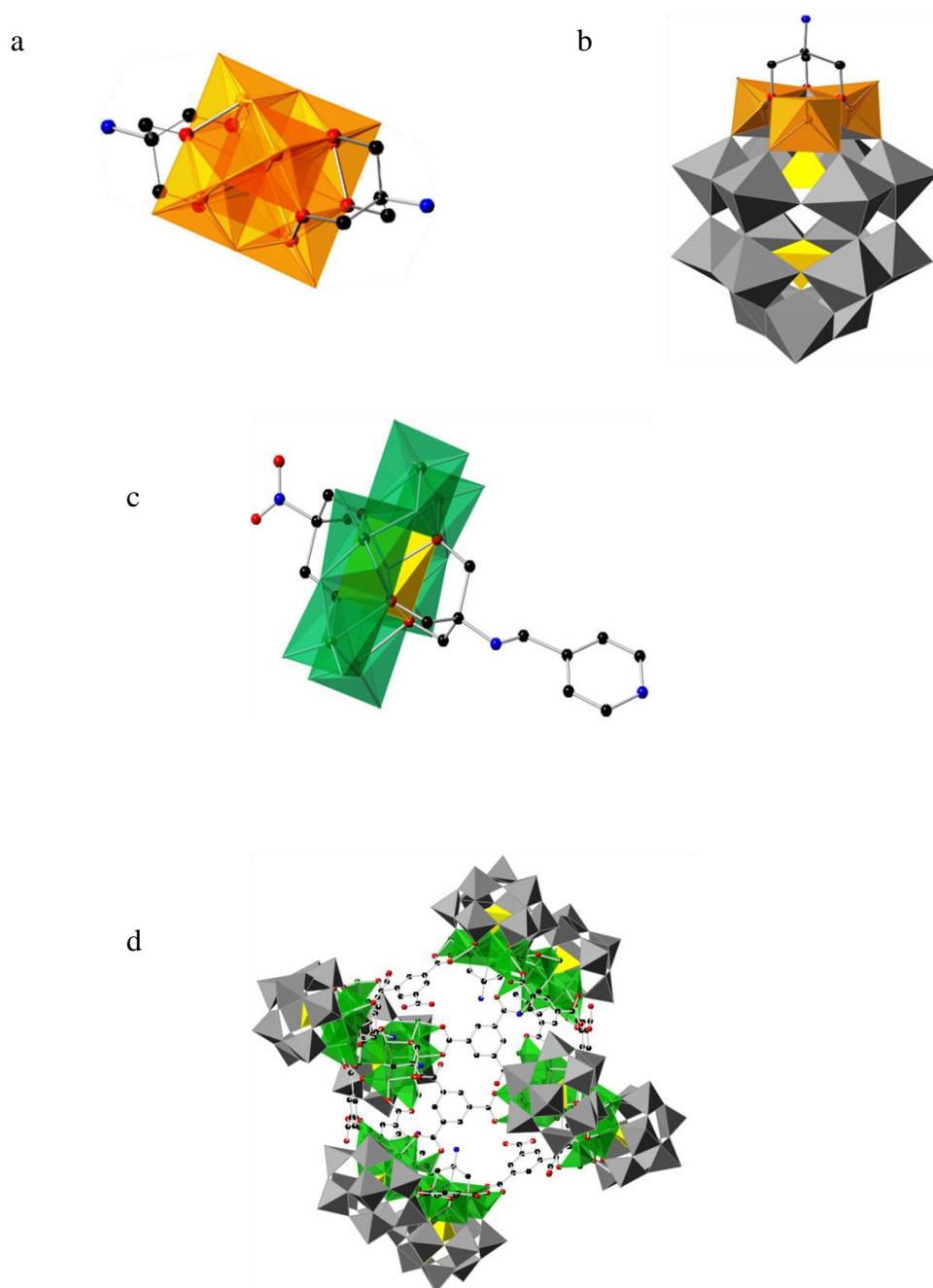


Figure 1-8. Type II organic-POM hybrids: a) Linqvist $[V_6O_{13}\{(OCH_2)_3CNH_2\}_2]^{2-}$; b) Wells-Dawson $[H_2NC(CH_2O)_3P_2V_3W_{15}O_{59}]^{6-}$; c) Anderson $[MnMo_6O_{18}\{(OCH_2)_3CNH_2\}\{(OCH_2)_3CNHCH_2C_5H_4N\}]^{3-}$; d) the molecular cage $[Ni_6(Tris)(ethylenediamine)_3(1,3,5\text{-benzenetricarboxylate})_{1.5}(B\text{-}\alpha\text{-PW}_9O_{34})_8]^{6-}$

Organic groups covalently linked to POM via Si-O bonds

Organosilyl derivatives of POMs can be obtained by reaction of lacunary polyanions with organosilanes (Figure 1-9). The nucleophilicity of the oxygen atoms located on the vacant sites renders them highly reactive towards electrophilic R_3SiX groups, where R and X are usually alkyl and halide substituents.^{64-77, 78-84, 85-88} The silylation process can be classified into two types based on the reaction solvents. One involves silylation conducted in organic solvents, such as acetonitrile, dimethylformamide, dichloromethane, etc., in the presence of phase transfer reagents such as tetraalkylammonium halides. Another method involves reaction in water or in water-polar organic solvent systems. Depending on the pH-dependent stability of lacunary POMs in water, these two approaches are selectively employed. Sometimes inorganic acids or organic bases are used to control the hydrolysis and condensation level of organosilane compounds in order to attach one or more organic groups to the POM.

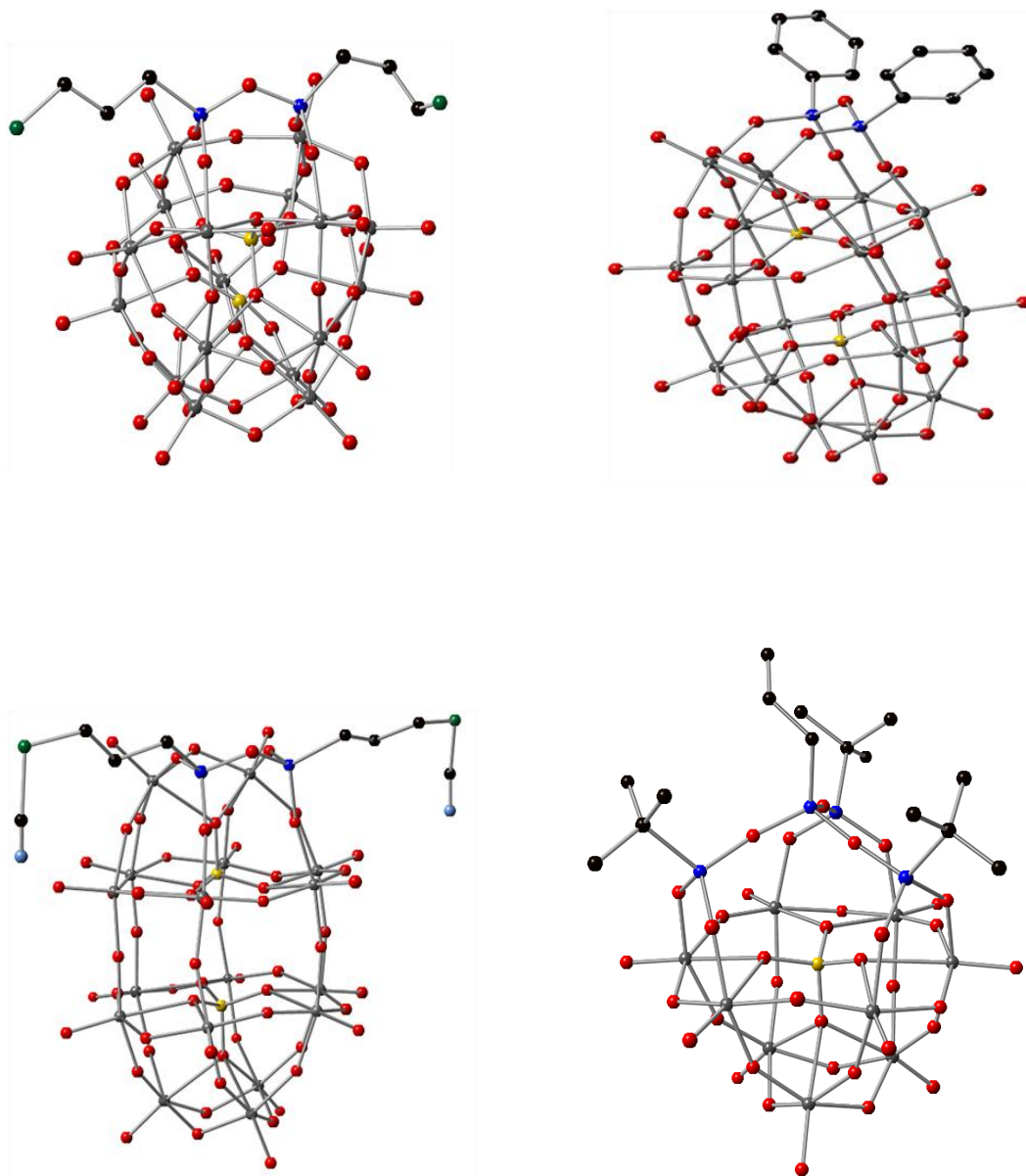
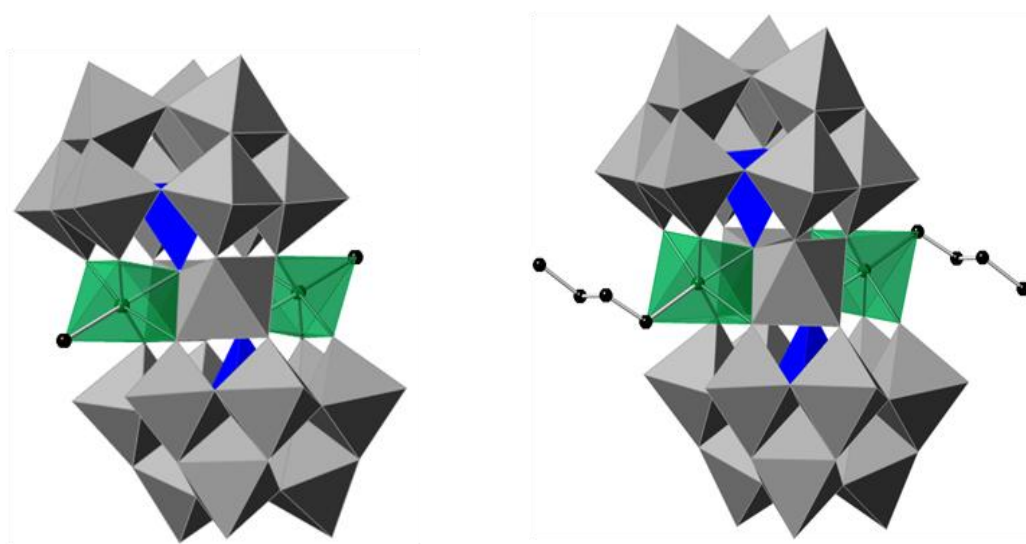


Figure 1-9. Type II organic-inorganic POM hybrids. $[\alpha_2\text{-P}_2\text{W}_{17}\text{O}_{61}\{\text{OR}\}_2]^{6-}$ where: a) R = $\text{Si}(\text{CH}_2)_3\text{SH}$; b) R = SiPh ; c) R = $\text{Si}(\text{CH}_2)_3\text{SCN}$; d) $(\text{A-}\beta\text{-PW}_9\text{O}_{34})_8]^{3-}$ with $[(^t\text{BuSiO})_3(\text{Si-CH}_2\text{-CH=CH}_2)]$ groups.

Organic groups covalently linked to POM via Ge-O or Sn-O bonds

There are only a few organogermyl and organotin POM derivatives; a few samples are illustrated in Figure 1-10. One example of the organogermyl derivatives is $[\text{PW}_{11}\text{O}_{39}\text{NbO}(\text{GeMe}_3)]^{3-}$ and the Ge-O-Nb linkage was confirmed by single crystal X-ray diffraction.^{25a, 26} However, this type of hybrid is prone to degradation in the presence of Lewis acids. In contrast, organotin-POM hybrids demonstrate higher stability toward hydrolysis and have been extensively studied in the past ten years.⁸⁹⁻⁹⁷ Recently, a type of phenyl-tin POM was reported to have effectively no crystallographically-imposed disorder and this opens a new synthetic route for controlled synthesis of organic-POM hybrid species.



a

b

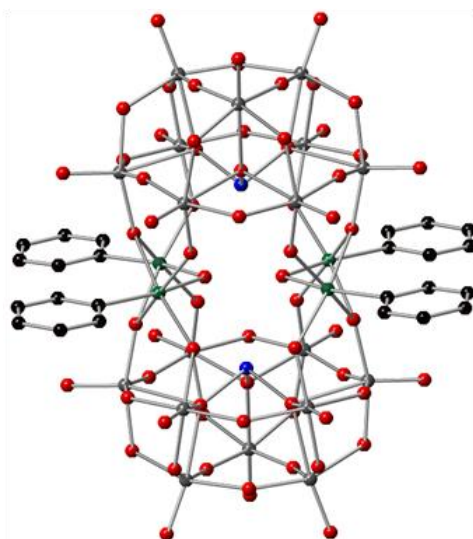


Figure 1-10. Type II organic-inorganic POM hybrids: $[\text{WZn}(\text{RSn})_2(\text{ZnW}_9\text{O}_{34})_2]^{10-}$ a) $\text{R} = \text{CH}_3$; b) $\text{R} = n\text{-C}_4\text{H}_9$; c) $[(\text{SnPh})_4(\alpha\text{-AsW}_9\text{O}_{34})_2]^{10-}$

Organic groups covalently linked to POM via N-M multiple bonds

Organic-POM hybrids with N-M (M = Mo or W) linkage include two types: organoimido and organodiazenido derivatives (Figure 1-11).^{55,98-103} The organoimido hybrids are mostly derived from the condensation reaction of Linqvist polyoxomolybdates and N-containing organic precursors. In general, there are three strategies to synthesize this type of material. The first approach reported by Maatta is the reaction between $[\text{Mo}_6\text{O}_{19}]^{2-}$ and $\text{Ph}_3\text{P}=\text{NR}$ to produce $[\text{Mo}_6\text{O}_{18}(\text{NR})]^{2-}$.¹⁰⁴ The second approach, which proceeds with higher efficiency, is to reflux $[\text{Mo}_6\text{O}_{19}]^{2-}$ and isocyanates RNCO (R = *n*-butyl, cyclohexyl, 2,6-diisopropylphenyl) in pyridine solvent.^{105,106} The third one reported by Peng is using dicyclohexylcarbodiimide (DCC) as a dehydration reagent, which is assumed to activate the terminal $\text{Mo}=\text{O}$ bonds in anhydrous polar aprotic solvents.¹⁰⁷⁻¹¹⁴ This method is much more efficient than the previous two and has been employed to produce dozens of new organoimido derivatives, which include single or multiple substituted (*cis*- or *trans*- isomers).¹¹⁵

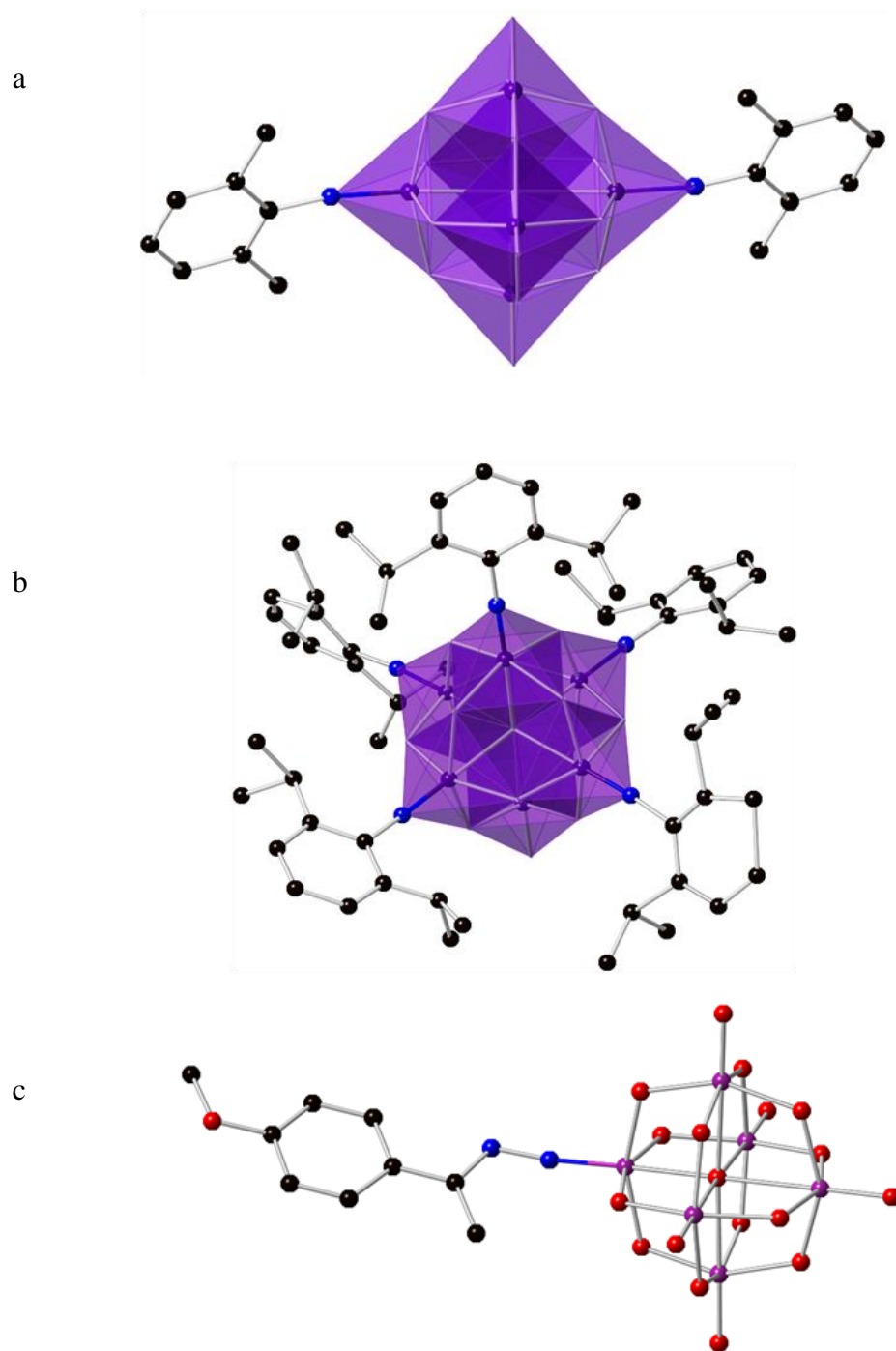


Figure 1-11. Type II organic-inorganic POM hybrids: a) *trans*-[Mo₆O₁₇{N(2,6-dimethylphenyl)}₂]; b) *cis*-[Mo₆O₁₄{N(2,6-diisopropylphenyl)}₅]²⁻; c) [Mo₆O₁₈(N=N=C(C₆H₄OCH₃)CH₃)]²⁻

Organic groups covalently linked to POM via P-O, As-O, or Sb-O bonds

A series of organophosphonate, organoarsenate, and organoantimony derivatives have been extensively studied since the first example, $[(RP)_2Mo_5O_{21}]^{4-}$ (R = H, Me, Et, Ph, $C_2H_4NH_3^+$, $p-CH_2C_6H_4NH_3^+$) was reported by Pope in 1975.¹¹⁶ Monophosphonate and diphosphonate¹¹⁷⁻¹²⁶ ligands can react with isopolyanions such as polyoxomolybdates¹²⁷⁻¹²⁹ and polyoxovanadates, or lacunary heteropolyanions, such as the monolacunary $PW_{11}O_{39}^{7-}$,^{130,131=} the dilacunary $[\gamma-XW_{10}O_{36}]^{8-}$ (X = Si, Ge),^{81, 132} and the trivacant $[PW_9O_{34}]^{9-}$ (Figure 1-12).^{133,134} These families of hybrids are usually synthesized under solvothermal conditions. One interesting observation is that organophosphonate can selectively react with POMs in the presence of some other organic functional groups, such as the carboxylic acid, primary amine, hydroxyl, and cyano.

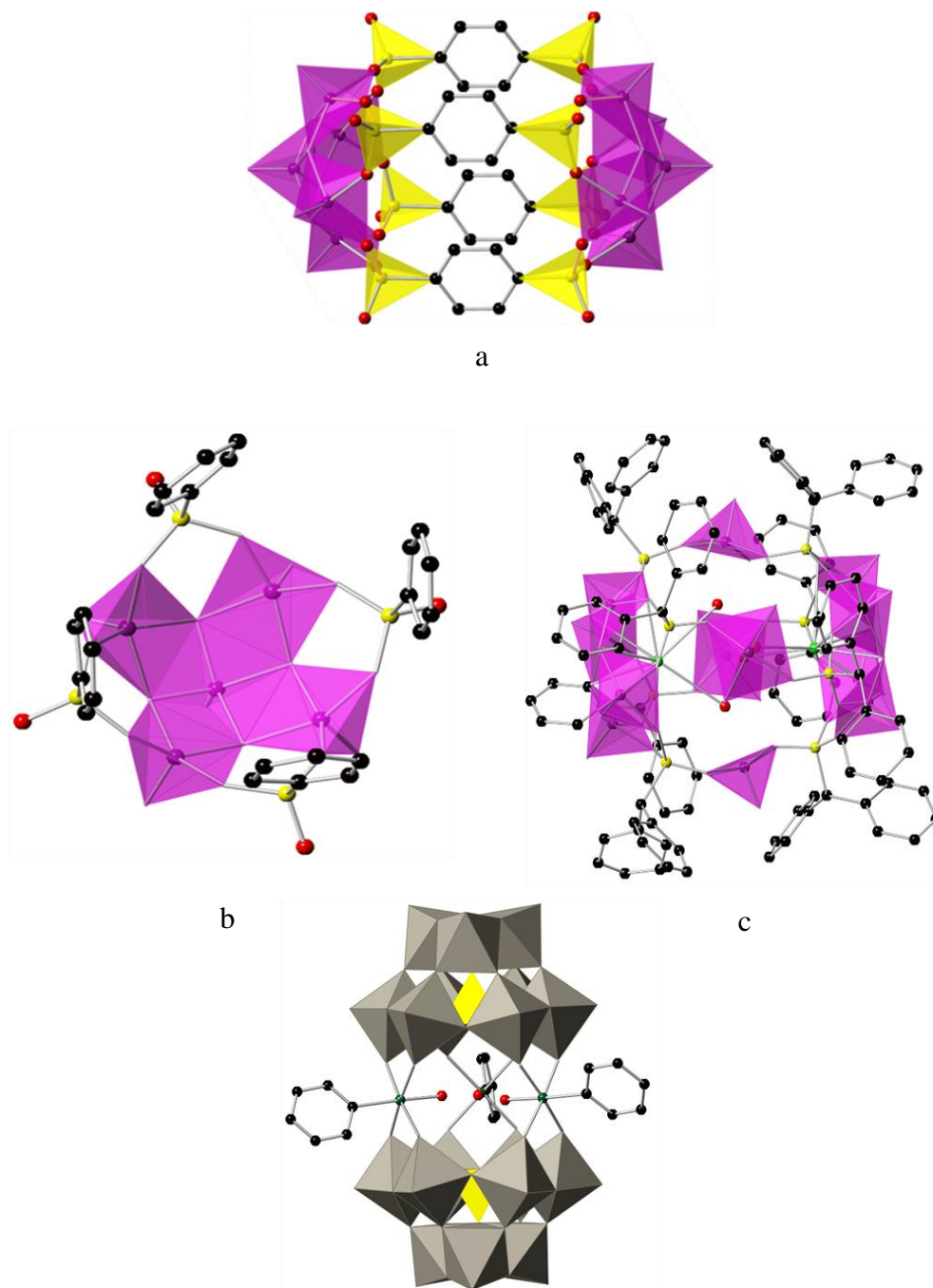


Figure 1-12. Type II organic-POM hybrids: a) $[\text{H}_2\text{V}_{10}\text{O}_{18}(\text{O}_3\text{PC}_6\text{H}_4\text{PO}_3)_4]^{8-}$; b) $[\text{V}_5\text{O}_9(\text{O}_3\text{AsC}_6\text{H}_4\text{-4-NH}_2)_4]^{5-}$; c) $[\text{V}_{12}\text{O}_{12}(\text{OH})_4(\text{O}_3\text{AsC}_6\text{H}_4\text{-4-NH}_2)_{10}]^{4-}$; d) $[\{\text{PhSbOH}\}_3(\text{A-}\alpha\text{-PW}_9\text{O}_{34})_2]^{9-}$

1-3. Overview of polyoxometalates as catalysts for oxidation of organic compounds and water

In the past decade, POMs and their transition metal-substituted derivatives, TMSPs, have attracted increasing attention because several classes are efficient acid and oxidation catalysts. One of several prominent commercial POMs is $[\text{PMo}_{12}\text{O}_{40}]^{3-}$ which is used to catalyze the oxidation of isobutylene to *tert*-butyl alcohol on a 10,000-ton industrial scale in Japan since 1984.¹³⁵

Several TMSPs catalyze the oxidation of organic substrates with high selectivity and high rates. They can act as either stoichiometric oxidants or as catalysts in conjunction with environmentally friendly oxidants such as O_2 and H_2O_2 .¹³⁶ One area of intense investigation has been the TMSP-catalyzed oxidation of alkanes to alcohols and ketones under a wide variety of conditions.^{137,138} One example is the application of mono-substituted polyoxotungstate $[\text{PW}_{11}(\text{M})\text{O}_{39}]^{5-}$ ($\text{M} = \text{Mn}^{2+}, \text{Fe}^{2+}, \text{Co}^{2+}, \text{Cu}^{2+}$) as a homogeneous catalyst for the high yield oxidation of alkane oxidation by oxo-transfer in the presence of *tert*-butyl hydroperoxide. Some such systems are sufficiently stable to sustain alkane functionalization for thousands of turnovers.¹³⁷

Recently, a divanadium-substituted phosphotungstate, $[\gamma\text{-H}_2\text{PV}_2\text{W}_{10}\text{O}_{40}]^{3-}$ was reported to be an effective catalyst for oxidation of sp^3 C-H in alkanes (Figure 1-13). High chemoselectivity (for alcohol relative to the products of overoxidation) and regioselectivity (for secondary over more reactive tertiary C-H bonds) in the hydroxylation of alkanes with H_2O_2 as an oxidant were observed.¹³⁹

In addition, important advances in the development of Pd-catalyzed oxidative coupling reactions of benzene with benzofuran¹⁴⁰ and olefination of unactivated sp^3 C-H bonds¹⁴¹ have been reported. The monovanadium-substituted polyoxomolybdate, $H_4PMo_{11}VO_{40}$, was employed as a co-catalyst for aerobic oxidation during the catalytic C-H activation/C-C coupling process, which leads to an increase in selectivity: >20:1 for primary over secondary sp^3 C-H bonds (Figure 1-13).

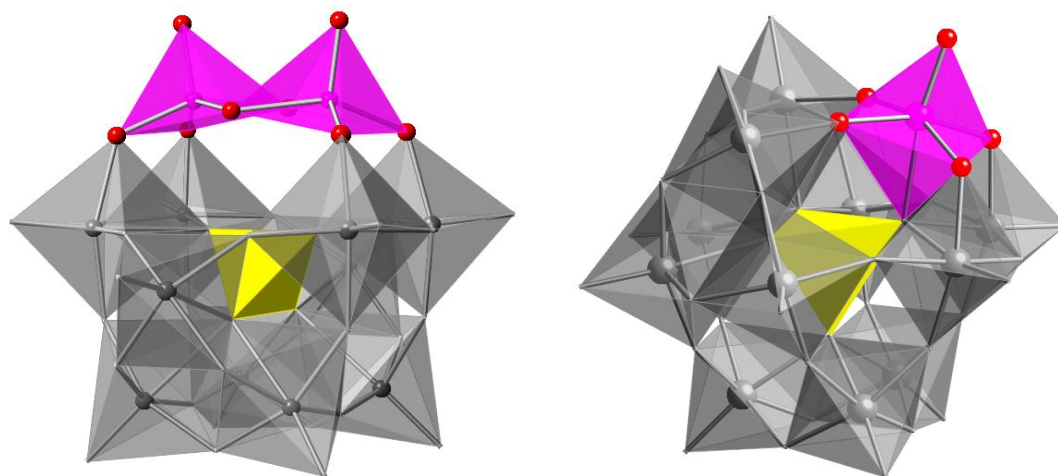


Figure 1-13. $[\gamma-H_2PV_2W_{10}O_{40}]^{3-}$ (left) and $[PMo_{11}VO_{40}]^{4-}$ (right).

In addition, these TMSPs also used as effective catalysts for epoxidation and hydroxylation of alkenes.¹⁴²⁻¹⁴⁴ The applications of TMSPs in decontamination of toxic reagents through hydrolysis or oxidation reactions such as sulfoxidation and thiol oxidation have been explored under ambient conditions.^{18,145,146}

In order to pursue renewable energy to meet future needs, application of TMSPs has been extended to the water splitting reaction to generate hydrogen and oxygen. The catalytic challenges in this area include facilitating the 4-electron oxidation of H₂O to O₂ and the 2-electron reduction of H₂O to H₂ with high catalyst stability under practical environmental conditions. There is also considerable interest these days to develop catalysts constituted by cheap, readily available, and abundant metals rather than noble metals.¹⁴⁷

Recently, several POMs with multiple d-electron transition metal centers have proved to constitute of a novel class of soluble, carbon-free molecular catalysts that integrate both high efficiency and robustness in one structure, under both dark and visible light-driven conditions. The ruthenium-containing POM, Ru₂Zn₂(H₂O)₂(ZnW₉O₃₄)₂]¹⁴⁻,¹⁴⁸ was shown to be an efficient electrochemical catalyst for water oxidation to molecular oxygen. However, its synthesis remains very problematic (many research groups have failed to agree on the final composition of this complex). Another polyanion, one with a tetraruthenium core, [Ru^{IV}₄O₄(OH)₂(H₂O)₄(γ-SiW₁₀O₃₆)₂]¹⁰⁻ was recently reported simultaneously by two research groups to catalyze water oxidation under either thermal or photochemical conditions (Figure 1-14 and Scheme 1-1).^{21,149}

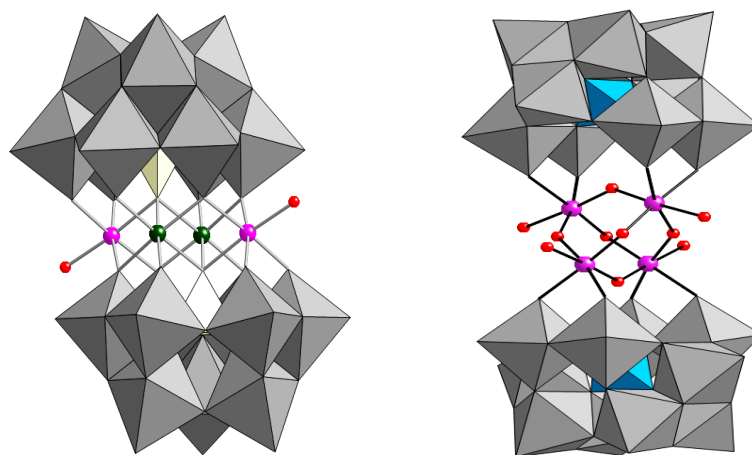
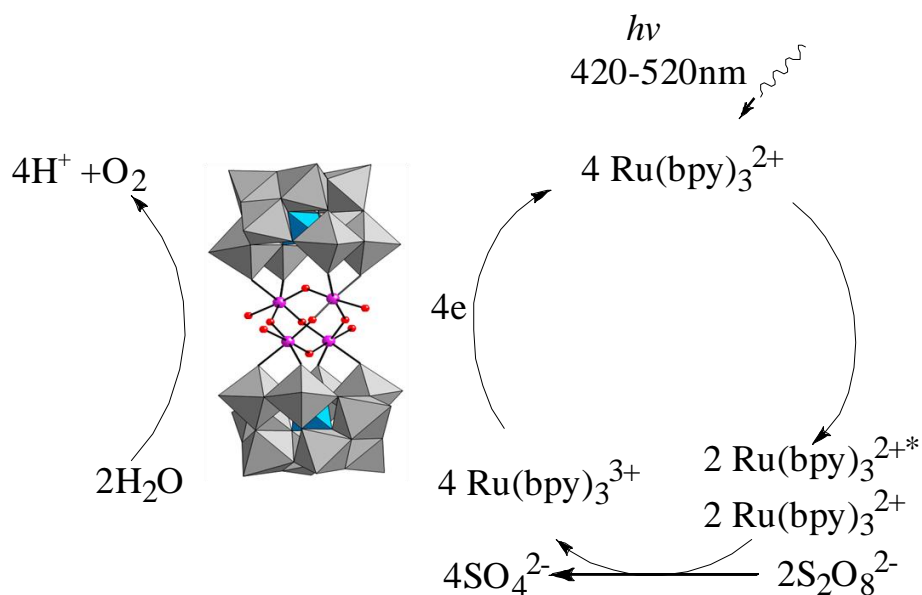


Figure 1-14. X-Ray structures of $\text{Ru}_2\text{Zn}_2(\text{H}_2\text{O})_2(\text{ZnW}_9\text{O}_{34})_2]^{11-}$ (left) and $[\text{Ru}^{\text{IV}}_4\text{O}_4(\text{OH})_2(\text{H}_2\text{O})_4(\gamma\text{-SiW}_{10}\text{O}_{36})_2]^{10-}$ (right) in combined polyhedral (polytungstate ligands) and ball-and-stick notation. Ru: purple, O: red; WO_6 octahedra: gray, SiO_4 tetrahedra: blue. ZnO_4 tetrahedra: pale white.



Scheme 1-1. Light-driven water oxidation catalyzed by $[\text{Ru}^{\text{IV}}_4\text{O}_4(\text{OH})_2(\text{H}_2\text{O})_4(\gamma\text{-SiW}_{10}\text{O}_{36})_2]^{10-}$ using $[\text{Ru}(\text{bpy})_3]^{2+}$ as a photosensitizer and persulfate as a sacrificial electron acceptor.

Most recently, $[\text{Co}_4(\text{H}_2\text{O})_2(\alpha\text{-PW}_9\text{O}_{34})_2]^{10-}$, another carbon-free POM, was documented to be the fastest homogeneous catalyst for water oxidation to date with turnover frequencies for O_2 production $\geq 5 \text{ s}^{-1}$ at pH 8 under thermal oxidation conditions (Figure 1-15 and Scheme 1-2).¹⁵⁰ In addition, this polyanion was shown to be hydrolytically and oxidatively stable during catalytic turnover. Later, its catalytic activity under visible light-driven conditions was also reported.¹⁵¹

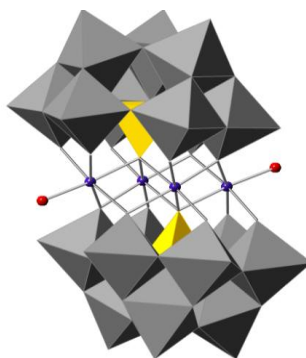
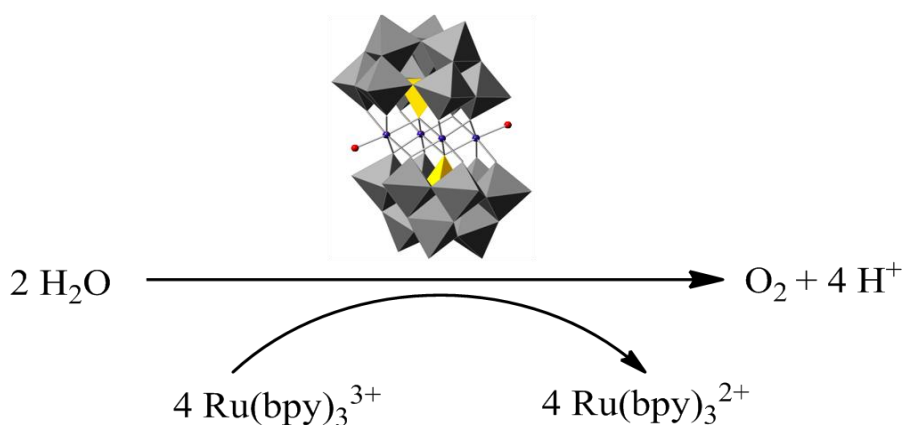


Figure 1-15. X-ray structure of $[\text{Co}_4(\text{H}_2\text{O})_2(\alpha\text{-PW}_9\text{O}_{34})_2]^{10-}$ in combined polyhedral (polytungstate ligands) and ball-and-stick notation. Co: blue, O: red; WO_6 octahedra: gray, PO_4 tetrahedra: yellow.



Scheme 1-2. Thermal oxidation of water catalyzed by $[\text{Co}_4(\text{H}_2\text{O})_2(\alpha\text{-PW}_9\text{O}_{34})_2]^{10-}$ using $[\text{Ru}(\text{bpy})_3]^{3+}$ as an oxidant.

References

- (1) Pope, M. T. *Heteropoly and Isopoly Oxometalates*; Springer-Verlag: Berlin, 1983.
- (2) Berzelius, J. J. *Poggendorfs Ann. Phys. Chem.* **1826**, 6, 369.
- (3) Hill, C. L. *Chem. Rev.* **1998**, 98, 1.
- (4) Katsoulis, D. E. *Chem. Rev.* **1998**, 98, 359.
- (5) Maekawa, S.; Tohyama, T.; Barnes, S. E.; Ishihara, S.; Koshibae, W.; Khaliullin, G. *Springer, Berlin: 2004, p 1. 2004.*
- (6) Pope, M. T. In *Comprehensive Coordination Chemistry*; Wilkinson, G., Gillard, R. D., McCleverty, J. A., Eds.; Pergamon Press: New York, 1987; Vol. 3, p Chapter 38.
- (7) Pope, M. T.; Müller, A. *Angew. Chem.* **1991**, 103, 56.
- (8) Hill, C. L.; Prosser-McCartha, C. M. *Coord. Chem. Rev.* **1995**, 143, 407.
- (9) Okuhara, T.; Mizuno, N.; Misono, M. *Advances in Catalysis* **1996**, 41, 113.
- (10) *Polyoxometalate Chemistry From Topology via Self-Assembly to Applications*; Pope, M. T.; Müller, A., Eds.; Kluwer Academic Publishers: Dordrecht, 2001.
- (11) Barrows, J. N.; Pope, M. T. *Inorg. Chim. Acta* **1993**, 213, 91.
- (12) Moffat, J. B. *Metal-Oxygen Clusters: The Surface and Catalytic Properties of Heteropoly Oxometalates.*; Kluwer Academic/Plenum Publishers: New York, 2001; Vol. 9.

- (13) *Polyoxometalate Chemistry for Nano-Composite Design*; Yamase, T.; Pope, M. T., Eds.; Kluwer Academic/Plenum Publishers: New York, 2002; Vol. 2.
- (14) Keggin, J. F. *Nature* **1933**, *131*, 908.
- (15) Brown, G. M.; Noe-Spirlet, M. R.; Busing, W. R.; Levy, H. A. *Acta Crystallogr., Sect. B: Struct. Sci.* **1977**, *B33*, 1038.
- (16) Baker, L. C. W.; Figgis, J. S. *J. Am. Chem. Soc.* **1970**, *92*, 3794.
- (17) Tézé A.; Hervé G. In *Inorg. Synth.*; Ginsberg, A. P., Ed.; John Wiley and Sons: New York, 1990; Vol. 27, p 85.
- (18) Okun, N. M.; Tarr, J. C.; Hilleshiem, D. A.; Zhang, L.; Hardcastle, K. I.; Hill, C. L. *J. Mol. Catal. A. Chem.* **2006**, *246*, 11.
- (19) Xin, F.; Pope, M. T.; Long, G. J.; Russo, U. *Inorg. Chem.* **1996**, *35*, 1207.
- (20) Nozaki, C.; Kiyoto, I.; Minai, Y.; Misono, M.; Mizuno, N. *Inorg. Chem.* **1999**, *38*, 5724.
- (21) Geletii, Y. V.; Botar, B.; Kögerler, P.; Hillesheim, D. A.; Musaev, D. G.; Hill, C. L. *Angew. Chem. Int. Ed.* **2008**, *47*, 3896.
- (22) Luo, Z.; Kögerler, P.; Cao, R.; Hill, C. L. *Polyhedron* **2009**, *28*, 215.
- (23) Luo, Z.; Kögerler, P.; Cao, R.; Hakim, I.; Hill, C. L. *Dalton Trans.* **2008**, 54.
- (24) Bassil, B. S.; Nellutla, S.; Kortz, U.; Stowe, A. C.; Tol, J. v.; Dalal, N. S.; Keita, B.; Nadjo, L. *Inorg. Chem.* **2005**, *44*, 2659.
- (25) Bassil, B. S.; Kortz, U.; Tigan, A. S.; Clemente-Juan, J. M.; Keita, B.; Oliveira, P. d.; Nadjo, L. *Inorg. Chem.* **2005**, *44*, 9360.

- (26) Okun, N. M.; Anderson, T. M.; Hill, C. L. *J. Am. Chem. Soc.* **2003**, *125*, 3194.
- (27) Randall, W. J.; Droege, M. W.; Mizuno, N.; Nomiya, K.; Weakley, T. J. R.; Finke, R. G. In *Inorg. Synth.*; Cowley, A. H., Ed.; John Wiley & Sons, Inc.: New York, 1997; Vol. 31, p 167.
- (28) *Special Thematic Issue on Polyoxometalates*; Hill, C. L., Ed., 1998; Vol. 98, No. 1.
- (29) Rhule, J. T.; Hill, C. L.; Judd, D. A.; Schinazi, R. F. *Chem. Rev.* **1998**, *98*, 327.
- (30) Dolbecq, A.; Dumas, E.; Mayer, C. R.; Mialane, P. *Chem. Rev.* **2010**, *110*, 6009.
- (31) Liu, T. *J. Am. Chem. Soc.* **2003**, *125*, 312.
- (32) Liu, T.; Diemann, E.; Li, H.; Dress, A. W. M.; Muller, A. *Nature* **2003**, *426*, 59.
- (33) Pradeep, C. P.; Misrahi, M. F.; Li, F.-Y.; Zhang, J.; Xu, L.; Long, D.-L.; Liu, T.; Cronin, L. *Angew. Chem. Int. Ed.* **2009**, *48*, 8309.
- (34) Liu, T.; Langston, M. L. K.; Li, D.; Pigga, J. M.; Pichon, C.; Todea, A. M.; Müller, A. *Science* **2011**, *331*, 1590.
- (35) Li, H.; Sun, H.; Qi, W.; Xu, M.; Wu, L. *Angew. Chem. Int. Ed.* **2007**, *46*, 1300.
- (36) Wang, H.; Yan, Y.; Li, B.; Bi, L.; Wu, L. *Chem. Eur. J.* **2011**, *17*, 4273.
- (37) Gouzerh, P.; Proust, A. *Chem. Rev.* **1998**, *98*, 77.

- (38) Sanchez, C.; Soler-Illia, G. J. d. A. A.; Ribot, F.; Lalot, T.; Mayer, C. R.; Cabuil, V. *Chem. Mater.* **2001**, *13*, 3061.
- (39) Coronado, E.; Giménez-Saiz, C.; Gómez-García, C. J. *Coord. Chem. Rev.* **2005**, *249*, 1776.
- (40) Akutagawa, T.; Endo, D.; Noro, S.-I.; Cronin, L.; Nakamura, T. *Coord. Chem. Rev.* **2007**, *251*, 2547.
- (41) Yu, R.; Kuang, X.-F.; Xiao-YuanWu; Lu, C.-Z.; Donahue, J. P. *Coord. Chem. Rev.* **2009**, *253*, 2872.
- (42) Proust, A.; Thouvenot, R.; Gouzerh, P. *Chem. Commun.* **2008**, 1837.
- (43) Allain, C.; Favette, S.; Chamoreau, L.-M.; Vaissermann, J.; Ruhlmann, L.; Hasenknopf, B. *Eur. J. Inorg. Chem.* **2008**, 3433.
- (44) Hasenknopf, B.; Micoine, K.; Lacôte, E.; Thorimbert, S.; Malacria, M.; Thouvenot, R. *Eur. J. Inorg. Chem.* **2008**, 5001.
- (45) Kortz, U.; Müller, A.; van Slageren, J.; Schnack, J.; Dalal, N. S.; Dressel, M. *Coord. Chem. Rev.* **2009**, *253*, 2315.
- (46) Müller, A.; Serain, C. *Acc. Chem. Res.* **2000**, *33*, 2.
- (47) Han, J. W.; Hill, C. L. *J. Am. Chem. Soc.* **2007**, *129*, 15094.
- (48) Song, Y.-F.; Long, D.-L.; Cronin, L. *Angew. Chem. Int. Ed.* **2007**, *46*, 3900.
- (49) Song, Y.-F.; Long, D.-L.; Kelly, S. E.; Cronin, L. *Inorg. Chem.* **2008**, *47*, 9137.
- (50) Song, Y.-F.; McMillan, N.; Long, D.-L.; Thiel, J.; Ding, Y.; Chen, H.; Gadegaard, N.; Cronin, L. *Chem. Eur. J.* **2008**, *14*, 2349.

- (51) Zhang, J.; Song, Y.-F.; Cronin, L.; Liu, T. *J. Am. Chem. Soc.* **2008**, *130*, 14408.
- (52) Song, Y.-F.; McMillan, N.; Long, D.-L.; Kane, S.; Malm, J.; Riehle, M. O.; Pradeep, C. P.; Gadegaard, N.; Cronin, L. *J. Am. Chem. Soc.* **2009**, *131*, 1340.
- (53) Song, J.; Luo, Z.; Zhu, H.; Huang, Z.; Lian, T.; Kaledin, A. L.; Musaev, D. G.; Lense, S.; Hardcastle, K.; Hill, C. L. *Inorg. Chim. Acta* **2010**, *363*, 4381.
- (54) Song, Y.-F.; Long, D.-L.; Cronin, L. *CrystEngComm* **2010**, *12*, 109.
- (55) Bustos, C.; Hasenknopf, B.; Thouvenot, R.; Vaissermann, J.; Proust, A.; Gouzerh, P. *Eur. J. Inorg. Chem.* **2003**, *2003*, 2757.
- (56) Micoine, K.; Hasenknopf, B.; Thorimbert, S.; Lacôte, E.; Malacria, M. *Org. Lett.* **2007**, *9*, 3981.
- (57) Zeng, H.; Newkome, G. R.; Hill, C. L. *Angew. Chem. Int. Ed.* **2000**, *39*, 1771.
- (58) Pradeep, C. P.; Long, D.-L.; Newton, G. N.; Song, Y.-F.; Cronin, L. *Angew. Chem. Int. Ed.* **2008**, *47*, 4388.
- (59) Villanneau, R.; Delmont, R.; Proust, A.; Gouzerh, P. *Chem. Eur. J.* **2000**, *6*, 1184.
- (60) Aronica, C.; Chastanet, G.; Zueva, E.; Borshch, S. A.; Clemente-Juan, J. M.; Luneau, D. *J. Am. Chem. Soc.* **2008**, *130*, 2365.
- (61) Müller, A.; Meyer, J.; Bögge, H.; Stammler, A.; Botar, A. *Chem. Eur. J.* **1998**, *4*, 1388.
- (62) Li, J.; Huth, I.; Chamoreau, L.-M.; Hasenknopf, B.; Lacôte, E.; Thorimbert, S.; Malacria, M. *Angew. Chem. Int. Ed.* **2009**, *48*, 2035.

- (63) Zheng, S.-T.; Zhang, J.; Li, X.-X.; Fang, W.-H.; Yang, G.-Y. *J. Am. Chem. Soc.* **2010**, *132*, 15102.
- (64) Knoth, W. H. *J. Am. Chem. Soc.* **1979**, *101*, 759.
- (65) Carlisle Chambers, R.; Osburn Atkinson, E. J.; McAdams, D.; Hayden, E. J.; Ankeny Brown, D. J. *Chem. Commun.* **2003**, 2456.
- (66) Agustin, D.; Dallery, J.; Coelho, C.; Proust, A.; Thouvenot, R. *Journal of Organomet. Chem.* **2007**, *692*, 746.
- (67) De bruyn, M.; Neumann, R. *Adv. Synth. & Cat.* **2007**, *349*, 1624.
- (68) Mirkhani, V.; Moghadam, M.; Tangestaninejad, S.; Mohammadpoor-Baltork, I.; Rasouli, N. *Inorg. Chem. Commun.* **2007**, *10*, 1537.
- (69) Mirkhani, V.; Moghadam, M.; Tangestaninejad, S.; Mohammadpoor-Baltork, I.; Shams, E.; Rasouli, N. *Appl. Cata. A: General* **2008**, *334*, 106.
- (70) Mirkhani, V.; Moghadam, M.; Tangestaninejad, S.; Mohammadpoor-Baltork, I.; Rasouli, N. *Cat. Commun.* **2008**, *9*, 219.
- (71) Mayer, C. R.; Roch-Marchal, C.; Lavanant, H.; Thouvenot, R.; Sellier, N.; Blais, J.-C.; S écheresse, F. *Chem. Eur. J.* **2004**, *10*, 5517.
- (72) Cannizzo, C.; Mayer, C. R.; S écheresse, F.; Larpent, C. *Adv. Mater.* **2005**, *17*, 2888.
- (73) Kato, C. N.; Kasahara, Y.; Hayashi, K.; Yamaguchi, A.; Hasegawa, T.; Nomiya, K. *Eur. J. Chem.* **2006**, 4834.
- (74) Hasegawa, T.; Kasahara, Y.; Yoshida, S.; Kurashina, T.; Aoki, S.; Yoza, K.; Nomiya, K. *Inorg. Chem. Commun.* **2007**, *10*, 1416.

- (75) Boujtita, M.; Boixel, J.; Blart, E.; Mayer, C. R.; Odobel, F. *Polyhedron* **2008**, *27*, 688.
- (76) Hasegawa, T.; Murakami, H.; Shimizu, K.; Kasahara, Y.; Yoshida, S.; Kurashina, T.; Seki, H.; Nomiya, K. *Inorg. Chim. Acta* **2008**, *361*, 1385.
- (77) Odobel, F.; S  verac, M.; Pellegrin, Y.; Blart, E.; Fosse, C.; Cannizzo, C.; Mayer, C. R.; Elliott, K. J.; Harriman, A. *Chem. Eur. J.* **2009**, *15*, 3130.
- (78) Mayer, C. R.; Thouvenot, R.; Lalot, T. *Macromolecules* **2000**, *33*, 4433.
- (79) Bonchio, M.; Carraro, M.; Scorrano, G.; Bagno, A. *Adv. Synth. Catal.* **2004**, *346*, 648.
- (80) Chen, H.; Xie, L.; Lu, H.; Yang, Y. *J. Mater. Chem.* **2007**, *17*, 1258.
- (81) Mayer, C. M.; Herson, P.; Thouvenot, R. *Inorg. Chem.* **1999**, *38*, 6152.
- (82) Mayer, C. R.; Cabuil, V.; Lalot, T.; Thouvenot, R. *Angew. Chem. Int. Ed.* **1999**, *38*, 3672.
- (83) Mayer, C. R.; Cabuil, V.; Lalot, T.; Thouvenot, R. *Adv. Mater.* **2000**, *12*, 417.
- (84) Schroden, R. C.; Blanford, C. F.; Melde, B. J.; Johnson, B. J. S.; Stein, A. *Chem. Mater.* **2001**, *13*, 1074.
- (85) Mazeaud, A.; Dromzee, Y.; Thouvenot, R. *Inorg. Chem.* **2000**, *39*, 4735.
- (86) Agustin, D.; Coelho, C.; Mazeaud, A.; Herson, P.; Proust, A.; Thouvenot, R. *Z. Anorg. Allg. Chem.* **2004**, *630*, 2049.
- (87) Niu, J.; Zhao, J.; Wang, J.; Li, M. *J. Mole. Struct.* **2003**, *655*, 243.
- (88) Bannani, F.; Thouvenot, R.; Debbabi, M. *Eur. J. Inorg. Chem.* **2007**, *2007*, 4357.

- (89) Bareyt, S.; Piligkos, S.; Hasenknopf, B.; Gouzerh, P.; Lacôte, E.; Thorimbert, S.; Malacria, M. *J. Am. Chem. Soc.* **2005**, *127*, 6788.
- (90) Yang, Q.; Dai, H.; Liu, J. *Trans. Metal Chem.* **1997**, *23*, 93.
- (91) Wang, X.-H.; Dai, H.-C.; Liu, J.-F. *Trans. Metal Chem.* **1999**, *24*, 600.
- (92) Hussain, F.; Kortz, U.; Keita, B.; Nadjo, L.; Pope, M. T. *Inorg. Chem.* **2005**, *45*, 761.
- (93) Hussain, F.; Dickman, M.; Kortz, U.; Keita, B.; Nadjo, L.; Khitrov, G.; Marshall, A. *J. Cluster Sci.* **2007**, *18*, 173.
- (94) Reinoso, S.; Dickman, M. H.; Matei, M. F.; Kortz, U. *Inorg. Chem.* **2007**, *46*, 4383.
- (95) Reinoso, S.; Dickman, M. H.; Praetorius, A.; Piedra-Garza, L. F.; Kortz, U. *Inorg. Chem.* **2008**, *47*, 8798.
- (96) Reinoso, S.; Dickman, M. H.; Kortz, U. *Eur. J. Inorg. Chem.* **2009**, *2009*, 947.
- (97) Piedra-Garza, L. F.; Dickman, M. H.; Moldovan, O.; Breunig, H. J.; Kortz, U. *Inorg. Chem.* **2009**, *48*, 411.
- (98) Moore, A. R.; Kwen, H.; Beatty, A. M.; Maatta, E. A. *Chem. Commun.* **2000**, 1793.
- (99) Hsieh, T. C.; Zubieta, J. A. *Polyhedron* **1986**, *5*, 305.
- (100) Hsieh, T. C.; Zubieta, J. *Inorg. Chem.* **1985**, *24*, 1287.
- (101) Kwen, H.; Young, J. V. G.; Maatta, E. A. *Angew. Chem. Int. Ed.* **1999**, *38*, 1145.

- (102) Carey, D. M.-L.; Muñoz-Castro, A.; Bustos, C. J.; Manríquez, J. M.; Arratia-Pérez, R. *J. Phys. Chem. A* **2007**, *111*, 6563.
- (103) Janjua, M. R. S. A.; Guan, W.; Liu, C. G.; Muhammad, S.; Yan, L.; Su, Z. *Eur. J. Inorg. Chem.* **2009**, *2009*, 5181.
- (104) Du, Y. H.; Rheingold, A. L.; Maatta, E. A. *J. Am. Chem. Soc.* **1992**, *114*, 345.
- (105) Strong, J. B.; Yap, G. P. A.; Ostrander, R.; Liable-Sands, L. M.; Rheingold, A. L.; Thouvenot, R.; Gouzerh, P.; Maatta, E. A. *J. Am. Chem. Soc.* **2000**, *122*, 639.
- (106) Kwen, H.; Beatty, A. M.; Maatta, E. A. *Compt. Rend. Chim.* *8*, 1025.
- (107) Wei, Y.; Xu, B.; Barnes, C. L.; Peng, Z. *J. Am. Chem. Soc.* **2001**, *123*, 4083.
- (108) Xu, B.; Peng, Z.; Wei, Y.; Powell, D. R. *Chem. Commun.* **2003**, 2562.
- (109) Xu, L.; Lu, M.; Xu, B.; Wei, Y.; Peng, Z.; Powell, D. R. *Angew. Chem. Int. Ed.* **2002**, *41*, 4129.
- (110) Lu, M.; Wei, Y.; Xu, B.; Cheung, C. F.-C.; Peng, Z.; Powell, D. R. *Angew. Chem. Int. Ed.* **2002**, *41*, 1566.
- (111) Peng, Z. *Angew. Chem. Int. Ed.* **2004**, *43*, 930.
- (112) Li, Q.; Wu, P.; Wei, Y.; Wang, Y.; Wang, P.; Guo, H. *Inorg. Chem. Commun.* **2004**, *7*, 524.
- (113) Roesner, R. A.; McGrath, S. C.; Brockman, J. T.; Moll, J. D.; West, D. X.; Swearingen, J. K.; Castineiras, A. *Inorg. Chim. Acta* **2003**, *342*, 37.

- (114) Kang, J.; Nelson, J. A.; Lu, M.; Xie, B.; Peng, Z.; Powell, D. R. *Inorg. Chem.* **2004**, *43*, 6408.
- (115) Xia, Y.; Wei, Y.; Wang, Y.; Guo, H. *Inorg. Chem.* **2005**, *44*, 9823.
- (116) Kwak, W.; Pope, M. T.; Scully, T. F. *J. Am. Chem. Soc.* **1975**, *97*, 5735.
- (117) Kortz, U.; Pope, M. T. *Inorg. Chem.* **1995**, *34*, 2160.
- (118) Dolbecq, A.; Lisnard, L.; Mialane, P.; Marrot, J.; B énard, M.; Rohmer, M.-M.; S écheresse, F. *Inorg. Chem.* **2006**, *45*, 5898.
- (119) Dolbecq, A.; Compain, J.-D.; Mialane, P.; Marrot, J.; S écheresse, F.; Keita, B.; Holzle, L. R. B.; Miserque, F.; Nadjo, L. *Chem. Eur. J.* **2009**, *15*, 733.
- (120) Keita, B.; Zhang, G.; Dolbecq, A.; Mialane, P.; S écheresse, F.; Miserque, F.; Nadjo, L. *J. Phys. Chem. C* **2007**, *111*, 8145.
- (121) Zhang, G.; Keita, B.; Dolbecq, A.; Mialane, P.; S écheresse, F.; Miserque, F.; Nadjo, L. *Chem. Mater.* **2007**, *19*, 5821.
- (122) Dumas, E.; Sassoie, C.; Smith, K. D.; Sevov, S. C. *Inorg. Chem.* **2002**, *41*, 4029.
- (123) Calin, N.; Sevov, S. C. *Inorg. Chem.* **2003**, *42*, 7304.
- (124) Burkholder, E.; Golub, V.; O'Connor, C. J.; Zubieta, J. *Chem. Commun.* **2003**, 2128.
- (125) Finn, R. C.; Burkholder, E.; Zubieta, J. *Chem. Commun.* **2001**, 1852.
- (126) Peloux, C. d.; Dolbecq, A.; Mialane, P.; Marrot, J.; Secheresse, F. *Dalton Trans.* **2004**, 1259.
- (127) Kortz, U.; Marquer, C.; Thouvenot, R.; Nierlich, M. *Inorg. Chem.* **2003**, *42*, 1158.

- (128) Mayer, C. R.; Marrot, J.; S écheresse, F. *J. Mole. Struct.* **2004**, *704*, 59.
- (129) Carraro, M.; Sartorel, A.; Scorrano, G.; Maccato, C.; Dickman, M. H.; Kortz, U.; Bonchio, M. *Angew. Chem. Int. Ed.* **2008**, *47*, 7275.
- (130) Kim, G. S.; Hagen, K. S.; Hill, C. L. *Inorg. Chem.* **1992**, *31*, 5316.
- (131) Sun, Z.-G.; You, W.-S.; Li, J.; Liu, J.-F. *Inorg. Chem. Commun.* **2003**, *6*, 238.
- (132) Carraro, M.; Modugno, G.; Sartorel, A.; Scorrano, G.; Bonchio, M. *Eur. J. Inorg. Chem.* **2009**, 5164.
- (133) Mayer, C. R.; Thouvenot, R. *J. Chem. Soc. Dalton Trans.* **1998**, 7.
- (134) Zhen-Gang, S.; Zai-Ming, Z.; Wan-Sheng, Y.; Xue-Fang, Z.; Yuan-Peng, G. *Chinese J. Chem.* **2005**, *23*, 530.
- (135) Br égeault, J.-M. *Dalton Trans.* **2003**, *17*, 3289.
- (136) Kozhevnikov, I. V. *Chem. Rev.* **1998**, *98*, 171.
- (137) Faraj, M.; Hill, C. L. *J. Chem. Soc., Chem. Commun.* **1987**, 1487.
- (138) Lyons, J. E.; Ellis, P. E., Jr.; Durante, V. A. In *Studies in Surface Science and Catalysis*; Grasselli, R. A., Sleight, A. W., Eds.; Elsevier Scientific: Amsterdam, 1991; Vol. 67, p 99.
- (139) Kamata, K.; Yonehara, K.; Nakagawa, Y.; Uehara, K.; Mizuno, N. *Nature Chem.* **2010**, *2*, 478.
- (140) Dwight, T. A.; Rue, N. R.; Charyk, D.; Josselyn, R.; DeBoef, B. *Org. Lett.* **2007**, *9*, 3137.
- (141) Stowers, K. J.; Fortner, K. C.; Sanford, M. S. *J. Am. Chem. Soc.* **2011**, *133*, 6541.

- (142) Neumann, R.; Abu-Gnim, C. J. *J. Am. Chem. Soc.* **1990**, *112*, 6025.
- (143) Rong, C.; Pope, M. T. *J. Am. Chem. Soc.* **1992**, *114*, 2932.
- (144) Khenkin, A. M.; Hill, C. L. *Mendeleev Commun.* **1993**, *3*, 140.
- (145) Okun, N. M.; Anderson, T. M.; Hardcastle, K. I.; Hill, C. L. *Inorg. Chem.* **2003**, *42*, 6610.
- (146) Rossi, L. I.; Martín, S. E. *Appl. Catal. A* **2003**, *250*, 271.
- (147) Geletii, Y. V.; Yin, Q.; Hou, Y.; Huang, Z.; Ma, H.; Song, J.; Besson, C.; Luo, Z.; Cao, R.; O'Halloran, K. P.; Zhu, G.; Zhao, C.; Vickers, J.; Ding, Y.; Mohebbi, S.; Kuznetsov, A. E.; Musaev, D. G.; Lian, T.; Hill, C. L. *Isr. J. Chem.* **2011**, *51*, 238.
- (148) Howells, A. R.; Sankarraj, A.; Shannon, C. *J. Am. Chem. Soc.* **2004**, *126*, 12258.
- (149) Geletii, Y. V.; Huang, Z.; Hou, Y.; Musaev, D. G.; Lian, T.; Hill, C. L. *J. Am. Chem. Soc.* **2009**, *131*, 7522.
- (150) Yin, Q.; Tan, J. M.; Besson, C.; Geletii, Y. V.; Musaev, D. G.; Kuznetsov, A. E.; Luo, Z.; Hardcastle, K. I.; Hill, C. L. *Science* **2010**, *328*, 342.
- (151) Huang, Z.; Luo, Z.; Geletii, Y. V.; Vickers, J.; Yin, Q.; Wu, D.; Hou, Y.; Ding, Y.; Song, J.; Musaev, D. G.; Hill, C. L.; Lian, T. *J. Am. Chem. Soc.* **2011**, *133*, 2068.

— CHAPTER —

2

**Covalently-linked Organic-POM Hybrids: Synthesis,
Characterization, and Catalytic Removal of Toxic
Chemicals**

Abstract

Polyoxometalates (POMs) are a large class of early transition metal oxide clusters with a range of potential applications in sensing, medicine, and catalysis. Covalently linking organic molecules with POMs would not only enrich the hybrid species that could be further employed as new building blocks for supramolecular assembly but also help extend their applications to biological systems and in organic media. The typically-employed “one-pot” hydrothermal/solvothermal technique of synthesis of covalently-tethered organic-POMs *via* the esterification reaction is demonstrated here by synthesis of one hybrid POM-based dendrimer, $(\text{TBA})_2[\text{V}_6\text{O}_{13}\{(\text{OCH}_2)_3\text{C}(\text{CH}_2)\text{O}(\text{CH}_2)\text{C}(\text{CH}_2\text{OH})_3\}_2]$ (**1**). The catalytic activity of **1** was also tested in the removal of toxic industrial chemicals (TICs), such as thiols, aldehydes, and hydrogen sulfide. However, the yield *via* solvothermal synthesis is generally low. More importantly, the reactivity of POMs with organic molecules is still challenging to investigate due to their completely different physical properties such as size, structure, and charge density, which render systematic investigation of the reactivity of all POMs difficult. We report an efficient method to synthetically modify the amine-containing side-chains of POM esters, including the Linqvist-type $[\text{V}_6\text{O}_{13}\{(\text{OCH}_2)_3\text{CNH}_2\}_2]^{2-}$ (**2**) triesters and Anderson-type $[\text{MnMo}_6\text{O}_{18}\{(\text{OCH}_2)_3\text{CNH}_2\}_2]^{3-}$ (**3**). This chemistry could be used to generate myriad organic-POM hybrids which in turn undergo supramolecular assembly and find potential application in functional materials. In this work, we screened several methods and demonstrate that a range of organic anhydrides can selectively react with the amine groups on triesters instead of the negatively-charged POM oxygen atoms which are minimally nucleophilic. The reactions are usually carried out in nonprotic polar solvents

at room temperature and completed in several hours with nearly quantitative yields.

Introduction

Polyoxometalates (POMs)¹⁻⁷ are a class of metal oxide clusters with many replaceable components, modifiable structures, and adjustable geometries, which consequently have an ensemble of fascinating properties at the molecular level and applications in the catalysis of organic transformations, especially C-H bond activation⁸ and decontamination of toxic chemicals.⁹⁻¹³ This versatility (tunability) of POMs has also led to materials applications in magnetism and other areas.¹⁴ Most recently, tetraruthenium-containing and tetracobalt-containing POMs were reported to be the first oxidative, hydrolytically and thermally stable, molecular water oxidation catalysts. They are also the fastest reported to date..¹⁵⁻²¹

Considering these proven and constantly emerging properties, POMs themselves are promising building blocks for functional molecular devices and nano-materials accessible through supramolecular assembly.^{7,22-40} However, POM surface negative charge densities, geometries, and coordination modes, generally prevent the direct application of these complexes as building block rules following the molecular packing hierarchy principle already established in coordination chemistry. This in turn thus makes formulation of strategies to construct larger functional architectures based on POMs quite challenging.⁴¹

One way to confront this synthetic difficulty and thus extend the scope of POM applications is to functionalize POMs with organic molecules to produce hybrid

compounds, in which the organic parts can act as structure-directing moieties that function to guide self assembly into larger (nanoscale) aggregates. In addition, the resulting hybrid materials can not only combine the properties of both inorganic and organic moieties, but also provide a platform and scaffold for further synthetic and functional elaboration. One example is the synthesis of 3D metal-organic frameworks (MOFs) assembled from the vanadium-containing POM building blocks, which retain the ability of the POMs to catalyze aerobic organic oxidations.⁴²

Usually, the favored synthetic approach to organic-POM derivatives is the hydrothermal (or solvothermal) method, by which some new products. This frequently produces unanticipated structures, often in high yield. In this chapter, we first demonstrate application of the hydrothermal method to the synthesis of a new generation-zero dendrimer, $(\text{TBA})_2[\text{V}_6\text{O}_{13}\{(\text{OCH}_2)_3\text{C}(\text{CH}_2)\text{O}(\text{CH}_2)\text{C}(\text{CH}_2\text{OH})_3\}_2]$ (**1**), which has six covalently-linked hydroxy groups as termini emanating from a hexavanadate core. These hydroxy group can be further functionalized by esterification reactions. In addition, we show the effectiveness of **1** in catalyzing the degradation of toxic industrial chemicals (TICs), such as 1-propanethiol, acetaldehyde, and hydrogen sulfide. However, extremely low yields and occasionally sensitive reaction conditions complicate this technique. The final product's structure depends greatly on many subtle reaction parameters including but not limited to temperature, reaction time, solvent used etc. More importantly, most organic compounds, especially these with fragile functional groups cannot survive the harsh reaction conditions (high temperature and pressure) of hydrothermal or solvothermal synthetic conditions. Such conditions can make incorporation of fragile organic molecules, like some chiral groups, challenging. Thus, the solvothermal

approach is frequently only applicable to few specific reactions and cannot be employed as a general method for organic-POM hybrid synthesis.

A controllable, more general effective and efficient route to rationally functionalize POMs has been pursued with great effort but such chemistry was almost nonexistent at the outset of my work in this area. Based on the some previous pioneering work, particularly that of Zubieta group, reacting triols, and in particular tris(hydroxymethyl)aminomethane (Tris) derivatives, with POMs, it was evident that there was considerable promise for such chemistry to be extended and generalized. Functionalization of the product POM triesters could then lead, with some control, to structure-controlled nanoscale functional materials.⁴³⁻⁴⁵ However, the yields of functionalized POM triesters are usually low due to the involvement of negatively-charged POM moiety, which impedes the continuing effort to study them. Following the hydrothermal synthesis of hybrid **1**, we report here an efficient method to functionalize two types of POM triesters, those of the Linqvist-type $[V_6O_{13}\{(OCH_2)_3CNH_2\}_2]^{2-}$ (**2**) and Anderson-type $[MnMo_6O_{18}\{(OCH_2)_3CNH_2\}_2]^{3-}$ (**3**). All the compounds have been fully characterized by 1H and ^{13}C NMR, FT-IR, and elemental analysis. One of the hybrid molecules was also characterized by single crystal X-ray diffraction and its self-assembly process in solid state is dictated based on the supramolecular interactions.

Experimental Section

General: All reagents including deuterated solvent were obtained from commercial chemical vendors and used without further purification. All reactions were carried out under a dry argon atmosphere with anhydrous solvents under anhydrous conditions and magnetically stirred with Teflon stir bars, and temperatures were measured externally. Reactions requiring anhydrous conditions were carried out in oven-dried (120 °C, 24 h) glassware. All reactions were monitored by proton nuclear magnetic resonance (^1H NMR) spectroscopy. Yields refer to spectroscopically (^1H NMR spectroscopy) homogeneous materials. ^1H and ^{13}C NMR spectra were recorded on a Varian INOVA 400 MHz instrument and chemical shifts (δ) were measured in parts per million (ppm) relative to the deuterated solvent used in the experiment. ^{51}V NMR spectra were recorded on a Varian Unity 600 MHz instrument and referenced externally by the sample replacement method to a 10 mM solution of $\text{H}_4\text{PVMo}_{11}\text{O}_{40}$ in 0.60 M NaCl solution (-533.6 ppm relative to neat VOCl_3) and chemical shifts were reported relative to VOCl_3 . Multiplicities were designated as singlet (s), doublet (d), triplet (t), quartet (quar), quintet (qi), sextet (sext), or multiplet (m). Broad or obscured peaks were indicated as “br” or “obs” respectively. Infrared spectra (IR) were recorded as KBr pellets on a Nicolet 510 FT-IR spectrophotometer and peak strengths were designated as strong (s), mild (m), or weak (w). Elemental analyses for C, H and, N were performed by Atlantic Microlab, Norcross, GA and elemental analyses for all other elements were performed either by Desert Analytics, Tucson, AZ or by Kanti Lab Ltd, Mississauga, Ontario. Mass spectra were recorded on a JEOL JMS-SX102/SX102A/E mass spectrometer (ESI). X-ray

crystallography studies were carried out in the X-ray Crystallography Laboratory at Emory University on a Bruker Smart 1000 CCD diffract meter.

Synthesis of $(\text{TBA})_2[\text{V}_6\text{O}_{13}\{(\text{OCH}_2)_3\text{C}(\text{CH}_2)\text{O}(\text{CH}_2)\text{C}(\text{CH}_2\text{OH})_3\}_2]$ (1).

Dipentaerythritol (0.2261 g, 0.8890 mmol) and $[(n\text{-C}_4\text{H}_9)_4\text{N}]_3[\text{H}_3\text{V}_{10}\text{O}_{28}]$ (0.5g, 0.296 mmol) were dissolved in 3.0 mL of dimethyl formamide (DMF). The orange solution was stirred at 80 °C for 18 h under an Ar atmosphere. The red-brown solution was cooled to room temperature and then added to diethyl ether (30 mL). The resulting sticky precipitate was obtained by decanting the solvent. The crude product was redissolved in acetonitrile/DMF (40 mL, v/v = 1/1) and then diethyl ether (150 mL) was added to re-precipitate the product. The material was filtered and washed with acetone-diethyl ether (2 × 10 mL, v/v = 1/2) and purified by crystallization from acetonitrile/DMF (20/15 mL) by diffusion of diethyl ether. Yield: 2.1 g, 81.5 % yield based on vanadium. X-ray quality single crystals were grown in very dilute solvents by the liquid-liquid diffusion method. ^1H NMR (400 MHz, DMSO- d_6 , 25 °C): 0.92 (t, 24H), 1.30 (sextet, 16H), 1.55 (quintet, 16H), 3.15 (t, 16H), 4.89 (s, 12H), 4.21 (t, 6H). ^{51}V NMR (600 MHz, DMSO- d_6 , 25 °C): -508.1. FT-IR (KBr): 3530 (s, br), 2978 (s), 2923 (m), 2890 (m), 1612 (w), 1476 (m), 1422 (w), 1389 (m), 1239 (m), 1180 (w), 1078 (s), 957 (s), 811 (s), 790 (s), 719 (s), 582(m), 421 (m) cm^{-1} . Elemental Analysis for $\text{C}_{52}\text{H}_{110}\text{N}_2\text{O}_{27}\text{V}_6$: Calc. H, 7.39; C, 41.61; N, 1.89; V, 20.3. Found: H, 7.45; C, 41.42; N, 2.04; V, 19.5.

Catalytic study of oxidation of 1-propanethiol by 1. In a typical experiment, 60.0 μL (6.62×10^{-4} mol) of propanethiol (PrSH), 18.0 μL (6.2×10^{-5} mol) of decane (internal standard) and 40 mg of **1** were stirred in 2.9 mL of chlorobenzene in a schlenk tube fitted

with PTFE septum stopper under dioxygen at 45 °C for 5 days. Aliquots were withdrawn from the schlenk tube at approximately 10 h intervals, and the products were quantified by gas chromatography. In order to prevent the PrSH from leaking, the reaction solution was placed in an ice-water bath for 20 minutes. After opening the schlenk tube, 0.2 μL of cooled reaction solution was withdrawn as quickly as possible and the atmosphere in the tube filled with dioxygen gas carefully.

Catalytic study of oxidation of acetaldehyde by 1. In a typical reaction, the catalyst **1** (0.05 mmol, 75.0 mg) was weighed and added to a clean, dry pressure tube and the complete experimental assembly was flushed with air and weighed. The reaction was initiated by addition of acetaldehyde (17.82 mmol, 785 mg, 1.0 mL) in deuterated water (6.0 mL) containing DMSO as internal standard (1.48 mmol, 116 mg, 0.11 mL). The reaction vessel was then sealed quickly and the reaction solution was stirred at room temperature. The reaction was monitored by ¹H NMR (400 MHz, D₂O, 25 °C) for kinetics studies.

Catalytic formaldehyde oxidation. The procedure and operation are the same as in acetaldehyde reaction but the ratios of reactants were different. Typically, the catalyst (0.05 mmol, 75.0 mg) was added to a freshly prepared stock solution containing CH₃CN (20.5 mg, internal standard), Formaline (37%, 81.15 mg), and deuterated water (0.6 mL), and the reaction was monitored by ¹H NMR (400 MHz, D₂O, 25 °C) for kinetics studies.

Catalytic H₂S oxidation. In a typical reaction, the catalyst **1** (0.05 mmol, 75.0 mg) was weighed and added to a clean, dry pressure tube and the complete experimental assembly was flushed with oxygen or air and weighed. The reaction was initiated by

addition of saturated H₂S aqueous solution (0.1 mol/l, pH=4.8, 20 mL). The reaction vessel was then sealed quickly and the reaction solution was stirred at room temperature. After several hours, the clear colorless solution became cloudy and the yellow elemental sulfur precipitated on the wall of reaction vial. After 24 hours, the solid reaction mixture was weighed after separated by centrifugation and dried in vacuum for another 24 hours. The yields of solid sulfur are 24.0 (TON=14.1) mg for oxygen-based catalysis and 25.5 mg (TON=15.0) for air-based catalysis, respectively.

Synthesis of Triesters (2, NH₂V₆ and 3, NH₂Mo₆)

Linqvist-type triester [(*n*-C₄H₉)₄N]₂[V₆O₁₃{(OCH₂)₃CNH₂}₂] (2, NH₂V₆). The solid mixture of tris(hydroxymethyl)aminomethane (1.39 g, 11.1 mmol) and [(*n*-C₄H₉)₄N]₃[H₃V₁₀O₂₈] (6.24 g, 3.70 mmol) were dissolved in 75 mL of dry dimethylacetamide (DMA). The orange solution was stirred at 90 °C for overnight (20 h). The resulting dark reddish brown solution was cooled to room temperature and added to 200 mL of diethyl ether to induce precipitation. To the gray precipitate, 40 mL of CH₃CN was added, and a small amount of insoluble solid was filtered off. To the filtrate, 20 mL of 6 N HCl was added over 1-2 min. While 6 N HCl was added to the filtrate, the color of solution was changed from the initial dark reddish brown to green and finally to deep red, and a red precipitate was formed. The solution was stirred for 1 hour at room temperature. At the end of the stirring, the color of solution turned to green. The precipitate was filtered and washed with water, CH₃CN, and diethyl ether. The red solid was suspended in 20 mL of CH₃CN/DMF (1/1). To the suspension, 6 mL of 1.0 M tetrabutylammonium hydroxide (TBAOH) in water was added dropwise. The red solid

was completely dissolved when about 3.0 mL of 1.0 M TBAOH in water was added. The resulting solution was added to 200 mL of diethyl ether to be precipitated. The sticky precipitate was redissolved in ca. 30 mL mixed solvent (CH₃CN/DMF = 2:1), and diffusion of ether into the solution over one week resulted in the formation of needle-like crystals that was used for the following amide reactions. Yield: 5.9% (based on vanadium). ¹H NMR (400 MHz, DMSO-*d*₆, 25 °C) 4.66 (s, 12H; -C(CH₂O)₃-), 3.19 (t, 16H; (CH₃CH₂CH₂CH₂)₄N⁺), 1.56 (quin, 16H; (CH₃CH₂CH₂CH₂)₄N⁺), 1.47 (s, 4H; -NH₂), 1.34-1.29 (sext, 16H; (CH₃CH₂CH₂CH₂)₄N⁺) 0.94-0.91 ppm (t, 24H; (CH₃CH₂CH₂CH₂)₄N⁺); ¹³C NMR (100 MHz, [D₆] DMSO, 25 °C): δ=86.3(-C(CH₂O)₃-), 57.5 ((CH₃CH₂CH₂CH₂)₄N⁺), 48.5 (-C(CH₂O)₃-), 23.1 ((CH₃CH₂CH₂CH₂)₄N⁺), 19.2 ((CH₃CH₂CH₂CH₂)₄N⁺), 13.5 ((CH₃CH₂CH₂CH₂)₄N⁺) ppm ; ⁵¹V NMR (600 MHz, DMSO-*d*₆, 25 °C): δ= 494.8 ppm; FT-IR (KBr): $\tilde{\nu}$ =: 3364 (br), 2961 (m), 2784 (m), 2845 (m, sh), 1482 (m), 1379 (w), 1061 (s), 950 (s), 821 (m), 796 (s), 720 (s), 577 (m), 515 (w), 470 (w), 418 (s) cm⁻¹; elemental analysis calcd (%) for C₄₀H₈₈N₄O₁₉V₆: C, 38.91; H, 7.18; N, 4.54; V, 24.75; found: C 38.78; H 7.24, N 4.49, V 24.65.

Anderson-type Triester [(*n*-C₄H₉)₄N]₃[MnMo₆O₁₈{(OCH₂)₃CNH₂}₂] (3, NH₂Mo₆). The preparation followed the literature method with modification. A solid mixture of tris(hydroxymethyl)aminomethane (1.55 g, 12.8 mmol), Mn(CH₃COO)₃ · 2H₂O (1.50 g, 5.6 mmol) and [(*n*-C₄H₉)₄N]₄[α-Mo₈O₂₆] (8.00 g, 3.70 mmol) were dissolved in dry dimethylformamide (75 ml) and heated at 90 °C under argon in dark for 24 h. The resulting orange solution was cooled to room temperature and a small amount of black solid was filtered via fine fritter. The solution was precipitated with excess ether and the

collected solid was crystallized at least two times by using diffusion of ether into the acetonitrile solution. Yield: 60% (based on molybdenum). ^1H NMR (400 MHz, $[\text{D}_6]$ DMSO, 25 °C) 61.1 (s, 12H; $-\text{C}(\text{CH}_2\text{O})_3-$), 3.14 (m, 24H; $(\text{CH}_3\text{CH}_2\text{CH}_2\text{CH}_2)_4\text{N}^+$), 1.55 (m, 24H; $(\text{CH}_3\text{CH}_2\text{CH}_2\text{CH}_2)_4\text{N}^+$), 1.31 (m, 24H; $(\text{CH}_3\text{CH}_2\text{CH}_2\text{CH}_2)_4\text{N}^+$) 0.94-0.91 ppm (t, 36H; $(\text{CH}_3\text{CH}_2\text{CH}_2\text{CH}_2)_4\text{N}^+$) and solvent (acetonitrile) peaks; ^{13}C NMR (100 MHz, $[\text{D}_6]$ DMSO, 25 °C): $\delta=57.5$ ($(\text{CH}_3\text{CH}_2\text{CH}_2\text{CH}_2)_4\text{N}^+$), 23.1 ($(\text{CH}_3\text{CH}_2\text{CH}_2\text{CH}_2)_4\text{N}^+$), 19.3 ($(\text{CH}_3\text{CH}_2\text{CH}_2\text{CH}_2)_4\text{N}^+$), 13.6 ($(\text{CH}_3\text{CH}_2\text{CH}_2\text{CH}_2)_4\text{N}^+$) ppm; FT-IR (KBr): $\tilde{\nu} = 3366$ (br), 3285 (w), 3199 (w), 2959(m), 2922(s), 2872(m), 2852(m), 1656(m), 1633(w), 1483 (m), 1378(w), 1343(w), 1270(w) , 1129(w), 1104(w), 1040(s), 938(s), 918(s), 900(s), 796(w), 663(s), 563(m), 511(w), 458(m), 413(m) cm^{-1} ; elemental analysis calcd (%) for $\text{C}_{56}\text{H}_{124}\text{MnMo}_6\text{N}_5\text{O}_{24} \cdot \text{CH}_3\text{CN}$: C, 36.22; H, 6.66; Mn, 2.86; Mo, 29.93; N, 4.37; found: C 36.11, H 6.75 Mn, 2.78; Mo, 29.65; N, 4.29.

General procedure for the Functionalization of Triesters (2 and 3) with Anhydrides The anhydride (0.22 mmol) and the Triester (0.1 mmol) were dissolved in anhydrous DMF (3.0 mL) and anhydrous triethylamine (0.22mmol) was injected into the reaction solution. A little heating was necessary to dissolve some anhydrides at the beginning of the reaction. The resulting orange-red hexavanadate derivatives or orange-yellow hexamolybdate solution was usually stirred continuously for 6-12 hr at ambient temperature; the bulky substrates frequently require a longer time or higher temperature for reaction completion. The reaction solution was then added dropwise to anhydrous diethyl ether (50 mL) to get yellow precipitate. This precipitate was then re-dissolved with anhydrous DMF and re-precipitated with anhydrous diethyl ether twice to remove the slight excess of anhydride. After drying the precipitate under vacuum for 2 hours, it

was re-dissolved in DMF-acetonitrile (10 mL, v/v= 2:1) and then ether was allowed to slowly diffuse into the solution to induce crystallization. Orange-red (for **2**, NH_2V_6) or orange-yellow (for **3**, NH_2Mo_6) crystals formed after one week and were characterized after drying under vacuum overnight. The reaction time was monitored by ^1H NMR spectra and the yields are referred to spectroscopically homogeneous materials.

Data for 2-a (Benzoic Anhydride): ^1H NMR (400 MHz, $[\text{D}_6]$ DMSO, 25 °C) $\delta=7.97$ (br, 2H; $-\text{C}(\text{O})\text{NH}-$), 7.52-7.36 (m, 6H; ArH), 5.23 (s, 12H; $-\text{C}(\text{CH}_2\text{O})_3-$), 3.17 (t, 16H, $(\text{CH}_3\text{CH}_2\text{CH}_2\text{CH}_2)_4\text{N}^+$), 1.56 (quin, 16H; $(\text{CH}_3\text{CH}_2\text{CH}_2\text{CH}_2)_4\text{N}^+$), 1.33-1.27 (sext, 16H; $(\text{CH}_3\text{CH}_2\text{CH}_2\text{CH}_2)_4\text{N}^+$), 0.95-0.91 ppm (t, 24H; $(\text{CH}_3\text{CH}_2\text{CH}_2\text{CH}_2)_4\text{N}^+$) and solvent (DMF) peaks; ^{13}C NMR (100 MHz, $[\text{D}_6]$ DMSO, 25°C) $\delta=169.1, 168.4, 143.4, 136.7, 133.5, 131.2, 130.6, 125.9, 89.0, 74.3, 57.5, 23.0, 19.2, 13.5$ ppm; FT-IR (KBr): $\tilde{\nu}=3418(\text{br}), 3023(\text{w}), 2960(\text{s}), 2927(\text{s}), 2872(\text{s}), 1716(\text{m}), 1659(\text{s}), 1543(\text{m}), 1480(\text{m}), 1380(\text{m}), 1322(\text{m}), 1282(\text{m}), 1107(\text{m}), 1081(\text{m}), 1051(\text{s}), 955(\text{s}), 875(\text{w}), 810(\text{s}), 720(\text{s}), 582(\text{m}), 512(\text{w}), 471(\text{w}), 419(\text{s})\text{cm}^{-1}$; elemental analysis calcd (%) for $\text{C}_{56}\text{H}_{96}\text{N}_4\text{O}_{25}\text{V}_6 \cdot \text{DMF}$: C 44.18, H 6.47, N 4.37; found: C 43.99, H 6.50, N 4.35.

Data for 2-b (Diphenic Anhydride): ^1H NMR (400 MHz, $[\text{D}_6]$ DMSO, 25 °C) $\delta=7.63$ (br, 2H; $-\text{C}(\text{O})\text{NH}-$), 7.46-7.43 (m, 4H; ArH), 7.38-7.34 (m, 6H; ArH), 7.08-7.03 (m, 6H; ArH), 4.70 (s, 12H; $-\text{C}(\text{CH}_2\text{O})_3-$), 3.14 (t, 16H, $(\text{CH}_3\text{CH}_2\text{CH}_2\text{CH}_2)_4\text{N}^+$), 1.54 (quin, 16H; $(\text{CH}_3\text{CH}_2\text{CH}_2\text{CH}_2)_4\text{N}^+$), 1.32-1.23 (sext, 16H; $(\text{CH}_3\text{CH}_2\text{CH}_2\text{CH}_2)_4\text{N}^+$), 0.92-0.88 ppm (t, 24H; $(\text{CH}_3\text{CH}_2\text{CH}_2\text{CH}_2)_4\text{N}^+$) and solvent (DMF) peaks; ^{13}C NMR (100 MHz, $[\text{D}_6]$ DMSO, 25°C) $\delta = 164.0, 162.0, 135.7, 135.2, 133.4, 132.9, 132.6, 131.8, 129.5, 128.9, 128.3, 127.0, 123.1, 120.1, 85.5, 76.4, 57.5, 23.0, 19.2, 13.5$ ppm; FT-IR (KBr): $\tilde{\nu}$

= 3400(br), 3263(br), 3059(w), 2960(s), 2925(s), 2854(s), 2100-1900(w), 1717(m), 1667(s), 1554(m), 1479(m), 1382(m), 1325(m), 1291(w), 1103(s), 1055(s), 954(s), 878(w), 809(s), 762(m), 719(s), 637(w), 581(m), 511(w), 463(w), 419(s)cm⁻¹; elemental analysis calcd (%) for C₆₈H₁₀₄N₄O₂₅V₆ · DMF: C 48.55, H 6.37, N 3.99; found: C 48.38, H 6.34, N 3.98.

Data for 2-c (Glutaric Anhydride): ¹H NMR (400 MHz, [D₆] DMSO, 25 °C) δ=7.40 (s, 2H; -C(O)NH-), 5.08 (s, 12H; -C(CH₂O)₃-), 3.17 (t, 16H; (CH₃CH₂CH₂CH₂)₄N⁺), 2.16 (t, 4H; -CH₂-C(O)NH-), 2.09 (t, 4H; -CH₂-C(O)OH), 1.64 (quin, 4H; -CH₂CH₂CH₂-) 1.57 (quin, 16H; (CH₃CH₂CH₂CH₂)₄N⁺), 1.34-1.28 (sext, 16H; (CH₃CH₂CH₂CH₂)₄N⁺), 0.95-0.91 ppm (t, 24H; (CH₃CH₂CH₂CH₂)₄N⁺); ¹³C NMR (100 MHz, [D₆] DMSO, 25°C) δ = 178.1, 172.2, 82.3, 74.6, 57.5, 33.6, 32.9, 23.0, 21.2, 19.2, 13.4 ppm; FT-IR (KBr): ν̃ = 3400(br), 3273(m), 3077(w), 2961(s), 2926(s), 2872(s), 1717(m), 1655(m), 1636(m), 1554(m), 1463(m), 1380(m), 1192(w), 1117(w), 1078(s), 1040(m), 954(s), 933(s), 883(w), 808(s), 721(s), 582(m), 512(w), 459(w), 417(s)cm⁻¹; elemental analysis calcd (%) for C₅₀H₁₀₀N₄O₂₅V₆: C 41.44, H 7.02, N 4.56; found: C 41.29, H 7.04, N 4.55.

Data for 2-d (4-Dimethyl-tert-butyl silicon-Glutaric Anhydride): ¹H NMR (400 MHz, [D₆] DMSO, 25 °C) δ=7.41 (s, 2H; -C(O)NH-), 5.09 (s, 12H; -C(CH₂O)₃-), 4.14(quin, 2H; CH₂CHCH₂) 3.17 (t, 16H; (CH₃CH₂CH₂CH₂)₄N⁺), 2.35-2.17 (m, 4H; -CH₂-C(O)OH and -CH₂-C(O)NH-), 1.57 (quin, 16H; (CH₃CH₂CH₂CH₂)₄N⁺), 1.33-1.28 (sext, 16H; (CH₃CH₂CH₂CH₂)₄N⁺), 0.95-0.91 ppm (t, 24H; (CH₃CH₂CH₂CH₂)₄N⁺) and solvent (DMF) peaks; ¹³C NMR (100 MHz, [D₆] DMSO, 25°C) δ= 178.2, 173.4, 85.6,

73.0, 64.7, 57.5, 40.1, 38.1, 35.8, 28.3, 23.0, 19.2, 13.5, -3.1 ppm; FT-IR (KBr): $\tilde{\nu}$ =3417(br), 3300(m), 3067(w), 2961(s), 2927(s), 2872(s), 1730(m), 1659(s), 1636(m), 1551(m), 1467(m), 1382(m), 1194(w), 1107(w), 1063(s), 954(s), 933(s), 881(w), 798(s), 718(s), 582(m), 512(w), 460(w), 418(s)cm⁻¹; elemental analysis calcd (%) for C₆₂H₁₂₈N₄O₂₇Si₂V₆ · 3DMF: C 43.89, H 7.73, N 5.05; found: C 43.67, H 7.81, N 4.98.

Data for 2-e (Antherecene Anhydride): ¹H NMR (400 MHz, [D₆] DMSO, 25 °C) δ =8.76 (s, 2H; ArH), 8.71 (s, 2H; ArH), 8.58 (s, 2H; ArH), 8.14-8.11 (m, 6H; ArH), 8.14-8.11 (m, 2H; -C (O) NH-), 7.60-7.58 (m, 4H; ArH), 5.32 (s, 12H; -C (CH₂O)₃-), 3.16 (t, 16H, (CH₃CH₂CH₂CH₂)₄N⁺), 1.56 (quin, 16H; (CH₃CH₂CH₂CH₂)₄N⁺), 1.33-1.27 (sext, 16H; (CH₃CH₂CH₂CH₂)₄N⁺), 0.94-0.90 ppm (t, 24H; (CH₃CH₂CH₂CH₂)₄N⁺) and solvent (DMF) peaks; ¹³C NMR (100 MHz, [D₆] DMSO, 25 °C) δ = 168.4, 162.3, 138.4, 136.0, 135.6, 132.5, 131.7, 127.9, 127.4, 126.7, 82.3, 74.1, 57.5, 23.0, 19.2, 13.5 ppm; FT-IR (KBr): $\tilde{\nu}$ = 3417(br), 3025(w), 2960(s), 2927(s), 2872(s), 1717(m), 1662(s), 1541(m), 1459(m), 1383(m), 1319(m), 1278(m), 1252(m), 1105(m), 1067(m), 1042(m), 953(s), 875(w), 809(s), 720(s), 582(m), 512(w), 471(w), 419(s)cm⁻¹; elemental analysis calcd (%) for C₇₂H₁₀₄N₄O₂₅V₆ · 2DMF: C 49.90, H 6.34, N 4.48; found: C 49.60, H 6.40, N 4.45.

Data for 2-f (Tartaric Anhydride): ¹H NMR (400 MHz, [D₆] DMSO, 25 °C) δ =8.05 (s, 2H; -C (O) NH-), 7.98-7.94 (m, 8H; ArH), 7.70-7.67 (m, 4H; ArH), 7.57-7.52 (m, 8H; ArH), 5.86 (d, 2H; HO(O)CCHCHC(O)NH-), 5.68 (d, 2H; HO(O)CCHCHC(O)NH-), 4.98 (s, 12H; -C (CH₂O)₃-), 3.16 (t, 16H, (CH₃CH₂CH₂CH₂)₄N⁺), 1.56 (quin, 16H; (CH₃CH₂CH₂CH₂)₄N⁺), 1.33-1.27 (sext, 16H; (CH₃CH₂CH₂CH₂)₄N⁺), 0.94-0.90 ppm (t, 24H; (CH₃CH₂CH₂CH₂)₄N⁺) and solvent

(DMF) peaks; ^{13}C NMR (100 MHz, $[\text{D}_6]$ DMSO, 25°C) $\delta = 173.8, 170.4, 162.3, 139.3, 129.3, 129.1, 128.8, 91.0, 86.7, 83.3, 81.7, 57.5, 23.0, 19.2, 13.5$ ppm; FT-IR (KBr): $\tilde{\nu} = 3411(\text{br}), 3062(\text{w}), 2961(\text{s}), 2927(\text{s}), 2872(\text{s}), 1729(\text{s}), 1659(\text{s}), 1601(\text{m}), 1539(\text{m}), 1452(\text{m}), 1382(\text{m}), 1317(\text{m}), 1251(\text{m}), 1178(\text{w}), 1106(\text{s}), 1068(\text{s}), 1043(\text{m}), 955(\text{s}), 888(\text{w}), 808(\text{s}), 717(\text{s}), 583(\text{m}), 511(\text{w}), 460(\text{w}), 419(\text{s})\text{cm}^{-1}$; elemental analysis calcd (%) for $\text{C}_{76}\text{H}_{112}\text{N}_4\text{O}_{33}\text{V}_6 \cdot \text{DMF}$: C 47.72, H 6.03, N 3.52; found: C 47.50, H 6.11, N 3.46.

Data for 2-g (Maleic Anhydride): ^1H NMR (400 MHz, $[\text{D}_6]$ DMSO, 25 °C) $\delta = 6.27$ (d, 2H; $\text{HO}(\text{O})\text{CCH}=\text{CHC}(\text{O})\text{NH}-$), 6.08 (d, 2H; $\text{HO}(\text{O})\text{CCH}=\text{CHC}(\text{O})\text{NH}-$), 5.11 (s, 12H; $-\text{C}(\text{CH}_2\text{O})_3-$), 3.14 (t, 16H, $(\text{CH}_3\text{CH}_2\text{CH}_2\text{CH}_2)_4\text{N}^+$), 1.54 (quin, 16H; $(\text{CH}_3\text{CH}_2\text{CH}_2\text{CH}_2)_4\text{N}^+$), 1.32-1.23 (sext, 16H; $(\text{CH}_3\text{CH}_2\text{CH}_2\text{CH}_2)_4\text{N}^+$), 0.92-0.88 ppm (t, 24H; $(\text{CH}_3\text{CH}_2\text{CH}_2\text{CH}_2)_4\text{N}^+$) and solvent (DMF) peaks; ^{13}C NMR (100 MHz, $[\text{D}_6]$ DMSO, 25°C) $\delta = 165.6, 162.3, 144.3, 139.3, 84.1, 81.9, 57.5, 23.0, 19.2, 13.5$ ppm; FT-IR (KBr): $\tilde{\nu} = 3424(\text{br}), 3247(\text{br}), 3060(\text{w}), 3030(\text{w}), 2961(\text{s}), 2925(\text{s}), 2872(\text{s}), 1719(\text{s}), 1660(\text{s}), 1630(\text{s}), 1603(\text{m}), 1561(\text{s}), 1482(\text{s}), 1385(\text{m}), 1316(\text{m}), 1270(\text{m}), 1218(\text{w}), 1110(\text{m}), 1064(\text{s}), 955(\text{s}), 882(\text{w}), 847(\text{w}), 812(\text{s}), 719(\text{s}), 582(\text{m}), 512(\text{w}), 460(\text{w}), 418(\text{s})\text{cm}^{-1}$; elemental analysis calcd (%) for $\text{C}_{48}\text{H}_{92}\text{N}_4\text{O}_{25}\text{V}_6 \cdot 2\text{DMF}$: C 41.12, H 6.77, N 5.33; found: C 40.96, H 6.85, N 5.22.

Data for 2-h (2,3-Dihydro-1,4-dithiino[2,3-c]furan-5,7-dione Anhydride): ^1H NMR (400 MHz, $[\text{D}_6]$ DMSO, 25 °C) $\delta = 8.43$ (br, s, 2H; $-\text{C}(\text{O})\text{NH}-$), 5.09 (s, 12H; $-\text{C}(\text{CH}_2\text{O})_3-$), 3.16 (t, 8H, $(\text{CH}_3\text{CH}_2\text{CH}_2\text{CH}_2)_4\text{N}^+$), 3.12-3.06 (m, 8H; $-\text{SCH}_2\text{CH}_2\text{S}-$), 3.01 (q, 18H; $(\text{CH}_3\text{CH}_2)_3\text{NH}^+$), 1.56 (quin, 8H; $(\text{CH}_3\text{CH}_2\text{CH}_2\text{CH}_2)_4\text{N}^+$), 1.34-1.26 (sext, 8H; $(\text{CH}_3\text{CH}_2\text{CH}_2\text{CH}_2)_4\text{N}^+$), 1.12 (t, 27H; $(\text{CH}_3\text{CH}_2)_3\text{NH}^+$), 0.95-0.91 ppm (t, 12H;

($\text{CH}_3\text{CH}_2\text{CH}_2\text{CH}_2$) $_4\text{N}^+$) and solvent (DMF) peaks; ^{13}C NMR (100 MHz, $[\text{D}_6]$ DMSO, 25°C) $\delta = 164.3, 156.9, 142.9, 132.4, 85.8, 73.9, 57.4, 45.5, 34.1, 23.0, 19.2, 13.5, 8.87$ ppm; FT-IR (KBr): $\tilde{\nu} = 3422(\text{br}), 3200(\text{br}), 3020(\text{w}), 2922(\text{s}), 2852(\text{s}), 1657(\text{s}), 1605(\text{m}), 1555(\text{m}), 1467(\text{m}), 1344(\text{m}), 1315(\text{m}), 1270(\text{m}), 1180(\text{w}), 1082(\text{m}), 1045(\text{s}), 954(\text{s}), 800(\text{s}), 718(\text{s}), 583(\text{m}), 513(\text{w}), 461(\text{w}), 420(\text{s})\text{cm}^{-1}$; elemental analysis calcd (%) for $[\text{Anion}^{2-} + \text{TBA}^+ + \text{TEAH}^+] \cdot \text{DMF} \cdot 2\text{TEA}$: $\text{C}_{42}\text{H}_{76}\text{N}_4\text{O}_{25}\text{S}_4\text{V}_6 \cdot \text{DMF}$: C 39.20, H 6.52, N 5.61; found: C 38.99, H 6.60, N 5.54.

Data for 2-i (Diallylpyrocarbonate Anhydride): ^1H NMR (400 MHz, $[\text{D}_6]$ DMSO, 25 °C) $\delta=7.17$ (br, 2H; -C (O) NH-), 5.86(m, 2H; $\text{CH}_2=\text{CHCH}_2\text{O}$ -), 5.28-5.24(d, 2H; *trans*- $\text{CHH}=\text{CHCH}_2\text{O}$ -), 5.16-5.14(d, 2H; *cis*- $\text{CHH}=\text{CHCH}_2\text{O}$ -), 5.04 (d, 12H; -C (CH_2O) $_3$ -), 4.41-4.40(d, 4H; $\text{CH}_2=\text{CHCH}_2\text{O}$ -), 3.17 (t, 16H, ($\text{CH}_3\text{CH}_2\text{CH}_2\text{CH}_2$) $_4\text{N}^+$), 1.57 (quin, 16H; ($\text{CH}_3\text{CH}_2\text{CH}_2\text{CH}_2$) $_4\text{N}^+$), 1.35-1.26 (sext, 16H; ($\text{CH}_3\text{CH}_2\text{CH}_2\text{CH}_2$) $_4\text{N}^+$), 0.95-0.91 ppm (t, 24H; ($\text{CH}_3\text{CH}_2\text{CH}_2\text{CH}_2$) $_4\text{N}^+$) and solvent (DMF) peaks; ^{13}C NMR (100 MHz, $[\text{D}_6]$ DMSO, 25°C) $\delta = 169.2, 129.2, 118.7, 86.3, 78.9, 57.5, 23.0, 19.2, 13.5$; FT-IR (KBr): $\tilde{\nu} = 3361(\text{br}), 2959(\text{s}), 2925(\text{s}), 2873(\text{s}), 2851(\text{s}), 1720(\text{m}), 1655(\text{s}), 1605(\text{w}), 1479(\text{s}), 1381(\text{m}), 1314(\text{w}), 1237(\text{w}), 1151(\text{w}), 1061(\text{s}), 950(\text{s}), 880(\text{w}), 820(\text{m}), 797(\text{s}), 721(\text{s}), 582(\text{s}), 515(\text{w}), 462(\text{w}), 418(\text{s})\text{cm}^{-1}$; elemental analysis calcd (%) for $\text{C}_{48}\text{H}_{96}\text{N}_4\text{O}_{23}\text{V}_6 \cdot \text{DMF}$ C 41.50, H 7.03, N 4.74, found: C 41.35, H 7.10, N 4.71;

Data for 2-j (Isonicotinic Anhydride): ^1H NMR (400 MHz, $[\text{D}_6]$ DMSO, 25 °C) $\delta=8.68$ (d, 4H; ArH), 8.06 (s, 2H;-C(O)NH-), 7.70 (d, 4H; ArH), 5.28 (s, 12H, -C(CH_2O) $_3$ -), 3.16 (t, 16H, ($\text{CH}_3\text{CH}_2\text{CH}_2\text{CH}_2$) $_4\text{N}^+$), 1.56 (quin, 16H; ($\text{CH}_3\text{CH}_2\text{CH}_2\text{CH}_2$) $_4\text{N}^+$), 1.35-1.26 (sext, 16H; ($\text{CH}_3\text{CH}_2\text{CH}_2\text{CH}_2$) $_4\text{N}^+$), 0.95-0.91 ppm (t,

24H; $(\text{CH}_3\text{CH}_2\text{CH}_2\text{CH}_2)_4\text{N}^+$) and solvent (DMF) peaks; ^{13}C NMR (100 MHz, $[\text{D}_6]$ DMSO, 25°C) δ = 166.3, 150.5, 142.7, 122.3, 82.7, 58.1, 53.9, 23.7, 19.9, 14.2 ppm; FT-IR (KBr): $\tilde{\nu}$ = 3350(br), 3272(br), 3027(w), 2962(s), 2930(s), 2874(s), 1730(w), 1667(s), 1597(w), 1540(m), 1483(m), 1407(w), 1381(w), 1319(m), 1279(w), 1178(w), 1153(w), 1108(s), 1050(s), 952(s), 812(s), 798(m), 721(s), 642(m), 583(m), 517(w), 461(w), 413(m) cm^{-1} ; elemental analysis calcd (%) for $\text{C}_{52}\text{H}_{94}\text{N}_6\text{O}_{27}\text{V}_6 \cdot \text{DMF}$: C, 40.93; H, 6.31; N, 6.07; found: C, 40.62; H, 6.40; N, 6.00.

Data for 2-k (*o*-Acetylsalicylic Anhydride): ^1H NMR (400 MHz, $[\text{D}_6]$ DMSO, 25 °C) δ =7.92 (d, 2H; *ArH*), 7.48-7.44 (m, 2H; -C(O)NH-), 7.48-7.44 (m, 2H; *ArH*), 7.27 (t, 2H; *ArH*), 7.16 (d, 2H; *ArH*), 5.20 (s, 12H; -C(CH₂O)₃-), 3.16 (t, 16H, (CH₃CH₂CH₂CH₂)₄N⁺), 2.18 (s, 6H; CH₃C(O)O-), 1.56 (quin, 16H; (CH₃CH₂CH₂CH₂)₄N⁺), 1.35-1.26 (sext, 16H; (CH₃CH₂CH₂CH₂)₄N⁺), 0.95-0.81 ppm (t, 24H; (CH₃CH₂CH₂CH₂)₄N⁺) and solvent (DMF) peaks; ^{13}C NMR (100 MHz, $[\text{D}_6]$ DMSO, 25°C): δ = 168.5, 166.1, 147.3 143.1, 130.5, 129.4, 122.6, 121.7, 82.0, 72.6, 57.5, 23.0, 20.7 19.2, 13.5 ppm; FT-IR (KBr): $\tilde{\nu}$ = 3410(br), 3260(br), 3060(w), 2961(s), 2928(s), 2872(s), 1765(m), 1666(s), 1606(w), 1526(m), 1480(m), 1379(m), 1321(m), 1283(w), 1198(m), 1110(m), 1094(m), 1053(s), 952(s), 878(w), 810(s), 721(s), 629(w), 583(m), 512(w), 460(w), 418(s) cm^{-1} ; elemental analysis calcd (%) for $\text{C}_{58}\text{H}_{100}\text{N}_4\text{O}_{25}\text{V}_6 \cdot \text{DMF}$: C 44.89, H 6.61, N 4.29; found: C 44.72, H 6.67, N 4.24.

Data for 2-l (Tetraphenylphthalic Anhydride): ^1H NMR (400 MHz, $[\text{D}_6]$ DMSO, 25 °C) δ =7.65 (br, 2H; -C(O)NH-), 7.08-7.00 (m, 20H; *ArH*), 6.84-6.72(m, 20H; *ArH*), 4.72(s, 12H; -C(CH₂O)₃-), 3.16 (t, 16H, (CH₃CH₂CH₂CH₂)₄N⁺), 1.56 (quin, 16H;

($\text{CH}_3\text{CH}_2\text{CH}_2\text{CH}_2$) $_4\text{N}^+$), 1.33-1.27 (sext, 16H; ($\text{CH}_3\text{CH}_2\text{CH}_2\text{CH}_2$) $_4\text{N}^+$), 0.95-0.91 ppm (t, 24H; ($\text{CH}_3\text{CH}_2\text{CH}_2\text{CH}_2$) $_4\text{N}^+$); ^{13}C NMR (100 MHz, $[\text{D}_6]$ DMSO, 25°C) δ = 173.3, 166.9, 155.7, 147.3, 137.2, 134.8, 134.6, 134.2, 130.8, 127.8, 129.1, 128.2, 84.6, 83.0, 57.5, 23.0, 19.2, 13.5 ppm; FT-IR (KBr): $\tilde{\nu}$ = 3417(br), 3056(w), 3026(w), 2960(s), 2928(s), 2872(s), 1718(m), 1669(s), 1601(w), 1557(w), 1518(w), 1466(m), 1380(m), 1343(m), 1254(m), 1195(w), 1114(m), 1048(s), 1026(s), 953(s), 885(w), 809(s), 776(w), 720(s), 701(w), 655(w), 581(m), 532(w), 460(w), 419(s) cm^{-1} ; elemental analysis calcd (%) for $\text{C}_{104}\text{H}_{128}\text{N}_4\text{O}_{25}\text{V}_6$: C 58.38, H 6.03, N 2.62; found: C 58.14, H 6.06, N 2.59.

Data for 2-m (Tetrafluorophthalic Anhydride): ^1H NMR (400 MHz, $[\text{D}_6]$ DMSO, 25 °C) δ =8.27 (br, 2H; -C(O)NH-), 5.14 (s, 12H; -C(CH₂O)₃-), 3.17 (t, 16H, ($\text{CH}_3\text{CH}_2\text{CH}_2\text{CH}_2$) $_4\text{N}^+$), 1.53 (quin, 16H; ($\text{CH}_3\text{CH}_2\text{CH}_2\text{CH}_2$) $_4\text{N}^+$), 1.31-1.25 (sext, 16H; ($\text{CH}_3\text{CH}_2\text{CH}_2\text{CH}_2$) $_4\text{N}^+$), 0.92-0.88 ppm (t, 24H; ($\text{CH}_3\text{CH}_2\text{CH}_2\text{CH}_2$) $_4\text{N}^+$) and solvent (DMF) peaks; ^{13}C NMR (100 MHz, $[\text{D}_6]$ DMSO, 25°C) δ = 168.5, 167.2, 153.6, 150.1, 144.4, 142.4, 124.2, 122.7, 91.9, 80.9, 57.5, 23.0, 19.2, 13.5 ppm; FT-IR (KBr): $\tilde{\nu}$ = 3417(br), 3026(w), 2961(s), 2925(s), 2873(s), 1720(m), 1662(s), 1640(s), 1562(m), 1510(m), 1469(m), 1379(m), 1317(w), 1250(w), 1185(w), 1076(m), 1048(s), 955(s), 885(w), 802(s), 718(s), 619(w), 583(m), 513(w), 459(w), 420(s) cm^{-1} ; elemental analysis calcd (%) for $\text{C}_{56}\text{H}_{88}\text{F}_8\text{N}_4\text{O}_{25}\text{V}_6 \cdot \text{DMF}$: C 40.54, H 5.48, N 4.01; found: C 40.27, H 5.53, N 3.95.

Data for 2-n (2.3-Pyrazinedicarboxylic Anhydride): ^1H NMR (400 MHz, $[\text{D}_6]$ DMSO, 25 °C) δ =8.77-8.75 (d, 4H; ArH), 8.30 (s, 2H; -C(O)NH-), 5.23 (s, 12H; -C(CH₂O)₃-), 3.16 (t, 16H, ($\text{CH}_3\text{CH}_2\text{CH}_2\text{CH}_2$) $_4\text{N}^+$), 1.56 (quin, 16H;

($\text{CH}_3\text{CH}_2\text{CH}_2\text{CH}_2$) $_4\text{N}^+$), 1.33-1.27 (sext, 16H; ($\text{CH}_3\text{CH}_2\text{CH}_2\text{CH}_2$) $_4\text{N}^+$), 0.94-0.91 ppm (t, 24H; ($\text{CH}_3\text{CH}_2\text{CH}_2\text{CH}_2$) $_4\text{N}^+$) and solvent (DMF) peaks; ^{13}C NMR (100 MHz, $[\text{D}_6]$ DMSO, 25°C) δ = 176.6, 166.9, 153.2, 147.4, 145.5, 138.7, 90.2, 79.1, 57.5, 23.1, 19.2, 13.6 ppm; FT-IR (KBr): $\tilde{\nu}$ = 3364(br), 3280(br), 3058(w), 2960(s), 2926(s), 2872(s), 1730(m), 1662(s), 1564(m), 1522(m), 1480(m), 1414(w), 1384(m), 1320(m), 1270(w), 1215(w), 1164(w), 1094(s), 1049(s), 954(s), 886(w), 808(s), 719(s), 659(m), 583(m), 465(w), 419(s) cm^{-1} ; elemental analysis calcd (%) for $\text{C}_{52}\text{H}_{92}\text{N}_8\text{O}_{25}\text{V}_6 \cdot 3\text{DMF}$: C 63.14, H 8.48, N 7.36; found: C 62.87, H 8.53, N 7.26.

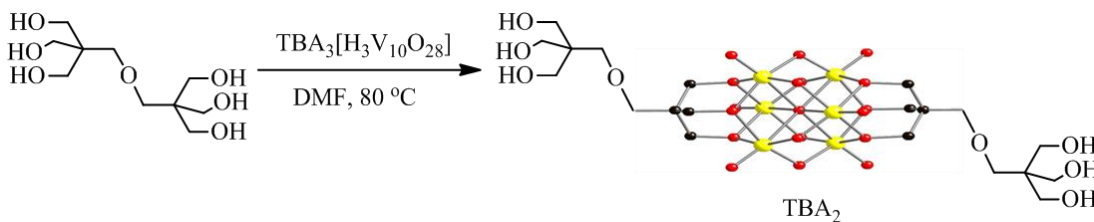
Data for 2-o (1-Pyrenebutyric Anhydride): ^1H NMR (400 MHz, $[\text{D}_6]$ DMSO, 25 °C) δ =8.32-7.33 (m, 18H; ArH and s, 2H; -C(O)NH-), 5.12 (s, 12H; -C(CH₂O)₃-), 3.26(t, 4H; ArCH₂CH₂CH₂C(O)NH-), 3.12 (t, 16H, ($\text{CH}_3\text{CH}_2\text{CH}_2\text{CH}_2$) $_4\text{N}^+$), 2.19(t, 4H; ArCH₂CH₂CH₂C(O)NH-), 1.94(quin, 4H; ArCH₂CH₂CH₂C(O)NH-) 1.53 (quin, 16H; ($\text{CH}_3\text{CH}_2\text{CH}_2\text{CH}_2$) $_4\text{N}^+$), 1.30-1.24 (sext, 16H; ($\text{CH}_3\text{CH}_2\text{CH}_2\text{CH}_2$) $_4\text{N}^+$), 0.92-0.88 ppm (t, 24H; ($\text{CH}_3\text{CH}_2\text{CH}_2\text{CH}_2$) $_4\text{N}^+$) and solvent (DMF) peaks; ^{13}C NMR (100 MHz, $[\text{D}_6]$ DMSO, 25°C) δ = 171.4, 136.5, 131.2, 130.8, 129.2, 128.4, 127.3, 127.2, 126.4, 126.1, 125.0, 124.8, 124.3, 124.1, 123.3, 81.6, 78.8, 57.4, 49.6, 37.2, 31.4, 23.0, 19.2, 13.5 ppm; FT-IR (KBr): $\tilde{\nu}$ =3421(br), 3290(br), 3027(w), 2958(s), 2923(s), 2852(s), 1662(s), 1603(w), 1540(m), 1466(s), 1378(m), 1307(w), 1245(w), 1184(w), 1118(w), 1074(s), 952(s), 848(m), 810(s), 799(w), 721(s), 583(s), 459(w), 416(s) cm^{-1} ; elemental analysis calcd (%) for $\text{C}_{80}\text{H}_{116}\text{N}_4\text{O}_{21}\text{V}_6 \cdot \text{DMF}$: C 53.93, H 6.71, N 3.79; found: C 53.68, H 6.77, N 3.76.

Data for 3-a (Maleic Anhydride): ^1H NMR (400 MHz, $[\text{D}_6]$ DMSO, 25 °C) $\delta=65.29$ (br,s, 12H, $-\text{C}(\text{CH}_2\text{O})_3-$), 13.62(br,s, 2H; $-\text{COOH}$), 8.55 (s, 2H; $-\text{C}(\text{O})\text{NH}-$), 6.51 (d, 2H; $\text{HO}(\text{O})\text{CCH}=\text{CHC}(\text{O})\text{NH}-$), 6.01 (d, 2H; $\text{HO}(\text{O})\text{CCH}=\text{CHC}(\text{O})\text{NH}-$), 3.16 (t, 24H, $(\text{CH}_3\text{CH}_2\text{CH}_2\text{CH}_2)_4\text{N}^+$), 1.56 (quin, 24H; $(\text{CH}_3\text{CH}_2\text{CH}_2\text{CH}_2)_4\text{N}^+$), 1.35-1.26 (sext, 24H; $(\text{CH}_3\text{CH}_2\text{CH}_2\text{CH}_2)_4\text{N}^+$), 0.95-0.91 ppm (t, 36H; $(\text{CH}_3\text{CH}_2\text{CH}_2\text{CH}_2)_4\text{N}^+$) and solvent (DMF) peaks; ^{13}C NMR (100 MHz, $[\text{D}_6]$ DMSO, 25°C) $\delta=185.9, 167.8, 135.6, 134.7, 57.5, 23.0, 19.2, 13.5$ ppm; FT-IR (KBr): $\tilde{\nu}=3432(\text{br}), 3272(\text{br}), 3058(\text{w}), 3025(\text{w}), 2962(\text{s}), 2930(\text{s}), 2874(\text{s}), 1719(\text{s}), 1657(\text{s}), 1627(\text{s}), 1604(\text{m}), 1569(\text{s}), 1483(\text{s}), 1381(\text{m}), 1319(\text{m}), 1279(\text{m}), 1218(\text{w}), 1178(\text{w}), 1153(\text{w}), 1108(\text{m}), 1034(\text{s}), 942(\text{s}), 921(\text{s}), 852(\text{w}), 817(\text{w}), 672(\text{s}), 567(\text{m}), 551(\text{m}), 461(\text{w}), 411(\text{w})\text{cm}^{-1}$; elemental analysis calcd (%) for $\text{C}_{64}\text{H}_{128}\text{MnMo}_6\text{N}_5\text{O}_{30} \cdot \text{DMF}$: C 37.40, H 6.32, N 3.91; found: C 37.21, H 6.41, N 3.86.

Data for 3-b (Isonicotinic Anhydride): ^1H NMR (400 MHz, $[\text{D}_6]$ DMSO, 25 °C) $\delta=61.75$ (br, 12H, $-\text{C}(\text{CH}_2\text{O})_3-$), 8.65 (s, 4H; ArH), 7.65 (s, 4H; ArH), 3.16 (t, 24H, $(\text{CH}_3\text{CH}_2\text{CH}_2\text{CH}_2)_4\text{N}^+$), 1.56 (quin, 24H; $(\text{CH}_3\text{CH}_2\text{CH}_2\text{CH}_2)_4\text{N}^+$), 1.35-1.26 (sext, 24H; $(\text{CH}_3\text{CH}_2\text{CH}_2\text{CH}_2)_4\text{N}^+$), 0.95-0.91 ppm (t, 36H; $(\text{CH}_3\text{CH}_2\text{CH}_2\text{CH}_2)_4\text{N}^+$); ^{13}C NMR (100 MHz, $[\text{D}_6]$ DMSO, 25°C) $\delta = 174.1, 148.9, 148.4, 132.2, 57.5, 23.0, 19.2, 13.5$ ppm; FT-IR (KBr): $\tilde{\nu} = 3425(\text{br}), 3267(\text{br}), 3060(\text{w}), 2960(\text{s}), 2929(\text{s}), 2872(\text{s}), 1733(\text{w}), 1663(\text{s}), 1542(\text{s}), 1480(\text{s}), 1381(\text{m}), 1322(\text{w}), 1285(\text{w}), 1152(\text{w}), 1103(\text{m}), 1037(\text{s}), 939(\text{s}), 919(\text{s}), 902(\text{s}), 780(\text{w}), 662(\text{s}), 564(\text{m}), 551(\text{m}), 461(\text{w}), 414(\text{w}) \text{cm}^{-1}$; elemental analysis calcd (%) for $\text{C}_{68}\text{H}_{130}\text{MnMo}_6\text{N}_7\text{O}_{26}$: C 39.03, H 6.26, N 4.69; found: C 38.91, H 6.34, N 4.60.

Results and Discussion

A new type of polyoxometalate (POM)-containing material, a hexavanadate covalently tethered with two groups bearing functionalizable termini via a triester linkage, hereforth noted “**1**”, are synthesized by the hydrothermal technique (Scheme 2-1). Such pendant groups if they contain another function(s) could be used in principle not only to directly tune the redox and acid-base chemistry of the catalyst active site, the hexavanadate unit itself in the case we report here, but also to immobilize these POMs on high surface area supports, incorporate them into otherwise functional supramolecular materials and to induce their proximity to our target substrates such as toxic industrial chemicals (TICs) and chemical warfare agents (CWAs).



Scheme 2-1. Hydrothermal synthesis of hybrid dendrimer **1**. Yellow: V; red: O.

The crystal structure of **1** clearly shows the covalent linkage of alkyl chains with the hexavanadate cluster via C-O bond formation (Figure 2-1 and Table 2-1). This molecule could be viewed as G-zero dendrimer, which contains a central POM core and an external surface groups with six hydroxyl-terminated branches.⁴⁶ The six hydroxyl termini could further be functionalized either by organic molecules to construct a higher level of more branched dendritic structures or POMs, such as Wells-Dawson type $[\text{P}_2\text{V}_3\text{W}_{15}\text{O}_{62}]^{9-}$, or to make “POM-dumbbells” (Scheme 2-2).⁴⁷ Formation of the hybrid POM-dumbbell is confirmed by both NMR techniques (Figure 2-2).

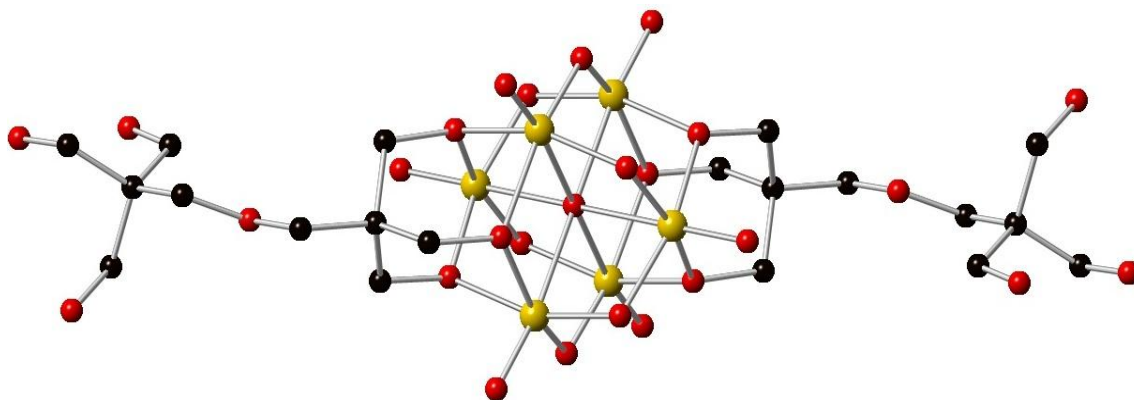
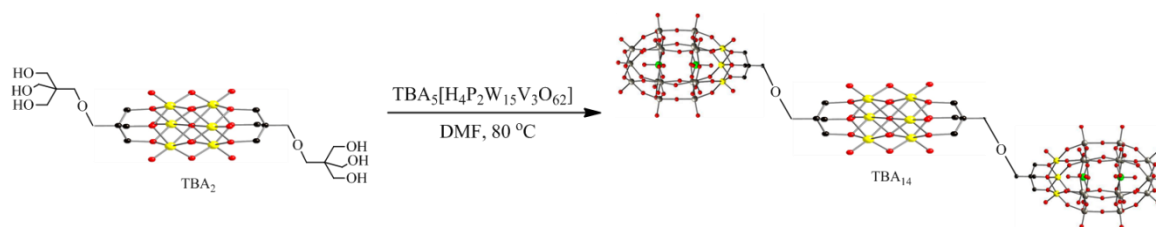


Figure 2-1. X-ray single crystal structure of **1**. Yellow: V; red: O; Black: C. (H atoms and counterions omitted for clarity)

Table 2-1. Crystallographic Data and Structure Refinement for **1**.

	1
empirical formula	C ₅₄ H ₁₁₀ N ₂ O ₂₈ V ₆
formula weight	1541.08g mol ⁻¹
crystal system	Monoclinic
space group	P2(1)/n
unit cell	a = 16.3560(6) Å α = 90° b = 13.5673(5) Å β = 104.210(2)° c = 16.9476(6) Å γ = 90°
volume	3645.7(2) Å ³
Z	2
density (calcd)	1.404 g cm ⁻³
temperature	173(2)K
wavelength	0.71073 Å
abs. coeff	0.814 mm ⁻¹
Reflections collected	44320
Independent reflections	7491 [R(int) = 0.0947]
GOF	1.039
final R ₁ ^a [I > 2σ(I)]	0.0765
final wR ₂ ^b [I > 2σ(I)]	0.2053

$$^a R_1 = \frac{\sum ||F_o| - |F_c||}{\sum |F_o|}; wR_2 = \frac{\sum [w(F_o^2 - F_c^2)^2]}{\sum [w(F_o^2)^2]}^{1/2}$$



Scheme 2-2. Linqvist and Wells-Dawson hybrid POM-dumbbell.

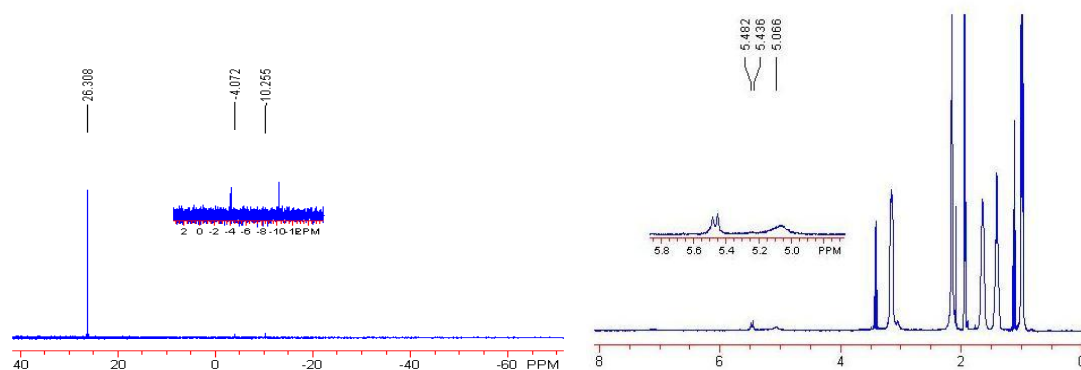
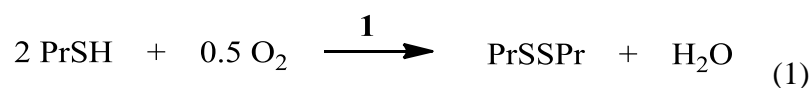


Figure 2-2. ^{31}P and ^1H NMR of the POM-dumbbell.

In preliminary evaluations, **1** shows catalytic activity for one of the most challenging but potentially useful classes of reactions, selective air-based oxidations. Such molecules could provide a catalytic, not just a stoichiometric, capability for decontaminating a range of toxic substances without the need for any other reagent or energy source. The latter point reflects the fact that oxidation of all organic compounds, which includes key TICs like formaldehyde, as well as many inorganic compounds, including other TICs, is thermodynamically favorable. Figure 2-3 shows the initial results, namely air-based oxidation of propane thiol (PrSH) catalyzed by **1** (equation 1). We chose a thiol as the substrate not because it's a TIC or a CWA (it's neither) but for two reasons: (1) its oxidative transformations can be far more readily and thus quickly investigated than those of actual TICs or CWAs (and thus central mechanistic insights for all catalyzed oxidations can be obtained rapidly), and (2) because thiol oxidation facilitated by POMs and POM-based materials including others developed recently by the Hill group, whether

they be stoichiometric or catalytic, often parallel oxidations of TICs such as formaldehyde and H₂S as well as the CWAs, mustard (HD) and VX (simulants or live agents).

The dendritic hybrid **1** effectively catalyzes thiol oxidation and interestingly does so via pseudo-zero-order kinetics to 100% consumption of PrSH. There is almost no reaction in the absence of catalyst (the volatile thiol was leaking slowly from the reaction vials). The detectable limit of the GC analysis is at 2-3 orders of magnitude less than the size of the GC peaks for organic substrate and product.



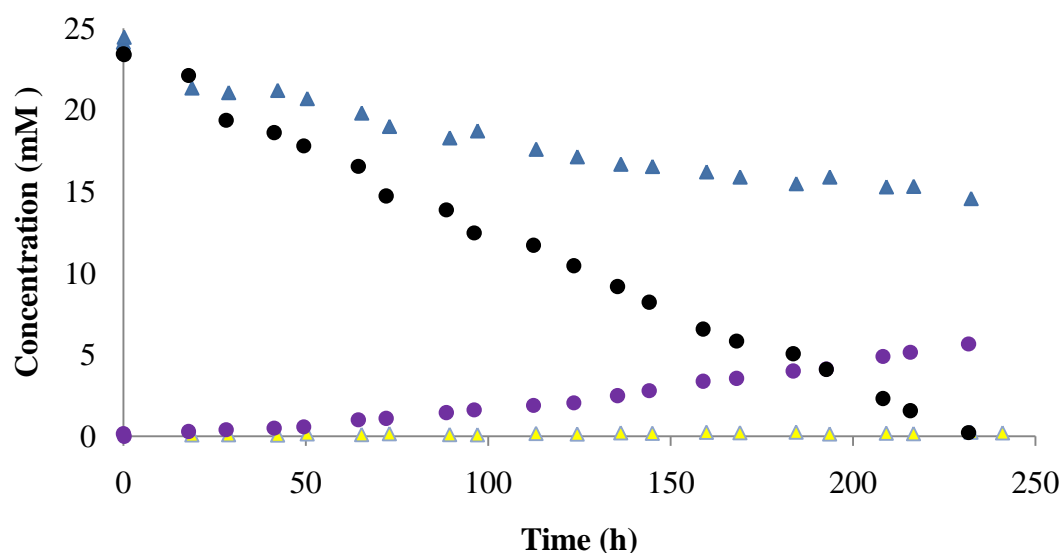


Figure 2-3. Dioxxygen oxidation of PrSH catalyzed by **1**. The upper lines show the consumption of PrSH; the bottom lines show the formation of PrSSPr. Triangles: control reaction without catalyst; dots: reaction in the presence of **1**.

In addition, **1** also catalyzes the oxidation of acetaldehyde to acetic acid using only ambient air (equation 2 and figure 2-4). The air-based oxidation of acetaldehyde catalyzed by **1** gives 280 turnovers in 10 weeks. In the absence of catalyst the oxidation of acetaldehyde is very slow. Acetaldehyde oxidation is a model for formaldehyde oxidation. While acetaldehyde is a TIC, it is low on the priority list; whereas formaldehyde is high on this list and our ultimate target in this particular effort. It is likely that other reaction conditions (solvent, optimal pH, etc) would considerably speed up the reaction.

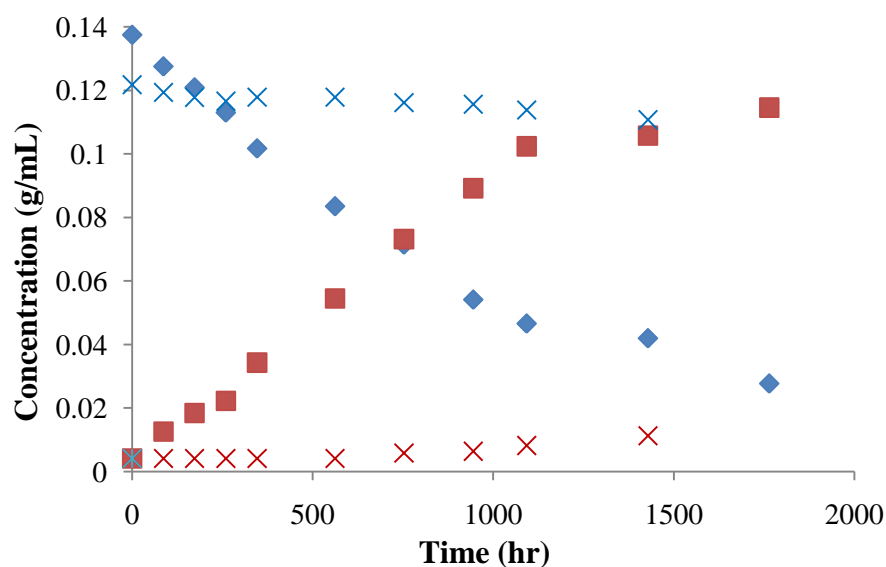
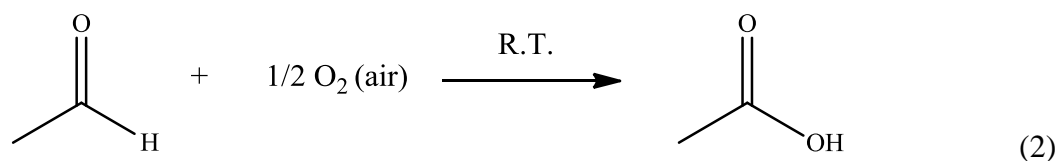


Figure 2-4. Aerobic oxidation of acetaldehyde (blue) to acetic acid (red) at room temperature. Crosses (control reaction without catalyst); squares (reaction in the presence of **1**).

The hybrid **1** was also used to catalyze aerobic oxidation of formaldehyde under ambient conditions, but no reaction was observed for 7 days. The possible reason might be that the commercial available Formalin contains 10–12% methanol as stabilizer to limit oxidation and polymerization. Another reason is that formaldehyde in water is nearly all in the form of the hydrate $\text{H}_2\text{C}(\text{OH})_2$ and its polymers; it is not present in the carbonyl form. It should be noted that aldehyde oxidation is also likely to be co-catalyzed by addition of appropriate transition metal counterions for **1**.

Complex **1** catalyzes the air-based oxidation of hydrogen sulfide to sulfur. Preliminary results show that **1** gives 14~15 turnovers under either air or oxygen at room temperature in 24 hours. Again, no significant reaction is seen in the absence of this organic-POM hybrid catalyst.

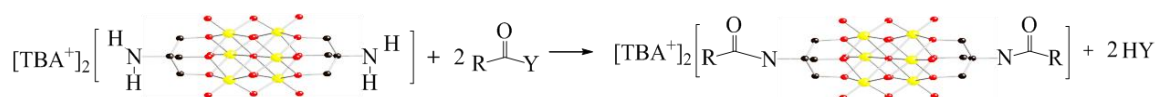
In addition to the hydrothermal synthesis of new types of organic-POM hybrids, we also explored the further functionalization of organic POMs derivatives.

In the early attempt to functionalize a POM triester by its terminal primary amine group,^{42,48} we found that the POM unit itself could function as a nucleophile and compete with the primary amine thus rendering the amine derivatization complicated and low yield.^{37,49-61} In terminal amine group functionalization, we favor amide bond formation because these reactions proceed in high yield, and amides are relatively robust ($\Delta H^\circ = 86 \text{ kcal mol}^{-1}$) and rigid (sp^2 hybridization of carbon on carbonyl group) facilitating subsequent synthetic elaboration of POM-amides and incorporation of these units into reactive materials such as POM-containing metal-organic frameworks recently reported by our group.

We initially examined reaction of the amine in **1** with acyl halides (Scheme 2-3 and Table 2-2). These reactions resulting only in reduction and decomposition of the POM triesters even at low temperatures (-10°C). We then turned our attention to the possible use of carboxylic acids as substrates for dehydration coupling in part because there are several highly effective dehydrating agents that could be used in these reactions. The coupling reagents dicyclohexylcarbodiimide (DCC), N-(3-Dimethylaminopropyl)-3-ethylcarbodiimide (EDC), and (Benzotriazol-1-yloxy)tris(dimethylamino)phosphonium hexafluorophosphate (BOP), were evaluated and all gave desirable products but in

unacceptably low yields based on proton NMR (< 10%). The POM units themselves were undergoing various reactions in the presence of these dehydrating agents as well, thus isolation of the desired side chain coupling products proved very difficult.

In order to avoid the use of a dehydration reagent, we studied amide formation by direct reaction of less reactive carboxylic acid esters with POM-triester terminal amine groups and drove the reaction equilibrium to products by removing the low-boiling alcohol byproducts as they were formed. However, there were virtually no reaction even at elevated temperature (120 °C) for a day. If the reaction time was elongated, obvious POM decomposition products could be observed and unidentified products formed.



Scheme 2-3. Functionalization of hexavanadate **2** triesters by amidation reaction. Yellow, V; red, O.

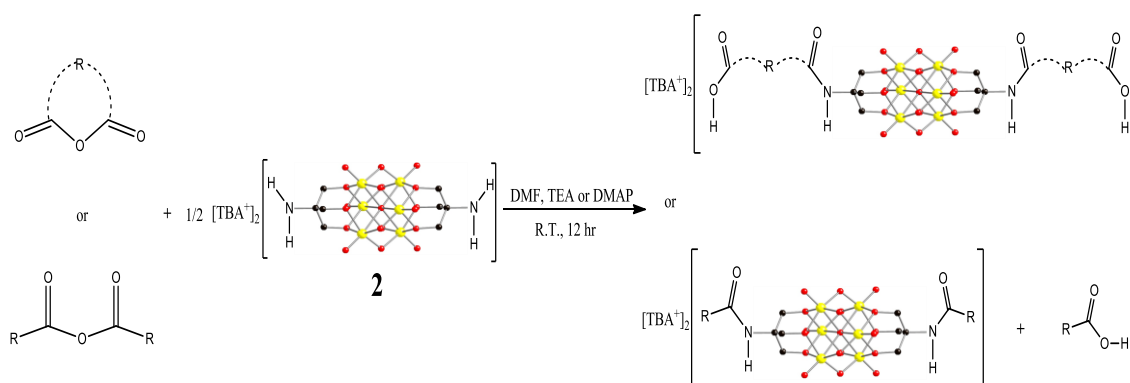
Table 2-2. Reaction of **2** with acyl chlorides, carboxylic acids, and esters.

Entry	Y	R	Reagents	Temp / Time	Conversion (%) ^[a]
1	Cl	Me	Pyr., MeCN	0 °C /4 hr	– ^[b]
2	Cl	Et	Pyr., MeCN	0 °C /4 hr	– ^[b]
3	Cl	Ph	Pyr., MeCN	0 °C /2 hr, then r.t. /12 hr	16 ^[c]
4	Cl	2-Pyridyl	Pyr. or K ₂ CO ₃ (s), MeCN	0 °C /2 hr, then r.t. /6 hr	– ^[b]
5	OH	Me	Method ^[d] (1), (2), (3), (4)		7 ^[e] /11 ^[e] /17 ^[e] /– ^[b]
6	OH	Et	Method ^[d] (1) & (2) & (3)		9 ^[e] /12 ^[e] /15 ^[e]
7	OH	Ph	Method ^[d] (1) & (3)		12 ^[e] /23 ^[e]
8	OH	2-Pyridyl	Method ^[d] (1) & (3)		16 ^[e] /19 ^[e]
9	OMe	Me	MeCN	reflux/24hr	8 ^[e]
10	OMe	Et	MeCN	reflux/24hr	11 ^[e]
11	OMe	Ph	DMF	120°C/24hr	8 ^[c]
12	OMe	2-Pyridyl	DMF	120°C/24hr	6 ^[c]

[a] Conversion based on hexavanadate triesters; all reactions tracked by ¹H NMR. [b] Unidentified product. [c] Desired product was accompanied by large amounts of green color decomposed POM. [d] Method (1): DCC, NHS, MeCN, r.t/12hr; (2): *t*-BuOH, EDC, MeCN, r.t/12hr; (3): EEDQ, MeCN, r.t/12hr; (4): BOP, MeCN, r.t/12hr.

[e] Product accompanying with partially decomposed POM could not be isolated.

The reactions explored indicated we needed reactants and conditions that would allow us to discriminate between the POM oxygens and the terminal amines as nucleophiles. We switched our focus to anhydrides and found that selected anhydrides fulfill these requirements perfectly. Anhydride based coupling was then systematically optimized (Scheme 2-4). These POM triester functionalization reactions exhibit high yield, high selectivity, and convenient purification without chromatography, etc. the features of “click-chemistry”.



Scheme 2-4. Reaction of hexavanadate triesters with cyclic or non-cyclic anhydrides.

The non-protic polar solvents in which the tetrabutylammonium (TBA) salt of POM triesters have relatively good solubility, such as CH₃CN, DMF, DMA, DMSO, NMP, could be effectively used depending on the solubility of anhydrides; sometimes a little heating is needed to dissolve the anhydrides at the beginning of the reaction. These anhydride couplings demonstrated good tolerance to organic bases such as stoichiometric triethylamine (TEA), pyridine or a catalytic amount of DMAP. Addition of such bases to the coupling processes could shorten the reaction time. It should be noted that in some reactions the negatively charged POM itself could play the same role as the base and thus addition of these bases have little effect. No added base simplified purification of the coupling product. Due to the localized D_{4h} symmetry of the anionic part of the bulky triesters **2** (~ 1.1 nm), the linear arrangement of two primary amines on each side did not impose much steric effect on the amidation reactions. Thus, most of the reactions reported here could be run at ambient temperature, although elevated temperature clearly shortens the reaction time especially for the sterically-hindered anhydride substrates.

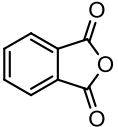
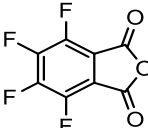
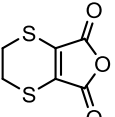
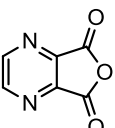
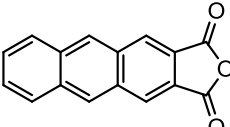
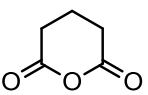
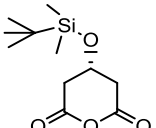
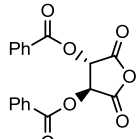
Another advantage of this approach is the convenient workup process. The products are normally insoluble in anhydrous Et₂O and so can be precipitated easily from the reaction solution by addition of this solvent. A small amount of excess of the

anhydride was thus left in the solvent and separated from the major product because because it is either soluble in ether or so soluble in reaction solvents, such as DMF, that it could not be precipitated from this solvent by ether addition. Further purification was effected by re-dissolving the products in anhydrous DMF and/or CH₃CN and then re-precipitating them with anhydrous ether. Crystallization by vapor diffusion works effectively for the final crystallization step. In most of the cases, single crystals of the products formed and the pure products were collected as crystalline solids.

To assess the generality of this synthetic route, the viability of normal anhydrides and the compatibility of POMs with other functionalities on the introduced anhydrides, were studied. Two major classes of anhydrides, cyclic anhydrides ranging from 7-membered to 5-membered rings and open-chain anhydrides, were intentionally selected for use in these reactions (Table 2-3 and 4). For all the cases shown here, the negatively charged POM species showed no evident side reaction with the other functional group(s) on the anhydride. For the condensation of the triesters with cyclic anhydrides, the reaction exhibits atom economy and the new carboxylic acid groups could also be simultaneously incorporated into the products. Significantly, these function groups deliberately incorporated into the hybrid molecules could be directly used as new coordination sites for further development of POM-containing coordination compounds. The well-elaborated principles of supramolecular architecture, including building block design, are applicable to the product functionalized POM-triester hybrids. The possibilities and rules for self assembly of POM-only (carbon-free) supramolecular structures aren't fully clear yet, but the myriad of organic-POM hybrids readily available through this mild anhydride coupling method should help address this intellectual and

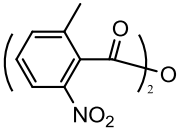
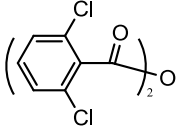
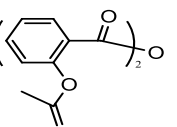
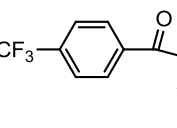
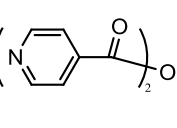
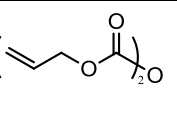
practical deficit. In addition, considering the commercial availability of thousands of anhydrides and the convenient preparation methods for many others in lab, this amide formation approach should be highly useful.

Table 2-3. Amidation of **1** with cyclic anhydrides

Entry	Anhydride	Reaction time/hr	Product, yield
1		8	2-a, 95
2		8	2-b, 95
3		10 ^[a]	2-c, 90
4		6	2-d, 94
5		16 ^[b]	2-e, 88
6		10	2-f, 96
7		10	2-g, 90
8		8	2-h, 96

[a] Stoichiometric amount of TEA was used. [b] Catalytic amount of DMAP was used and the reaction was heated to 60 °C for 30 minutes at the beginning.

Table 2-4. Amidation of of **1** with acyclic anhydrides

Entry	Anhydride	Reaction time/hr	Product, yield (%) ^[c]
1		8 ^[a]	2-i, 85
2		8	2-g, 90
3		16 ^[b]	2-k, 89
4		8	2-l, 91
5		12	2-m, 95
6		16 ^[b]	2-n, 80

[a] Stoichiometric amount of DMAP was used and the reaction temperature was 80 °C. [b]

Catalytic amount of DMAP was used and the reaction temperature was 70 °C.

We also proved the applicability of this synthetic route to other POM triesters by using the Anderson-type triester, [(MnMo₆O₂₄)NH₂]³⁻ (**3**).

The good crystallizability of the functionalized triesters portends well for study of the self-assembly of these molecules and the role of organic linkers in the solid state. Consider the crystal structure of fluorescent anthracyl functionalized **2** (Figure 2-5). The single crystal structure confirms amide bond formation and that the hybrid molecules exist only in the pure *trans*-configuration isomer (carboxylate-bearing side chains on

opposite sides of the POM and directly away from each other). This and X-ray structures of other organic-POM hybrids reveal the interactions that lead to self assembly of a 3-D network but also larger architectures.

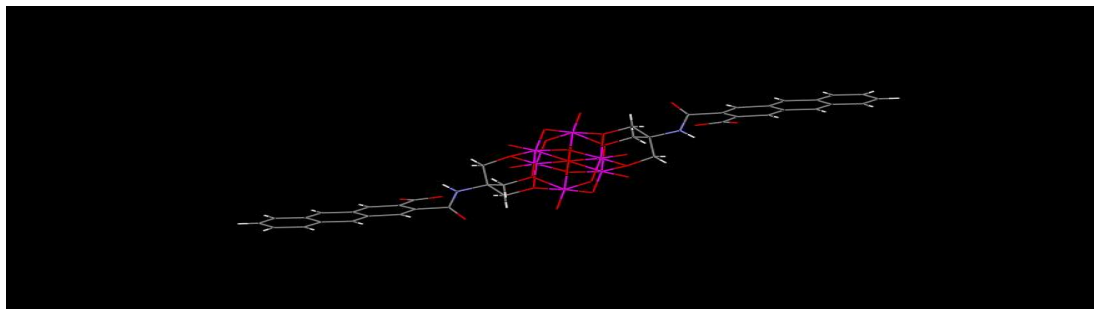


Figure 2-5. Single crystal structure of **2-e**. Cations and solvent molecules omitted for clarity.

Specifically, two adjacent molecules are connected by two p - π stacking interactions between the parallel aromatic anthracyl rings and two carbonyl groups of carboxylic acids with a distance of 3.370 Å (Figure 2-6). The well-ordered connection is further reinforced by the $H_{Anthracyl} \cdots O_{POM, terminal}$ hydrogen bonding (2.487 Å) between one hydrogen on the aromatic ring in one molecule and one terminal oxygen on the POM unit on another molecule. These interactions are relayed continuously to form the 1-D “ladder-shaped” chain (Figure 2-6).

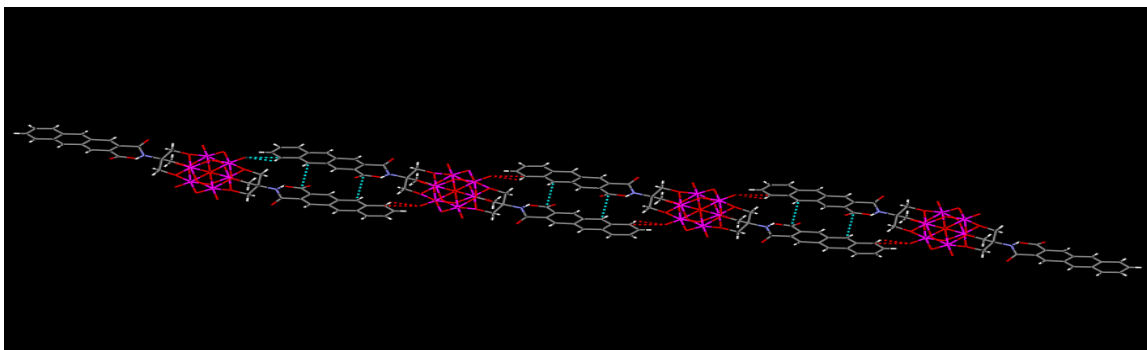


Figure 2-6. 1-D chain assembly of **2-e** via p- π stacking and H-bonding ($H_{org} \cdots O_{POM}$).

This 1-D ladder chain further connects with other adjacent parallel 1-D ladder chains via van der Waals forces to form 2-D “grandstand-like” network structures (Figure 2-7). One terminal oxygen and one bridging oxygen on a POM species in the first 1-D chain interacts with one hydrogen ($H_{Anthracyl} \cdots O_{POM, terminal} = 2.590 \text{ \AA}$) and two hydrogens ($H_{Anthracyl} \cdots O_{POM, bridging} = 2.522, 2.592 \text{ \AA}$) on one anthracyl ring in the second 1-D chain respectively.

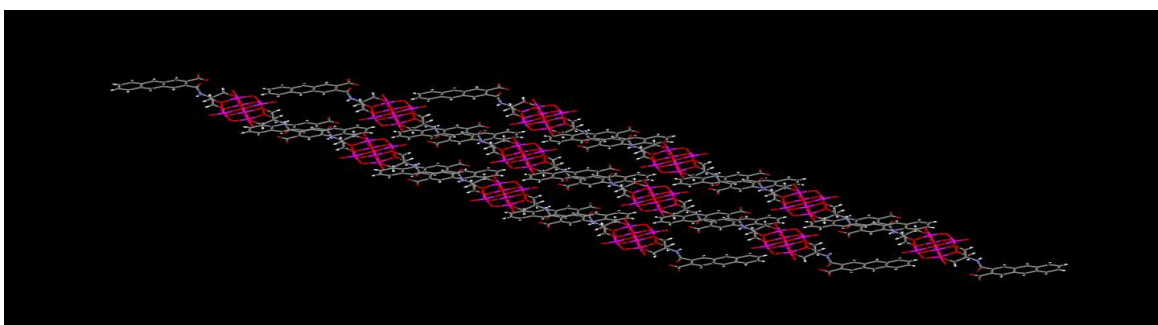


Figure 2-7. 2-D grandstand network of **2-e**.

Finally, the 3-D framework is constructed from the well-ordered 2-D grandstand network in a layer-by-layer fashion (layer-layer distance is *ca.* 11.50 \AA , see Figure 2-8).

TBA cations function as connectors between layers of the 2-D grandstand network, in which the weak van der Waals interactions such as $\text{C-H}_{TBA^+} \cdots \text{O}_{POM}$ and $\text{C-H}_{TBA^+} \cdots \text{H}_{Triester}\text{-C}$ interactions are evident. In addition to these weak forces, the stronger ionic attraction between anionic POM species and cationic TBA also directs the formation of the 3-D framework. The TBA cations also function as a template. Microporous channels form along the crystallographic a-axis, in which the longest and shortest dimensions were 11.818 and 8.384 Å respectively (Figure 2-9). Such 3-dimensional architectures lend themselves to exploration of the origins of micro-porosity, fluorescent properties of the conjugated aromatic systems, and catalytic activity of the vanadium-containing POMs. The free carboxylic acid groups on the walls of these channels could be further covalently modified or utilized as ligands to complex transition metals in the construction of POM-incorporated MOFs.

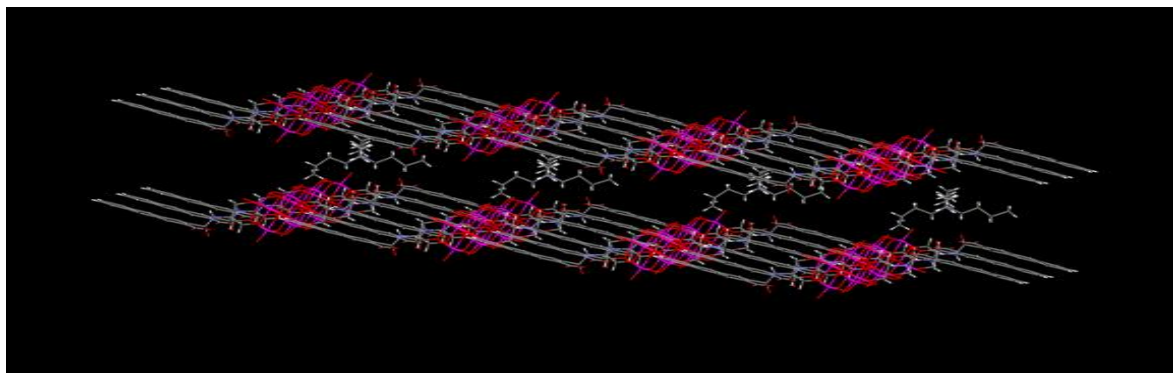


Figure 2-8. 3-D framework assembly of **2-e**. $\text{C-H}\cdots\text{O}$ -POM interaction and ionic attraction between POMs and TBA salts.

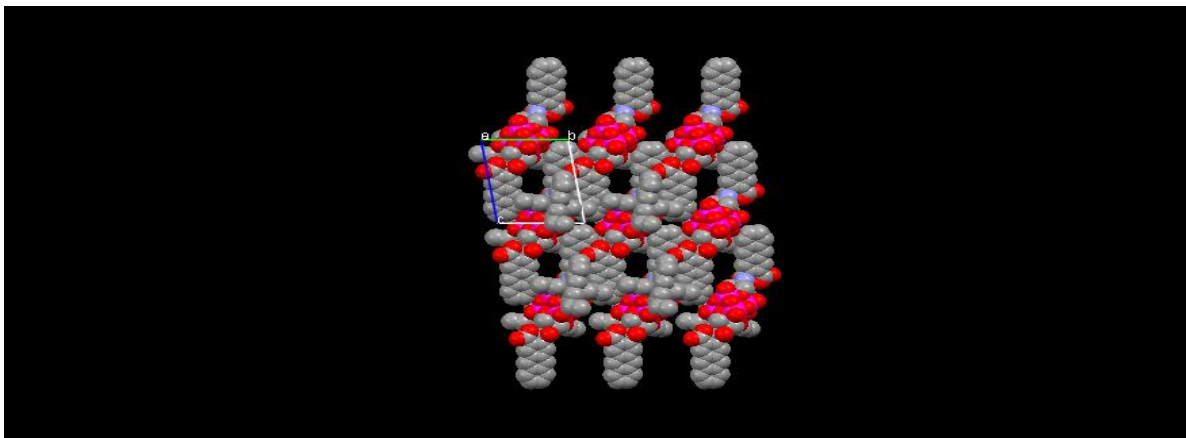


Figure 2-9. Space-filled 3-D framework of **2-e** showing its channels along *a*-direction.

Conclusions

A new dendritic POM, a hexavanadate with covalently-linked termini bearing six hydroxy groups has been prepared, structurally characterized and its catalytic applications in degradation of thiol, aldehyde, and hydrogen sulfide by aerobic oxidation under ambient conditions documented. This dendritic hexavanadate material can further react with Wells-Dawson polyanions via esterification to yield covalently-connected dumbbell-like hybrids. In addition, we have developed an efficient and broadly applicable protocol for the functionalization POM triesters using anhydrides, which could lead to very substantial family of organic-POM hybrids bearing a variety of functional groups. Such hybrids are of interest in context with potential applications in catalysis and supramolecular chemistry.

References

- (1) Hill, C. L. *Chem. Rev.* **1998**, *98*, 1.
- (2) Pope, M. T.; Müller, A. *Angew. Chem.* **1991**, *103*, 56.
- (3) Borrás-Almenar, J. J.; Coronado, E.; Müller, A.; Pope, M. T. *Polyoxometalate Molecular Science*; Kluwer Academic Publishers: Dordrecht, 2003; Vol. 98.
- (4) Hill, C. L. In *Comprehensive Coordination Chemistry-II: From Biology to Nanotechnology*; Wedd, A. G., Ed.; Elsevier Ltd.: Oxford, UK, 2004; Vol. 4, p 679.
- (5) Pope, M. T. In *Comprehensive Coordination Chemistry II: From Biology to Nanotechnology*; Wedd, A. G., Ed.; Elsevier Ltd.: Oxford, UK, 2004; Vol. 4, p 635.
- (6) Kögerler, P.; Cronin, L. *Angew. Chem. Int. Ed.* **2005**, *44*, 844.
- (7) Long, D.-L.; Burkholder, E.; Cronin, L. *Chem. Soc. Rev.* **2007**, *36*, 105.
- (8) Li, Q.; Wei, Y.; Hao, J.; Zhu, Y.; Wang, L. *J. Am. Chem. Soc.* **2007**, *129*, 5810.
- (9) Hill, C. L.; Okun, N. M.; Hillesheim, D. A.; Geletii, Y. V. In *Anti-Terrorism and Homeland Defense: Polymers and Materials, ACS Symposium Series 980, Chapter 12*; Reynolds, J. G., Lawson, G. E., Koester, C. J., Eds.; American Chemical Society: Washington, D.C., 2007, p 198.
- (10) Okun, N. M.; Anderson, T. M.; Hill, C. L. *J. Mol. Catal. A: Chem.* **2003**, *197*, 283.
- (11) Kholdeeva, O. A.; Timofeeva, M. N.; Maksimov, G. M.; Maksimovskaya, R. I.; Neiwert, W. A.; Hill, C. L. *Inorg. Chem.* **2005**, *44*, 666.
- (12) Okun, N. M.; Tarr, J. C.; Hilleshiem, D. A.; Zhang, L.; Hardcastle, K. I.; Hill, C. L. *J. Mol. Catal. A. Chem.* **2006**, *246*, 11.

- (13) Hill, C. L. *J. Mol. Catal. A: Chem.* **2007**, *262*, 2.
- (14) Müller, A.; Peters, F.; Pope, M. T.; Gatteschi, D. *Chem. Rev.* **1998**, *98*, 239.
- (15) Geletii, Y. V.; Botar, B.; Kögerler, P.; Hillesheim, D. A.; Musaev, D. G.; Hill, C. L. *Angew. Chem. Int. Ed.* **2008**, *47*, 3896.
- (16) Geletii, Y. V.; Huang, Z.; Hou, Y.; Musaev, D. G.; Lian, T.; Hill, C. L. *J. Am. Chem. Soc.* **2009**, *131*, 7522.
- (17) Geletii, Y. V.; Besson, C.; Hou, Y.; Yin, Q.; Musaev, D. G.; Quinonero, D.; Cao, R.; Hardcastle, K. I.; Proust, A.; Kögerler, P.; Hill, C. L. *J. Am. Chem. Soc.* **2009**, *131*, 17360.
- (18) Besson, C.; Huang, Z.; Geletii, Y. V.; Lense, S.; Hardcastle, K. I.; Musaev, D. G.; Lian, T.; Proust, A.; Hill, C. L. *Chem. Commun.* **2010**, 2784.
- (19) Yin, Q.; Tan, J. M.; Besson, C.; Geletii, Y. V.; Musaev, D. G.; Kuznetsov, A. E.; Luo, Z.; Hardcastle, K. I.; Hill, C. L. *Science* **2010**, *328*, 342.
- (20) Huang, Z.; Luo, Z.; Geletii, Y. V.; Vickers, J.; Yin, Q.; Wu, D.; Hou, Y.; Ding, Y.; Song, J.; Musaev, D. G.; Hill, C. L.; Lian, T. *J. Am. Chem. Soc.* **2011**, *133*, 2068.
- (21) Geletii, Y. V.; Yin, Q.; Hou, Y.; Huang, Z.; Ma, H.; Song, J.; Besson, C.; Luo, Z.; Cao, R.; OHalloran, K. P.; Zhu, G.; Zhao, C.; Vickers, J.; Ding, Y.; Mohebbi, S.; Kuznetsov, A. E.; Musaev, D. G.; Lian, T.; Hill, C. L. *Isr. J. Chem.* **2011**, *51*, 238.
- (22) Long, D.-L.; Abbas, H.; Kögerler, P.; Cronin, L. *J. Am. Chem. Soc.* **2004**, *126*, 13880.
- (23) Long, D.-L.; Kögerler, P.; Cronin, L. *Angew. Chem. Int. Ed.* **2004**, *43*, 1817.
- (24) Long, D.-L.; Kögerler, P.; Farrugia, L. J.; Cronin, L. *Chem. Asi. J.* **1**,

352.

- (25) Long, D.-L.; Streb, C.; Kögerler, P.; Cronin, L. *J. Cluster Sci.* **2006**, *17*,

257.

- (26) Miras, H. N.; Cooper, G. J. T.; Long, D.-L.; Bögge, H.; Müller, A.; Streb, C.; Cronin, L. *Science* **2010**, *327*, 72.

- (27) Miras, H. N.; Wilson, E. F.; Cronin, L. *Chem. Commun.* **2009**, 1297.

- (28) Mitchell, S. G.; Khanra, S.; Sanchez, P. M.; Miras, H. N.; Long, D.-L.; Cronin, L. *Angew. Chem.* **2011**, in preparation for submission.

- (29) Mitchell, S. G.; Streb, C.; Miras, H. N.; Boyd, T.; Long, D.-L.; Cronin, L. *Nature Chem.* **2010**, *2*, 308.

- (30) Noro, S.-i.; Tsunashima, R.; Kamiya, Y.; Uemura, K.; Kita, H.; Cronin, L.; Akutagawa, T.; Nakamura, T. *Angew. Chem. Int. Ed.* **2009**, *48*, 8703.

- (31) Pickering, A. L.; Long, D.-L.; Cronin, L. *Inorg. Chem.* **2004**, *43*, 4953.

- (32) Pradeep, C. P.; Long, D.-L.; Newton, G. N.; Song, Y.-F.; Cronin, L. *Angew. Chem. Int. Ed.* **2008**, *47*, 4388.

- (33) Ritchie, C.; Cooper, G. J. T.; Song, Y.-F.; Streb, C.; Yin, H.; Parenty, A. D. C.; MacLaren, D. A.; Cronin, L. *Nature Chem.* **2009**, *1*, 47.

- (34) Ritchie, C.; Ferguson, A.; Nojiri, H.; Miras, H. N.; Song, Y.-F.; Long, D.-L.; Burkholder, E.; Murrie, M.; Kögerler, P.; Brechin, E. K.; Cronin, L. *Angew. Chem. Int. Ed.* **2008**, *47*, 5609.

- (35) Song, Y.-F.; Long, D.-L.; Cronin, L. *Angew. Chem. Int. Ed.* **2007**, *46*, 3900.

- (36) Song, Y.-F.; Long, D.-L.; Cronin, L. *CrystEngComm* **2010**, *12*, 109.

- (37) Song, Y.-F.; McMillan, N.; Long, D.-L.; Kane, S.; Malm, J.; Riehle, M. O.;

Pradeep, C. P.; Gadegaard, N.; Cronin, L. *J. Am. Chem. Soc.* **2009**, *131*, 1340.

(38) Song, Y.-F.; McMillan, N.; Long, D.-L.; Thiel, J.; Ding, Y.; Chen, H.;

Gadegaard, N.; Cronin, L. *Chem. Eur. J.* **2008**, *14*, 2349.

(39) Yan, J.; Gao, J.; Long, D. L.; Miras, H. N.; Cronin, L. *J. Am. Chem. Soc.*

2010, *132*, 11410.

(40) Yan, J.; Long, D.-L.; Wilson, E. F.; Cronin, L. *Angew. Chem. Int. Ed.* **2009**,

48, 4376.

(41) Long, D.-L.; Cronin, L. *Chem. Eur. J.* **2006**, *12*, 3698.

(42) Han, J. W.; Hill, C. L. *J. Am. Chem. Soc.* **2007**, *129*, 15094.

(43) Khan, M. I.; Chen, Q.; Zubieta, J.; Goshorn, D. P. *Inorg. Chem.* **1992**, *31*,

1556.

(44) Khan, M. I.; Chen, Q.; Hope, H.; Parkin, S.; O'Connor, C. J.; Zubieta, J.

Inorg. Chem. **1993**, *32*, 2929.

(45) Daniel, C.; Hartl, H. *J. Am. Chem. Soc.* **2009**, *131*, 5101.

(46) Zeng, H.; Newkome, G. R.; Hill, C. L. *Angew. Chem. Int. Ed.* **2000**, *39*,

1771.

(47) Pradeep, C. P.; Misrahi, M. F.; Li, F.-Y.; Zhang, J.; Xu, L.; Long, D.-L.;

Liu, T.; Cronin, L. *Angew. Chem. Int. Ed.* **2009**, *48*, 8309.

(48) Han, J. W.; Hardcastle, K. I.; Hill, C. L. *Eur. J. Inorg. Chem.* **2006**, 2598.

(49) Chen, Q.; Goshorn, D. P.; Scholes, C. P.; Tan, X. L.; Zubieta, J. *J. Am.*

Chem. Soc. **1992**, *114*, 4667.

(50) Allain, C.; Favette, S.; Chamoreau, L.-M.; Vaissermann, J.; Ruhlmann, L.;

Hasenknopf, B. *Eur. J. Inorg. Chem.* **2008**, *2008*, 3433.

- (51) Hou, Y.; Hill, C. L. *J. Am. Chem. Soc.* **1993**, *115*, 11823.
- (52) Song, Y.-F.; McMillan, N.; Long, D.-L.; Kane, S.; Malm, J.; Riehle, M. O.; Pradeep, C. P.; Gadegaard, N.; Cronin, L. *J. Am. Chem. Soc.* **2009**, *131*, 1340.
- (53) Bonchio, M.; Carraro, M.; Scorrano, G.; Bagno, A. *Adv. Synth. Catal.* **2004**, *346*, 648.
- (54) Khan, M. I.; Chang, Y.; Chen, O.; Hope, H.; Parking, S.; Goshorn, D. P.; Zubieta, J. *Angew. Chem. Int. Ed.* **1992**, *31*, 1197.
- (55) Gouzerh, P.; Proust, A. *Chem. Rev.* **1998**, *98*, 77.
- (56) Khan, M. I.; Chen, Q.; Goshorn, D. P.; Hope, H.; Parkin, S.; Zubieta, J. *J. Am. Chem. Soc.* **1992**, *114*, 3341.
- (57) Johnson, B. J. S.; Geers, S. A.; Brennessel, W. W.; Young, J. V. G.; Stein, A. *Dalton Trans.* **2003**, 4678.
- (58) Kortz, U.; Vaissermann, J.; Thouvenot, R.; Gouzerh, P. *Inorg. Chem.* **2003**, *42*, 1135.
- (59) Johnson, B. J. S.; Schroden, R. C.; Zhu, C.; Young, V. G.; Stein, A. *Inorg. Chem.* **2002**, *41*, 2213.
- (60) Kortz, U.; Savelieff, M. G.; Ghali, F. Y. A.; Khalil, L. M.; Maalouf, S. A.; Sinno, D. I. *Angew. Chem. Int. Ed.* **2002**, *41*, 4070.
- (61) Breen, J. M.; Schmitt, W. *Angew. Chem. Int. Ed.* **2008**, *47*, 6904.

———— CHAPTER ————

3

**Inorganic-Organic Hybrid Vesicles with Counterion-
and pH-Controlled Fluorescent Properties**

Abstract

Two inorganic-organic hybrid clusters with one or two covalently-linked pyrene fluorescent probes, $[(n\text{-C}_4\text{H}_9)_4\text{N}]_2[\text{V}_6\text{O}_{13}\{(\text{OCH}_2)_3\text{C}(\text{NH}(\text{CO})\text{CH}_2\text{CH}_2\text{CH}_2\text{C}_{16}\text{H}_9)\}\{(\text{OCH}_2)_3\text{C}(\text{NH}_2)\}]$ (**(TBA⁺)₂1**) and $[(n\text{-C}_4\text{H}_9)_4\text{N}]_2[\text{V}_6\text{O}_{13}\{(\text{OCH}_2)_3\text{C}(\text{NH}(\text{CO})\text{CH}_2\text{CH}_2\text{CH}_2\text{C}_{16}\text{H}_9)\}_2]$ (**(TBA⁺)₂2**), are synthesized from Linqvist-type polyoxometalates (POMs). The incorporation of pyrene into POMs results in amphiphilic hybrid molecules and simultaneously offers a great opportunity to study the interaction between hybrid clusters and their counterions. 2D-NOESY NMR and fluorescence techniques have been used to study the role of counterions such as tetrabutyl ammonium (TBA) in the vesicle formation of the hybrid clusters. The TBA⁺ ions not only screen the electrostatic repulsions between the POM head groups but also are involved in the hydrophobic region of the vesicular structure where they interrupt the formation of pyrene excimers which greatly perturbs the luminescence signal from the vesicle solution. By replacing the TBA⁺ counterions with protons, the new vesicles demonstrate interesting pH-dependent fluorescence properties.

Introduction

Smart supramolecular assemblies that respond to single or multiple external stimuli, such as temperature,¹ ionic strength,² pH,³ redox,⁴ light,⁵ ultrasound⁶ and magnetic field⁷, are of great interest for their potential applications in drug delivery, oil recovery and design of new sensors and catalysts.⁸⁻¹³ While most smart supramolecular assemblies are constructed from organic molecules or block copolymers, incorporating

functional inorganic components (such as quantum dots, silica, transition metal ions, *etc.*) into organic building blocks to make functional hybrid assemblies represents an interesting new direction.^{5,6,14} Polyoxometalates (POMs), a large group of early-transition-metal oxide clusters, represents structurally well-defined inorganic molecules with diversified structures and properties.¹⁵⁻¹⁷ The synergistic combination of POMs and organic components gives these hybrids noteworthy properties of potential utility.¹⁸ For instance, polymers with grafted POMs can be used in photovoltaic cells or in trapping magnetic nanoparticles,^{19,20} and surfaces that are covered with hybrid POMs (SAM-POM-pyrene) show specific cell adhesion ability.²¹ Organo-POM hybrids²²⁻²⁶ have been shown to exhibit unusual spectroscopic properties²⁷ or catalyze oxidation reactions,²⁸⁻³⁰ organometallic POM clusters has been tested for norbornene and cyclohexene oxygenation as precatalysts³¹ and a recent study on a photoresponsive surfactant-encapsulated POM complex has shown an interesting dynamic structure transition in solution.³² The new hybrids with surfactant-like amphiphilic solution properties are particularly interesting because they can be compatible with both hydrophilic and hydrophobic environments and therefore can enhance the applications of the functional clusters. Interesting supramolecular structures such as micelles, vesicles, liquid crystals and 2D-films have been reported in various amphiphilic hybrid solutions.^{33,34,35} The self-assembly is dependent upon solvent polarity,³⁶ the hydrocarbon chain length,³⁷ the type and length of organic linkers,³⁸ and the architecture of the hybrids, as well as temperature.

Meanwhile, the development of fluorescent tags or probes opens new opportunities for smart molecules. Applying fluorescent probes to investigate biochemical micro-environments is a powerful technique which can often provide unique

and critical information. Pyrene, a highly symmetrical polyaromatic hydrocarbon fluorophore possessing restricted modes of motion, can exhibit fine structure in its absorbance and fluorescence spectra at room temperature.³⁹ One important application of the pyrene fluorescence stems from its ability to probe the polarity of the local micro-environment, either in a hydrophobic or hydrophilic media, from the change of specific emission peaks in the spectrum.^{40,41} Therefore, amphiphilic hybrid POM clusters with pendent pyrene fluorescent probes are of potential interest for the construction of smart supramolecular assemblies via macroion-counterion interaction.

It is an interesting question how the hybrid surfactants arrange themselves to form closely packed regions in the supramolecular structures. These hybrids differ from conventional surfactants in that they have large polar head groups making close packing of hydrophobic domains very difficult due to the spatial obstruction. We proposed, but without solid evidence, that the counter-ions might be important by perturbing the solvophobic layer formation.³⁸ The newly synthesized hybrid clusters with pyrene as fluorescent probes offer a unique opportunity to study this phenomenon.

Experimental section

Materials and Instruments. All reagents including deuterated solvent were obtained from commercial chemical vendors and used without further purification. Syntheses of two precursors, triester of Linqvist-type hexavanadate, $[(n\text{-C}_4\text{H}_9)_4\text{N}]_2[\text{V}_6\text{O}_{13}\{(\text{OCH}_2)_3\text{CNH}_2\}_2]$ (TBA-NH₂V₆) and 1-pyrenebutyric acid *N*-hydroxysuccinimide ester (PASE), were developed and reported here in details. All reactions were carried out under a dry argon atmosphere with anhydrous solvents under

anhydrous conditions and magnetically stirred with Teflon stir bars; temperatures were measured externally. Synthetic experiments were monitored by proton nuclear magnetic resonance (^1H NMR) spectroscopy recorded on a Varian INOVA 400 MHz instrument and chemical shifts (δ) were measured in parts per million (ppm) relative to the deuterated solvent used in the experiment. Yields refer to spectroscopically (^1H NMR spectroscopy) homogeneous materials. ^{51}V NMR spectra were recorded on a Varian Unity 600 MHz instrument and referenced externally by the sample replacement method to a 10 mM solution of $\text{H}_4\text{PVMo}_{11}\text{O}_{40}$ in 0.60 M NaCl solution (-533.6 ppm relative to neat VOCl_3) and chemical shifts were reported relative to VOCl_3 . Infrared spectra (IR) were recorded as KBr pellets on a Nicolet 510 FT-IR. Elemental analyses for C, H and, N were performed by Atlantic Microlab, Norcross, GA and elemental analyses for V all other elements were performed by Galbraith Laboratories, Knoxville, TN. X-ray crystallography studies were carried out in the X-ray Crystallography Laboratory at Emory University on a Bruker D8 SMART APEX CCD diffract meter.

Triester of Linqvist-type hexavanadate $[(n\text{-C}_4\text{H}_9)_4\text{N}]_2[\text{V}_6\text{O}_{13}\{(\text{OCH}_2)_3\text{CNH}_2\}_2]$ (TBA- NH_2V_6). The solid mixture of tris(hydroxymethyl)aminomethane (1.39 g, 11.1 mmol) and $[(n\text{-C}_4\text{H}_9)_4\text{N}]_3 [\text{H}_3\text{V}_{10}\text{O}_{28}]$ (6.24 g, 3.70 mmol) were dissolved in 75 mL of dry dimethylacetamide (DMA). The orange solution was stirred at 90 °C overnight (24 h). The resulting dark reddish brown solution was cooled to room temperature and added to 200 mL of diethyl ether to induce precipitation. To the gray precipitate, 40 mL of CH_3CN was added, and a small amount of insoluble solid was filtered off. To the filtrate, 20 mL of 6 M HCl was added over 1-2 min. While 6 M HCl was added to the filtrate, the color of solution was changed from the initial dark reddish brown to green and finally to deep

red, and a red precipitate formed. The solution was stirred for 1 h at room temperature. At the end of the stirring, the color of solution turned to green. The resulting precipitate was filtered and washed with water, CH₃CN, and diethyl ether. The red solid was suspended in 20 mL of CH₃CN/DMF (1/1). To the suspension, 6 mL of 1.0 M tetrabutylammonium hydroxide (TBAOH) in water was added dropwise. The red solid was completely dissolved when about 3.0 mL of 1.0 M TBAOH in water was added. The resulting solution was added to 200 mL of diethyl ether to be precipitated. The sticky precipitate was redissolved in ca. 30 mL mixed solvent (CH₃CN/DMF = 2:1), and diffusion of ether into the solution over one week resulted in the formation of needle-like crystals that was used for the following amide reactions. Yield: 5.9% (based on vanadium). ¹H NMR (400 MHz, DMSO-*d*₆, 25 °C) 4.66 (s, 12H; -C(CH₂O)₃-), 3.19 (t, 16H; (CH₃CH₂CH₂CH₂)₄N⁺), 1.56 (quin, 16H; (CH₃CH₂CH₂CH₂)₄N⁺), 1.47 (s, 4H; -NH₂), 1.34-1.29 (sext, 16H; (CH₃CH₂CH₂CH₂)₄N⁺) 0.94-0.91 ppm (t, 24H; (CH₃CH₂CH₂CH₂)₄N⁺); ¹³C NMR (100 MHz, DMSO-*d*₆, 25 °C): δ=86.3(-C(CH₂O)₃-), 57.5 ((CH₃CH₂CH₂CH₂)₄N⁺), 48.5(-C(CH₂O)₃-), 23.1((CH₃CH₂CH₂CH₂)₄N⁺), 19.2((CH₃CH₂CH₂CH₂)₄N⁺), 13.5 ((CH₃CH₂CH₂CH₂)₄N⁺) ppm ; ⁵¹V NMR (600 MHz, DMSO-*d*₆, 25 °C): δ = 494.8 ppm; FT-IR (KBr): ν̃= 3364 (br), 2961 (m), 2784 (m), 2845 (m, sh), 1482 (m), 1379 (w), 1061 (s), 950 (s), 821 (m), 796 (s), 720 (s), 577 (m), 515 (w), 470 (w), 418 (s) cm⁻¹; elemental analysis calcd (%) for C₄₀H₈₈N₄O₁₉V₆: C, 38.91; H, 7.18; N, 4.54; V, 24.75; found: C 38.78; H 7.24, N 4.49, V 24.65. Tetramethylammonium (TMA⁺), tetraethylammonium (TEA⁺), and zwitterion salts, TMA-NH₂V₆, TEA-NH₂V₆ and NH₃V₆ were obtained via cation-exchange resin from the TBA⁺ salt and confirmed by ¹H NMR. X-ray single crystal structures of TBA-NH₂V₆ and NH₃V₆ were solved and

shown here.

1-Pyrenebutyric acid *N*-hydroxysuccinimide ester (PASE)

An anhydrous CH₃CN (5 mL) solution of *N*-hydroxysuccinimide (0.115 g, 1.0 mmol), 1-pyrenebutyric acid (0.288 g, 1.0 mmol) and dicyclohexylcarbodiimide (0.227 g, 1.1 mmol) was vigorously stirred under argon for over 24 hr at room temperature. Then the reaction solution was filtered quickly through a fine-porosity frit and the solvent was removed under reduced pressure to give the yellow solid target compound. Further purification was made using methanol diffusion into acetonitrile solution or by crystallization from methanol. Yield 0.30 g (77.8%) ¹H NMR (400 MHz, CDCl₃, 25 °C): 2.25 (m, 2H; PyCH₂CH₂CH₂), 2.66 (t, 2H; PyCH₂CH₂CH₂CO), 2.77 (s, 4H; COCH₂CH₂CO), 3.39 (t, 2H; ArCH₂CH₂), 8.22-7.77 (m, 9H; PyH).

Synthesis of hybrid clusters. The synthesis of these two covalently-linked pyrene-POM molecules with tetrabutylammonium cations ($[(n\text{-C}_4\text{H}_9)_4\text{N}]^+$ or TBA⁺), $[(n\text{-C}_4\text{H}_9)_4\text{N}]_2[\text{V}_6\text{O}_{13}\{(\text{OCH}_2)_3\text{C}(\text{NH}(\text{CO})\text{CH}_2\text{CH}_2\text{CH}_2\text{-C}_{16}\text{H}_9)\}\{(\text{OCH}_2)_3\text{C}(\text{NH}_2)\}]$ ((TBA⁺)₂1), and $[(n\text{-C}_4\text{H}_9)_4\text{N}]_2[\text{V}_6\text{O}_{13}\{(\text{OCH}_2)_3\text{C}(\text{NH}(\text{CO})\text{CH}_2\text{CH}_2\text{CH}_2\text{C}_{16}\text{H}_9)\}_2]$ ((TBA⁺)₂2) is described below in detail and also depicted in Scheme 3-1. (TMA⁺)₂1, (TEA⁺)₂1, (TMA⁺)₂2 and (TEA⁺)₂2 were correspondingly synthesized by either using TMA-NH₂V₆ and TEA-NH₂V₆ as starting materials or cation-exchanging method from (TBA⁺)₂1 or (TBA⁺)₂2.

Synthesis of (TBA⁺)₂1 Under an argon atmosphere, a solution of PASE (16.2 mg, 0.041 mmol) in anhydrous DMF (5 mL) was slowly injected into the solution of TBA-NH₂V₆ (500 mg, 0.411 mmol) and a catalytic amount of 4-dimethylaminopyridine (~ 1 mg) in anhydrous DMF (25 mL) over a period of 8 hours. The resulting orange-red solution was

stirred under argon at room temperature for another 24 hours. When the reaction was finished, the reaction solution was dropwise added to anhydrous diethyl ether (150 mL) to get yellow precipitate. The precipitate was then collected by centrifugation and re-dissolved with anhydrous DMF and re-precipitate with anhydrous diethyl ether twice to remove the side products. After drying the precipitate under vacuum for 2 hours, it was re-dissolved in DMF-acetonitrile (5 mL, v/v = 2:1) and HCl solution (0.5 mL of 10 M in aqueous solution or 3 mL of 2.0 M in diethyl ether) was dropwise added to this solution with vigorously stirring. After stirring for 30 minutes, the resulting solution was centrifuged to remove any precipitate from the red solution and then added dropwise to diethyl ether (50 mL). The product yellow precipitate that was collected and dried using a fine-porosity frit by suction filtration. The yellow powder was then dissolved in anhydrous DMF (2 mL) and titrated with two equivalents of TBAOH in methanol. The mixture in the resulting solution was crystallized by slow ether diffusion. Orange-yellow crystalline solids formed after 7 days and were isolated, crystallized a second time, and dried under vacuum overnight before characterization. The reaction and purification process via cation exchange method were monitored by ^1H NMR spectra. Yield 0.027 g (46%) ^1H NMR (400 MHz, $\text{DMSO-}d_6$, 25°C) $\delta=8.32-7.32$ (m, 9H; ArH and s, 2H; -C(O)NH-), 5.14 (s, 6H; -C(O)NHC(CH₂O)₃-), 4.67 (s, 6H; NH₂C(CH₂O)₃-), 3.25 (t, 4H; ArCH₂CH₂CH₂C(O)NH-), 3.12 (t, 16H, (CH₃CH₂CH₂CH₂)₄N⁺), 2.19 (t, 4H; ArCH₂CH₂CH₂C(O)NH-), 1.94 (quin, 4H; ArCH₂CH₂CH₂C(O)NH-) 1.53 (quin, 16H; (CH₃CH₂CH₂CH₂)₄N⁺), 1.30-1.24 (sext, 16H; (CH₃CH₂CH₂CH₂)₄N⁺), 0.92-0.88 ppm (t, 24H; (CH₃CH₂CH₂CH₂)₄N⁺) and solvent (DMF) peaks; ^{13}C NMR (100 MHz, $\text{DMSO-}d_6$, 25°C) $\delta = 170.9, 136.2, 130.8, 130.1, 129.8, 128.2, 126.8, 126.9, 126.6, 126.0, 125.5,$

123.8, 122.5, 123.3, 123.1, 81.2, 77.8, 72.8, 56.9, 48.1, 36.4, 30.9, 22.3, 18.6, 13.2 ppm; FT-IR (KBr): $\tilde{\nu}$ =3430(br), 3260(br), 3019(w), 2973(s), 2917(s), 2862(s), 1666(s), 1610(w), 1554(m), 1476(s), 1383(m), 1312(w), 1254(w), 1176(w), 1122(w), 1068(s), 947(s), 845(m), 806(s), 796(w), 716(s), 586(s), 451(w), 410(s) cm^{-1} ; elemental analysis calcd (%) for $\text{C}_{60}\text{H}_{102}\text{N}_4\text{O}_{20}\text{V}_6 \cdot 2\text{DMF}$: C 48.00, H 7.08, N 5.09; found: C 46.76, H 7.60, N 4.89.

Synthesis of $(\text{TBA}^+)_2\mathbf{2}$ Pyrenebutyric acid *N*-hydroxysuccinimide ester (34.3 mg, 0.089 mmol), TBA- NH_2V_6 (50 mg, 0.041 mmol) and 4-dimethylaminopyridine (~ 1 mg) were dissolved in anhydrous DMF (3.0 mL) and the resulting orange-red solution was stirred under argon at room temperature for around 24 hours. When the reaction was finished, the reaction solution was dropwise added to anhydrous diethyl ether (50 mL) to get yellow precipitate. The precipitate was then collected and re-dissolved with anhydrous DMF and re-precipitate with anhydrous diethyl ether twice to remove the side products and a slight excess of unreacted pyrenebutyric acid *N*-hydroxysuccinimide ester. After drying the precipitate under vacuum, compound **2** was further purified by re-dissolving in DMF-acetonitrile (5 mL, v/v = 2:1) and allowing ether to slowly diffuse into the solution to facilitate crystallization. Orange-red single crystals formed after 3 days and were used for characterization after drying under vacuum overnight. Yield 0.068 g (85%). ^1H NMR (400 MHz, $\text{DMSO-}d_6$, 25 $^\circ\text{C}$) δ =8.32-7.33 (m, 18H; ArH and s, 2H; -C(O)NH-), 5.12 (s, 12H; -C(CH₂O)₃-), 3.26 (t, 4H; ArCH₂CH₂CH₂C(O)NH-), 3.12 (t, 16H, (CH₃CH₂CH₂CH₂)₄N⁺), 2.19 (t, 4H; ArCH₂CH₂CH₂C(O)NH-), 1.94 (quin, 4H; ArCH₂CH₂CH₂C(O)NH-) 1.53 (quin, 16H; (CH₃CH₂CH₂CH₂)₄N⁺), 1.30-1.24 (sext, 16H; (CH₃CH₂CH₂CH₂)₄N⁺), 0.92-0.88 ppm (t, 24H; (CH₃CH₂CH₂CH₂)₄N⁺) and solvent

(DMF) peaks; ^{13}C NMR (100 MHz, $\text{DMSO-}d_6$, 25°C) δ = 171.4, 136.5, 131.2, 130.8, 129.2, 128.4, 127.3, 127.2, 126.4, 126.1, 125.0, 124.8, 124.3, 124.1, 123.3, 81.6, 78.8, 57.4, 49.6, 37.2, 31.4, 23.0, 19.2, 13.5 ppm; FT-IR (KBr): $\tilde{\nu}$ =3421(br), 3290(br), 3027(w), 2958(s), 2923(s), 2852(s), 1662(s), 1603(w), 1540(m), 1466(s), 1378(m), 1307(w), 1245(w), 1184(w), 1118(w), 1074(s), 952(s), 848(m), 810(s), 799(w), 721(s), 583(s), 459(w), 416(s) cm^{-1} ; elemental analysis calcd (%) for $\text{C}_{80}\text{H}_{116}\text{N}_4\text{O}_{21}\text{V}_6 \cdot \text{DMF}$: C 53.93, H 6.71, N 3.79; found: C 53.68, H 6.77, N 3.76.

X-ray Crystallography. X-ray quality crystals of NH_3V_6 , $\text{TBA-NH}_2\text{V}_6$, and $(\text{TBA}^+)_2\mathbf{2}$ were coated with Paratone N oil and mounted on a small fiber loop for index and intensity data collection. The X-ray diffraction data were collected under a nitrogen stream at 173 K on a Bruker D8 SMART APEX CCD single-crystal diffractometer with graphite monochromated Mo $\text{K}\alpha$ ($\lambda = 0.71073 \text{ \AA}$) radiation. Data collection, indexing, and initial cell refinements were processed using the SMART⁴² software; while frame integration and final cell refinements were carried out using the SAINT⁴³ software. The final cell parameters were determined from the least-squares refinement of total reflections. The structures were determined through direct methods (SHELXS97) and difference Fourier maps (SHELXL97). The final results of crystal data and structure refinement are summarized in Table 3-1. The Cambridge Crystallographic Data Centre deposition number for NH_3V_6 , $\text{TBA-NH}_2\text{V}_6$, and $(\text{TBA}^+)_2\mathbf{2}$ are CCDC 821763, 821764, and 821765, respectively.

Cation Exchange. Counterion replacement of TBA^+ with H^+ was achieved by using a

cation-exchange resin column. For a typical experiment, 5 mg of hybrid cluster **1** or **2** was dissolved in 2 mL of acetonitrile. This solution was then applied to a pre-packed, cation-exchange resin column (Amberjet 1200 hydrogen form purchased from Sigma-Aldrich) rinsed with D. I. water and acetonitrile. An additional 20 to 50 mL of acetonitrile was used to elute the column and the yellow fraction was collected. The post elution was further washed with 5 mL of diethyl ether to remove organic impurities. The final solution was transferred into a glass culture plate and kept in the dark for several days to fully evaporate the solvent. Yellow colored fine powders were collected and could be easily dissolved in water or DMSO for further study.

Laser Light Scattering. Both Dynamic Light Scattering (DLS) and Static Light Scattering (SLS) techniques were used to characterize the self-assembly of hybrids in solution. A Brookhaven Instruments *Inc.* light scattering spectrometer, equipped with a diode-pumped solid-state (DPSS) laser operating at 532 nm and a BI-9000AT multi-channel digital correlator was used for all experiments. The SLS was performed over a broad range of scattering angles from 30 ° to 130 °, with a 2 ° interval. The radius of gyration (R_g) and the weight-average molecular mass (M_w) of the large assemblies were calculated using the Rayleigh-Gans-Debye equation⁴⁴:

$$Hc/R_{90} = 1/M_w + 2A_2 * c \quad (1)$$

where H is an optical parameter; M_w is the weight-average molecular mass of the solutes; A_2 is the second virial coefficient and c is the solute concentration. The $2A_2c$ term is neglected during calculations because the sample solutions examined in this study have very low concentrations.

For DLS measurements, the intensity-intensity time correlation functions were analyzed by the constrained regularized (CONTIN) method in order to ascertain the average hydrodynamic radius (R_h) of the large assemblies. The average apparent translational diffusion coefficient, D_{app} was determined from the normalized distribution function of the characteristic line width, $\Gamma(G)$. The hydrodynamic radius R_h is converted from D through the Stokes–Einstein equation:

$$R = k_B T / 6\pi\eta D \quad (2)$$

where k_B is the Boltzmann constant and η the viscosity of the solvent at temperature T . The particle size distribution in solution can be obtained by plotting $\Gamma G(\Gamma)$ versus R_h , with $\Gamma_i G_i$ (Γ_i) being proportional to the angular-dependent scattered intensity of particle i having an apparent hydrodynamic radius $R_{h,i}$. The temperature in the sample chamber was controlled to within ± 0.1 °C. More details about SLS and DLS can be found in our previous publications.⁴⁵

All the catalytic experiments were set up, carried out, and analyzed by Dr. Zhen Luo.

Transmission Electron Microscopy (TEM). Samples for electron microscopy characterization were prepared by pipeting 5 μ L of diluted solution onto a carbon-coated TEM grid. The TEM samples were left under ambient conditions for several hours until the solvent completely evaporated. Bright-field (BF) TEM imaging was performed on a JEOL 2000FX transmission electron microscope having an accelerating voltage of 200 kV.

Zeta (z) Potential Analysis. All the z potential analysis measurements were performed on a Brookhaven Instrument Inc. Zeta PALS Analyzer. The instrument is equipped with a red laser operating at 660 nm wavelength and has an accuracy of $\pm 2\%$ for filtrated samples. The sample chamber was kept at 25 ± 0.1 °C and all sample solutions were loaded 30 min prior to measurements in order to achieve thermal equilibrium with the chamber.

Nuclear Magnetic Resonance Spectroscopy. All 1D and 2D ^1H NMR measurements in the liquid state were performed on a Bruker Avance 500 spectrometer equipped with a 5 mm triple-axis gradient (TXI) probe. 2-D Nuclear Overhauser Enhancement Spectroscopy (2-D NOESY) spectra were recorded with 256 t_1 increments and 64 scans under the pulse program of noesygp19 provided with Topspin 1.3. The relaxation delay D1 varied from 1 – 2s and the mixing time D8 changed from 0.1 – 0.5s. Baseline correction and noise reduction were performed when appropriate. All spectra were taken at room temperature and FIDs were processed and analyzed with the NMR software provided by Bruker.

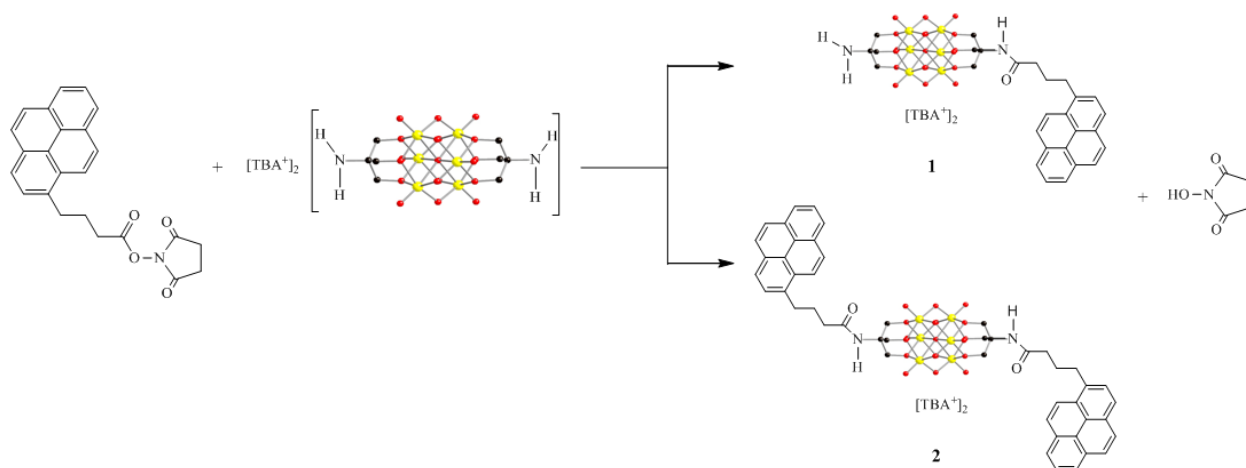
Fluorescence Measurements. Fluorescence spectra were recorded at room temperature on a Cary Eclipse fluorescence spectrophotometer. The excitation wavelength, λ_{exc} , used was 335 nm and the spectrum width was from 350 nm to 700 nm. An emission filter of 360 nm - 1100 nm was used. Each spectrum was obtained by averaging three scans and corrected for scatter of the equivalent blank sample. In calculations of the excimer-to-monomer intensity ratio, the monomer (I_M) and the excimer (I_E) were determined by

taking the integrals under the fluorescence peaks from 350 to 430 nm for the pyrene monomer and from 430 to 700 nm for the pyrene excimer.³⁹

Results and Discussion

Synthesis and characterization of hybrid (TBA⁺)₂1** and (TBA⁺)₂**2**.** The synthetic protocol was developed here to efficiently construct a new type of POM-based inorganic-organic hybrid (Scheme 3-1). Based on the idea that succinate (NHS) esters show high reaction selectivity to N-termini in negatively-charged protein modification, the primary amine groups symmetrically attached on the two opposite faces of a negatively-charged hexavanadate were further functionalized by reacting with a pyrene-containing succinate ester (**PASE**) at room temperature, to give the desired hybrids via efficient amide bond formation. By tuning the PASE/TBA-NH₂V₆ molar ratio in the reaction, asymmetric hybrid compounds, **1** (only one amine group reacted) and symmetric hybrid compounds, **2** (both of two amine groups reacted), were obtained, respectively, in high yield and selectivity. In general, when two equivalents of **PASE** were used, the symmetric product, **2**, is produced in 85% yield and the asymmetric product, **1**, in 46% yield. The reaction process could be conveniently tracked using ¹H NMR to monitor the chemical shift of methylene group protons, -C(O)NHC(CH₂O)₃-, which are directly linked to the hexavanadate via oxygen. The separation and consequent purification of **2** is relatively easier than that of **1** due to the excess of the hexavanadate precursor, TBA-NH₂V₆, in the reaction solution. However, the purification method developed here, adding HCl to protonate the amine groups and precipitation of the extra precursor by forming charge-neutral zwitterions, work effectively to isolate the target

hybrid from the reaction mixture. The organic by-product, *N*-hydroxylsuccinimide could be removed by using the solubility difference in DMF-ether solution. The purity of the final products was confirmed by multiple techniques, with 1D and 2D ^1H NMR providing especially informative data on the solution properties of these hybrid polyanions.



Scheme 3-1. The construction of hybrids **1** and **2**.

The molecular structures of $\text{TBA-NH}_2\text{V}_6$ and **2** were also determined from single crystal X-ray diffraction (Table 3-1). In $\text{TBA-NH}_2\text{V}_6$, TBA cations form honeycomb-like structure and the hexavanadate anions with two negative charges are trapped in each of the channels. For comparison, hybrid **2** with the same charge as its precursor packs in a layer-by-layer fashion, in which the pyrene groups of the hybrid POM anions are in one layer (but not overlapping), the $[\text{V}_6\text{O}_{19}]$ units reside in a second layer and the TBA cations reside in third. Although we have not been able to obtain high quality single crystals of **1** suitable for X-ray study to date, the packing mode of this asymmetric hybrid could be different from both its precursor and **2** due to its one-side hydrophilic POM head (Figure 3-1).

Table 3-1. Crystallographic Data for NH_3V_6 , TBA- NH_2V_6 and TBA-2

	NH_3V_6	TBA- NH_2V_6	TBA-2
empirical formula	$\text{C}_{16}\text{H}_{42}\text{N}_2\text{O}_{23}\text{S}_4\text{V}_6$	$\text{C}_{40}\text{H}_{88}\text{N}_4\text{O}_{19}\text{V}_6$	$\text{C}_{75}\text{H}_{103}\text{N}_{4.5}\text{O}_{22.5}\text{V}_6$
formula weight	1064.40	1234.78	1733.26
crystal system	monoclinic	orthorhombic	monoclinic
space group	$P2(2)/c$	$Ibca$	$C2/c$
unit cell	$a = 11.9050(17) \text{ \AA}$ $b = 14.3684(19)$ $c = 11.9050(17)$ $\alpha = 90^\circ$ $\beta = 117.48$ $\gamma = 90$	$a = 20.8395(7) \text{ \AA}$ $b = 20.0194(7)$ $c = 24.8572(8)$ $\alpha = 90^\circ$ $\beta = 90$ $\gamma = 90$	$a = 37.7321(12) \text{ \AA}$ $b = 18.0806(5)$ $c = 24.0340(8)$ $\alpha = 90^\circ$ $\beta = 109.719(2)$ $\gamma = 90$
$V/\text{\AA}^3$	1806.6(4)	11924.3(7)	15434.9(8)
Z	2	8	8
$D_c/\text{g} \cdot \text{cm}^{-3}$	1.957	1.376	1.492
T/K	173(2)	173(2)	173(2)
μ/mm^{-1}	Semi-empirical from equivalents	0.967	0.775
reflns collected	18227	64944	61681
unique reflns	2966	6113	15770
GOF	1.022	1.027	1.021
final $R_1^a [I > 2\sigma(I)]$	0.0781	0.0418	0.0867
final $wR_2^b [I > 2\sigma(I)]$	0.1690	0.1056	0.2193

$$^a R_1 = \frac{\sum ||F_0| - |F_c||}{\sum |F_0|}; \quad ^b wR_2 = \frac{\sum [w(F_0^2 - F_c^2)^2]}{\sum [w(F_0^2)^2]}^{1/2}$$

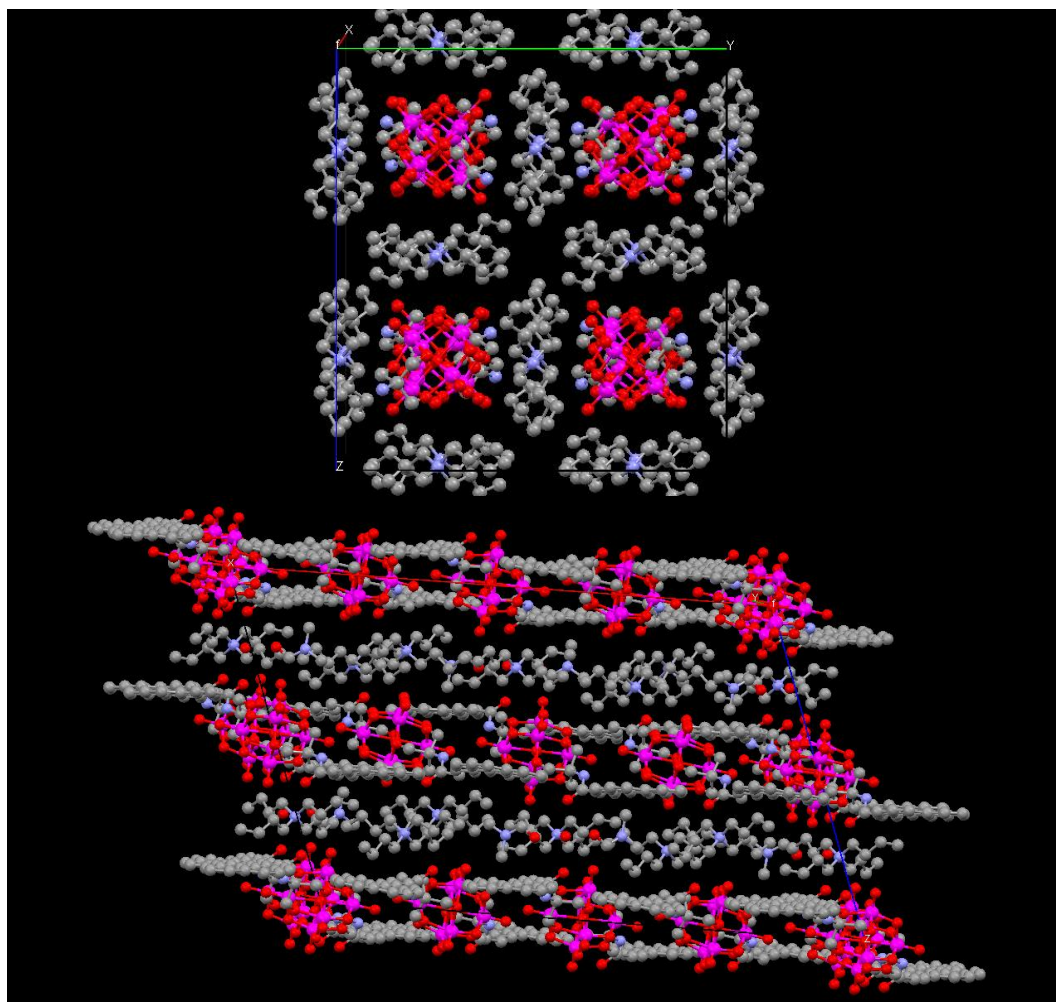


Figure 3-1. Three-dimensional packing of TBA-NH₂V₆ (**top**) and TBA-2 (**bottom**) (views along a-axis) showing the arrangement of TBA cations around associated POMs (bottom).

Molecular packing in the unit cells of (TBA⁺)₂2 shows several supramolecular interactions between the polyanions in solid state, which include limited pyrene-pyrene π stacking (the closest distance between two adjacent carbons on two pyrene rings is *ca.* 0.335 nm) and H-bonding between the amide -NH- and a terminal POM oxygen (the N...O distance is *ca.* 0.286 nm) (Figure 3-2).

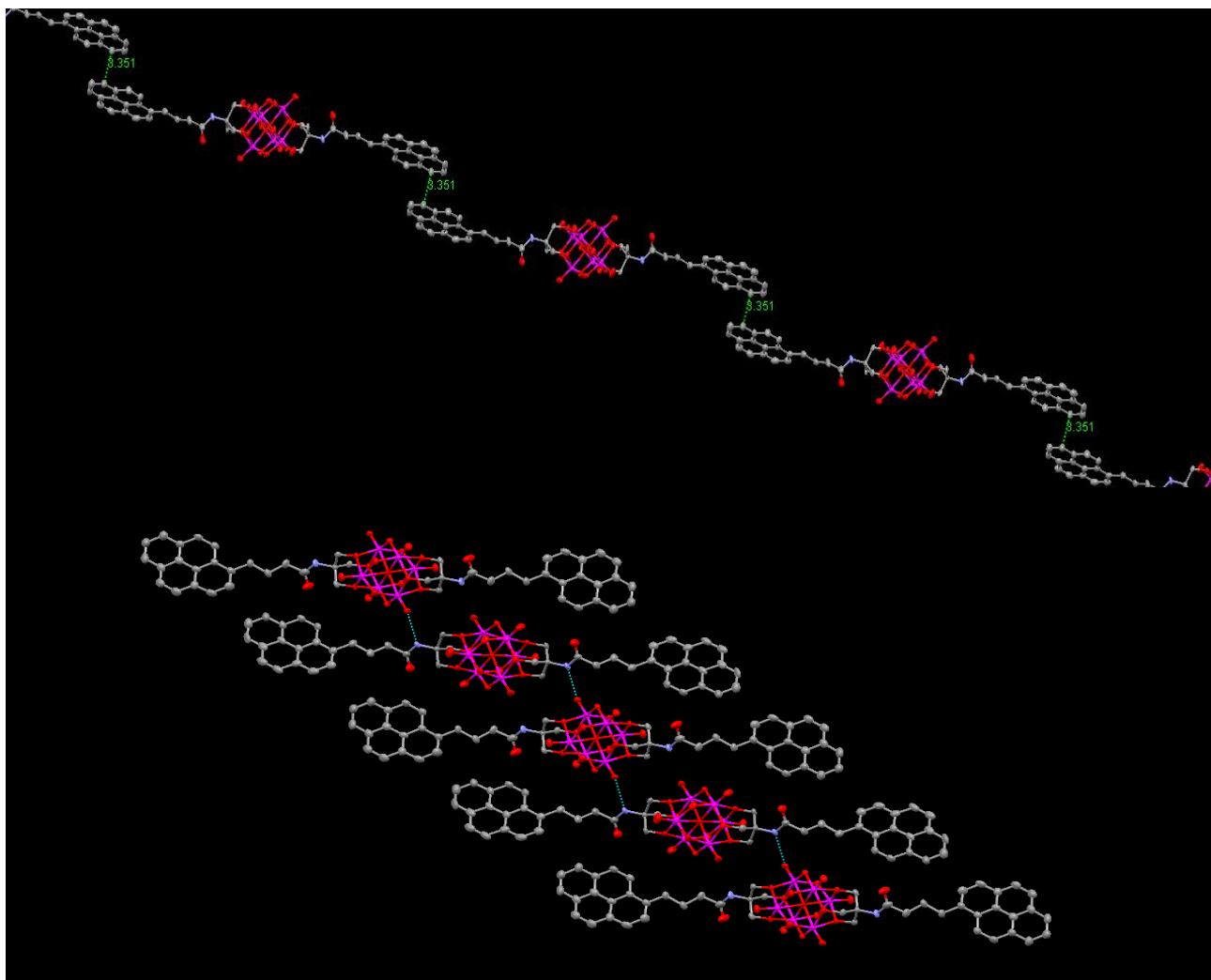
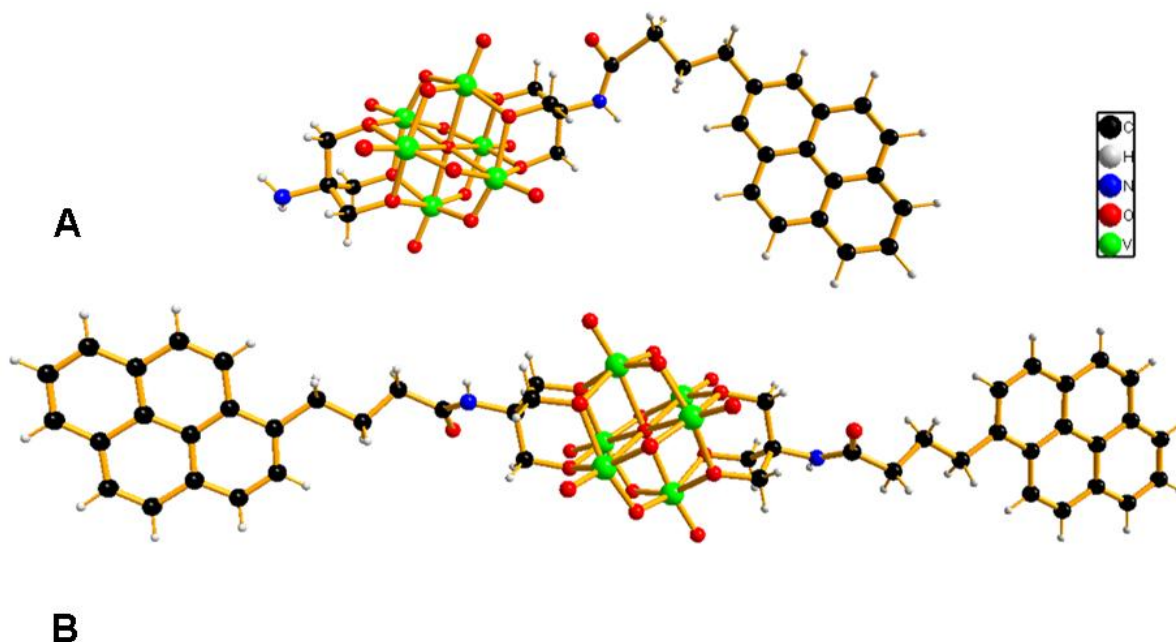


Figure 3-2. Weak intermolecular interactions between the hybrid cluster **2**. Top: π - π staking between two adjacent pyrene groups (distance between two aromatic planes are less than 3.351 Å and the green dot line shows the most adjacent two carbon atoms on two pyrenes). Bottom: H-bonding between the hydrogen atoms on amide groups in one POM and one of the terminal oxygens on another.

Such interactions could well be operable in the vesicles and are expected to play a role in solution aggregation. The length of the hydrophobic region is critical to the overall amphiphilic property of the hybrid cluster, as well as the self-assembled supramolecular

structures. At the same time, POMs are well-known electron acceptors so fluorescence quenching by the clusters was a concern at the outset.⁴⁶ Therefore, we targeted complexes in which the pyrene fluorophores were separated from the POM head groups by a four-carbon hydrocarbon chain. Later we determined that this hydrocarbon chain maintains flexibility in the hydrophobic component and also preserves the pyrene fluorescence.



Scheme 3-2. The molecular structure of two novel polyoxometalates hybrid cluster anions **1** and **2** shown in combined ball-and-stick representation. Atoms are represented by: V green, N blue, O red, C black, H white.

Characterization of the amphiphilic properties of hybrids 1 and 2 in polar solvents. As shown in Scheme 3-2, two novel POM based inorganic-organic hybrids are constructed by incorporating one or two pyrene functional groups onto one Lindqvist-type polyoxovanadate $[V_6O_{13}\{(OCH_2)_3CNH_2\}]^{2-}$. The linkage of flexible, hydrophobic organic tails to the inorganic POM head groups renders these new species amphiphilic.

Hybrids (TBA⁺)₂**1** and (TBA⁺)₂**2** are insoluble in water but can be readily dissolved in dimethyl sulfoxide (DMSO), dimethyl formamide (DMF) and other polar organic solvents. For 0.1 mg/mL of hybrid (TBA⁺)₂**1** in DMSO, a very low scattered intensity (~45 Kcps) was collected from SLS measurements (for comparison, the scattered intensity of pure solvent is ~ 40 Kcps), indicating that the hybrid molecules prefer to remain as monomers in solution rather than large assemblies. However, when additional water was introduced to make a solvent containing up to 70 vol% water, the total scattered intensity starts to increase significantly, and supramolecular structures are observed under DLS, as shown in Figure 3-3.

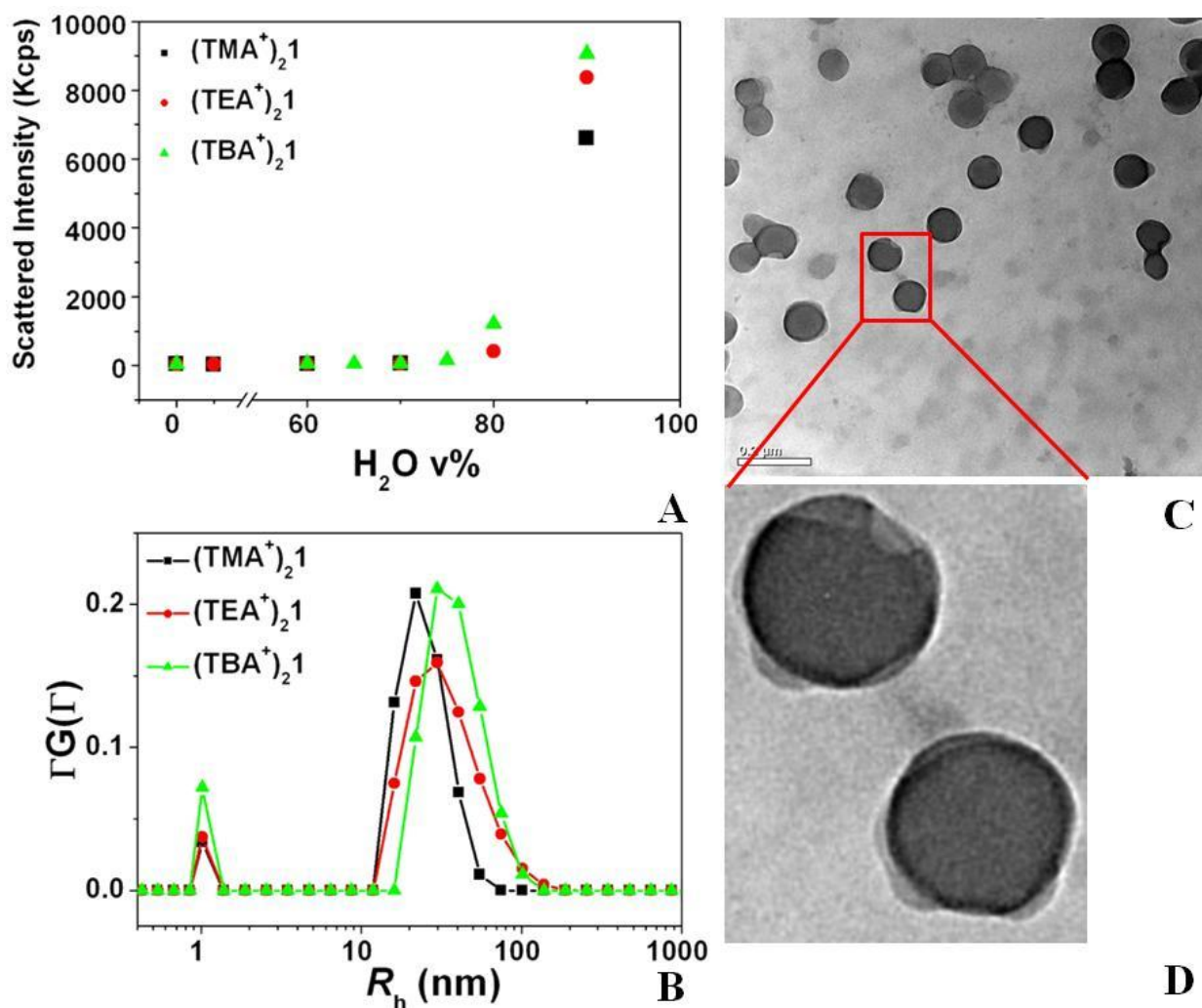


Figure 3-3. (A) The total scattered intensity recorded by SLS for hybrid cluster **1** with different counterions in H₂O/DMSO mixed solvents. (B) CONTIN plot of the size distribution of vesicular structures formed by hybrid cluster **1** with different counterions in 80:20 v/v H₂O/DMSO mixed solvents. (C) A TEM image of the vesicular structure formed in 80:20 v/v H₂O/DMSO mixed solvents (bar = 0.2 μ m). (D) An enlarged region of (C) in order to show the structural details of the hollow spherical vesicular structures.

The CONTIN analysis of the DLS measurement on this solution reveals a peak corresponding to assemblies with a very narrow size distribution and an average hydrodynamic radius (R_h) of 50 nm. The R_h value does not show angular dependence

which suggests that the supramolecular structures are likely spherical (Figure 3-4).⁴⁴ The radius of gyration (R_g) of the assemblies measured by SLS is 48 nm (Figure 3-5). The relation of $R_{h,0} \approx R_g$ strongly suggests that the supramolecular structures have a hollow spherical vesicular structure, which is also clearly confirmed by the TEM studies (Figure 3-3C). The TEM image shown in Figure 3-3D reveals several important aspects: First, the different contrast shown inside (lighter color) and around (darker color) the vesicular structures indicate they are hollow, which is quite similar to the vesicles formed by phospholipids.⁴⁷ Secondly, these vesicles collapsed on the carbon film due to the evaporation of internal solvent under high vacuum condition, indicating a soft and flexible nature of the vesicles' membrane. In order to form such vesicular structures in the mixed solvents as shown here, it is reasonable to assume that the hybrids use their polar POM clusters to face the hydrophilic solvent while their organic tails form a hydrophobic domain. The addition of water induces dissociation of the TBA⁺ counterions from the POM cluster and increases the overall negative charge on the polar head groups, which in turn changes the amphiphilicity of the hybrid molecules and leads to the vesicle formation.

When the original TBA⁺ counterions of **1** are replaced by TEA⁺ or TMA⁺, similar vesicular structures were observed. However, compared with the case of TBA⁺, the total scattered light intensity becomes lower and more water is needed to trigger the vesicle formation. The R_h of the large vesicular structures also changes from 50 nm to 30 nm and 23 nm in the same solvent system (80:20 v/v H₂O:DMSO) (Figure 3-3A and B), respectively. The decrease of the vesicle size should be attributed to the shorter alkyl chains of the counterions, which decreases the size of the hydrophobic domain and

consequently increases the curvature of the vesicles. These results indicate that the counterions play an important role in regulating the amphiphilic nature of the hybrid clusters and the electrostatic interactions between them.

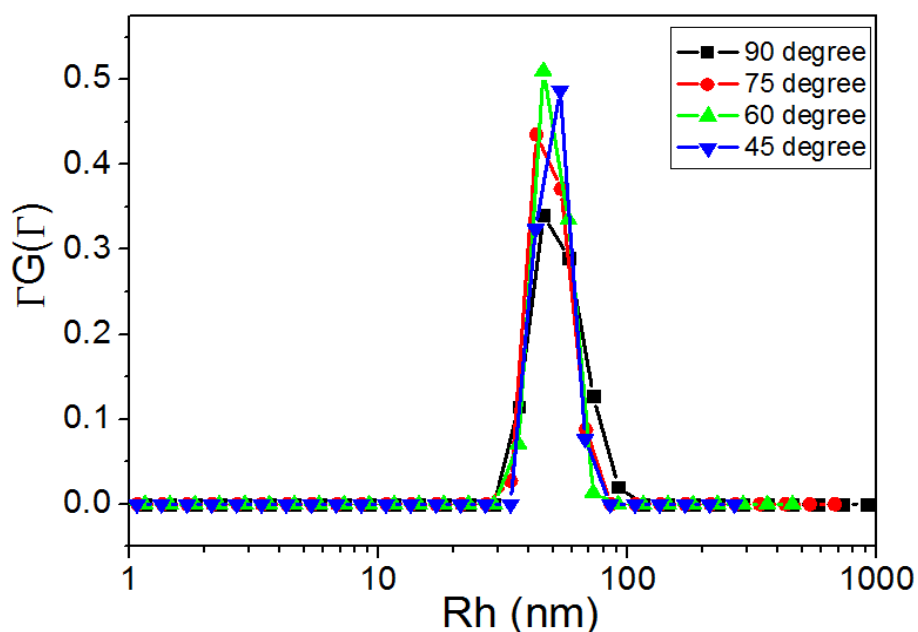


Figure 3-4. The size distribution plot of hybrid **1** in 80:20 v/v H₂O:DMSO solution under different scattering angles shows no obvious angular dependence.

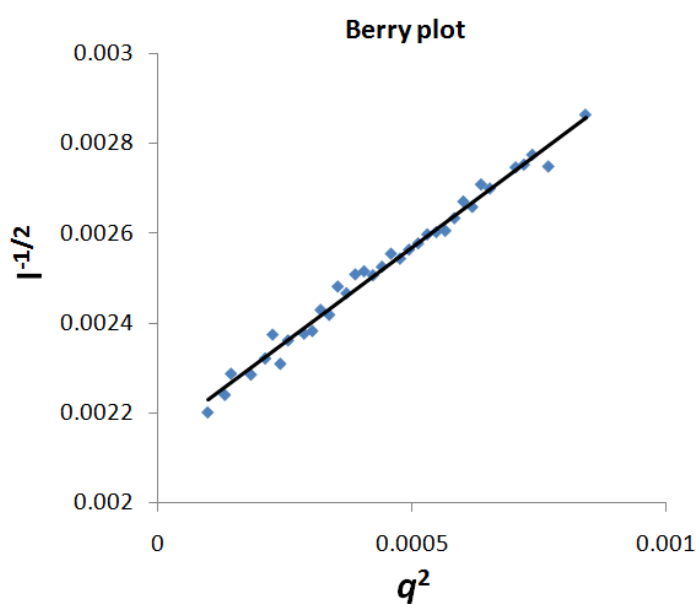


Figure 3-5. The Berry plot of hybrid **1** in 80:20 v/v H₂O:DMSO solution from which the R_g is determined to be 48 nm.

Hybrid $(\text{TBA}^+)_2\mathbf{2}$ in mixed solvents ($\text{H}_2\text{O}/\text{DMSO}$, $\text{H}_2\text{O}/\text{acetonitrile}$, *etc.*) show similar self-assembly behavior as hybrid $(\text{TBA}^+)_2\mathbf{1}$ does. However, the vesicular structures formed by hybrid $\mathbf{2}$ are smaller than those formed by hybrid $\mathbf{1}$ under the same condition. This is because an additional bending energy is needed to properly fold the two hydrophobic tails of hybrid $\mathbf{2}$ into the vesicular structure and therefore leads to a higher curvature or smaller vesicles (Figure 3-6).⁴⁸

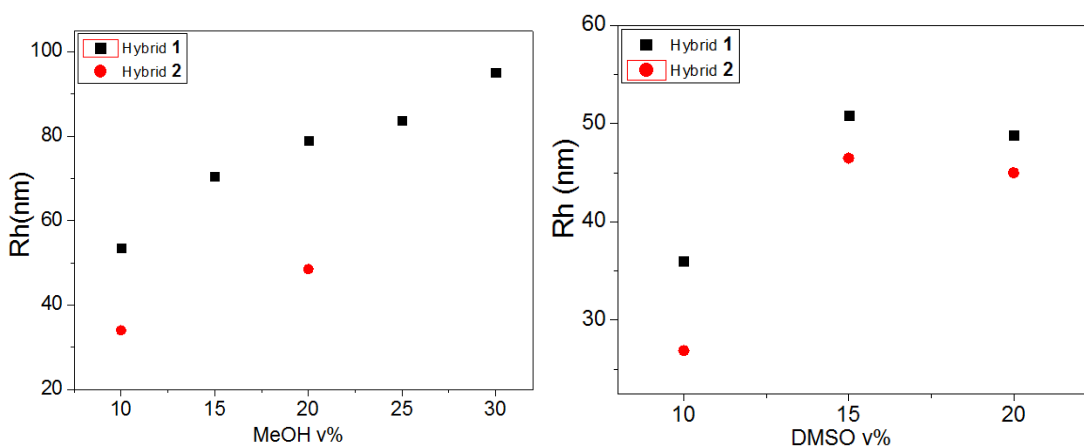


Figure 3-6. The average R_h of vesicles formed by hybrid $\mathbf{1}$ and $\mathbf{2}$ in different mixed solvents.

Counterions affect the packing of hybrid clusters in vesicles. Fluorescent probes are highly useful in monitoring polarity changes of microenvironments in macromolecules and membranes. The general dependence of probe fluorescence on polarity has been attributed to the dipole-dipole interaction between the singlet excited state of the fluorophores and the solvent molecules. Specifically, the fine structural pattern in the fluorescence of the pyrene monomers is found to be independent of excitation conditions or collisional quenching, but highly dependent on solvent polarity.⁴¹ Therefore, any changes in the pyrene fluorescence will reveal interactions between counterions and the

hybrid clusters (Figure 3-7).

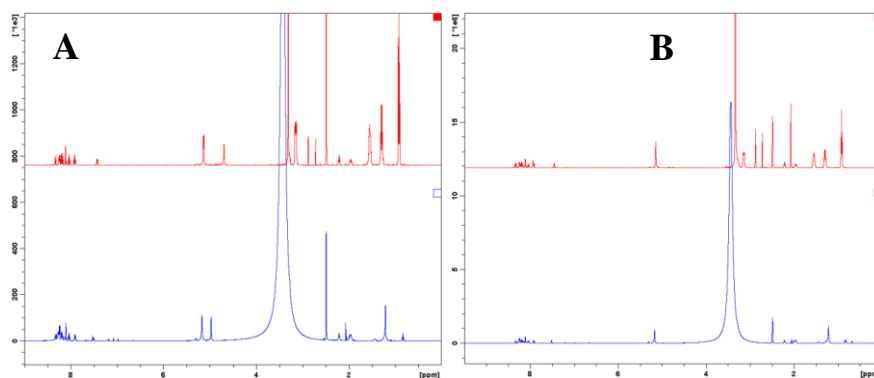


Figure 3-7. (A) ^1H NMR spectra of hybrid **1** with TBA (top) and H (bottom) as counterions in $\text{DMSO-}d_6$ (B) ^1H NMR spectra of hybrid **2** with TBA (top) and H (bottom) as counterions in $\text{DMSO-}d_6$.

As shown in Figure 3-8, when counterions are TBA^+ , TEA^+ or TMA^+ , the fluorescence intensity primarily comes from the pyrene monomer and no excimer peak is observed. Under these conditions, vesicular structures have already formed in the solution. Therefore, the fluorescence spectra indicate that the pyrene groups on the vesicle surface are not spatially close enough to form excimers. However, the fluorescence spectra are significantly different when H^+ counterions are present in the solution. The emission peaks of the monomer become less well-defined and the peak of the excimer centered at 480 nm becomes the dominant one for both $\text{H}_2\mathbf{1}$ and $\text{H}_2\mathbf{2}$. Secondly, it has been shown in the literature that the polarity of the micro-environment around the pyrene group is reflected by the ratio of the emission peak at 375 nm to the peak at 395 nm: the lower the ratio, the less polar the pyrene environment.^{39,40} Figure 3-8B clearly shows that the pyrene groups are more solvated when large counterions (for example TBA^+) are present in the assemblies. In contrast, when H^+ ions are the counterions, the pyrene groups stay closer to each other. This data confirms that

counterions with long alkyl chains can prevent the close packing of the hybrid clusters in the vesicular structures.

More direct evidence comes from the 2D NOESY NMR measurements. In general, when a saturated or inverted proton undergoes dipolar cross-relaxation, another spatially close proton may experience an intensity enhancement, a common phenomenon termed the Nuclear Overhauser Effect (NOE).⁴⁹ The NOE is unique among the NMR phenomena because it does not rely on through-bond J couplings but depends only on the spatial proximity between protons.^{50,51} In other words, the strength of the NOE can be used to estimate how close two protons are.^{52,53} In the current system, there are two possible scenarios for TBA interaction with the vesicular structure, either strongly bound to the vesicles or as free counterions in solution. Since no covalent chemical bonds are present between TBA cations and the hybrid cluster, it is quite possible that a dynamic exchange and equilibrium exists between bound and free cations. Free TBA cations show very weak to no NOE, while the bound TBAs are explicitly revealed through strong, negative NOE cross peaks. Moreover, the strong, negative NOE from bound TBA cations will outweigh that from free cations and dominate the NOESY spectrum, even when the free TBAs are in considerable excess.⁵⁰ Figure 3-3 shows that in a 0.25 mg/mL (TBA)₂**1** solution in pure DMSO-*d*₆, the TBA protons exhibit positive NOE cross peaks between adjacent protons indicating that the TBA counterions exist as free ions. The NOE cross peak pattern is identical to that of the control compound TBAI (tetrabutylammonium iodide). This is because there is no vesicle formation in solution and the TBA counterions interact only very weakly with the monomeric hybrids. However, when vesicular structures form in 90:10 v/v D₂O:DMSO-*d*₆ solution, the NOE spectra for (TBA⁺)₂**1**

dramatically changes. First, the previously positive NOE cross peaks become negative, indicating strong binding between the TBA cations and the vesicles. More interestingly, a set of new negative NOE cross peaks appears between cations and the fluorescent pyrene groups on **1** (Figure 3-9D), which do not appear in Figure 3-9B. This clearly indicates that the amphiphilic TBA cations interact with the hydrophobic domains in the vesicles. It is almost certain that this interaction interrupts the formation of pyrene excimers that in turn greatly affects the fluorescence pattern of the pyrene (Scheme 3-3). Previously, we noticed that the dumb-bell shaped POM hybrids could form vesicles in water/acetone mixed solvents.³⁸ The interesting question is how these hybrids could form closely packed hydrophobic layers in their vesicles. The giant POM head groups make the close packing of the alkyl chains very difficult due to spatial hindrance. We speculate that the alkyl chains of the TBA cations interact with the hydrophobic domains, but there is no direct evidence for this. From the 2D NOESY NMR study, we can confirm that the amphiphilic TBA cations are distributed partly into the hydrophobic regions of the vesicular structures.

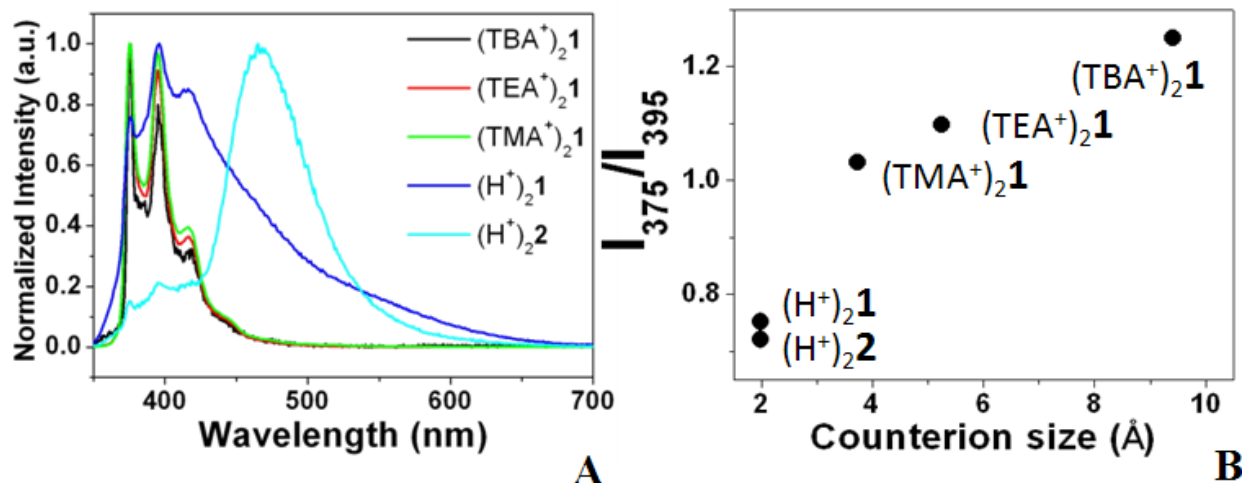


Figure 3-8. (A) Fluorescence spectra of hybrid clusters **1** and **2** with different counterions. (For the TBA, TEA and TMA salts, the solvent is 80:20 v/v H₂O:DMSO; for the H salt, the solvent is H₂O). (B) Plot of the pyrene monomer fluorescence peak $I(375\text{nm})/I(395\text{nm})$ versus the counterion size for hybrid clusters **1** and **2** with different counterions.

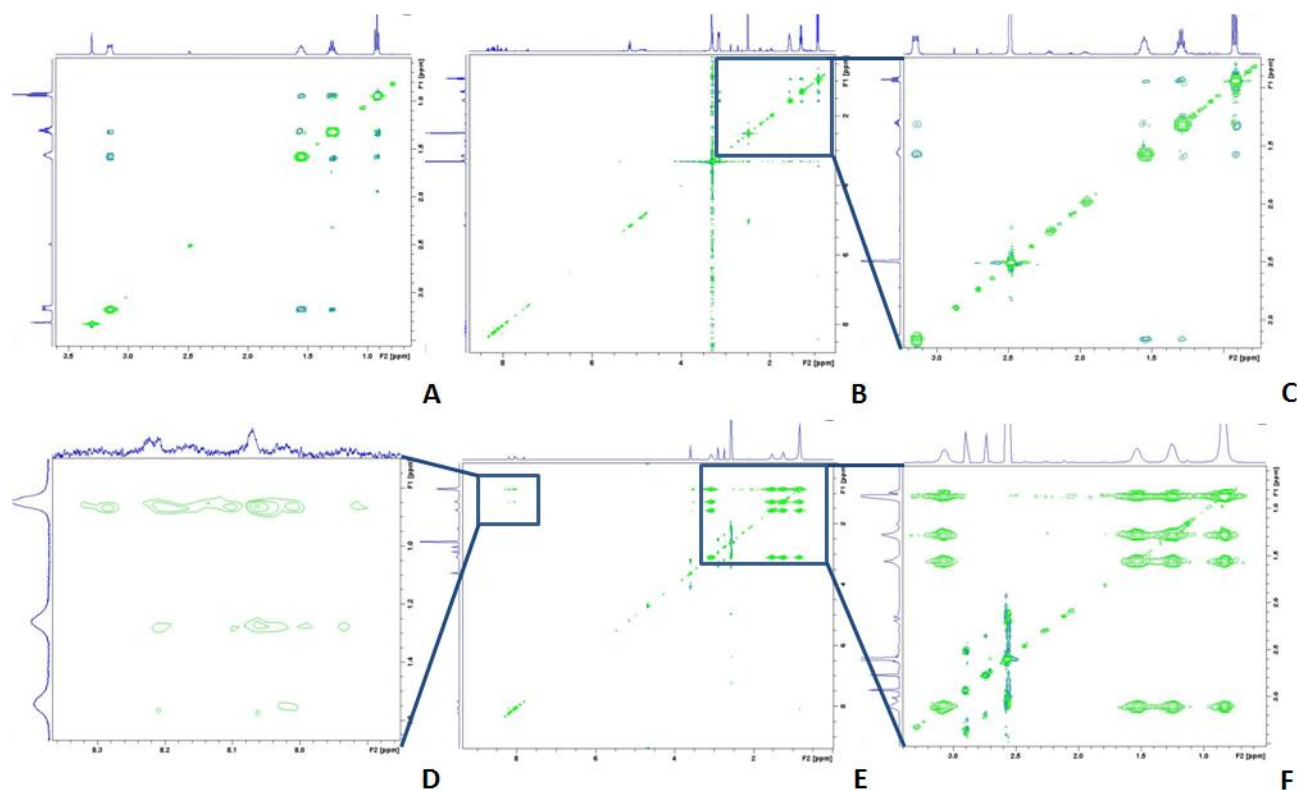
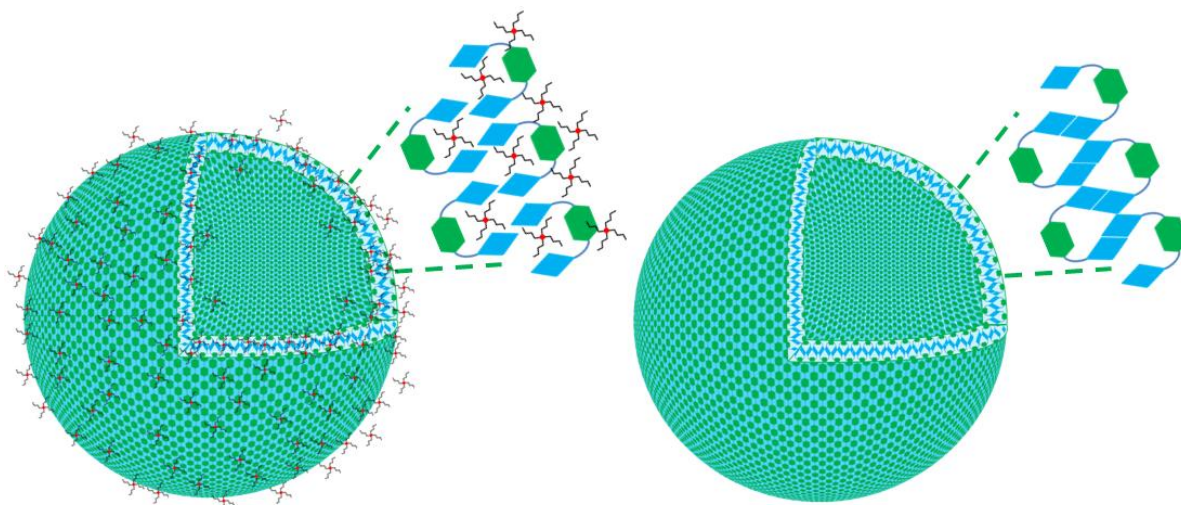


Figure 3-9. (A) 2D NOESY spectrum of TBAI in DMSO-*d*₆. (B) 2D NOESY spectrum of (TBA⁺)₂1 in DMSO-*d*₆. (C) An enlarged region of B showing the TBA cross peaks. (D) An enlarged region of E showing the TBA-pyrene cross peaks. (E) 2D NOESY spectrum of (TBA⁺)₂1 in 90:10 v/v D₂O:DMSO-*d*₆ mixed solvent. (F) An enlarged region of E show the TBA cross peaks. (Positive NOE peaks are in dark green color while negative NOE peaks are in light green color.)



Scheme 3-3. An illustration of possible vesicular structures formed by hybrid clusters, **2**, in polar solvents, and how the TBA counterions may be arranged in the packing of individual clusters. The hexagons, parallelograms and four-legged stars represent the POM, pyrene, and TBA cations, respectively.

pH sensitive vesicles. When two pyrene groups are spatially close to each other (less than 0.5 nm) without any interruption, an excimer peak appears.³⁹ We have shown earlier in the paper that replacement of the original TBA counterions by H^+ through cation exchange changes the fluorescence spectra of the appended pyrene: the peaks due to pyrene excimers become dominant relative to those from pyrene monomers, indicating a much closer packing of the hybrid clusters in the vesicular structure. This unique property gives us a great opportunity to construct a smart, pH sensitive vesicular structure and study the effect of pH on the assembly and disassembly of vesicular structures (Figure 3-10).

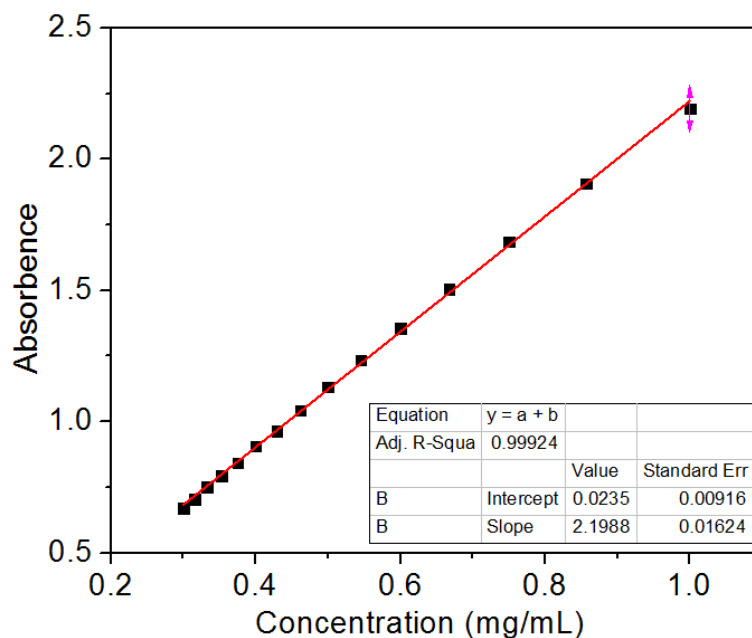


Figure 3-10. The calibration curve of hybrid **2** to determine the concentration of $(H^+)_{22}$ in water.

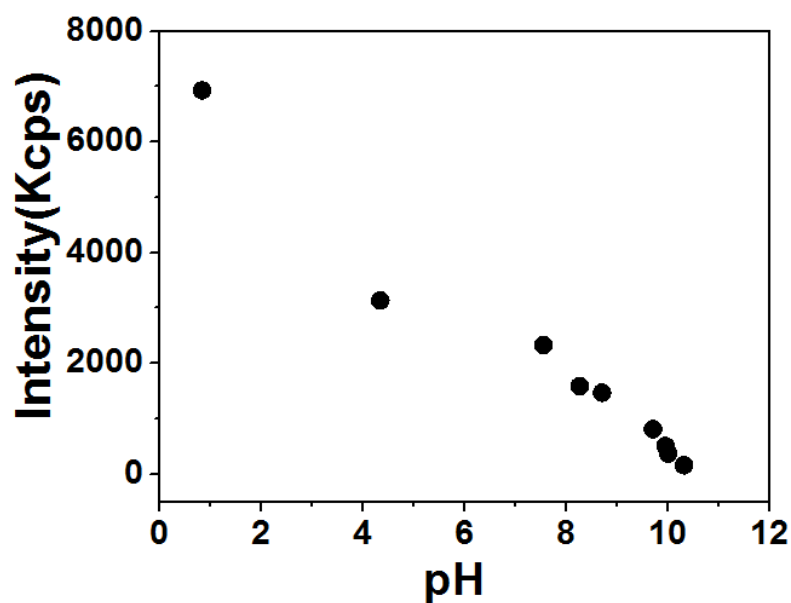


Figure 3-11. pH effect on the vesicular structure determined by total scattered intensity recorded by SLS for hybrid H_{22} in different solution pH values.

Figure 3-12 shows that the initial pH for an aqueous solution of hybrid cluster **2** (ca. 0.44 mg/mL based on UV absorption calibration) after counterion exchange is 3.41,

and the dominant fluorescence comes from the pyrene excimers. The molar ratio of hybrid **2** divided by free H^+ in solution is 0.87 based on solution pH, which indicates only a portion of the H^+ ions are released into solution and contribute to the pH, while a large amount of H^+ counterions are closely associated with the hybrids. (If protons are free in solution, the molar ratio should be 0.5). When dilute NaOH solution is slowly titrated into the solution of POM hybrid, a gradual decrease of the excimer peak along with a continuous increase in the pyrene monomer peaks occurs, indicating that the distance between pyrene excimers increases (larger than 0.5 nm). Because Na^+ has a weaker affinity for the hybrid macroanions in solution than H^+ does,⁵⁴ which leads to less screening of the POM cluster from neighboring groups, the drop of proton concentration in solution will increase the repulsion between adjacent POM groups in the vesicles. When the solution pH approaches 7, the decrease in the ratio of [excimer]/[monomer] peak areas becomes much slower, indicating that the distance between hybrid clusters becomes less sensitive to pH due to the limited amount of available protons. More interestingly, in the pH range of 1 - 7, the whole process is reversible. In other words, the average pyrene-to-pyrene distance between adjacent clusters is reversibly tunable by changing pH.

The average vesicle size recorded by DLS at 90 degree scattering angle also shows pH dependence: the R_h of vesicles decreases with increasing pH. Since stronger electrostatic repulsion between hybrid clusters will result in a high curvature, i.e., a smaller vesicle, for the assemblies, the current general trend clearly shows how the counterions affect the close packing of hybrid clusters. Meanwhile, the Zeta potential of the vesicular structures becomes more negative with increasing pH and becomes nearly

neutral at a low pH, indicating that the net charge on the vesicles increases with increasing pH.

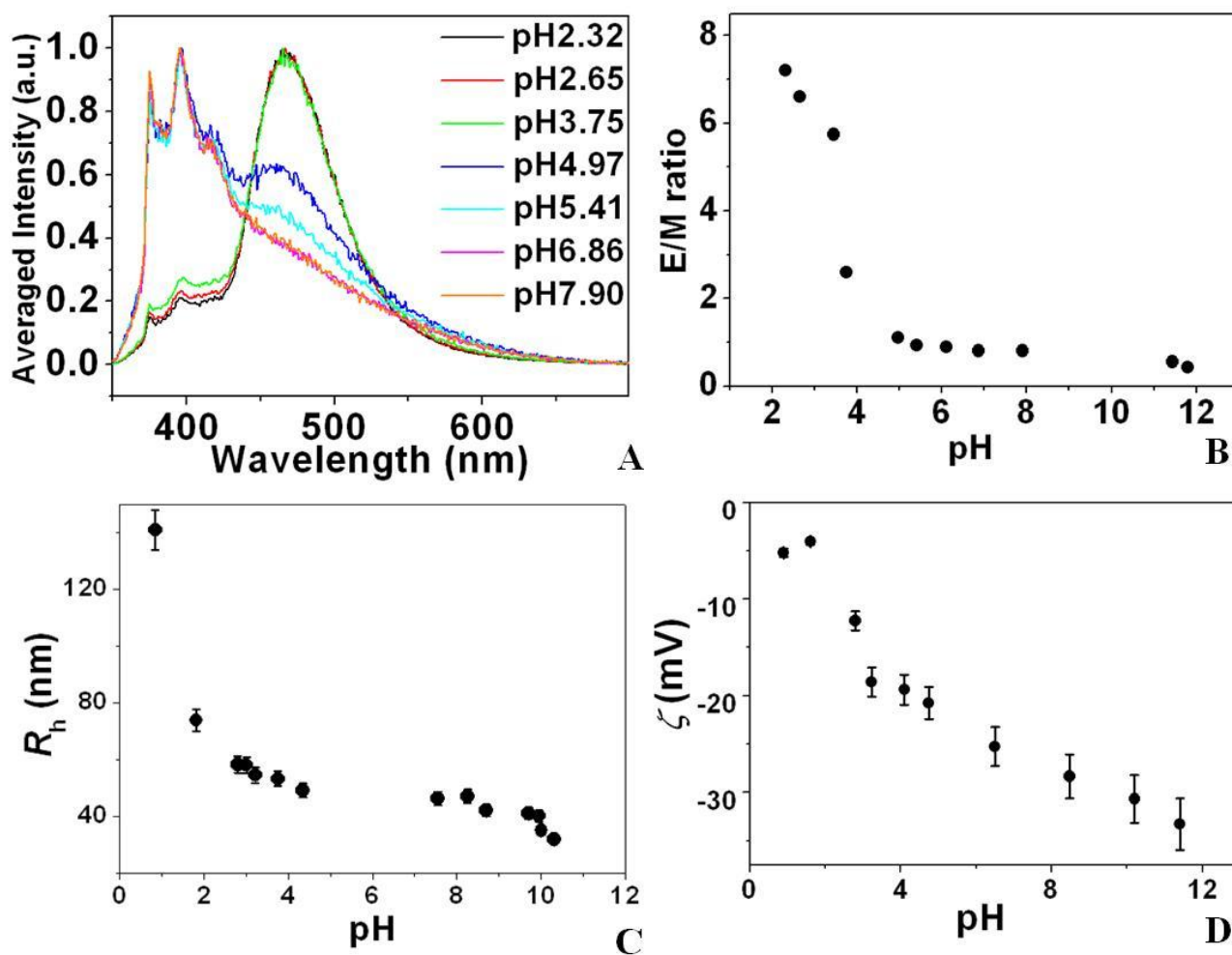


Figure 3-12. (A) Fluorescence spectra of hybrid clusters $(H^+)_{22}$ in water at different pH values (the fluorescence intensity has been normalized). (B) Plot of pyrene excimer/monomer intensity ratio versus solution pH for hybrid clusters $(H^+)_{22}$. (C) Change in the vesicular structure size with solution pH for $(H^+)_{22}$. (D) Zeta potential of the vesicular structure with solution pH for $(H^+)_{22}$.

Conclusions

In summary, two novel POM-based hybrid clusters were synthesized by connecting one or two organic pyrene tails with a Lindqvist type polyoxovanadate head cluster through triester capping groups. These two hybrid clusters demonstrate noteworthy amphiphilic properties by forming spherical vesicular structures in polar solvents. Four different counterions (TBA, TEA, TMA and H⁺) have been used to study the counterion effect on the vesicular structures and their consequent role in the fluorescent properties of the pyrene groups on vesicle surface. TBA counterions not only interact with POM polar head groups, but also move into the hydrophobic regions and interrupt the close packing of pyrene groups. More importantly, when TBA counterions are replaced by protons, a dramatic change of the pyrene fluorescence pattern occurs, and the vesicle size, the fluorescence pattern, and the effective charge on the vesicles change correspondingly and reversibly with solution pH. The construction of pH sensitive vesicular structures could well have application to artificial cell studies, nanoreactors, as well as drug and gene delivery systems.

References

- (1) Lee, E.; Kim, J.-K.; Lee, M. *Macromol. Rapid Commun.* **2010**, *31*, 975.
- (2) Li, M.-H.; Keller, P. *Soft Matter* **2009**, *5*, 927.
- (3) Zhang, X.; Rehm, S.; Safont-Sempere, M. M.; Würthner, F. *Nat. Chem.* **2009**, *1*, 623.
- (4) Roberts, M. C.; Hanson, M. C.; Massey, A. P.; Karren, E. A.; Kiser, P. F. *Adv. Mater.* **2007**, *19*, 2503.

- (5) Wang, M.-S.; Xu, G.; Zhang, Z.-J.; Guo, G.-C. *Chemical Communications* **2010**, 46, 361.
- (6) Bardelang, D.; Zaman, M. B.; Moudrakovski, I. L.; Pawsey, S.; Margeson, J. C.; Wang, D.; Wu, X.; Ripmeester, J. A.; Ratcliffe, C. I.; Yu, K. *Adv. Mater.* **2008**, 20, 4517.
- (7) Katagiri, K.; Nakamura, M.; Koumoto, K. *ACS Appl. Mater.* **2010**, 2, 768.
- (8) Hu, J.; Liu, S. *Macromolecules* **2010**, 43, 8315.
- (9) Haag, R. *Angew. Chem. Int. Ed.* **2004**, 43, 278.
- (10) Griset, A. P.; Walpole, J.; Liu, R.; Gaffey, A.; Colson, Y. L.; Grinstaff, M. W. *J. Am. Chem. Soc.* **2009**, 131, 2469.
- (11) Aryal, S.; Hu, C.-M. J.; Zhang, L. *ACS Nano* **2009**, 4, 251.
- (12) Shi, N. E.; Dong, H.; Yin, G.; Xu, Z.; Li, S. H. *Adv. Funct. Mater.* **2007**, 17, 1837.
- (13) Ali, M.; Yameen, B.; Cervera, J.; Ramírez, P.; Neumann, R.; Ensinger, W.; Knoll, W.; Azzaroni, O. *J. Am. Chem. Soc.* **2010**, 132, 8338.
- (14) Wang, R.; Jiang, X.; Di, C.; Yin, J. *Macromolecules* **2010**, 43, 10628.
- (15) Müller, A.; Peters, F. *Chem. Rev.* **1998**, 98, 239.
- (16) Long, D. L.; Burkholder, E.; Cronin, L. *Chem. Soc. Rev.* **2007**, 36, 105.
- (17) Rhule, J. T.; Hill, C. L.; Judd, D. A.; Schinazi, R. F. *Chem. Rev.* **1998**, 98, 327.
- (18) Dolbecq, A.; Dumas, E.; Mayer, C. d. R.; Mialane, P. *Chem. Rev.* **2010**, 110, 6009.
- (19) Xu, L.; Lu, M.; Xu, B.; Wei, Y.; Peng, Z.; Powell, D. R. *Angew. Chem. Int. Ed.* **2002**, 41, 4129.
- (20) Mayer, C. R.; Cabuil, V.; Lalot, T.; Thouvenot, R. *Angew. Chem. Int. Ed.* **1999**, 38, 3672.
- (21) Song, Y.-F.; McMillan, N.; Long, D.-L.; Kane, S.; Malm, J.; Riehle, M. O.;

- Pradeep, C. P.; Gadegaard, N.; Cronin, L. *J. Am. Chem. Soc.* **2009**, *131*, 1340.
- (22) Khan, M. I.; Chen, Q.; Goshorn, D. P.; Hope, H.; Parkin, S.; Zubieta, J. *J. Am. Chem. Soc.* **1992**, *114*, 3341.
- (23) Chen, Q.; Goshorn, D. P.; Scholes, C. P.; Tan, X. L.; Zubieta, J. *J. Am. Chem. Soc.* **1992**, *114*, 4667.
- (24) Gouzerh, P.; Proust, A. *Chem. Rev.* **1998**, *98*, 77.
- (25) Proust, A.; Thouvenot, R.; Gouzerh, P. *Chem. Commun.* **2008**, 1837.
- (26) Joo, N.; Renaudineau, S.; Delapierre, G.; Bidan, G.; Chamoreau, L.-M.; Thouvenot, R.; Gouzerh, P.; Proust, A. *Chem. Eur. J.* **2010**, *16*, 5043.
- (27) Bar-Nahum, I.; Cohen, H.; Neumann, R. *Inorg. Chem.* **2003**, *42*, 3677.
- (28) Hou, Y.; Hill, C. L. *J. Am. Chem. Soc.* **1993**, *115*, 11823.
- (29) Zeng, H.; Newkome, G. R.; Hill, C. L. *Angew. Chem. Int. Ed.* **2000**, *39*, 1771.
- (30) Bar-Nahum, I.; Khenkin, A. M.; Neumann, R. *J. Am. Chem. Soc.* **2004**, *126*, 10236.
- (31) Weiner, H.; Hayashi, Y.; Finke, R. G. *Inorg. Chem.* **1999**, *38*, 2579.
- (32) Yan, Y.; Wang, H.; Li, B.; Hou, G.; Yin, Z.; Wu, L.; Yam, V. W. W. *Angew. Chem. Int. Ed.* **2010**, *49*, 9233.
- (33) Carlisle R, C.; Osburn Atkinson, E. J.; McAdams, D.; Hayden, E. J.; Ankeny Brown, D. J. *Chem. Commun.* **2003**, 2456.
- (34) Landsmann, S.; Lizandara-Pueyo, C.; Polarz, S. *J. Am. Chem. Soc.* **2010**, *132*, 5315.
- (35) Rosnes, M. H.; Musumeci, C.; Pradeep, C. P.; Mathieson, J. S.; Long, D.-L.; Song, Y.-F.; Pignataro, B.; Cogdell, R.; Cronin, L. *J. Am. Chem. Soc.* **2010**, *132*, 15490.

- (36) Zhang, J.; Liu, T.; Mal, S. S.; Kortz, U. *Eur. J. Inorg. Chem.* **2010**, 2010, 3195.
- (37) Zhang, J.; Song, Y.-F.; Cronin, L.; Liu, T. *Chem. Eur. J.* **2010**, 16, 11320.
- (38) Pradeep, C. P.; Misrahi, M. F.; Li, F.-Y.; Zhang, J.; Xu, L.; Long, D.-L.; Liu, T.; Cronin, L. *Angew. Chem. Int. Ed.* **2009**, 48, 8309.
- (39) Winnik, F. M. *Chem. Rev.* **1993**, 93, 587.
- (40) Kalyanasundaram, K.; Thomas, J. K. *J. Am. Chem. Soc.* **1977**, 99, 2039.
- (41) Glushko, V.; Thaler, M. S. R.; Karp, C. D. *Arch. Biochem. Biophys.* **1981**, 210, 33.
- (42) Bruker AXS, I.; 5.628 ed.; Analytical X-ray Systems: Madison, WI, 2003.
- (43) Bruker AXS, I.; 6.45 ed.; Analytical X-ray Systems: Madison, WI, 2003.
- (44) Hiemenz, P. C.; Rajagopalan, R. *Principles of Colloid and Surface Chemistry*; 3rd ed.; CRC Press: New York, 1997.
- (45) Liu, T.; Diemann, E.; Li, H.; Dress, A. W. M.; Müller, A. *Nature* **2003**, 426, 59.
- (46) Song, J.; Luo, Z.; Zhu, H.; Huang, Z.; Lian, T.; Kaledin, A. L.; Musaev, D. G.; Lense, S.; Hardcastle, K. I.; Hill, C. L. *Inorg. Chim. Acta.* **2010**, 363, 4381.
- (47) Beck, P.; Liebi, M.; Kohlbrecher, J.; Ishikawa, T.; Rügger, H.; Zepik, H.; Fischer, P.; Walde, P.; Windhab, E. *J. Phys. Chem. B* **2009**, 114, 174.
- (48) Zhang, J.; Song, Y.-F.; Cronin, L.; Liu, T. *J. Am. Chem. Soc.* **2008**, 130, 14408.
- (49) Ernst, R. R.; Bodenhausen, G.; Wokaun, A. *Principles of Nuclear Magnetic Resonance in One and Two Dimensions*; Oxford University Press, 1992.
- (50) Hassinen, A.; Moreels, I.; de Mello Donegá, C.; Martins, J. C.; Hens, Z. *J. Phys. Chem. Lett.* **2010**, 1, 2577.
- (51) Denkova, P. S.; Van Lokeren, L.; Willem, R. *J. Phys. Chem. B* **2009**, 113, 6703.
- (52) Yuan, H.-Z.; Cheng, G.-Z.; Zhao, S.; Miao, X.-J.; Yu, J.-Y.; Shen, L.-F.; Du, Y.-R.

Langmuir **2000**, *16*, 3030.

(53) Cros-Gagneux, A.; Delpech, F.; Nayral, C. I.; Cornejo, A.; Coppel, Y.; Chaudret, B. *J. Am. Chem. Soc.* **2010**, *132*, 18147.

(54) Pigga, J. M.; Teprovich, J. A.; Flowers, R. A.; Antonio, M. R.; Liu, T. *Langmuir* **2010**, *26*, 9449.

———— CHAPTER ————

4

**A Multi-unit Catalyst with Synergistic Stability and
Reactivity: A Polyoxometalate-Metal Organic
Framework for Aerobic Decontamination**

Abstract

A combination of polyanion size and charge allows the Keggin-type polyoxometalate (POM), $[\text{CuPW}_{11}\text{O}_{39}]^{5-}$, a catalyst for some air-based organic oxidations, to fit snugly in the pores of MOF-199 (HKUST-1), a metal-organic framework (MOF) with the POM counter-cations residing in alternative pores. This close matching of POM diameter and MOF pore size in this POM-MOF material, $[\text{Cu}_3(\text{C}_9\text{H}_3\text{O}_6)_2]_4[\{(\text{CH}_3)_4\text{N}\}_4\text{CuPW}_{11}\text{O}_{39}\text{H}]$ (**1**), results in a substantial synergistic stabilization of both the MOF and the POM. In addition, this heretofore undocumented POM-MOF interaction results in a dramatic increase in the catalytic turnover rate of the POM for air-based oxidations. While **1** catalyzes the rapid chemo- and shape-selective oxidation of thiols to disulfides, and more significantly, the rapid and sustained removal of toxic H_2S via $\text{H}_2\text{S} + \frac{1}{2}\text{O}_2 \rightarrow \frac{1}{8}\text{S}_8 + \text{H}_2\text{O}$ (4,000 turnovers in < 20 h), the POM or the MOF alone are catalytically slow or inactive. Three arguments are consistent with the catalytic reactions taking place inside the pores. POM activation by encapsulation in the MOF likely involves electrostatic interactions between the two components resulting in a higher reduction potential of the Cu(II) centers and thus a faster rate-limiting oxidation of the reduced sulfur species by Cu(II).

Introduction

MOFs as a class of crystalline materials offer high levels of porosity with considerable control over pore size and composition.¹⁻¹⁴ Such properties have led to the successful application of MOFs in gas adsorption,¹⁵⁻¹⁷ separation,¹⁸⁻²⁰ magnetism studies,^{21,22} nonlinear optical properties,²³ and more recently, catalysis. Several noteworthy studies on MOF-based catalysis are now published.^{11-13,24-26} POMs have been

successfully incorporated by covalent, electrostatic and other means into coordination polymers and large pore MOFs,^{10,27-35} and some POM-containing structures catalyze oxidation reactions.^{27,29-31,34} There is a 2007 publication describing the trapping and preconcentration of organic phosphonates by a metal-organic framework but it does not involve catalysis,³⁶ and a significant study was just reported on the hydrolytic decontamination of nerve agent simulants by a POM-MOF.³⁷

However, there remain two challenges in MOF catalysis that are both addressed in this study: making MOF derivatives that can catalyze reactions using the ambient environment, and making MOF catalysts more stable. Catalytic oxidations based on ambient air are of considerable interest because they promise the removal of many toxic or odorous molecules using only air without the need for energy sources, solvents or other reagents. Oxidizable undesirable compounds include toxic industrial chemicals, chemical warfare agents, indoor air contaminants and many environmental pollutants.^{38,39}

A logical approach to such effective aerobic oxidation catalysts would be to combine the high catalytic activity of particular polyoxometalates (POMs)⁴⁰⁻⁴⁵ for aerobic oxidations^{38,46-49} with the porosity and selective sorption properties of metal organic frameworks (MOFs)⁴⁻⁷ by encapsulating POM catalysts into appropriate MOFs. We henceforth refer to these materials as “POM-MOFs” and note that optimal POM retention logically requires MOF apertures smaller than the POM (with counterions) radius, although one type of POM-MOF has shown negligible loss of POM despite a MOF aperture size larger than the POM radius.^{31,34,50} We report here that a MOF with pore sizes closely matching a POM guest self assembles around this guest to make a material, unlike the POM-MOFs reported in the literature thus far, that has significantly different

properties than either the POM or MOF component alone. Specifically, MOF-199 (also known as HKUST-1)⁵¹ in the presence of $[\text{CuPW}_{11}\text{O}_{39}]^{5-}$, forms a POM-MOF material, $[\text{Cu}_3(\text{C}_9\text{H}_3\text{O}_6)_2]_4[\{(\text{CH}_3)_4\text{N}\}_4\text{CuPW}_{11}\text{O}_{39}\text{H}]\cdot 40\text{H}_2\text{O}$ (**1**) whose hydrolytic stability is far greater than that of either the MOF or the POM alone and whose strong POM-MOF interactions also dramatically (2 orders of magnitude) increase the rate of air-based oxidations catalyzed by the POM guest, $[\text{CuPW}_{11}\text{O}_{39}]^{5-}$ (shape-selective thiol oxidation and fast, sustained decontamination of the toxic industrial chemical H_2S , forming S_8 and water).

Experimental Section

General methods and materials. MOF-199, PW_{12} -MOF ($[\text{PW}_{12}\text{O}_{40}]^{3-}$, the saturated parent Keggin-type polyanion of $[\text{CuPW}_{11}\text{O}_{39}]^{5-}$, in MOF-199), $\text{K}_5[\text{CuPW}_{11}\text{O}_{39}]$, and $\text{TBA}_5[\text{CuPW}_{11}\text{O}_{39}]$, were prepared according to the literature methods,^{32,51,52} and their purity was confirmed by FT-IR and powder X-ray diffraction (XRD). The other reagents including $\text{H}_3\text{PW}_{12}\text{O}_{40}$, trimesic acid, $(\text{CH}_3)_4\text{NOH}$, $\text{Cu}(\text{NO}_3)_2$, and the thiols were purchased from Aldrich and used without further purification. Gas chromatography (GC) was performed on a Hewlett-Packard 5890 gas chromatograph equipped with a 5% phenyl methyl silicone capillary column, flame ionization detector, and a Hewlett-Packard 3390A series integrator using N_2 as the carrier gas. Elemental analyses for C, H, and N were performed by Atlantic Microlab (Norcross, Georgia). K, Na, Cu, P and W were performed by Galbraith Laboratories (Knoxville, Tennessee). The infrared spectrum (2% sample in KBr pellet) was recorded on a Nicolet™ 6700 FT-IR spectrometer from ThermoElectron Corporation. The thermogravimetric data were

collected on an ISI TGA 1000 instrument. Powder XRD was measured on an D8 Discover Powder Instrument on monochromatic Cu K α ($\lambda = 1.54060 \text{ \AA}$) radiation.

Synthesis of $[\text{Cu}_3(\text{C}_9\text{H}_3\text{O}_6)_2]_4\{[(\text{CH}_3)_4\text{N}]_4\text{CuPW}_{11}\text{O}_{39}\text{H}\} \cdot 40\text{H}_2\text{O}$ (1). To 10 mL of distilled water was added $\text{Cu}(\text{NO}_3)_2 \cdot 2.5\text{H}_2\text{O}$ (480 mg, 2.50 mmol) and $\text{K}_5\text{CuPW}_{11}\text{O}_{39}$ (400 mg, 0.14 mmol), and the resulting blue solution stirred for 10 minutes. Trimesic acid (420 mg, 2.0 mmol) and then $(\text{CH}_3)_4\text{NOH}$ (362.46 mg, 2.0 mmol) were added sequentially, with 10 minutes of stirring after each addition. The resulting solution with pH ~ 3 , was transferred to a Teflon-lined Parr bomb, heated up to 200 $^\circ\text{C}$ for 16 hours, programmatically cooled down to 100 $^\circ\text{C}$ for another 4 hours, and left to cool to ambient temperature. The resulting polyhedron-like deep-blue crystals were separated from the solution and washed with distilled water several times. Further purification was carried out by soaking the crystals in saturated KCl solution and distilled water and sonicating them at least 3 times for 30 minutes each time to exchange and remove any free metal ions. The product was dried *in vacuo* overnight to remove water molecules trapped in the pores of the product. Yield: 200 mg (ca. 25% based on POM). Elemental Analysis, Calcd (Found %) for $\text{C}_{88}\text{H}_{153}\text{N}_4\text{O}_{127}\text{Cu}_{13}\text{PW}_{11}$ (1): calc for C, 17.11; H, 2.50; N, 0.91; Cu, 13.37; W, 32.73, found for C, 15.85; H, 2.43; N, 0.92; Cu, 12.3; W, 35.1; FT-IR (cm^{-1}): 1649(s), 1452(m), 1374(s), 1080 (w), 987 (w), 898(w), 824(m), 752 (m), 728(m), 497(w).

X-ray Crystallography. An X-ray quality crystal of **1** was coated with Paratone N oil and mounted on a small fiber loop for index and intensity data collection. The X-ray diffraction data were collected under a nitrogen stream at 173 K on a Bruker D8

SMART APEX CCD single-crystal diffractometer using Mo K α (0.71073 Å) radiation. Data collection, indexing, and initial cell refinements were processed using the SMART⁵³ software. Frame integration and final cell refinements were carried out using the SAINT⁵⁴ software. The final cell parameters were determined from the least-squares refinement of total reflections. The structures were determined through direct methods (SHELXS97) for locating the tungsten atoms and difference Fourier maps (SHELXL97). The final results of the refinement are listed in Table 4-1.

Table 4-1. Crystallographic Data and Structure Refinement for **1**.

1	
empirical formula	C ₈₈ H ₁₅₃ Cu ₁₃ N ₄ O ₁₂₇ PW ₁₁
formula weight	6178.48 g mol ⁻¹
crystal system	Cubic
space group	<i>Fm-3m</i>
unit cell	$a = 26.307(2) \text{ \AA}$ $\alpha = 90^\circ$
Volume	18207(3) Å ³
<i>Z</i>	4
density (calcd)	2.254 g cm ⁻³
temperature	173(2)K
wavelength	0.71073 Å
abs. coeff	8.517 mm ⁻¹
Reflections collected	92628
Independent reflections	1439 [R(int) = 0.1641]
GOF	1.057
final R ₁ ^a [<i>I</i> > 2σ(<i>I</i>)]	0.0566
final wR ₂ ^b [<i>I</i> > 2σ(<i>I</i>)]	0.1827

$$^a R_1 = \frac{\sum ||F_0| - |F_c||}{\sum |F_0|}; wR_2 = \frac{\sum [w(F_0^2 - F_c^2)^2]}{\sum [w(F_0^2)^2]}^{1/2}$$

Stability tests of K₅[CuPW₁₁O₃₉] and the POM-MOF, 1. The stability of K₅[CuPW₁₁O₃₉] (10 mg in 1.0 mL of buffer) at different pH values was monitored by UV-vis spectroscopy. The POM-MOF complex, **1** (10 mg) was suspended in 1.0 mL of buffer at pH 7.0 (0.02 M sodium phosphate, NaPi, buffer); pH 8.0 (0.01 M NaPi buffer),

pH 9.0 (0.01 M NaPi buffer), pH 10.0 (0.01 M Na borate buffer), and pH 11.0 (0.01 M NaOH). After 12 hours, the solids were separated by centrifugation and the reflection IR spectra were measured using a Nicolet 6700 FT-IR with smart orbital ATR accessory.

Catalytic experiments:

Aerobic H₂S oxidation in aqueous solution. In a typical reaction, the catalyst (10.0 mg) was weighed and added to a clean, dry pressure tube and the complete experimental assembly was flushed with oxygen or air and weighed. The reaction was initiated by addition of a saturated aqueous solution of H₂S (0.1 mol/L, pH = 4.8, 75 mL). The reaction vessel was then sealed quickly and the reaction solution was stirred at room temperature for 20 hours. After several minutes, the clear colorless solution became cloudy and the yellow elemental sulfur began to precipitate on the walls of reaction vial. The solid reaction mixture, in parallel reactors for each specific reaction period, was separated by centrifugation, dried in vacuum overnight and weighed.

Aerobic H₂S oxidation under gas phase (solvent-free). In a typical reaction, the catalyst (150.0 mg) was weighed in a beaker and then placed in a desiccator. The H₂S gas was generated by mixing of solid K₂S (0.5051 g) with H₃PO₄ (100 mL) in another beaker placed in the same desiccator and then the cap of the desiccator was sealed tightly. The H₂S gas was circulated by a fan in the desiccator. Reaction with the dioxygen in the air takes place on the surface of the catalyst particles. After one week, the catalyst was dried and characterized by FT-IR. The weight of catalyst before and after reaction was assessed carefully 3 times.

Aerobic thiol oxidation. In a typical catalytic thiol oxidation experiment, 60.0 μL (6.62×10^{-4} mol) of propanethiol (PrSH), 18.0 μL (9.2×10^{-5} mol) of decane (internal standard) and 10 mg of **1** were stirred in 2.9 mL of chlorobenzene in a Schlenk tube fitted with PTFE septum stopper under dioxygen at 45 $^{\circ}\text{C}$ for 5 days. Aliquots were withdrawn from the Schlenk tube at approximately 10 h intervals, and the products were quantified by gas chromatography. In order to prevent the PrSH from leaking, the reaction solution was placed in an ice-water bath for 20 minutes. After opening the Schlenk tube, 0.1 μL of cooled reaction solution was withdrawn as quickly as possible and the atmosphere in the tube was carefully filled with dioxygen gas. All the catalytic experiments above and stability characterizations of **1** during turnovers were set up, carried out, and analyzed by Dr. Zhen Luo.

Results and Discussion

A solution of $\text{Cu}(\text{NO}_3)_2 \cdot 2.5\text{H}_2\text{O}$, $\text{K}_5\text{CuPW}_{11}\text{O}_{39}$, trimesic acid and $(\text{CH}_3)_4\text{NOH}$, treated under hydrothermal conditions, results in X-ray quality crystals of the POM-MOF, **1**, in *ca.* 25% yield (based on POM). These crystals were filtered, washed with distilled water, and dried in vacuum. The FT-IR spectrum of **1** clearly shows the characteristic peaks of both POM and MOF components (Figure 4-1).⁵¹ Both the UV-visible and FT-IR spectra of the concentrated filtrates from washing the purified **1** with water indicate that no POM whatsoever is lost from **1** by these procedures.

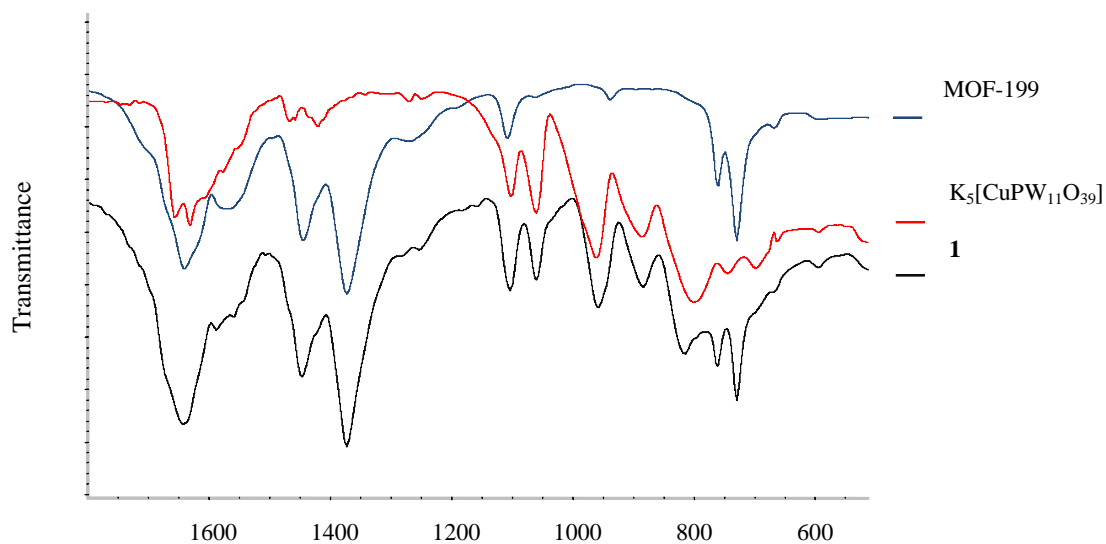


Figure 4-1. . FT-IR spectra of MOF-199 alone (blue), K₅[CuPW₁₁O₃₉] alone (red), and **1** (black).

The specific surface area of **1**, measured by the BET method, is 462 m²/g (Figure 4-2). The surface area of the POM-MOF is generally one third that of the isostructural bulk MOF-199 (1,264 m²/g) before guest molecule incorporation.^{39,51} The relatively low surface area indicates that most of the MOF pores are occupied by the POM and its counterions. The stoichiometries of formula of **1** were generated and defined on the basis of crystal structure, elemental analysis and thermal gravimetric analysis (Figure 4-3).

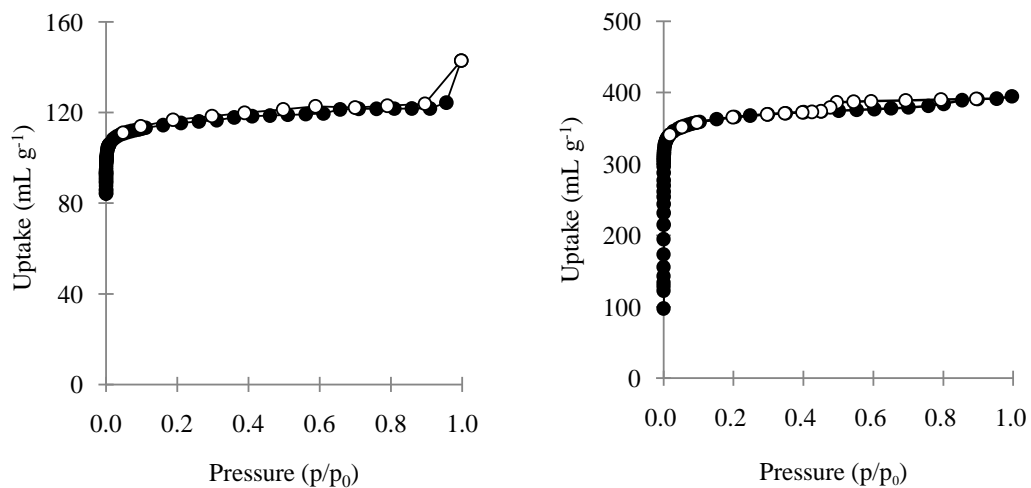


Figure 4-2. N₂ gas adsorption isotherms of **1** (left) and MOF-199 (right) measured at 77K. Filled symbols, adsorption; open symbols, desorption. The BET surface areas of **1** and MOF-199 alone are 462 and 1,264 m²/g, respectively.

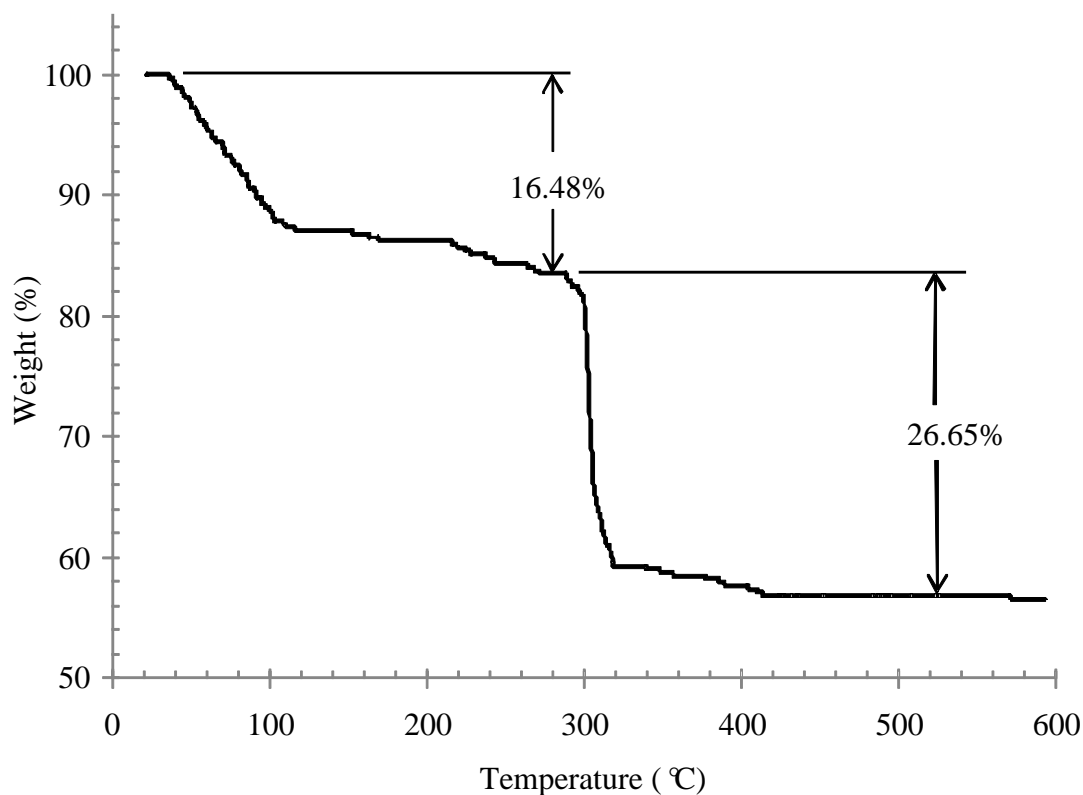


Figure 4-3. Thermogravimetric analysis of **1**. The calculated weight percentages of water + tetramethylammonium cations and the MOF framework are 16.46% and 26.82%, respectively, based on the molecular formula of **1**.

The powder XRD pattern and single crystal X-ray structure of **1** reveal that the parent MOF-199 framework has been maintained and that the catalytically active tetramethylammonium (TMA) salt of the Cu-containing POM, $[\text{CuPW}_{11}\text{O}_{39}]^{5-}$, has been introduced into this $[\text{Cu}_3(\text{C}_6\text{H}_3\text{O}_6)_2]_4$ -based MOF (Figures 4-4 and 4-5). The structure of **1** clearly reveals the high occupancy of the POMs and their counterions in the pores. Predictably, given the pore and POM volumes, the TMA counterions don't reside in the same pores as the POM polyanions, but in adjacent pores. Both the transition-metal-

substituted POM and countercations are disordered, leading to the location of the N atoms of only two of total four TMA cations. As in all X-ray structures of α -Keggin POMs with one substituted metal-oxo or metal-aqua unit, the polyanion is orientationally disordered so the substituted metal occurs at all 12 Keggin sites. Each encapsulated POM can be accessed via six adjacent pores, which contain the TMA ions.

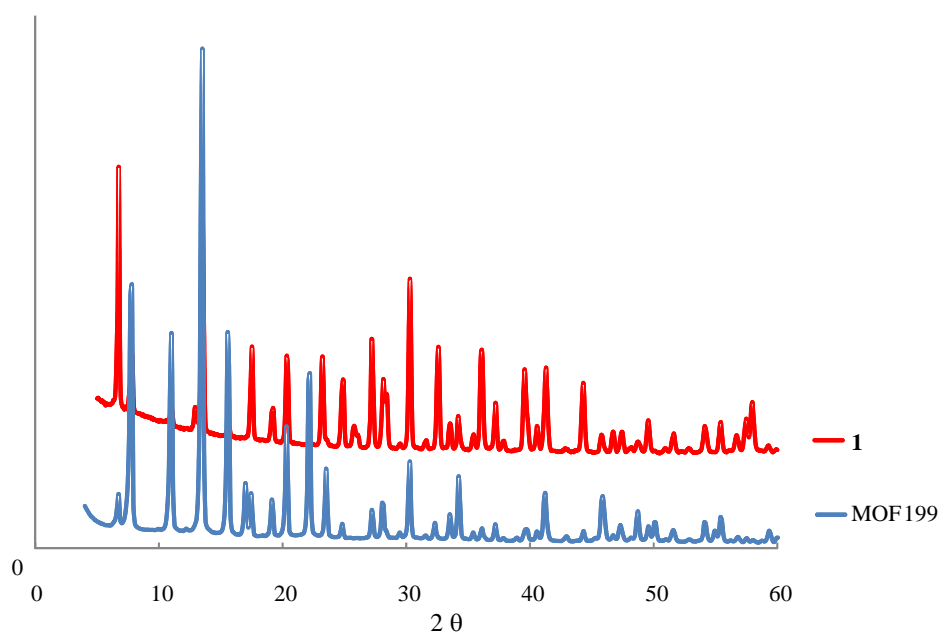


Figure 4-4. Powder X-ray diffraction patterns of **1** and MOF-199.

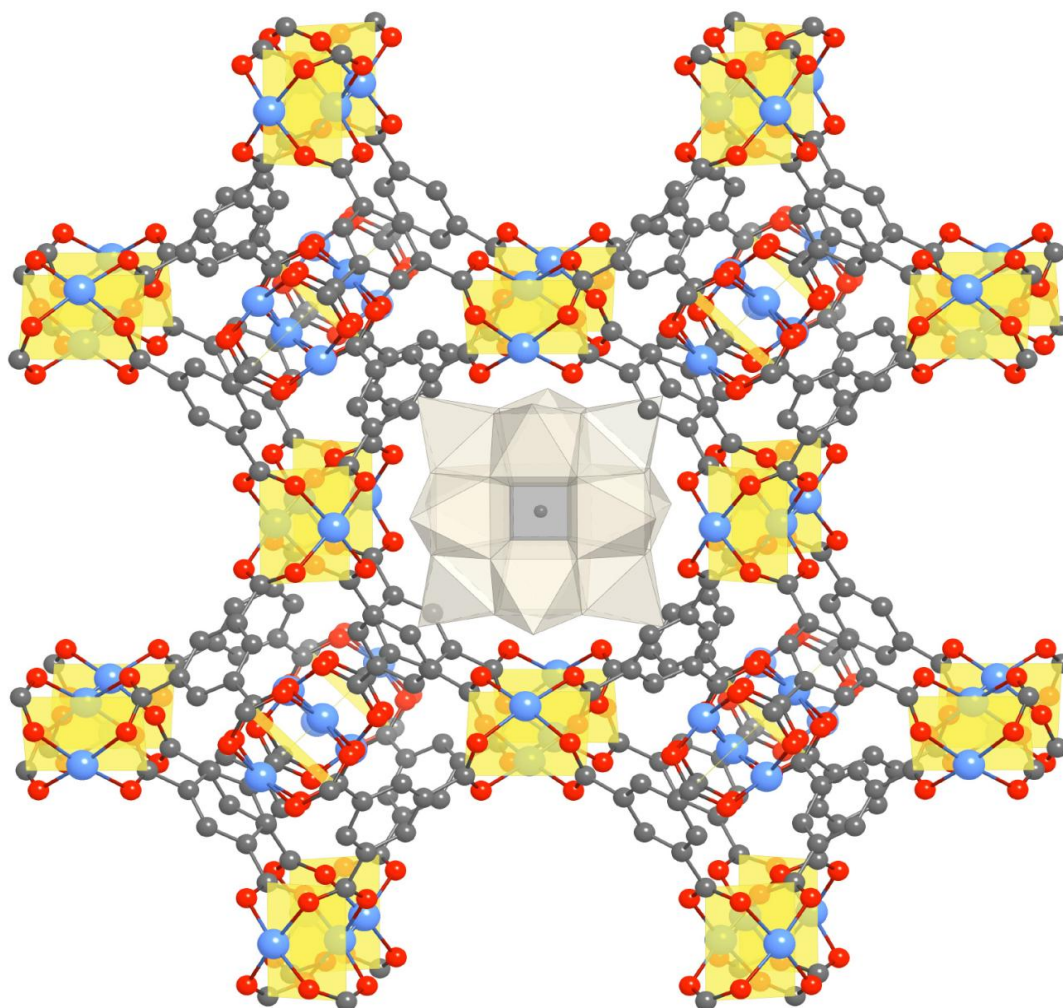
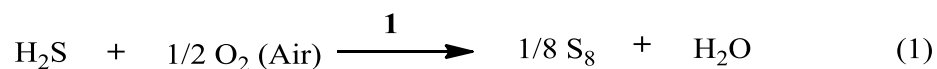


Figure 4-5. X-ray crystal structure of **1**. The POM, represented as off-white polyhedra, is orientationally disordered in the pores. The MOF-199 framework is represented in ball and stick form wherein C atoms are represented in gray, O in red, and Cu in blue. Yellow squares denote the geometry of the copper(II) acetate clusters. Tetramethylammonium (TMA) cations, which are disordered in the pores, and hydrogen atoms are omitted for clarity.

POM-MOF **1** is capable of catalyzing the air-based oxidative decontamination of a series of toxic industrial chemicals (TICs). Hydrogen sulfide is oxidatively converted

by **1** under ambient conditions via eq 1 (Figure 4-6, Table 4-2 and Table 4-3) in aqueous solution or gas phase. The produced yellow powder was confirmed to be elemental sulfur by its UV-Vis spectrum after extraction into chloroform solution. The turnover number (TON), based on H₂S consumed (1/8 S₈ formed) and POM units present in **1**, is *ca.* 4,000 in less than 20 hours in aqueous solution. In aqueous solution, the product inhibition (blockage of the pores in **1** by marginally soluble S₈ product) does little to inhibit the reaction at the outset and FT-IR shows that the integrity of the POM-MOF structure is maintained during reaction (Figure 4-7).



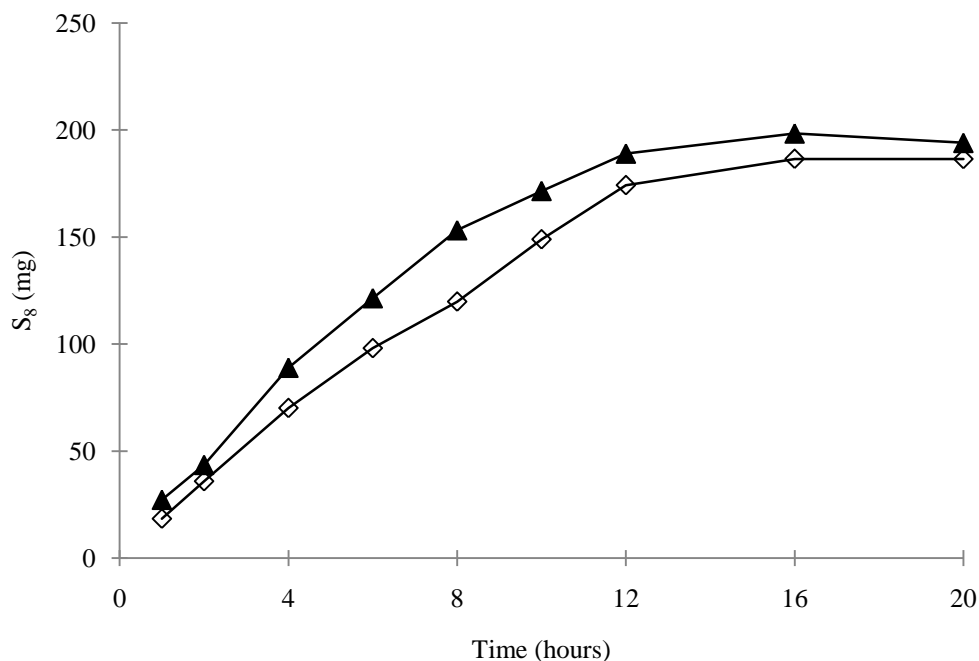


Figure 4-6. Aerobic oxidation of H₂S to S₈ catalyzed by the POM-MOF, **1**, in water. An aqueous solution of H₂S (0.1 mol/L, pH=4.8, 75 mL) containing **1** (10.0 mg) was flushed with oxygen (black triangles) or air (open squares) and stirred at room temperature for the duration of the reaction (20 hours). Parallel reactions were conducted and stopped at specific reaction times for product separation and measurement. Control experiments for POM only (10.0 mg) and MOF-199 (10.0 mg) only under identical conditions showed no catalytic activity (no production of S₈).

Table 4-2. The quantity of sulfur, produced via eq 1 in aqueous solution, catalyzed by 10 mg of the POM-MOF, **1**.

	weight of S ₈ (mg)	TON ^a
oxygen-based catalysis	223.4 ± 30	4,301
air-based catalysis	194.9 ± 20	3,755

^a Turnover Numbers (TON) = moles of H₂S consumed (or 8 x moles of product S₈ formed) per mol of catalyst used.

Table 4-3. The quantity of sulfur, produced via eq 1 in gas phase under ambient conditions, catalyzed by **1**, PW₁₂-MOF, MOF 199, and {CuPW₁₁}.

	catalysts (mg)	S ₈ formed (mg)	TON ^a
1	150	9.5 ± 0.1	10.5
PW ₁₂ -MOF	150	0.2 ± 0.1	0.2
MOF 199	150	0.2 ± 0.1	0.02
{CuPW ₁₁ }	150	~ ^b	~

^a Turnover Numbers (TON) = moles of H₂S consumed (or 8 x moles of product S₈ formed) per mol of catalyst used. ^b No detectable weight change when {CuPW₁₁} was used as catalyst.

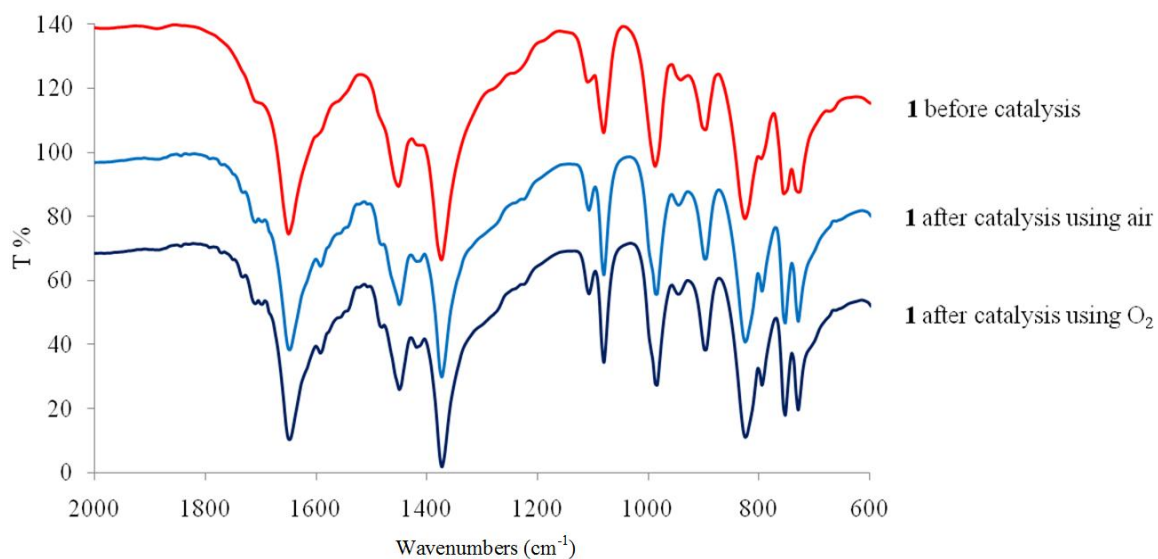
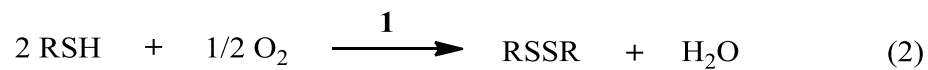


Figure 4-7. FT-IR spectra of **1** before and after the catalytic oxidation of H₂S using O₂ or air (approximately 4,000 turnovers).

Control experiments in aqueous solution using K₅[CuPW₁₁O₃₉] only or, separately, MOF-199 only showed no production of solid S₈. Additional experiments showed that the solid MOF decomposes in minutes based both on color change (blue to colorless) and dissolution of the material in the reaction solution (H₂O, pH 4.8). The POM-MOF was reproducibly much more stable to decomposition than the same MOF alone (no POM guest). The H₂S oxidation in gas phase catalyzed by **1** also exhibits the synergetic effects. No or very few oxidation products were detected in control experiments. Interestingly, the non-copper-containing polyanion, PW₁₂-MOF, showed very low activity in catalyzing H₂S oxidation. These results indicate that the Cu centers in the POM unit of **1** are very likely the active site for the H₂S oxidation. Production of S₈ by **1** in the gas phase stopped at TON ~ 10, in contrast to the aqueous solution H₂S oxidations, as expected because of the blockage of the pores in **1** by the oxidation product.

To assess the ability of **1** to catalyze other aerobic oxidations, the conversion of volatile mercaptans to less toxic and odorous disulfides was examined. Removal of sulfur-based harmful industrial chemicals^{55,56} is important in the deodorization and jet fuel sweetening industries.⁵⁷⁻⁵⁹ Aerobic mercaptan oxidation catalyzed by **1** was established to proceed readily under ambient conditions via the stoichiometry in eq 2.



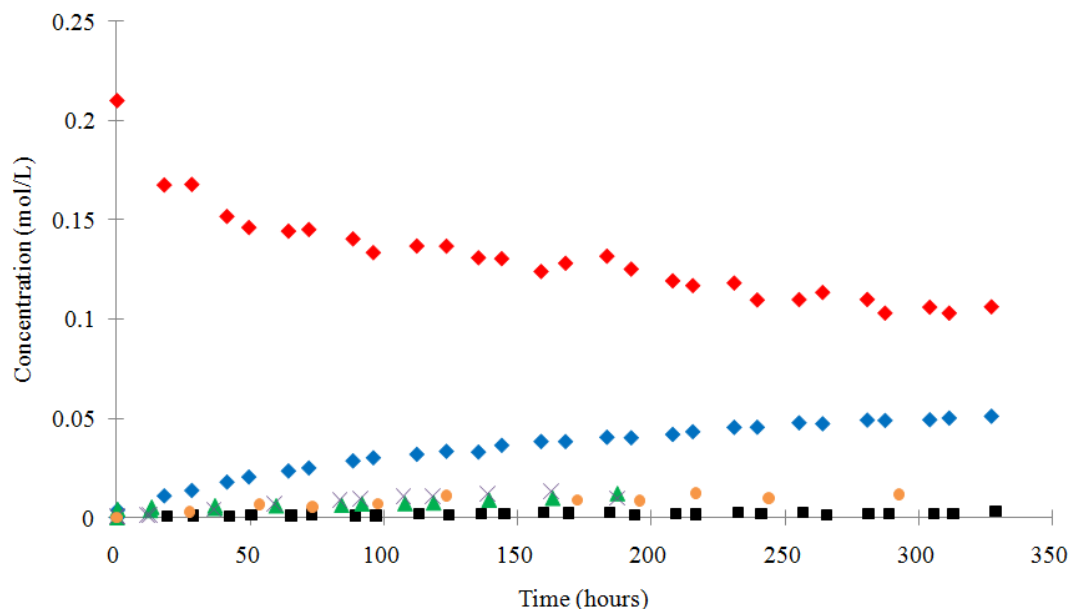


Figure 4-8. Aerobic oxidation of PrSH to PrSSPr catalyzed by **1**. PrSH (0.662 mmol) and the catalyst, **1** (10 mg, ~0.025 mmol), were stirred in chlorobenzene (2.9 mL) with decane (internal standard, 0.092 mmol) in a pressure tube fitted with a PTFE plug under 100% O₂ at 50 °C. Consumption of PrSH (red diamonds, ◆) and formation of PrSSPr (blue diamonds, ◆) catalyzed by **1**; PrSSPr concentration in presence of PW₁₂-MOF (orange circle, ●); PrSSPr concentration in presence of MOF-199 alone (green triangle, ▲); PrSSPr concentration in presence of TBA₅[CuPW₁₁O₃₉] alone (purple crosses, ×); and PrSSPr concentration in absence of any additives (black squares, ■).

Figure 4-8 shows the air-based oxidation of propanethiol (PrSH) in chlorobenzene solution catalyzed by **1**. Di-*n*-propyl disulfide was the only product detected by gas chromatography and mass spectrometry. Under the same reaction conditions where **1** produces 200 turnovers, the production of disulfide is negligible in the absence of the catalyst. Significantly, the activity of an equimolar amount of the tetrabutylammonium

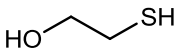
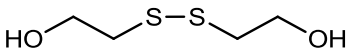
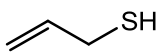
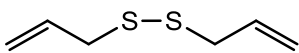
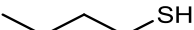
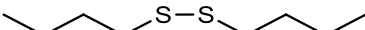
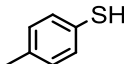
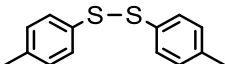
salt of the mono-copper-substituted-POM, $\text{TBA}_5[\text{CuPW}_{11}\text{O}_{39}]$, (homogeneous catalyst), POM-free MOF-199, and PW_{12} -MOF (heterogeneous) under identical conditions was assessed and shown to be *ca.* one order of magnitude lower than that of the new material, **1**, itself. Immobilization of homogeneous catalysts usually results in turnover rates that are one to three orders of magnitude lower than those for the same catalyst in solution, although we have noted modest increases in turnover rates when some POM catalysts are immobilized on cationic surfaces.^{46,60,61} It is likely that electrostatic interactions between the solvent-accessible Cu(II) centers of the MOF structure and the encapsulated $[\text{CuPW}_{11}\text{O}_{39}]^{5-}$ units are present in **1** and these stabilize **1** relative to its components. Such electrostatic POM-MOF interactions could simultaneously increase the potential of the Cu centers in the POM unit of **1** which would be expected to increase the rates of the substrate oxidation- $[\text{CuPW}_{11}\text{O}_{39}]^{5-}$ reduction step in the overall oxidations catalyzed by the POM-MOF. Reoxidation of Cu(I) centers in the reduced POM units of **1** by O_2 is not rate limiting because the overall oxidation rates are independent of O_2 pressure.

Table 4-4 summarizes the air-based oxidations of representative mercaptans varying in electron density, nucleophilicity and steric bulk around the sulfur atom catalyzed by **1** under similar conditions. Gas chromatographic analyses confirm the 99% chemoselective oxidation of all the evaluated mercaptans to disulfides. In addition, size and shape-dependent selectivity is clearly observed in these reactions. 2-Hydroxyethanethiol gives the highest conversion (95%) while *p*-toluenethiol gives less than a 30% yield of disulfide. Conversions decrease with an increase in the number of mercaptan carbon atoms. This is consistent with thiol oxidation by the POM units encapsulated in the MOF:

electronically similar but sterically larger thiols are less accessible to the POM units and thus are oxidized at lower rates. The disulfide products are also obtained in proportionally lower yields. The higher conversion for oxidation of 2-hydroxyethanethiol relative to other thiols is attributed to the higher affinity of this hydrogen-bonding thiol for the hydrophilic channels in the MOF. Again, the rates of propanethiol oxidation under air and pure O₂ catalyzed by **1** are very similar, indicating that POM reduction, and not reduced POM re-oxidation by O₂, is rate limiting.

The used catalyst, **1**, is readily separated from the catalytic oxidations described above by filtration. The separated supernatant of the reaction solution shows no catalytic activity for any of the aerobic oxidations reported here. The isolated catalyst was reused for these reactions after simple filtration, washing with dichloromethane and drying. The electronic absorption spectrum of the dichloromethane filtrate shows no leaching of the POM from **1** whatsoever.

Table 4-4. The aerobic oxidation of thiols to disulfides catalyzed by **1**.

Substrates	Products	Selectivity	Conversions
		99%	95%
		99%	77%
		99%	32%
		99%	27%

Conversion measured after 62 hours; in a typical kinetic experiment, substrate thiol (6.5×10^{-4} mol), decane (18.0 μL , 9.2×10^{-5} mol, internal standard) and **1** were stirred in chlorobenzene (2.9 mL) in a pressure tube fitted with a PTFE septum stopper under O_2 or air at 45 $^\circ\text{C}$. A control reaction conducted under the same conditions except without catalyst showed no oxidation products whatsoever.

Significantly, the integrated ensemble, **1**, is very robust in both aqueous and organic solutions during the catalysis. Enhanced structural and hydrolytic stability of both $[\text{CuPW}_{11}\text{O}_{39}]^{5-}$ and MOF-199 in **1** relative to the POM alone (e.g. the K_5 salt) or the MOF alone is clearly observed over a wide pH range. $[\text{CuPW}_{11}\text{O}_{39}]^{5-}$ is hydrolytically stable in solution only from pH 2.0 to 5.9⁵² and decomposes quickly in basic aqueous solution. MOF networks usually exist in a much narrower pH range and the host framework used, MOF-199, has been determined to be only metastable at pH 4.0. In contrast, both the FT-IR and UV-vis spectra demonstrate that $[\text{CuPW}_{11}\text{O}_{39}]^{5-}$ when present in **1**, remains intact at pH 11.0 for at least 12 hours (Figure 4-9). This dramatic enhancement of POM stability upon incorporation into some MOFs has positive implications for catalytic and other applications.^{62,63}

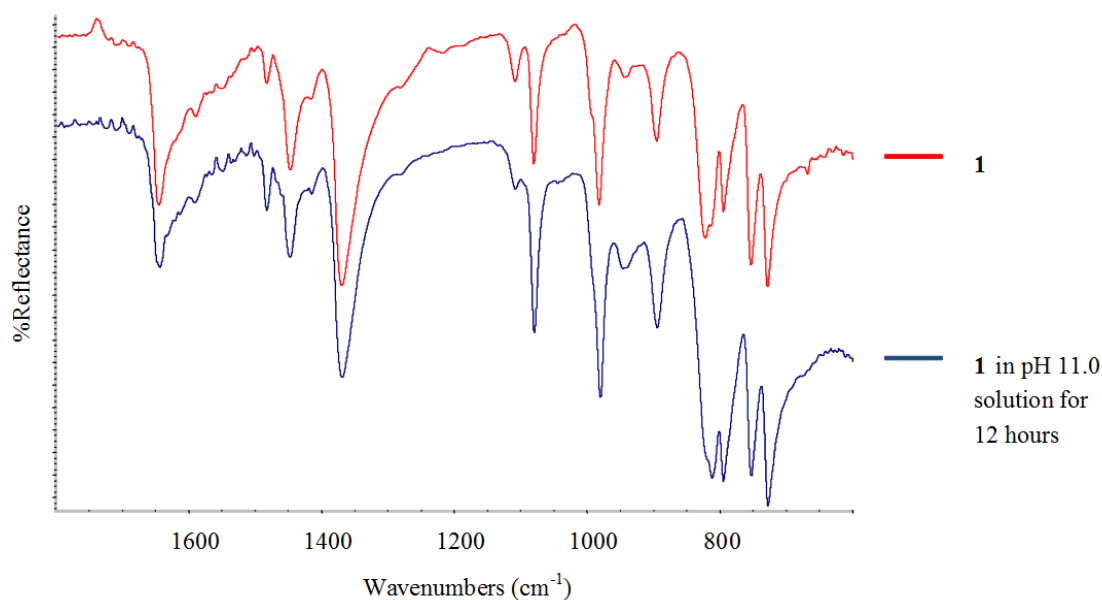


Figure 4-9. Reflect-IR of **1** before and after treatment in pH 11.0 aqueous solution for 12 hours.

Three lines of additional evidence indicate that **1** stays intact during the catalytic oxidation: (1) the recycled **1** catalyzes aerobic oxidation of H₂S and propanethiol for at least three cycles without significant activity loss; (2) the FT-IR of **1** after reaction retains all the characteristic peaks of the polyanion, [CuPW₁₁O₃₉]⁵⁻, and MOF-199, indicating that both structural components are stable (Figure 4-10); and (3) the X-ray powder diffraction patterns of **1** before and after use as a catalyst are identical (Figure 4-11).

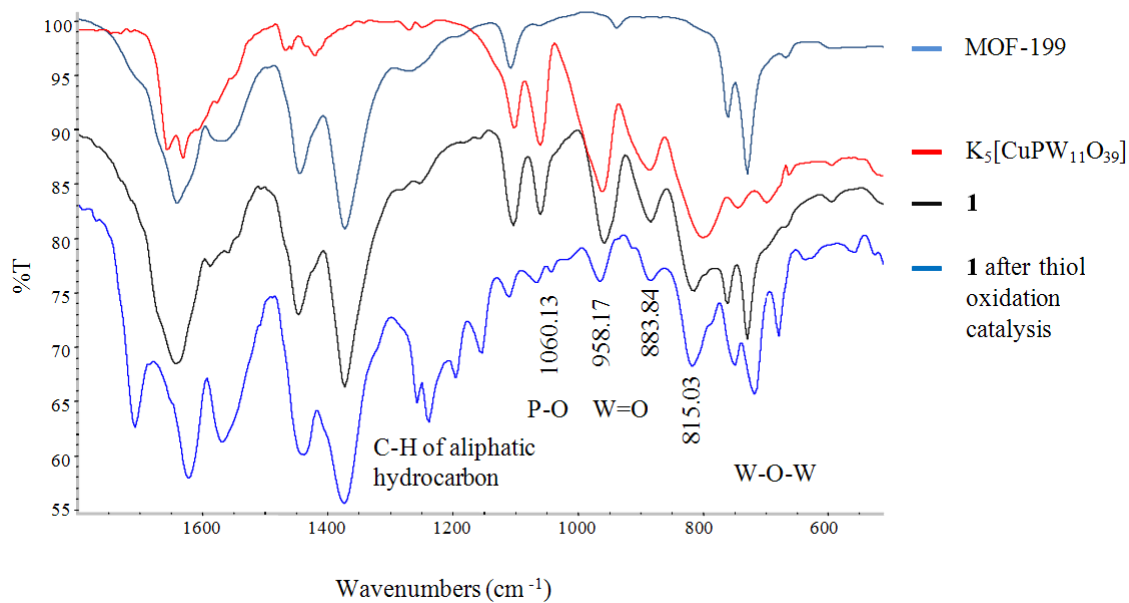


Figure 4-10. IR spectra of MOF-199, K₅[CuPW₁₁O₃₉], and **1** before and after the catalytic oxidation of propanethiol.

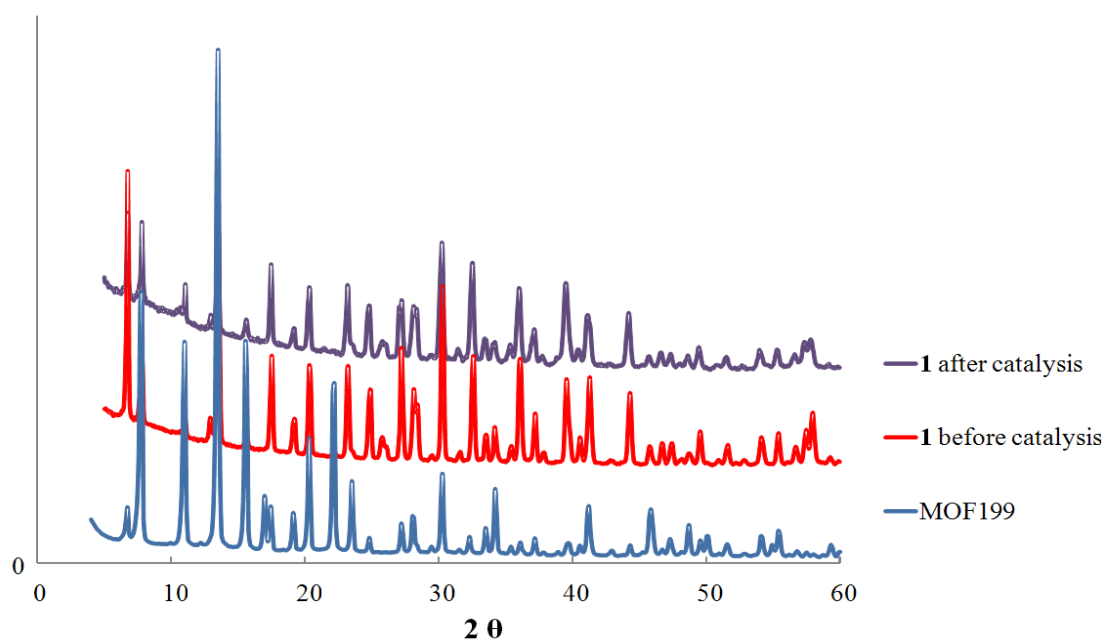


Figure 4-11. The powder X-ray diffraction patterns of MOF-199, **1**, and **1** after catalytic oxidation of propanethiol.

The present study clearly documents a new type of robust catalyst that exhibits the attractive features of both its components, the POM and the MOF, shows mutual enhancement of stability by each component, and efficiently catalyzes the detoxification of various sulfur compounds including H_2S to S_8 using only ambient air. Significantly, the synergy between the two structural components of **1** also extends to the catalytic activity of the polyanion: the $\{\text{CuPW}_{11}\}$ in **1** is one to several orders of magnitude faster under otherwise identical conditions in these aerobic oxidation reactions than it in solution. The fact that **1** is a readily re-isolated and re-used heterogeneous catalyst that requires only the ambient environment for some oxidation processes indicates its potential value as a versatile and robust catalytic decontaminant. Considering that both POMs and MOFs are two large classes of species with different compositions and structures, selective combinations of these two components would be expected to afford many new materials and this large experimental space could be tuned to target the catalytic removal of a range of other TICs and pollutants using just the ambient environment.

References

- (1) Kitagawa, S.; Kitaura, R.; Noro, S.-i. *Angew. Chem. Int. Ed.* **2004**, *43*, 2334
- (2) Long, J. R.; Yaghi, O. M. *Chem. Soc. Rev.* **2009**, *38*, 1213.
- (3) Tranchemontagne, D. J.; Mendoza-Cortes, J. L.; O'Keeffe, M.; Yaghi, O. M. *Chem. Soc. Rev.* **2009**, *38*, 1257.
- (4) O'Keeffe, M.; Peskov, M. A.; Ramsden, S. J.; Yaghi, O. M. *Acc. Chem. Res.* **2008**, *41*, 1782.
- (5) Ockwig, N. W.; Delgado-Friedrichs, O.; O'Keeffe, M.; Yaghi, O. M. *Acc. Chem. Res.* **2005**, *38*, 176.
- (6) Eddaoudi, M.; Moler, D. B.; Li, H.; Chen, B.; Reineke, T. M.; O'Keeffe, M.; Yaghi, O. M. *Acc. Chem. Res.* **2001**, *34*, 319.
- (7) Yaghi, O. M.; Li, H.; Davis, C.; Richardson, D.; Groy, T. L. *Acc. Chem. Res.* **1998**, *31*, 474.
- (8) Czaja, A. U.; Trukhan, N.; Muller, U. *Chem. Soc. Rev.* **2009**, *38*, 1284.
- (9) Duan, C.; Wei, M.; Guo, D.; He, C.; Meng, Q. *J. Am. Chem. Soc.* **2010**, *132*, 3321.
- (10) Zheng, S. T.; Zhang, J.; Yang, G. Y. *Angew. Chem. Int. Ed.* **2008**, *47*, 3909.
- (11) Alaerts, L.; Wahlen, J.; Jacobs, P. A.; Vos, D. E. D. *Chem. Commun.* **2008**, 1727.
- (12) Corma, A.; Garc ía, H.; Xamena, F. X. L. *Chem. Rev.* **2010**, *110*, 4606.
- (13) Ma, L.; Abney, C.; Lin, W. *Chem. Soc. Rev.* **2009**, *38*, 1248.
- (14) Férey, G. *Chem. Soc. Rev.* **2008**, *37*, 191.

- (15) Eddaoudi, M.; Kim, J.; Rosi, N.; Vodak, D.; Wachter, J.; O'Keeffe, M.; Yaghi, O. M. *Science* **2002**, *295*, 469.
- (16) Murray, L. J.; Dinca, M.; Long, J. R. *Chem. Soc. Rev.* **2009**, *38*, 1294.
- (17) Yoon, J. W.; Jhung, S. H.; Hwang, Y. K.; Humphrey, S. M.; Wood, P. T.; Chang, J.-S. *Adv. Mater.* **2007**, *19*, 1830.
- (18) Matsuda, R.; Kitaura, R.; Kitagawa, S.; Kubota, Y.; Belosludov, R. V.; Kobayashi, T. C.; Sakamoto, H.; Chiba, T.; Takata, M.; Kawazoe, Y.; Mita, Y. *Nature* **2005**, *436*, 238.
- (19) Li, J.-R.; Kuppler, R. J.; Zhou, H.-C. *Chem. Soc. Rev.* **2009**, *38*, 1477.
- (20) Chen, B.; et al. *Angew. Chem. Int. Ed.* **2006**, *45*, 1390.
- (21) Halder, G. J.; Kepert, C. J.; Moubaraki, B.; Murray, K. S.; Cashion, J. D. *Science* **2002**, *298*, 1762.
- (22) Cheng, X. N.; Zhang, W. X.; Lin, Y. Y.; Zheng, Y. Z.; Chen, X. M. *Adv. Mater.* **2007**, *19*, 1494.
- (23) Evans, O. R.; Lin, W. *Acc. Chem. Res.* **2002**, *35*, 511.
- (24) Seo, J. S.; Whang, D.; Lee, H.; Jun, S. I.; Oh, J.; Jeon, Y. J.; Kim, K. *Nature (London)* **2000**, *404*, 982.
- (25) Lee, J. Y.; Farha, O. K.; Roberts, J.; Scheidt, K. A.; Nguyen, S. B. T.; Hupp, J. T. *Chem. Soc. Rev.* **2009**, *38*, 1450.
- (26) Uemura, T.; Yanai, N.; Kitagawa, S. *Chem. Soc. Rev.* **2009**, *38*, 1228.
- (27) Zeng, H.; Newkome, G. R.; Hill, C. L. *Angew. Chem. Int. Ed.* **2000**, *39*, 1771.
- (28) Yang, L.; Naruke, H.; Yamase, T. *Inorg. Chem. Comm.* **2003**, *6*, 1020.

- (29) Han, J. W.; Hardcastle, K. I.; Hill, C. L. *Eur. J. Inorg. Chem.* **2006**, 2598.
- (30) Han, J. W.; Hill, C. L. *J. Am. Chem. Soc.* **2007**, *129*, 15094.
- (31) Maksimchuk, N. V.; Timofeeva, M. N.; Melgunov, M. S.; Shmakov, A. N.; Chesalov, Y. A.; Dybtsev, D. N.; Fedin, V. P.; Kholdeeva, O. A. *J. Catal.* **2008**, *257*, 315.
- (32) Sun, C.-Y.; Liu, S.-X.; Liang, D.-D.; Shao, K.-Z.; Ren, Y.-H.; Su, Z.-M. *J. Am. Chem. Soc.* **2009**, *131*, 1883.
- (33) Yu, R.; Kuang, X.-F.; Xiao-YuanWu; Lu, C.-Z.; Donahue, J. P. *Coord. Chem. Rev.* **2009**, *253*, 2872.
- (34) Maksimchuk, N. V.; Kovalenko, K. A.; Arzumanov, S. S.; Chesalov, Y. A.; Melgunov, M. S.; Stepanov, A. G.; Fedin, V. P.; Kholdeeva, O. A. *Inorg. Chem.* **2010**, *49*, 2920.
- (35) Inman, C.; Knaust, J. M.; Keller, S. W. A. *Chem. Commun.* **2002**, 156.
- (36) Ni, Z.; Jerrell, J. P.; Cadwallader, K. R.; Masel, R. I. *Anal. Chem.* **2007**, *79*, 1290.
- (37) Ma, F.-J.; Liu, S.-X.; Sun, C.-Y.; Liang, D.-D.; Ren, G.-J.; Wei, F.; Chen, Y.-G.; Su, Z.-M. *J. Am. Chem. Soc.* **2011**, *133*, 4178.
- (38) Hill, C. L.; Okun, N. M.; Hillesheim, D. A.; Geletii, Y. V. In *Anti-Terrorism and Homeland Defense: Polymers and Materials, ACS Symposium Series 980, Chapter 12*; Reynolds, J. G., Lawson, G. E., Koester, C. J., Eds.; American Chemical Society: Washington, D.C., 2007, p 198.
- (39) Britt, D.; Tranchemontagne, D.; Yaghi, O. M. *Proc. Natl. Acad. Sci.* **2008**, *105*, 11623.
- (40) Pope, M. T.; Müller, A. *Angew. Chem. Int. Ed. Engl.* **1991**, *30*, 34.

- (41) Borrás-Almenar, J. J.; Coronado, E.; Müller, A.; Pope, M. T. *Polyoxometalate Molecular Science*; Kluwer Academic Publishers: Dordrecht, 2003; Vol. 98.
- (42) Hill, C. L. In *Comprehensive Coordination Chemistry-II: From Biology to Nanotechnology*; Wedd, A. G., Ed.; Elsevier Ltd.: Oxford, UK, 2004; Vol. 4, p 679.
- (43) Pope, M. T. In *Comprehensive Coordination Chemistry II: From Biology to Nanotechnology*; Wedd, A. G., Ed.; Elsevier Ltd.: Oxford, UK, 2004; Vol. 4, p 635.
- (44) Kögerler, P.; Cronin, L. *Angew. Chem. Int. Ed.* **2005**, *44*, 844.
- (45) Long, D.-L.; Burkholder, E.; Cronin, L. *Chem. Soc. Rev.* **2007**, *36*, 105.
- (46) Okun, N. M.; Anderson, T. M.; Hill, C. L. *J. Mol. Catal. A: Chem.* **2003**, *197*, 283.
- (47) Kholdeeva, O. A.; Timofeeva, M. N.; Maksimov, G. M.; Maksimovskaya, R. I.; Neiwert, W. A.; Hill, C. L. *Inorg. Chem.* **2005**, *44*, 666.
- (48) Okun, N. M.; Tarr, J. C.; Hilleshiem, D. A.; Zhang, L.; Hardcastle, K. I.; Hill, C. L. *J. Mol. Catal. A: Chem.* **2006**, *246*, 11.
- (49) Hill, C. L. *J. Mol. Catal. A: Chem.* **2007**, *262*, 2.
- (50) Férey, G.; Mellot-Draznieks, C.; Serre, C.; Millange, F.; Dutour, J.; Surblé S.; Margiolaki, I. *Science* **2005**, *309*, 2040.
- (51) Chui, S. S.-Y.; Lo, S. M.-F.; Charmant, J. P. H.; Orpen, A. G.; Williams, I. D. *Science* **1999**, *283*, 1148.
- (52) Tourné C. M.; Tourné G. F.; Malik, S. A.; Weakley, T. J. R. *J. Inorg. Nucl. Chem.* **1970**, *32*, 3875.
- (53) Bruker AXS, I.; Analytical X-ray Systems: Madison, WI, 2003.

- (54) Bruker AXS, I.; Analytical X-ray Systems: Madison, WI, 2003.
- (55) Xu, L.; Boring, E.; Hill, C. *J. Catal.* **2000**, *195*, 394.
- (56) Hill, C. L.; Anderson, T. M.; Han, J.; Hillesheim, D. A.; Geletii, Y. V.; Okun, N. M.; Cao, R.; Botar, B.; Musaev, D. G.; Morokuma, K. *J. Mol. Catal. A: Chem.* **2006**, *251*, 234.
- (57) EPA, U. S. In *Profile of the Petroleum Refining Industry* 1995, p 30.
- (58) Basu, B.; Satapathy, S.; Bhatnagar, A. K. *Catal. Rev., Sci. Eng.* **1993**, *35*, 571.
- (59) Leitao, A.; Rodrigues, A. *Chem. Eng. Sci.* **1990**, *45*, 679.
- (60) Okun, N. M.; Anderson, T. M.; Hill, C. L. *J. Am. Chem. Soc.* **2003**, *125*, 3194.
- (61) Okun, N. M.; Ritorto, M. D.; Anderson, T. M.; Apkarian, R. P.; Hill, C. L. *Chem. Mater.* **2004**, *16*, 2551.
- (62) Cho, S.-H.; Ma, B.; Nguyen, S. T.; Hupp, J. T.; Albrecht-Schmitt, T. E. *Chem. Commun.* **2006**, 2563.
- (63) Isaeva, V. I.; Kustov, L. M. *Petr. Chem.* **2010**, *50*, 167.

———— CHAPTER ————

5

**Synthesis, Structure, and Characterization of Two
Polyoxometalate-Photosensitizer Hybrid Materials**

Abstract

Two hybrid materials based on the tris(bipyridine)ruthenium(II), $[\text{Ru}(\text{bpy})_3]^{2+}$ and Keggin-type polyoxometalates, $[\text{PW}_{11}\text{O}_{39}]^{7-}$ and $[\text{PW}_{12}\text{O}_{40}]^{3-}$, namely, $[\text{Ru}(\text{bpy})_3][\text{K}_5\text{PW}_{11}\text{O}_{39}]$ (**1**) and $[\text{Ru}(\text{bpy})_3][\text{KPW}_{12}\text{O}_{40}]$ (**2**) were synthesized. X-ray crystallographic studies of the red-colored complex, **2**, showed that it crystallizes in the orthorhombic space group P_{bcn} and the polyanions are associated with the cationic $[\text{Ru}(\text{bpy})_3]^{2+}$ by Coulombic forces and supramolecular interactions. The molecular complex is further connected and forms a three dimensional framework through C-H \cdots O_{POM} and other weak interactions. These complexes were further characterized by FT-IR, UV-vis, ^1H and ^{31}P NMR, luminescent spectra and computational studies. Significantly, these combined spectroscopic studies show that these polyoxometalate-dye hybrids have strong electronic interactions between the cationic dye and polyanion units.

Introduction

It is well-known that photosensitizers (henceforth “dyes”) play the key role in light harvesting and light-to-current conversion in the dye-sensitized solar cells (DSSCs). Grätzel and his co-workers long ago demonstrated that photoanodes comprising $[\text{Ru}(\text{bpy})_3]^{2+}$ bonded to TiO_2 not only generate photocurrent with visible light when interfaced with the iodine/iodide couple but also operate for thousands of hours with minimal degradation in performance^{1,2}. The counterions of cationic dyes affect the photoinjection quantum yields, in part because they impact charge separation and recombination rates and efficiencies.^{3,4} Polyoxometalates (POMs) are a wide class of negatively charged later transition metal oxide clusters with variable molecular

components, structures, and redox properties.^{5,6} Recently, particular d-electron-transition metal-substituted POMs were reported to be stable and fast water oxidation catalysts.⁷⁻¹² In the proposed catalytic cycle of water oxidation, the tris(bipyridine)ruthenium(II) chloride dye is used to induce the electron transfer process from the water molecule to the POM catalyst. The process initiated from excited dye produced either by chemical oxidants or by visible light demonstrates that the electron transfer between the dye and POM molecule is possible under selected experimental conditions. Interest in the synthesis of POM-dye hybrid materials is growing up in the past several years due to their potential applications,¹³⁻¹⁶ but few studies on the details of the POM-dye structure associated with the electron transfer process among these systems have been reported.¹⁷⁻²⁰

Here we report the synthesis of hybrid POM-tris(bipyridine)ruthenium dye complexes, $[\text{Ru}(\text{bpy})_3][\text{K}_5\text{PW}_{11}\text{O}_{39}]$ (**1**) and $[\text{Ru}(\text{bpy})_3][\text{KPW}_{12}\text{O}_{40}]$ (**2**), but significantly that spectroscopic measurements combined with theoretical calculations indicate strong interactions between the cationic and anionic moieties in these hybrid materials.

Experimental section

Material and instrumentation

$\text{K}_7[\text{PW}_{11}\text{O}_{39}]$ was synthesized according to the literature procedures²¹, and all the other starting materials were obtained commercially and used as received. ^1H and ^{31}P NMR spectra were recorded on a Varian INOVA 400 MHz instrument and chemical shifts were measured in parts per million (ppm) relative to the deuterated solvent used in the experiment. Infrared spectra (FT-IR) were obtained on a Nicolet 510 FT-IR

spectrophotometer with KBr pellets. UV-Vis spectra were acquired using 8453 spectrophotometer. Elemental analyses for C, H and, N were performed by Atlantic Microlab, Norcross, GA, and elemental analyses for all other elements were performed either by Columbia Analytical Services, Tucson, AZ or by Galbraith Laboratories, Inc., Knoxville, TN. Mass spectra were recorded on a JEOL JMS-SX102/SX102A/E mass spectrometer (ESI). X-ray crystallography studies were carried out in the X-ray Crystallography Laboratory at Emory University on a Bruker Smart Apex II CCD diffractometer. Steady-state emission spectra of the samples were measured using a SPEX FluoroLog-3 self-contained and fully automated spectrofluorometer.

Syntheses

[Ru(bpy)₃][K₅PW₁₁O₃₉] (1)

To a solution of K₇PW₁₁O₃₉ (0.49 g, 0.16 mmol) in distilled water (10 mL), was slowly added [Ru(bpy)₃]Cl₂ (0.1 g, 0.16 mmol) in distilled water (10 mL). The resulted suspension was placed in dark and stirred for 12 hours. Orange-red precipitates were collected by centrifuge and washed by water (10 mL × 3), acetone (10 mL × 3), and diethyl ether (10 mL × 3) successively. Thus obtained product was dried in vacuo at room temperature overnight before use. The hybrid POM-dye complexes are light-sensitive and thus covered with aluminum foil and stored in the dark. Yield: 0.51 g (91%, based on dye) for (1). ¹H NMR (δ, *d*-DMSO): 8.845 (2H, *d*), 8.184 (2H, *t*), 7.746 (2H, *d*), 7.556 (2H, *t*) ppm. ³¹P NMR (δ, *d*-DMSO): -8.679 ppm (in comparison to K₇PW₁₁O₃₉: -7.782). FT-IR (KBr, cm⁻¹): 3075.1(w), 1632.8 (m), 1602.6 (m), 1463.8 (m), 1445.4 (m), 1423.7 (m), 1077.0 (m), 1039.4 (vs), 943.5 (vs), 852.9(vs), 811.9(vs), 758.4 (vs), 591.7 (w),

511.6 (m); in comparison to $\text{H}_7\text{PW}_{11}\text{O}_{39}$: 1631.7 (m), 1087.4 (m), 1041.9 (m), 950.7 (vs), 901.2 (m), 857.0 (vs) 805.6 (vs), 729.6 (vs), 591.0 (w), 509.0 (m). Elemental analysis *Calc.* for $\text{C}_{30}\text{H}_{24}\text{K}_5\text{N}_6\text{O}_{39}\text{PRuW}_{11}$: C, 10.47; H, 0.70; N, 2.44; K, 5.68; P, 0.90; Ru, 2.94; W, 58.75. *Found*: C, 10.02; H, 0.82; N, 2.36; K, 5.28; P, 0.86; Ru, 2.84; W, 58.15.

[Ru(bpy)₃][KPW₁₂O₄₀] (2)

The title crystalline **2** was prepared by a slow diffusion of reactants by making three liquid layers: an aqueous solution (10 mL) containing $\text{H}_3\text{PW}_{12}\text{O}_{40}$ (0.46 g, 0.16 mmol) and KCl (0.03 g, 0.32 mmol) on the bottom, a mixed solvent (2 mL, $\text{H}_2\text{O}/\text{EtOH} = 2/1$; v/v) separating phase in the middle, and a $[\text{Ru}(\text{bpy})_3]\text{Cl}_2$ (0.1 g, 0.16 mmol) solution in EtOH (5 mL) on top of the mixed solvent layer. Orange-red crystals formed after 3 weeks and were removed by filtration, washed with water and air-dried. Yield: 0.52 g (94%, based on dye) for **2**. ^1H NMR (δ , *d*-DMSO): 8.828 (2H, *d*), 8.167 (2H, *t*), 7.732 (2H, *d*), 7.530 (2H, *t*) ppm. ^{31}P NMR (δ , *d*-DMSO): -12.798 ppm (in comparison to $\text{H}_3\text{PW}_{12}\text{O}_{40}$: -12.762). FT-IR (KBr, cm^{-1}): 3081.1(w), 1704.4 (m), 1655.2 (m), 1603.4 (m), 1464.0 (m), 1446.0 (m), 1079.2 (vs), 977.4 (vs), 897.6(vs), 814.1(vs), 759.4 (vs), 729.3 (m), 596.0 (w), 520.2 (m); in comparison to $\text{H}_3\text{PW}_{12}\text{O}_{40}$: 1616.8 (m), 1080.4 (vs), 984.5 (vs), 891.4(vs), 799.8 (vs), 595.1 (w), 524.0 (m). Elemental analysis *Calc.* for $\text{C}_{30}\text{H}_{24}\text{KN}_6\text{O}_{40}\text{PRuW}_{12}$: C, 10.34; H, 0.69; N, 2.41; P, 0.89; Ru, 2.90; W, 63.29. *Found*: C, 9.95; H, 0.79; N, 2.30; P, 0.81; Ru, 2.78; W, 59.49.

For comparison, the spectra of the thoroughly studied parent photosensitizer complex, [Ru(bpy)₃]Cl₂, are as follows: ¹H NMR (δ , *d*-DMSO): 8.844 (2H, *d*), 8.169 (2H, *t*), 7.727 (2H, *d*), 7.528 (2H, *t*). FT-IR (KBr, cm⁻¹): 3069.1(w), 1654.9 (m), 1601.6 (m), 1464.0 (m), 1443.7 (m), 1421.2 (m), 776.5 (vs), 730.6 (m). Both **1** and **2** were subjected to ESI-MS and MALDI-MS but both techniques failed to yield informative values.

X-ray crystallography

A crystal of complex **2** with size of 0.20 x 0.05 x 0.03 mm³ was mounted on a glass fiber capillary which was put on a Bruker Smart Apex II CCD diffractometer equipped with graphite monochromatic radiation and used for data collection. Data were collected at 173(2) K using MoK α radiation ($\lambda = 0.71073$ Å). The structure was solved by direct methods (SHELXTL-97) and refined by the full-matrix-block least-squares method on F^2 . All non-hydrogen atoms were refined with anisotropic displacement parameters. Heavy atoms (W and Ru) were refined with anisotropic displacement parameters and other atoms (O, C, N and P) were refined isotropically. Hydrogen atoms were included at calculated positions and refined with a riding model. A summary of the crystal data and refinement results are listed in **Table 5-1** and **5-3**. The CCDC reference number is 769589.

Table 5-1. Crystallographic parameters and refinement details for complex **2**.

2	
Empirical formula	C ₃₀ H ₂₄ KN ₆ O _{45.48} PRuW ₁₂
Formula weight	3573.57
T (K)	173(2) K
Crystal system	Orthorhombic
Space group	<i>Pbcn</i>
a (Å)	16.3036(17)
b (Å)	28.330(3)
c (Å)	16.4903(17)
β (°)	90
Volume (Å) ³	7616.4(13)
Z	4
Calculated density (Mg/m ³)	3.116
Absorption coefficient (mm ⁻¹)	18.395
Number of parameters/restraints	442, 0
Measured reflections	61348
Independent reflections	7962
R [I > 2σ (I)]	0.0850
R _w [I > 2σ (I)]	0.2506
Goodness-of-fit (GOF) on F ²	1.016
Largest difference peak and hole (e Å ⁻³)	2.733, -1.875

$$R = \frac{\sum |F_o| - |F_c|}{\sum |F_o|}, \quad R_w = \frac{[\sum w(F_o^2 - F_c^2)^2 / \sum w(F_o^2)^2]}^{1/2}$$

Static emission measurements.

Solutions of [Ru(bpy)₃]²⁺, [H₃PW₁₂O₄₀], and their mixtures were prepared and stored in the dark to avoid photodegradation. The solution of 5 μM [Ru(bpy)₂]²⁺ and less

than 30 μM $[\text{H}_3\text{PW}_{12}\text{O}_{40}]$ were used for all measurements due to the low solubility of the $[\text{Ru}(\text{bpy})_3]^{2+}/[\text{H}_3\text{PW}_{12}\text{O}_{40}]$ mixture in the used solvents. All solutions were degassed with N_2 before measurements. A 10x10 mm quartz cuvette and 1.8-nm excitation and emission slits were used. Samples were excited at 450 nm, and emission intensity data were collected and averaged over 615-620 nm at 20 $^\circ\text{C}$. Integration time was set at 0.05 s.

Computational methods

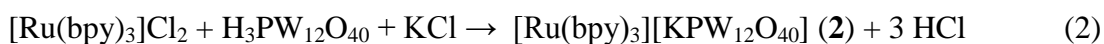
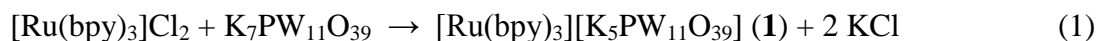
Full geometry optimization and energy calculation of the studied $[\text{Ru}(\text{bpy})_3]^{2+}$, $[\text{Ru}(\text{bpy})_3]^{3+}$, $[\text{PW}_{12}\text{O}_{40}]^{3-}$, $[\text{PW}_{12}\text{O}_{40}]^{4-}$ and the complex $\{[\text{Ru}(\text{bpy})_3]^{2+} \dots [\text{PW}_{12}\text{O}_{40}]^{3-}\}$ were performed in acetonitrile (at 300 K and 1 atm). In these calculations the BP86^{22,23} density functional and polarizable continuum model (PCM, with UFF atomic radii for all atoms)²⁴ in conjunction with lanl2dz basis sets²⁵⁻²⁷ for all atoms were utilized. Basis sets of P and N were augmented with polarization d-functions with exponents of 0.55 and 0.8, respectively. For Ru and W, the corresponding lanl2dz ECP²⁵⁻²⁷ were used. The calculations were carried out with Gaussian-09 quantum chemistry software package²⁸

Results and discussion

Syntheses

The two complexes were synthesized in one-step reaction with molar ratio of 1:1 by simply mixing solutions of the reactants. The resulting orange-red product could be purified by washing with pure water to remove the excess starting materials and byproduct, e.g. KCl or HCl (Scheme 5-1). Different photosensitizer-POM compounds

could be produced conveniently by varying the reactant molar ratio, reaction temperature, concentration and other solution variables.



Scheme 5-1. Synthesis of photosensitizer-POMs adducts.

Several crystal growth techniques including re-crystallization at high or low temperatures and vapor diffusion were employed; however, the only single X-ray quality crystals of **2** were obtained using the liquid-to-liquid diffusion method.

Crystal structure

Complex **2** crystallizes in the orthorhombic space group *Pbcn*. The asymmetric unit is composed of half a Keggin anion, one potassium cation, and half a tris(bipyridine)ruthenium(II) cation (**Figure 5-1**). The shortest distance between two Keggin anions is 2.946 Å and involves two terminal O(1) oxygen atoms. Each polyanion is surrounded by five adjacent $[\text{Ru}(\text{bpy})_3]^{2+}$ units. Some polyanion oxygen atoms are within hydrogen bonding distance of some bpy hydrogen atoms (key O--H distances are given in **Table 5-2** and others are in **Table 5-3**). According to the well-ordered packing of the anion and cation in the unit cell, all photosensitizer $[\text{Ru}(\text{bpy})_3]^{2+}$ units are separated quite uniformly from one another by the polyoxoanions, and as a consequence, there is no expected $\pi \cdots \pi$ or C-H $\cdots \pi$ interactions between the rigid bipyridine rings.

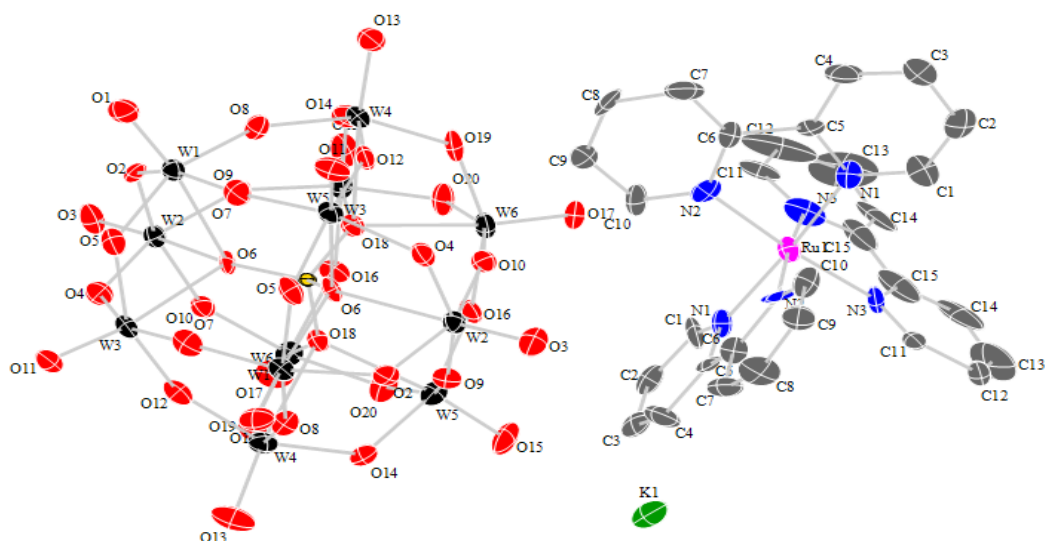


Figure 5-1. ORTEP diagram of the asymmetric unit of complex **2** with the atomic numbering scheme (30% thermal ellipsoids). Potassium (green), ruthenium (pink), carbon (green), tungsten (black), nitrogen (blue), and oxygen (red) phosphor (yellow). H atoms are omitted for clarity.

The crystal packing of **2** exhibits interesting three-dimensional structures (**Figure 5-2**). The crystal has large pores in all three crystallographic directions, and big channels of electrostatically attracted $[\text{Ru}(\text{bpy})_3]^{2+}$ and polyanion units exist along the *c*-axis. The microporous channels along the crystallographic *c*-axis exhibit longest and shortest dimensions of 10.067 and 9.700 Å, respectively. Such porous structures are potentially attractive for applications in sensor, adsorption and catalytic technologies. Nanostructures or devices that both detect and catalytically remove odorous and/or toxic agents are of considerable current interest²⁹.

Table 5-2. Atomic distances (Å) and angles (°) of $O_{POM} \cdots H_{pyr}$ interactions in the crystal structure of complex **2**.

	Bonding distance	Angle
O(7) \cdots H(14)C(14)	2.561	133.25
O(8) \cdots H(13)C(13)	2.899	98.67
O(10) \cdots H(9)C(9)	2.691	121.30
O(10) \cdots H(10)C(10)	2.683	124.33
O(11) \cdots H(13)C(13)	2.634	115.23
O(15) \cdots H(2)C(2)	2.563	116.00
O(15) \cdots H(3)C(3)	2.623	112.76
O(19) \cdots H(3)C(3)	2.903	88.84
O(19) \cdots H(9)C(9)	2.963	121.34

Table 5-3. Selected bond lengths (Å) and angles (°) for **2**. The bpy unit on the $[Ru(bpy)_3]^{2+}$ has disorder that could not be modeled well because the molecule sits on a symmetry site.

distance		angle	
C(1)-C(2)	1.36(6)	C(2)-C(1)-N(1)	127(4)
C(1)-N(1)	1.41(5)	C(3)-C(2)-C(1)	114(5)
C(2)-C(3)	1.31(5)	C(2)-C(3)-C(4)	123(4)
C(3)-C(4)	1.42(5)	C(3)-C(4)-C(5)	118(4)
C(4)-C(5)	1.43(4)	N(1)-C(5)-C(4)	120(3)

C(5)-N(1)	1.31(4)	N(1)-C(5)-C(6)	120(3)
C(5)-C(6)	1.44(5)	C(4)-C(5)-C(6)	120(3)
C(6)-C(7)	1.26(5)	C(7)-C(6)-C(5)	127(4)
C(6)-N(2)	1.45(5)	C(7)-C(6)-N(2)	122(4)
C(7)-C(8)	1.45(6)	C(5)-C(6)-N(2)	111(3)
C(8)-C(9)	1.38(5)	C(6)-C(7)-C(8)	118(4)
C(9)-C(10)	1.38(4)	C(9)-C(8)-C(7)	123(4)
C(10)-N(2)	1.32(3)	C(10)-C(9)-C(8)	112(3)
C(11)-N(3)	1.30(4)	N(2)-C(10)-C(9)	127(3)
C(11)-C(12)	1.3900	N(3)-C(11)-C(12)	121.5(19)
C(12)-C(13)	1.3900	C(13)-C(12)-C(11)	120.0
C(13)-C(14)	1.3900	C(14)-C(13)-C(12)	120.0
C(14)-C(15)	1.49(4)	C(13)-C(14)-C(15)	118.5(18)
C(15)-C(15)#1	1.34(8)	C(15)#1-C(15)-N(3)	117(2)
C(15)-N(3)	1.40(5)	C(15)#1-C(15)-C(14)	127.2(18)
K(1)-O(3W)#2	1.83(9)	N(3)-C(15)-C(14)	116(3)
K(1)-O(3W)#3	1.83(9)	C(5)-N(1)-C(1)	117(3)
K(1)-O(13W)	2.11(8)	C(5)-N(1)-Ru(1)	115(2)
K(1)-O(13W)#4	2.11(8)	C(1)-N(1)-Ru(1)	128(2)
K(1)-O(14W)#4	2.19(15)	C(10)-N(2)-C(6)	116(3)
K(1)-O(14W)	2.19(15)	C(10)-N(2)-Ru(1)	130(2)

K(1)-O(1W)#4	2.56(9)	C(6)-N(2)-Ru(1)	114(2)
K(1)-O(1W)	2.56(9)	C(11)-N(3)-C(15)	123(3)
K(1)-O(15W)	2.77(9)	C(11)-N(3)-Ru(1)	122(3)
K(1)-O(15W)#4	2.77(9)	C(15)-N(3)-Ru(1)	115(3)
K(1)-O(11W)#2	3.00(11)	N(2)-Ru(1)-N(2)#1	88.8(15)
K(1)-O(11W)#3	3.00(11)	N(2)-Ru(1)-N(1)#1	95.2(12)
N(1)-Ru(1)	2.05(3)	N(2)#1-Ru(1)-N(1)#1	79.6(12)
N(2)-Ru(1)	2.04(3)	N(2)-Ru(1)-N(1)	79.6(12)
N(3)-Ru(1)	2.07(3)	N(2)#1-Ru(1)-N(1)	95.2(12)
		N(2)-Ru(1)-N(3)#1	173.5(13)
		N(2)#1-Ru(1)-N(3)#1	97.0(13)
		N(1)#1-Ru(1)-N(3)#1	88.9(10)
		N(1)-Ru(1)-N(3)#1	96.7(10)
		N(2)-Ru(1)-N(3)	97.0(13)
		N(2)#1-Ru(1)-N(3)	173.5(13)
		N(1)#1-Ru(1)-N(3)	96.7(10)
		N(1)-Ru(1)-N(3)	88.9(10)
		N(3)#1-Ru(1)-N(3)	78(2)

Symmetry transformations used to generate equivalent atoms: #1 $-x, y, -z+3/2$; #2 $-x+1, -y+1, -z+1$; #3 $x-1, y, z$; #4 $-x, -y+1, -z+1$; #5 $-x, y, -z+1/2$; #6 $x+1, y, z$; #7 $-x+2, y, -z+3/2$.

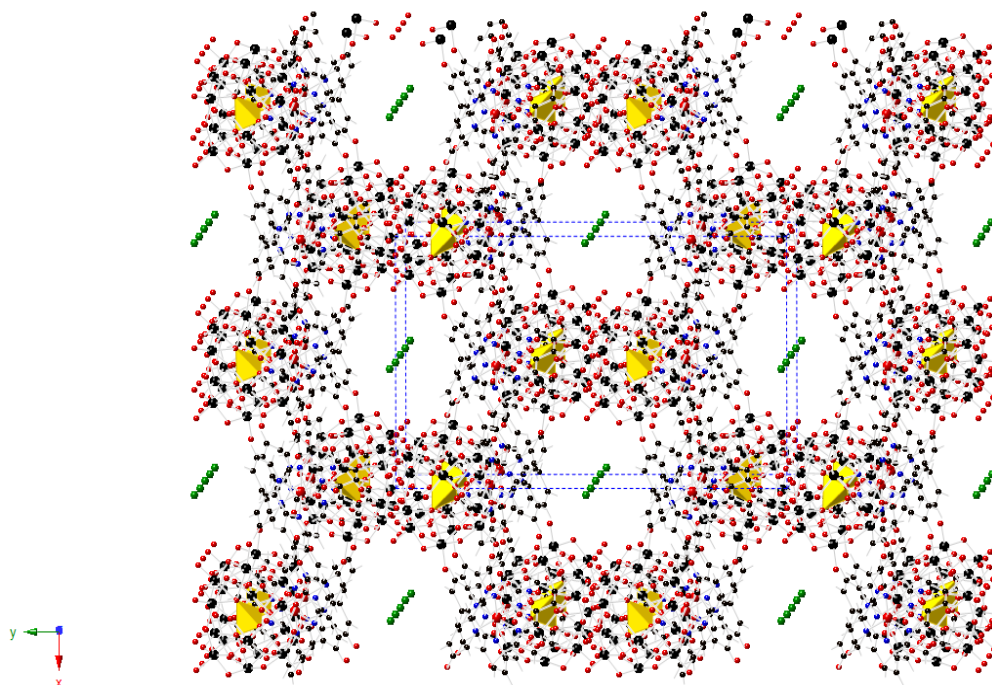


Figure 5-2. Three-dimensional structure of **2**: view of the ion channel of potassium in plane (001) or the z-axis.

Spectroscopic studies of the hybrid complexes

UV-vis and static emission spectra

The title complexes, **1** and **2**, were suspended in various solvents, followed by sonication and filtration. We used a mixed solvent for **2** because of its poor solubility in pure CH₃CN. **Figure 5-3** shows the UV/vis spectra of **1**, **2** and their components in different solvents. In pure DMSO, the absorption of each complex (**1** or **2**) is a sum of the absorptions of [Ru(bpy)₃]²⁺ and its POM counter ion ([K₅PW₁₁O₄₀]²⁻ or [PW₁₂O₄₀]³⁻), as shown in **Figure 5-3** for **2**.

However, for **1** in CH₃CN and for **2** in 9:1 CH₃CN/DMSO, the spectra show absorption bands centered at 540, 470 and 365 nm, respectively. These are significantly different from that of [Ru(bpy)₃]²⁺ suggesting the formation of strongly interacting complexes between the anionic POM and the [Ru(bpy)₃]²⁺ units. The nature of these new complexes and their absorption spectra are being investigated by computation and time-resolved spectroscopy.

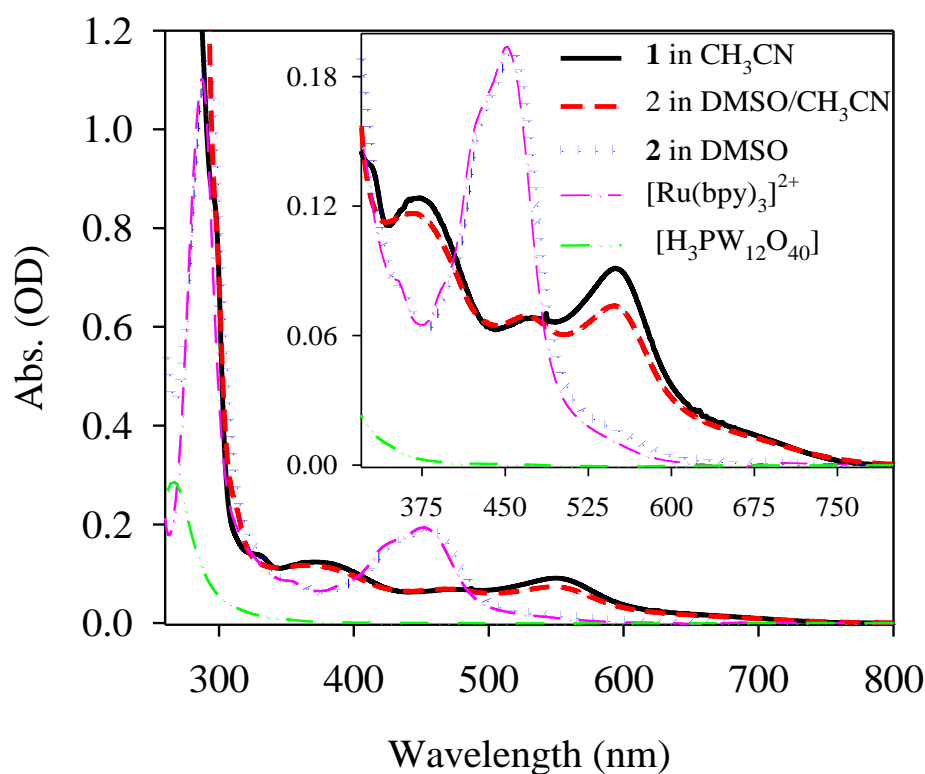


Figure 5-3. UV/vis spectra of **1** in CH₃CN (solid black line), **2** in CH₃CN/DMSO (9:1 in volume, dashed red line), **2** in DMSO (dotted blue curve), [Ru(bpy)₃]²⁺ in CH₃CN/DMSO (9:1 in volume, pink dash-dot-dash line), and [H₃PW₁₂O₄₀] in DMSO (green dash-dot-dot-dash line). The inset shows the enlarged spectra.

In addition, static emission quenching studies were carried out to verify the formation of ion pairs in DMSO/CH₃CN solution (**Figure 5-4 and 5-5**). The steady emission of [Ru(bpy)₃]²⁺ with (*I*) and without (*I*₀) [H₃PW₁₂O₄₀] was measured.

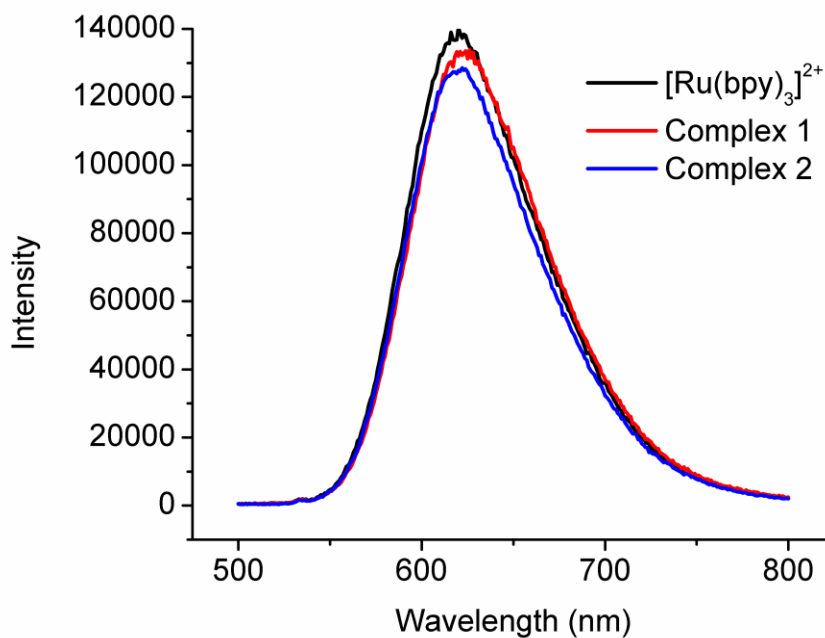


Figure 5-4. Emission spectra of the POM-Dye complexes in DMSO

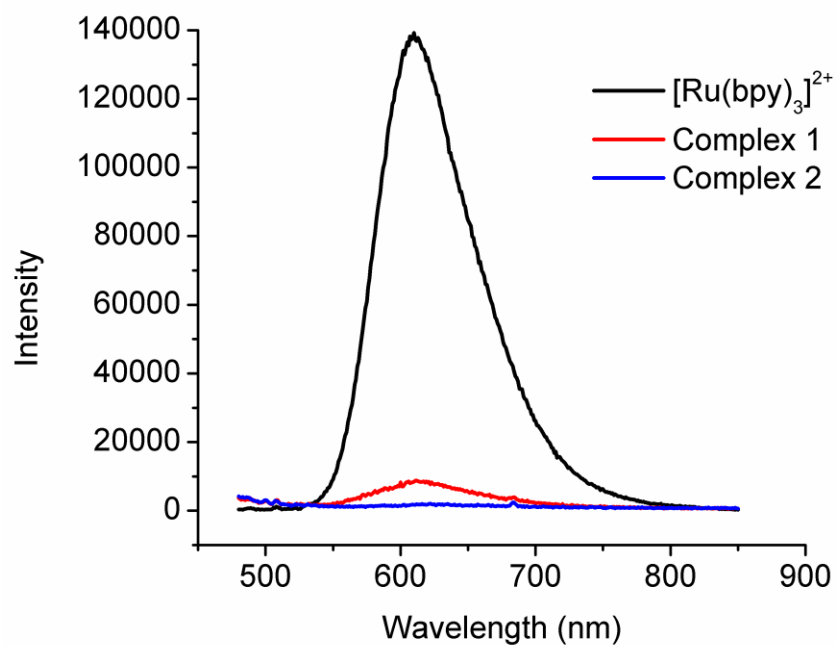


Figure 5-5. Emission spectra of the POM-Dye complexes in MeCN; fluorescence quenching were observed in MeCN solution

Figure 5-6 shows the resulting Stern-Volmer (SV) plots, I_0/I vs. $[\text{H}_3\text{PW}_{12}\text{O}_{40}]$. As seen from those plots, the $[\text{Ru}(\text{bpy})_3]^{2+}$ emission is quenched by the presence of $[\text{H}_3\text{PW}_{12}\text{O}_{40}]$. In pure DMSO, the SV plot is roughly linear within the range of the used $[\text{H}_3\text{PW}_{12}\text{O}_{40}]$ concentrations, suggesting a bimolecular emission quenching process that can be described using a typical linear SV equation:

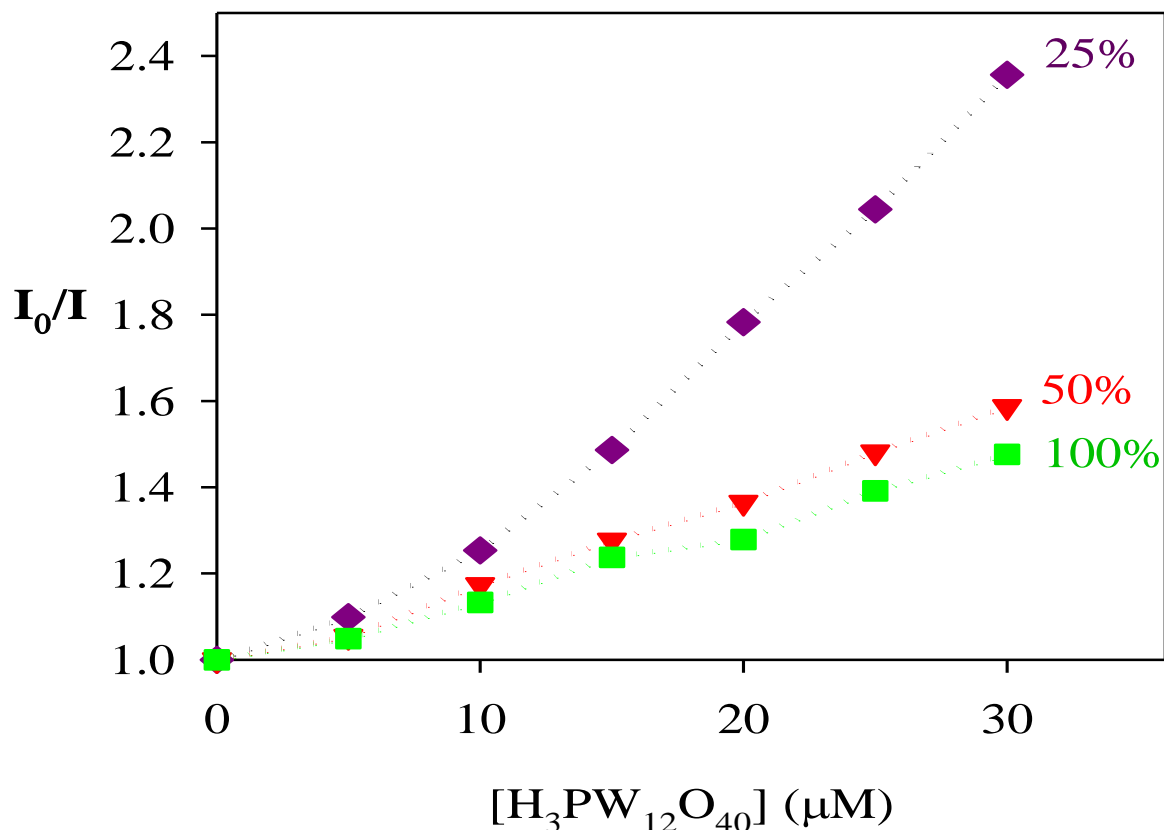


Figure 5-6. Stern-Volmer plots for samples in DMSO solutions containing 0% (green squares), 50% (red triangles) and 75% (purple diamonds) of CH₃CN in volume as indicated in the figure. All solutions contained 5 μM [Ru(bpy)₃]²⁺ and were purged with N₂. The emission intensities of [Ru(bpy)₃]²⁺ with (*I*) and without (*I*₀) [H₃PW₁₂O₄₀] were collected, averaged at 615 nm ~ 620 nm after 450 nm excitation.

$$I_0 / I = 1 + k_q \tau_0 [H_3PW_{12}O_{40}] \quad (1)$$

where k_q is the bimolecular quenching rate constant, and τ_0 is the intrinsic emission lifetime of the emitter, [Ru(bpy)₃]²⁺.

The quenching efficiency increases with increasing CH₃CN/DMSO ratio, suggesting that CH₃CN enhances the interaction between [Ru(bpy)₃]²⁺ and [PW₁₂O₄₀]³⁻. In addition, the presence of CH₃CN causes the SV plots to deviate from linearity and show an upward curvature. This may be caused by the formation of non-emitting ion pairs as seen in equation (2),

$$I_0 / I = (1 + k_q \tau_0 [\text{H}_3\text{PW}_{12}\text{O}_{40}]) (1 + K_{\text{eq}} [\text{H}_3\text{PW}_{12}\text{O}_{40}]) \quad (2)$$

where K_{eq} is the equilibrium constant of ion-pair formation. On the other hand, if emitting ion pairs form, the SV plot will show a downward curvature.^{30,31}

Therefore, our results imply that non-emitting or poorly-emitting ion pairs form in the solution, suggesting a fast photo-quenching process within the ion pair. Due to the lack of kinetic data, those plots were not able to be fit to the kinetic model outlined above. Kinetic studies by time-resolved fluorescence and transient spectroscopy to characterize the ion pairs are in progress.

FT-IR spectra

The FT-IR spectra are shown in **Figure 5-7**, and the major vibration modes are listed in **Table 5-4**. Both hybrid complexes exhibit several absorption peaks located in the range of 1423–1630 cm⁻¹, which correspond to the characteristic vibrations of the

2,2'-bpy ligand of the photosensitizer cation [12]. For complex **1**, the peaks at 1039 and 1077 cm^{-1} are attributed to the P–O stretches and the peak at 943 cm^{-1} is assigned to W=O stretches. In comparison with the lacunary complexes, $\text{K}_7\text{PW}_{11}\text{O}_{39}$, the bands at 750, 812 and 853 cm^{-1} could be assigned to the corner-shared ($\text{W}-\text{O}_c-\text{W}$) and edge shared ($\text{W}-\text{O}_b-\text{W}$) octahedra of the Keggin unit. For **2**, the similar peak shifts are also observed (Figure 5-7, Table 5-4). The higher energies for the W=O and P–O stretches is consistent with a strong interaction existing between POM anion with the dye $[\text{Ru}(\text{bpy})_3]^{2+}$ cation in the hybrids.³²

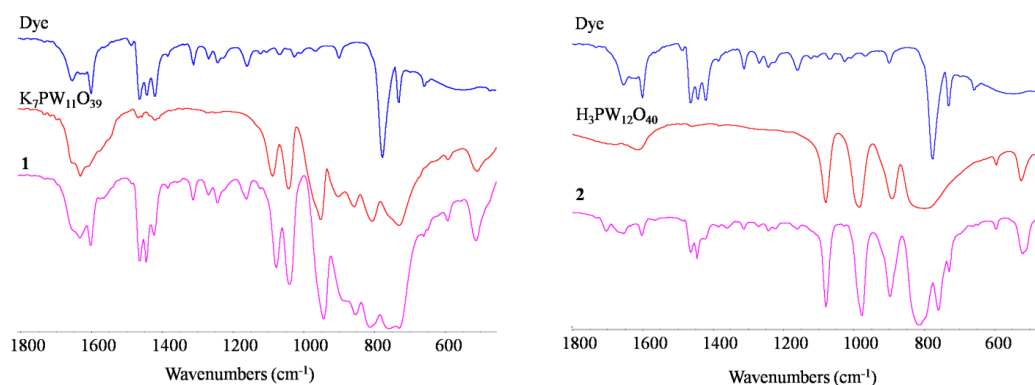


Figure 5-7. FT-IR spectra of the dye and the hybrid complexes.

Table 5-4. Major FT-IR peaks for $K_7PW_{11}O_{39}$, $H_3PW_{12}O_{40}$, $[Ru(bpy)_3]^{2+}$, and the two hybrid complexes, **1** and **2** (cm^{-1}).

	complex 1	$K_7PW_{11}O_{39}$	dye	complex 2	$H_3PW_{12}O_{40}$
W-O _c - W	750, 812	730, 805		814	799
W-O _b - W	853	857		897	891
W=O _d	943	950		977	984
P-O _a	1039, 1077	1041, 1087		1079	1080
2,2'-bpy	1423-1463, 1602-1632		1421-1464, 1601-1654	1425-1464, 1603-1655	

³¹P and ¹H NMR spectra

³¹P and ¹H NMR of the hybrid complexes were measured in deuterated DMSO solvent (**Table 5-5**). The ³¹P NMR spectra clearly demonstrate that the phosphorus peaks at -8.679 ppm for **1** and -12.798 ppm for **2** are moved to high field in comparison with the chemical shifts of $K_7PW_{11}O_{39}$ at -7.782 ppm and $H_3PW_{12}O_{40}$ at -12.762 ppm, respectively. The ¹H NMR spectra of both complexes also exhibit changes of chemical shift for protons on the bipyridine ligands.

Table 5-5. ^{31}P and ^1H NMR for $\text{K}_7\text{PW}_{11}\text{O}_{39}$, $\text{H}_3\text{PW}_{12}\text{O}_{40}$, $[\text{Ru}(\text{bpy})_3]^{2+}$, and the two hydrid complexes, **1** and **2** in *d*-DMSO (ppm).

	dye	$\text{K}_7\text{PW}_{11}\text{O}_{39}$	Complex (1)	$\text{H}_3\text{PW}_{12}\text{O}_{40}$	Complex (2)
^{31}P		-7.782	-8.679	-12.762	-12.798
^1H	8.844(2H, <i>d</i>), 8.169 (2H, <i>t</i>), 7.727 (2H, <i>d</i>), 7.528 (2H, <i>t</i>).		8.845 (2H, <i>d</i>), 8.184 (2H, <i>t</i>), 7.746 (2H, <i>d</i>), 7.556 (2H, <i>t</i>).		8.828(2H, <i>d</i>), 8.167 (2H, <i>t</i>), 7.732 (2H, <i>d</i>), 7.530 (2H, <i>t</i>).

Computational study.

As demonstrated in our previous paper³⁰ the ground electronic state of $[\text{Ru}(\text{bpy})_3]^{2+}$ is a closed-shell singlet state. Its few uppermost doubly occupied MOs (HOMOs) are primarily Ru d-orbitals. The first three lowest-unoccupied MOs (LUMOs) are localized on the bpy ligands and represent π^* -orbitals of the bpy rings. Removing an electron from $[\text{Ru}(\text{bpy})_3]^{2+}$ to yield a doublet $[\text{Ru}(\text{bpy})_3]^{3+}$ requires 6.1 eV.

The ground electronic state of the $[\text{PW}_{12}\text{O}_{40}]^{3-}$ polyoxoanion is also a closed-shell singlet. Its first few LUMOs are W-O antibonding (mostly W d-orbitals) orbitals, while the about forty uppermost doubly occupied orbitals are 2p-lone pairs of the oxygen centers. The next set of doubly occupied orbitals of $[\text{PW}_{12}\text{O}_{40}]^{3-}$, after the oxygen lone pairs, are the W-O bonding orbitals. Calculations show that the electron affinity of $[\text{PW}_{12}\text{O}_{40}]^{3-}$ is *ca* 4.6 eV.

The above presented thermodynamic data indicate that removing one electron from $[\text{Ru}(\text{bpy})_3]^{2+}$ and placing it on $[\text{PW}_{12}\text{O}_{40}]^{3-}$ requires 1.5 eV. In other words, the electron transfer from $[\text{Ru}(\text{bpy})_3]^{2+}$ to $[\text{PW}_{12}\text{O}_{40}]^{3-}$ cannot occur spontaneously at the ground states of the fragments. Therefore, one may expect that the mixing of ground state $[\text{Ru}(\text{bpy})_3]^{2+}$ with ground state $[\text{PW}_{12}\text{O}_{40}]^{3-}$ will lead to formation of a weakly bound $\{[\text{Ru}(\text{bpy})_3]^{2+} \dots [\text{PW}_{12}\text{O}_{40}]^{3-}\}$ complex, which may have several isomers. In **Figure 5-8** we present the energetically most stable isomer, where $[\text{Ru}(\text{bpy})_3]^{2+}$ is coordinated to the face of $[\text{PW}_{12}\text{O}_{40}]^{3-}$, which contains three W-centers, via three H-bonding (see **Figure 5-8**). This coordination motif is consistent with the X-ray structure of this complex. The calculated fragmentation energy of the fully optimized $\{[\text{Ru}(\text{bpy})_3]^{2+} \dots [\text{PW}_{12}\text{O}_{40}]^{3-}\}$ complex, in its ground singlet state, is found to be ~ 5.5 kcal/mol.

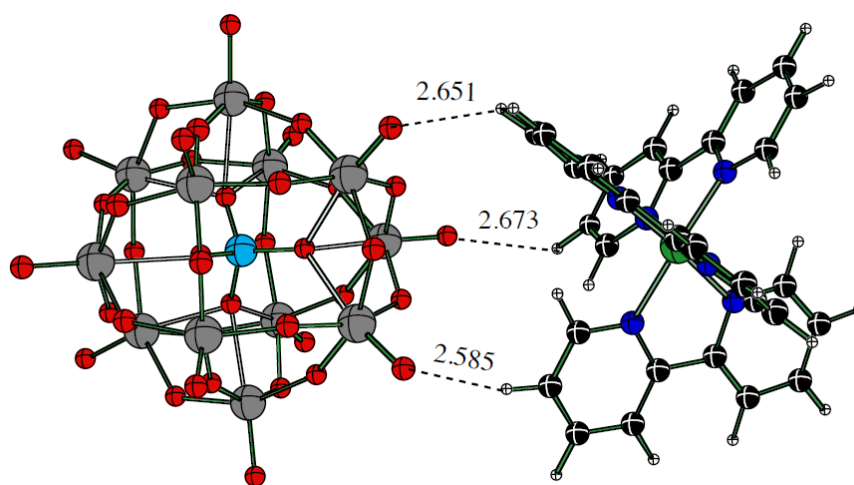


Figure 5-8. Calculated structure and important geometry parameters (in Å) of the $\{[\text{Ru}(\text{bpy})_3]^{2+} \dots [\text{PW}_{12}\text{O}_{40}]^{3-}\}$ complex.

However, charge transfer in the $\{[\text{Ru}(\text{bpy})_3]^{2+} \dots [\text{PW}_{12}\text{O}_{40}]^{3-}\}$ complex, i.e. complex $\{[\text{Ru}(\text{bpy})_3]^{3+} \dots [\text{PW}_{12}\text{O}_{40}]^{4-}\}$, can be achieved by photoexcitation of $[\text{Ru}(\text{bpy})_3]^{2+}$ from its **S0** (ground state) to **S1** (the first excited state). Previously, we calculated³⁰ the **S0** \rightarrow **S1** vertical excitation energy in water to be ~ 2.7 eV (459 nm) versus the measured value of 450 nm. Detailed studies of charge transfer in $\{[\text{Ru}(\text{bpy})_3]^{2+} \dots [\text{PW}_{12}\text{O}_{40}]^{3-}\}$ complex are in progress and will be reported elsewhere.

Conclusions

Two dye-POM complexes, $[\text{Ru}(\text{bpy})_3][\text{K}_5\text{PW}_{11}\text{O}_{39}]$ (**1**) and $[\text{Ru}(\text{bpy})_3][\text{KPW}_{12}\text{O}_{40}]$ (**2**), have been synthesized and characterized in both solid and solution state. The crystal structure of **2** demonstrates an interesting 3D packing with ion-channel-like porosity. All the spectroscopic and computational studies indicate that a strong interaction exists between the cationic dye and polyanion units. Future investigation will explore the electron transfer character including ET rate measurements between the cationic dye in its excited state and the polyanions.

References

- (1) Grätzel, M. *Inorg. Chem.* **2005**, *44*, 6841.
- (2) Grätzel, M. *Nature* **2001**, *414*, 338.
- (3) Bard, A. J.; Fox, M. A. *Acc. Chem. Res.* **1995**, *28*, 141.
- (4) Sun, X.; Du, Y.; Zhang, L.; Dong, S.; Wang, E. *Anal. Chem.* **2007**, *79*, 2588.
- (5) Hill, C. L. *Chem. Rev.* **1998**, *98*, 1.
- (6) *Polyoxometalate Chemistry for Nano-Composite Design*; Yamase, T.; Pope, M. T., Eds.; Kluwer Academic/Plenum Publishers: New York, 2002; Vol. 2.
- (7) Besson, C.; Huang, Z.; Geletii, Y. V.; Lense, S.; Hardcastle, K. I.; Musaev, D. G.; Lian, T.; Proust, A.; Hill, C. L. *Chem. Commun.* **2010**, 2784.
- (8) Geletii, Y. V.; Besson, C.; Hou, Y.; Yin, Q.; Musaev, D. G.; Quinonero, D.; Cao, R.; Hardcastle, K. I.; Proust, A.; Kögerler, P.; Hill, C. L. In *239th ACS National Meeting, Fuel Chemistry Division, "Solar Cells & Solar Fuels Symposium"* San Francisco, CA, March 21-25, 2010, p 1.
- (9) Yin, Q.; Tan, J. M.; Besson, C.; Geletii, Y. V.; Musaev, D. G.; Kuznetsov, A. E.; Luo, Z.; Hardcastle, K. I.; Hill, C. L. *Science* **2010**, *328*, 342.
- (10) Geletii, Y. V.; Besson, C.; Hou, Y.; Yin, Q.; Musaev, D. G.; Quinonero, D.; Cao, R.; Hardcastle, K. I.; Proust, A.; Kögerler, P.; Hill, C. L. *J. Am. Chem. Soc.* **2009**, *131*, 17360.
- (11) Geletii, Y. V.; Huang, Z.; Hou, Y.; Musaev, D. G.; Lian, T.; Hill, C. L. *J. Am. Chem. Soc.* **2009**, *131*, 7522.

- (12) Deng, Z.; Tseng, H.-W.; Zong, R.; Wang, D.; Thummel, R. *Inorg. Chem.* **2008**, *47*, 1835.
- (13) Bao, D.-M.; Gu, Y.-P.; Zhou, X.-S.; Hu, S.-X.; You, W.-S. *Liaoning Shifan Daxue Xuebao, Ziran Kexueban* **2003**, *26*, 59.
- (14) Mariotti, A. W. A.; Xie, J.; Abrahams, B. F.; Bond, A. M.; Wedd, A. G. *Inorg. Chem.* **2007**, *46*, 2530.
- (15) Wang, X.-L.; Han, Z.-B.; Wang, E.-B.; Zhang, H.; Hu, C.-W. *Electroanal.* **2003**, *15*, 1460.
- (16) Xie, J.; Abrahams, B. F.; Wedd, A. G. *Chem. Commun.* **2008**, 576.
- (17) Han, Z.; Wang, E.; Luan, G.; Li, Y.; Hu, C.; Wang, P.; Hu, N.; Jia, H. *Inorg. Chem. Commun.* **2001**, *4*, 427.
- (18) Bonchio, M.; Carraro, M.; Scorrano, G.; Bagno, A. *Adv. Synth. Catal.* **2004**, *346*, 648.
- (19) Fay, N.; Dempsey, E.; Kennedy, A.; McCormac, T. *J. Electroanal. Chem.* **2003**, *556*, 63.
- (20) Fay, N.; Hultgren, V. M.; Wedd, A. G.; Keyes, T. E.; Forster, R. J.; Leaned, D.; Bond, A. M. *Dalton Trans.* **2006**, 4218.
- (21) Tourné C.; Tourné G. *Bull. Soc. Chim. Fr.* **1969**, *4*, 1124.
- (22) Perdew, J. P. *Phys. Rev. A* **1986**, *B33*, 8822.
- (23) Becke, A. D. *Phys. Rev. A* **1988**, *38*, 3098.
- (24) Cancès, E.; Mennucci, B.; Tomasi, J. *J. Chem. Phys.* **1997**, *107*, 3032.
- (25) Hay, P. J.; Wadt, W. R. *J. Chem. Phys.* **1985**, *82*, 270.
- (26) Hay, P. J.; Wadt, W. R. *J. Chem. Phys.* **1985**, *82*, 299.

(27) Wadt, W. R.; Hay, P. J. *J. Chem. Phys.* **1985**, *82*, 284.

(28) M.J. Frisch, G. W. T., H.B. Schlegel, G.E. Scuseria, M.A. Robb, J.R. Cheeseman, G. Scalmani, V. Barone, B. Mennucci, G.A. Petersson, H. Nakatsuji, M. Caricato, X. Li, H.P. Hratchian, A.F. Izmaylov, J. Bloino, G. Zheng, J.L. Sonnenberg, M. Hada, M. Ehara, K. Toyota, R. Fukuda, J. Hasegawa, M. Ishida, T. Nakajima, Y. Honda, O. Kitao, H. Nakai, T. Vreven, J.A. Montgomery, Jr., J.E. Peralta, F. Ogliaro, M. Bearpark, J.J. Heyd, E. Brothers, K.N. Kudin, V.N. Staroverov, R. Kobayashi, J. Normand, K. Raghavachari, A. Rendell, J.C. Burant, S.S. Iyengar, J. Tomasi, M. Cossi, N. Rega, J.M. Millam, M. Klene, J.E. Knox, J.B. Cross, V. Bakken, C. Adamo, J. Jaramillo, R. Gomperts, R.E. Stratmann, O. Yazyev, A.J. Austin, R. Cammi, C. Pomelli, J.W. Ochterski, R.L. Martin, K. Morokuma, V.G. Zakrzewski, G.A. Voth, P. Salvador, J.J. Dannenberg, S. Dapprich, A.D. Daniels, O. Farkas, J.B. Foresman, J.V. Ortiz, J. Cioslowski, D.J. Fox, in, Gaussian, Inc., Wallingford, CT, 2009.

(29) Han, J. W.; Hill, C. L. *J. Am. Chem. Soc.* **2007**, *129*, 15094.

(30) Kaledin, A. L.; Huang, Z.; Geletii, Y. V.; Lian, T.; Hill, C. L.; Musaev, D. *G. J. Phys. Chem. A* **2010**, *114*, 73.

(31) White, H. S.; Becker, W. G.; Bard, A. J. *J. Phys. Chem.* **1984**, *88*, 1840.

(32) Mosa, J.; Larramona, G.; Durán, A.; Aparicio, M. *J. Membr. Sci.* **2008**, *307*, 21.

———— CHAPTER ————

6

**An Efficient Homogeneous Carbon-free Multi-cobalt
Water Oxidation Catalyst: New Structure and High
Activity**

Abstract:

The cobalt-substituted polyoxometalate, $\text{Na}_{12}[\text{WCo}_3(\text{H}_2\text{O})_2(\text{CoW}_9\text{O}_{34})_2]\cdot 46\text{H}_2\text{O}$ (**1**), has been shown to be a new catalyst for the effective production of dioxygen from water under visible light irradiation. The turnover number (TON) and turnover frequency (TOF) based on 0.2 μM catalyst concentration can reach around 1500 and 10 s^{-1} , respectively, indicating its high efficiency as a water oxidation catalyst (WOC). The catalyst is systematically characterized by FT-IR, UV-Vis, X-ray single crystal structures, elemental analysis, TGA, XPS, CV and etc. Now catalytic activity of **1** towards water oxidation and its stability under turnover conditions are reported.

Introduction

Efficient visible-light-driven water splitting into hydrogen and oxygen is anticipated to be centrally important in meeting future energy needs. As the core part of this green chemistry, catalysts for the 4-electron oxidation of H_2O to O_2 and the 2-electron reduction of H_2O to H_2 must be both highly active and stable (both thermodynamically and oxidatively) during turnover under practical environmental conditions. In addition, the development of cheap, readily available, and abundant metal-based catalyst as a substitute for noble metals is also a vital research topic in the catalysts exploration area.¹⁻⁶

Along with the extensive studies in catalytic water reduction to generate hydrogen, research on catalytic water oxidation to produce dioxygen proceeds extremely slowly because of the intrinsic difficulty in this thermodynamically unfavorable pathway. For this oxidation process, the heterogeneous catalysts, which are mainly metal oxides, such as TiO_2 , Fe_2O_3 , IrO_x , and RuO_x ,⁷⁻⁹ and recently reported Co-phosphate (Co-Pi)¹⁻³

and Ni-borate (Ni-Bi)¹⁰ materials, have been studied since the 1970's. However, the characterization of the catalytic species and tunability of catalytic properties in these heterogeneous systems are relatively more difficult than that in the homogeneous system. In order to investigate the mechanism of water oxidation and provide more detailed molecular information on the action mode, several homogeneous molecular catalysts have been reported demonstrating attractive WOC activity. A majority of these homogeneous catalysts are ruthenium-based,¹¹⁻¹⁶ iridium-based,^{17,18} manganese-based,¹⁹⁻²³ or most recently cobalt-based polypyridine complexes²⁴⁻²⁶. However, the problem is that the organic ligands involved are prone to be oxidatively decomposed under the catalytic redox cycle and limit their potential practical applications. In the line to develop new catalytic materials for water splitting, the ideal catalysts should demonstrate their stabilities during the catalytic cycle, which include the thermodynamic, hydrolytic, and redox stabilities. In addition to robustness of the desired catalysts, the high efficiency of water splitting, which is the speed of O₂ production quantified with its turn-over frequency, is highly pursued.⁶

Polyoxometalates (POMs),²⁷⁻²⁹ a large class of d⁰ metal oxide cluster anions with adjustable geometrical and electronic structures, are attractive multi-dentate ligands to stabilize multi-d-electron transition metal centers that have the redox properties needed to facilitate the multi-electron transfer processes in water splitting reaction. These POMs demonstrate high tunability, thermodynamical robustness towards oxidation, and hydrolytical stability in a broad range of pH, are the most prospective catalysts for this multi-electron process.

Recently we have reported several carbon-free water oxidation molecular catalysts, which are either Ru-based³⁰⁻³⁷ and earth abundant Co-based POMs.^{38,39} These all-inorganic POM catalysts demonstrate both high efficiency and robustness under dark and visible light-driven conditions. Based on our current work, the development of new but more efficient POM-based water oxidation catalysts that combine these advantages is the central effort in this direction.

Herein, we report the synthesis and characterization of a multi-cobalt containing polyanion, $\text{Na}_{12}[\text{Co}_3(\text{H}_2\text{O})_2\text{W}(\text{CoW}_9\text{O}_{34})_2]\cdot 46\text{H}_2\text{O}$ (**1**), which is like recently reported another sandwich-type polyanion WOC catalyst $\text{Na}_{10}[\text{Co}_4(\text{H}_2\text{O})_2(\text{PW}_9\text{O}_{34})_2]$ (**Co4**), shows high efficiency in producing dioxygen from water but significantly faster than the latter under the studied conditions. Several evidences including spectrochemical and kinetics studies support that **1** is also stable during turnover.

Materials and Methods

Synthesis of $\text{Na}_{12}[\text{Co}_3(\text{H}_2\text{O})_2\text{W}(\text{CoW}_9\text{O}_{34})_2]\cdot 46\text{H}_2\text{O}$ (**1**). Complex **1** is one of the Tourné type sandwich POMs containing $[\text{MMWM}(\text{XW}_9\text{O}_{34})_2]^{12-}$ polyanions (X= M= Zn or Co),⁴⁰ which are unusually hard to purify and characterize as can be seen in the many attempts to get a single pure isomer of “[WZnRu₂(OH)(H₂O)(ZnW₉O₃₄)₂]¹¹⁻ (the latter is isostructural with the title complex **1**).^{41,42} The reasons that render the synthesis difficult are (a) this family of complexes forms isomers with two or three d-electron metals in the central belt, (b) these isomers can co-crystallize, and (c) all the X-ray crystal structures have the metal ions in the central belt disordered. With the effort to make pure **1**, the target compound is hydrothermally synthesized in water from two salts of earth abundant elements, cobalt and tungsten, according to the literature but with some modifications. A

typical synthesis way was conducted as following procedure. $\text{Na}_2\text{WO}_4 \cdot 2\text{H}_2\text{O}$ (18.0 g, 55 mmol) was dissolved in deionized water (75 mL) and stirred violently when concentrated nitric acid ((75 mL)) was added slowly. Then, the solution was slowly heated to 70 °C and $\text{Co}(\text{OAc})_2 \cdot 4\text{H}_2\text{O}$ (4.5 g, 18 mmol) in deionized water (30 mL) was added dropwise to the former solution for about 2 hours. The resulting purple colored solution was heated to reflux for four hours before cooled down to room temperature. After centrifugation to remove any precipitate from the solution, the green supernatant was left to crystallize for 3-4 days to give deep-green plate-like crystals. Yield 2.14 g (12.5 % yield based on tungstate). Elemental analysis calcd (%) for 1: Co, 4.90; Na, 4.59; W, 58.0 found: Co, 4.44; Na, 4.60; W, 57.6. FT-IR (cm^{-1}) 920 (m), 875 (m), 760 (s), 875 (m), 712 (sh), 690 (sh), 545 (w), 445 (w), 410 (w). UV-vis: $\epsilon_{579} = 330 \text{ M}^{-1} \text{ cm}^{-1}$.

Tris(2,2'-bipyridyl)dichlororuthenium(II) hexahydrate ($\text{Ru}(\text{bpy})_3\text{Cl}_2 \cdot 6\text{H}_2\text{O}$) was purchased from Aldrich and recrystallized before use. $\text{Ru}(\text{bpy})_3\text{Cl}_2 \cdot 6\text{H}_2\text{O}$ (1.0 g) was dissolved in deionized H_2O (5 ml) at 80 °C in the dark. After cooling the solution to room temperature, the sample was collected and air dried. Yield: 50%.

Synthesis of $\text{Ru}(\text{bpy})_3(\text{ClO}_4)_3$. $\text{Ru}(\text{bpy})_3\text{Cl}_2 \cdot 6\text{H}_2\text{O}$ (375 mg, 0.5 mmol) was dissolved in the mixture of H_2O (9.7 mL) and concentrated H_2SO_4 (0.28 ml) with vigorously stirring, then excess amount of PbO_2 was slowly added to the solution. After the orange color turns to green, the mixture was continued to stir for 30 minutes.. The reaction solution was collected by filtration through a fine glass. To the green colored filtrate in ice bath concentrated HClO_4 was dropwise added and dark green crystals gradually precipitated in about 30 minutes. Then the green crystals were filtered through a fine glass filter and dried at room temperature in vacuum oven.

Synthesis of $\text{Na}_{10}[\text{Co}_4(\text{H}_2\text{O})_2(\alpha\text{-PW}_9\text{O}_{34})_2]$ (**Co4**). The preparation is the same as reported in our previous work.³⁹ A mixture of solid $\text{Na}_2\text{WO}_4 \cdot 2\text{H}_2\text{O}$ (35.62 g, 0.108 mol), $\text{Na}_2\text{HPO}_4 \cdot 7\text{H}_2\text{O}$ (3.22 g, 0.012 mol), and $\text{Co}(\text{NO}_3)_2 \cdot 6\text{H}_2\text{O}$ (6.98 g, 0.024 mol) was dissolved in distilled water (100 ml) and The pH value of the resulting solution was adjusted to 7 with dropwise addition of 0.1 M HCl. The resulting purple suspension was then refluxed for two hours. After reflux, the solution was saturated with NaCl and allowed to cool to room temperature before the purple crystals were collected. The final products were obtained by recrystallization in hot water, and the purity was assessed by FT-IR and UV-vis.

Instrumentation

X-ray diffraction. The complete datasets for **1** were collected at Emory University. A suitable crystal of **1** was coated with Paratone N oil, suspended in a small fiber loop and placed in a cooled nitrogen gas stream at 173 K on a Bruker D8 APEX II CCD sealed tube diffractometer with graphite monochromated $\text{MoK}\alpha$ (0.71073 Å) radiation. Data were measured using a series of combinations of phi and omega scans with 10 s frame exposures and 0.5° frame widths. Data collection, indexing and initial cell refinements were all carried out using APEX II software. Frame integration and final cell refinements were done using SAINT software. The final cell parameters were determined from least-squares refinement on 9978 reflections. The structure was solved using Direct methods and difference Fourier techniques (SHELXTL, V6.12) (S12). Only the Co, Na and W atoms were refined anisotropically; no hydrogen atoms were included in the final structure. Scattering factors and anomalous dispersion corrections are taken from the International Tables for X-ray Crystallography (S13). Structure solution,

refinement, graphics and generation of publication materials were performed by using SHELXTL, V6.12 software. Additional details of data collection and structure refinement are given in Table 6-1.

UV-Vis spectra were acquired using Agilent 8453 spectrophotometer equipped with a diode-array detector and an Agilent 89090A cell temperature controller unit. Steady state luminescence quenching was studied using a SPEX® FluoroLog®-3 self-contained and fully automated spectrofluorometer. Electrochemical data were obtained at room temperature using a BAS CV-50W electrochemical analyzer equipped with a glassy-carbon working electrode, a Pt-wire auxiliary electrode, and a Ag/AgCl (3 M NaCl) BAS reference electrode. All reduction potentials are measured relative to this reference electrode. Analysis of dioxygen in the reaction headspace was performed using a HP5890A model gas chromatograph equipped with thermal conductivity detector and a HP-MOLESIEVE capillary GC column (30m x 0.535 mm x 25.00 μm) packed with 5Å molecular sieves to separate O₂ and N₂. Argon was used as a carrier gas. A LED-lamp was used as a light source with the wavelength of 455 nm. A magnetically-coupled stirring system (SYS 114, SPECTROCELL) was used for reaction solutions. The stirring rate in revolutions per minute (RPM) was determined by a home-built set-up consisting of a helium-neon laser (IMATTRONIC), a magnetic stick (VP 736-1, V&P scientific), a photo-diode detector (PDA 55, ThorLabs), and an oscilloscope (LT262, LeCroy). The catalytic experiments were carried out by Hongjin Lv, stopped-flow experiments were done by James Vickers, and stability test of catalyst were done by Dr. Sajjad Mohebbi.

General Procedure of Photo-driven Water Oxidation

The general procedure of light-driven water oxidation was performed in a cylindrical cuvette (NSG, 32G10) with a total volume of ~2.5 ml. The cell was filled with 2 ml of reaction solution with the desired concentrations of Ru(bpy)₃Cl₂·6H₂O (1.0 mM), Na₂S₂O₈ (5 mM), catalyst (**1**) (0.2 - 6 μM) and buffer (40 mM sodium borate, initial pH 9.0). The reaction cell was then sealed with a rubber septum, carefully deaired and filled with Ar. All procedures were performed with a minimum exposure to ambient light. The reaction was initiated by turning on the LED-lamp (λ = 455 nm; light intensity 17 mW) with constant magnetic stirring (4 × 10³ RPM). The O₂ concentration in the headspace was analyzed for O₂ content. The solution pH was measured after the reaction. The O₂ yield was quantified as described by withdrawing a gas sample from the headspace without stopping the reaction. Briefly, 100 μl of the gas in the headspace of the reaction cell was withdrawn through a septum using a deaired gas-tight syringe and 50 μl of the gas was finally injected into gas chromatograph. Contamination of the headspace by air was corrected by quantification of N₂ present in the head-space (from the N₂ peak in the GC traces).

Quantum Efficiency Measurements

The quantum efficiency of O₂ formation defined as the number of O₂ molecules formed per two absorbed photons.

$$\Phi = N(O_2) / [N(h\nu) / 2]$$

where N(O₂) is the moles of O₂ formed, and N(hν) is the moles of photons absorbed by the reaction solution. The quantum yield is defined for per two absorbed photons because the formation of one molecule of O₂ requires four oxidative equivalents supplied by two molecules of persulfate after absorption of two photons. The amount of O₂ formed was quantified as described above at the reaction time < 5 min. The total amount of photons absorbed for a given reaction time *t* was calculated from the irradiation power and the absorbance of the reaction solution.

The irradiation power, 17 mW, was measured at the point right in front of the reaction cell using a laser power meter (Molelectron, model Max 500A). During illumination, the reaction solution remained orange colored, indicating that the photosensitizer was mostly present in reduced form as Ru(bpy)₃²⁺. Since the optical density of the reaction solution was much larger enough, all light entering the reaction solution was considered to be absorbed. The amount of absorbed light can be determined from the measured power in front of the reaction cell and the absorption loss (18%) by the optical glass (NSG cuvette manual, and by

UV/Vis spectrometer) and reflection loss (4%) at the glass/air interface. All scattering photons due to the solvent (H₂O) will be absorbed by the solution. The optimum experimental quantum efficiency was found to be ~55% with the concentration catalyst **1** of 6 μM.

Results and Discussion

In order to confirm the purity and metal composition of the product, we have characterized **1** by a combination of single crystal X-ray crystallography (Figure 6-1 and 6-2, Table 6-1 and 6-3), XPS (Figure 6-3), in addition to the usual spectroscopic methods TGA (Figure 6-4), UV-vis (Figure 6-5), FT-IR (Figure 6-6), and elemental analysis. All these techniques collectively make a strong case that **1** is the formula indicated.

The sodium salt of **1** crystallizes in the monoclinic space group $P 2(1)/n$ with two formula units per asymmetric unit (Table 6-1). The sandwich type cluster $[\text{Co}_3(\text{H}_2\text{O})_2\text{W}(\text{CoW}_9\text{O}_{34})_2]^{12-}$ consists of two α -B- $[\text{CoW}_9\text{O}_{34}]^{12-}$ lacunary subunits (Figure 6-1). The two tri-vacant subunits, which are derived from the parent *Keggin* structure by removal of three adjacent edge-sharing octahedral WO_6 , are linked together via a system of four coplanar metal atoms (three Co^{II} and one W atoms, that is two Co2, one Co3, and one W10) on the belt position. These four metal atoms on the belt position, however, differ in their connectivity and reveal distorted octahedral coordination sites in a close-packed arrangement.

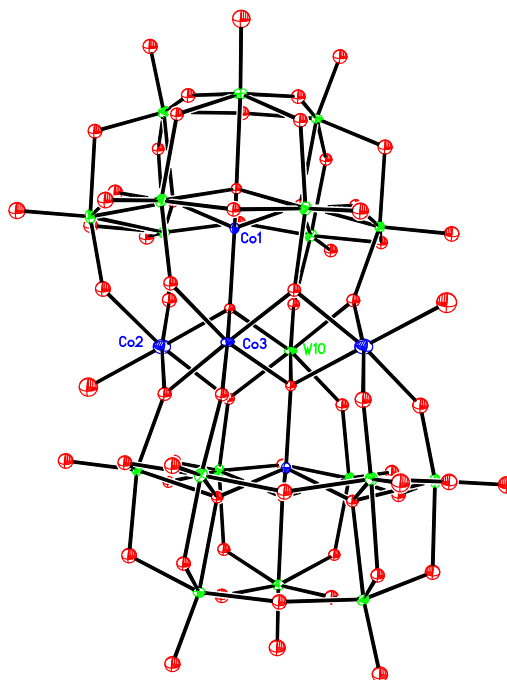


Figure 6-1. Ellipsoid and Ball-and-stick representations of X-ray single crystal structure of **1**. W (green), O (red), Co (blue).

Table 6-1. Crystallographic Data and Structure Refinement for **1**.

	1
Empirical formula	Co ₅ H ₈₈ Na ₁₂ O ₁₁₂ W ₁₉
Formula weight	5944.38 g·mol ⁻¹
Crystal system	Monoclinic
Space group	<i>P</i> 2(1)/n
Unit cell	a = 13.0689 (15) Å α = 90° b = 17.746 (2) Å β = 93.385(2)° c = 21.054(3) Å γ = 90°
Volume	4874.3(10) Å ³
Z	2
Density (calcd)	4.050 g cm ⁻³
Temperature	173(2)K
Wavelength	0.71073 Å
Abs. coeff	23.328 mm ⁻¹
Reflections collected	83541
Independent reflections	12101 [R(int) = 0.0931]
GOF	1.051
Final R ₁ ^a [I > 2σ(I)]	0.0413
Final wR ₂ ^b [I > 2σ(I)]	0.0916

^a R₁ = Σ||F_o| - |F_c|| / Σ|F_o|; ^b wR₂ = Σ[w(F_o² - F_c²)²] / Σ[w(F_o²)²]^{1/2}

Two sites containing one cobalt (Co3) and one tungsten (W10) that are related by inversion symmetry, are each surrounded by six oxygen atoms belonging to the two sub-units, α -B-[CoW₉O₃₄]¹²⁻ (Figure 6-2). Here, each is found randomly occupied either by a tungsten or by Co atom. The two other sites containing two cobalt (Co2) atoms remain equivalent, which are surrounded by six surrounding oxygen atoms, (five of them belong to sub-units and the sixth one being aqua ligand). Therefore, the five Co atoms in this structure can be cataloged to three types. Two cobalt atoms occupying the center of each lacunary anion have a tetrahedral environment of four oxygen atoms. Three cobalt atoms on the belt position of the polyanion have an octahedral coordination mode but different site arrangement. Among the three cobalt atoms on the belt, two of them (Co2), each coordinating with one water molecule, reside outside of the polyanion, and another cobalt atom (Co3), is opposite to one tungsten atom (W10). Each of the tetrahedral cobalt (Co1) is connected to each of the octahedral atoms via one of the oxygen atoms consisting of the tetrahedron. One mirror plan, consisting of two cobalt in the tetrahedral sites (Co1) and one cobalt (Co3) and one tungsten (W10) of the belt in the octahedral sites, is perpendicular to the Co2-Co2 bond on the belt position.

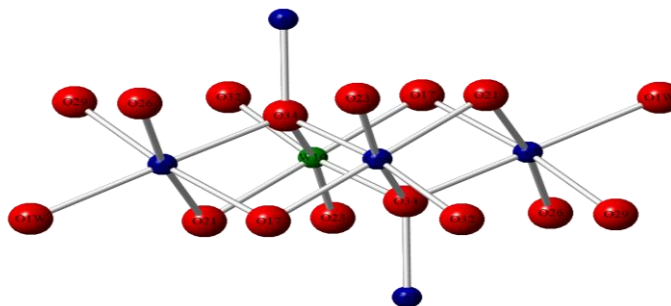


Figure 6-2. Coordination environment of tetrahedral (Co1) and octahedral cobalt (Co2).

Each belt atom reveals distorted octahedral coordination site in a close-packed arrangement. The W(10) – O bond lengths of the belt tungsten range from 1.954(8) to 2.041(7) Å and the Co (2) – O bond lengths of the belt cobalt from 2.083(7) to 2.210(10) Å.

The average Co-O bond lengths of the tetrahedral and octahedral Co are observed to be 1.925 and 2.078 Å, respectively. Relevant bond lengths and angles are summarized in Table 6-2.

Table 6-2. Selected bond lengths [Å] and angles [°] for **1**.

Co(1)-O(13)	1.905(7)	W(5)-O(21)-Co(2)#1	121.5(4)
Co(1)-O(5)	1.924(7)	W(5)-O(22)-W(6)	111.6(4)
Co(1)-O(34)#1	1.932(7)	W(6)-O(23)-Co(3)	145.0(4)
Co(1)-O(10)	1.938(7)	W(6)-O(24)-Na(3)	137.9(4)
Co(2)-O(34)#1	2.083(7)	W(6)-O(25)-W(7)	155.6(5)
Co(2)-O(26)	2.117(8)	W(7)-O(26)-Co(2)	136.7(5)
Co(2)-O(29)	2.117(8)	W(8)-O(28)-W(7)	110.9(4)
Co(2)-O(21)#1	2.175(8)	W(8)-O(29)-Co(2)	134.7(5)
Co(2)-O(17)#1	2.176(8)	W(9)-O(31)-W(8)	152.9(5)
Co(2)-O(1W)	2.210(10)	W(9)-O(32)-W(10)#1	143.4(4)
Co(3)-O(23)	1.929(7)	W(9)-O(32)-Co(3)#1	143.4(4)
Co(3)-O(32)#1	1.954(8)	W(10)#1-O(32)-Co(3)#1	0.00(5)
Co(3)-O(34)#1	1.995(7)	Co(1)#1-O(34)-W(10)#1	116.7(4)

Co(3)-O(34)	2.038(7)	Co(1)#1-O(34)-Co(3)#1	116.7(4)
Co(3)-O(17)#1	2.041(7)	W(10)#1-O(34)-Co(3)#1	0.00(5)
Co(3)-O(21)	2.104(8)	Co(1)#1-O(34)-Co(3)	115.3(3)
O(1)-W(1)	1.731(9)	W(10)#1-O(34)-Co(3)	102.4(3)
O(2)-W(9)	1.959(8)	Co(3)#1-O(34)-Co(3)	102.4(3)
O(2)-W(1)	1.969(7)	Co(1)#1-O(34)-Co(2)#1	118.1(3)
O(2)-Na(6)#13	2.449(11)	W(10)#1-O(34)-Co(2)#1	100.6(3)
O(3)-W(4)	1.973(8)	Co(3)#1-O(34)-Co(2)#1	100.6(3)
O(3)-W(1)	1.973(7)	Co(3)-O(34)-Co(2)#1	101.3(3)
O(4)-W(1)	1.854(8)	O(1)-W(1)-O(4)	101.9(4)
O(4)-W(3)	1.976(8)	O(1)-W(1)-O(6)	101.1(4)
O(5)-W(9)	2.152(7)	O(4)-W(1)-O(6)	87.2(3)
O(5)-W(4)	2.178(7)	O(1)-W(1)-O(2)	94.6(4)
O(5)-W(1)	2.180(7)	O(4)-W(1)-O(2)	90.1(3)
O(6)-W(1)	1.920(8)	O(6)-W(1)-O(2)	164.4(3)
O(6)-W(2)	1.942(8)	O(1)-W(1)-O(3)	97.1(4)
O(7)-W(2)	1.728(8)	O(4)-W(1)-O(3)	161.0(3)
O(8)-W(2)	1.938(8)	O(6)-W(1)-O(3)	88.5(3)
O(8)-W(5)	2.005(8)	O(2)-W(1)-O(3)	89.0(3)
O(9)-W(2)	1.966(8)	O(1)-W(1)-O(5)	165.7(3)
O(9)-W(6)	1.974(8)	O(4)-W(1)-O(5)	87.5(3)
O(10)-W(5)	2.137(7)	O(6)-W(1)-O(5)	90.1(3)
O(10)-W(6)	2.152(7)	O(2)-W(1)-O(5)	74.4(3)
O(10)-W(2)	2.202(7)	O(3)-W(1)-O(5)	74.0(3)
O(11)-W(2)	1.870(8)	O(7)-W(2)-O(11)	101.9(4)
O(11)-W(3)	1.956(8)	O(7)-W(2)-O(8)	98.6(4)
O(12)-W(3)	1.729(8)	O(11)-W(2)-O(8)	158.9(3)
O(13)-W(8)	2.138(7)	O(7)-W(2)-O(6)	98.9(4)
O(13)-W(7)	2.162(7)	O(11)-W(2)-O(6)	85.7(3)
O(13)-W(3)	2.252(7)	O(8)-W(2)-O(6)	86.3(3)
O(14)-W(3)	1.857(8)	O(7)-W(2)-O(9)	98.0(4)
O(14)-W(8)	2.120(8)	O(11)-W(2)-O(9)	90.7(3)
O(15)-W(3)	1.883(8)	O(8)-W(2)-O(9)	91.3(3)
O(15)-W(7)	2.122(8)	O(6)-W(2)-O(9)	163.1(3)
O(16)-W(4)	1.731(8)	O(7)-W(2)-O(10)	169.0(3)

O(17)-W(4)	1.906(8)	O(11)-W(2)-O(10)	86.4(3)
O(17)-W(10)#1	2.041(7)	O(8)-W(2)-O(10)	73.9(3)
O(17)-Co(3)#1	2.041(7)	O(6)-W(2)-O(10)	88.8(3)
O(17)-Co(2)#1	2.176(8)	O(9)-W(2)-O(10)	74.4(3)
O(18)-W(5)	1.891(7)	O(12)-W(3)-O(14)	99.9(4)
O(18)-W(4)	1.958(7)	O(12)-W(3)-O(15)	100.2(4)
O(19)-W(4)	1.897(8)	O(14)-W(3)-O(15)	96.9(3)
O(19)-W(9)	2.011(7)	O(12)-W(3)-O(11)	99.3(4)
O(19)-Na(2)#13	2.472(9)	O(14)-W(3)-O(11)	159.3(3)
O(20)-W(5)	1.745(8)	O(15)-W(3)-O(11)	87.5(3)
O(21)-W(5)	1.889(8)	O(12)-W(3)-O(4)	99.3(4)
O(21)-Co(2)#1	2.175(8)	O(14)-W(3)-O(4)	88.6(3)
O(22)-W(5)	1.965(8)	O(15)-W(3)-O(4)	158.5(3)
O(22)-W(6)	1.966(8)	O(11)-W(3)-O(4)	80.5(3)
O(23)-W(6)	1.910(8)	O(12)-W(3)-O(13)	173.3(3)
O(24)-W(6)	1.725(8)	O(14)-W(3)-O(13)	75.9(3)
O(25)-W(6)	1.883(8)	O(15)-W(3)-O(13)	75.5(3)
O(25)-W(7)	1.940(8)	O(11)-W(3)-O(13)	85.7(3)
O(26)-W(7)	1.785(8)	O(4)-W(3)-O(13)	85.8(3)
O(27)-W(7)	1.732(9)	O(16)-W(4)-O(19)	99.7(4)
O(28)-W(8)	1.938(8)	O(16)-W(4)-O(17)	102.5(3)
O(28)-W(7)	1.986(8)	O(19)-W(4)-O(17)	90.0(3)
O(29)-W(8)	1.790(8)	O(16)-W(4)-O(18)	100.0(3)
O(30)-W(8)	1.760(9)	O(19)-W(4)-O(18)	160.2(3)
O(31)-W(9)	1.885(8)	O(17)-W(4)-O(18)	86.6(3)
O(31)-W(8)	1.962(8)	O(16)-W(4)-O(3)	95.6(4)
O(32)-W(9)	1.913(8)	O(19)-W(4)-O(3)	88.8(3)
O(32)-W(10)#1	1.954(8)	O(17)-W(4)-O(3)	161.7(3)
O(32)-Co(3)#1	1.954(8)	O(18)-W(4)-O(3)	88.4(3)
O(33)-W(9)	1.735(8)	O(16)-W(4)-O(5)	168.7(3)
O(34)-Co(1)#1	1.932(7)	O(19)-W(4)-O(5)	75.7(3)
O(34)-W(10)#1	1.995(7)	O(17)-W(4)-O(5)	87.9(3)
O(34)-Co(3)#1	1.995(7)	O(18)-W(4)-O(5)	84.7(3)
O(34)-Co(2)#1	2.083(7)	O(3)-W(4)-O(5)	74.1(3)
O(19W)-O(26W)	0.64(4)	O(20)-W(5)-O(21)	102.2(4)

O(22W)-O(25W)	1.12(3)	O(20)-W(5)-O(18)	99.9(3)
O(23W)-O(24W)	1.55(3)	O(21)-W(5)-O(18)	90.1(3)
O(13)-Co(1)-O(5)	108.1(3)	O(20)-W(5)-O(22)	96.6(4)
O(13)-Co(1)-O(34)#1	109.7(3)	O(21)-W(5)-O(22)	88.5(3)
O(5)-Co(1)-O(34)#1	112.9(3)	O(18)-W(5)-O(22)	163.4(3)
O(13)-Co(1)-O(10)	107.8(3)	O(20)-W(5)-O(8)	94.3(4)
O(5)-Co(1)-O(10)	105.7(3)	O(21)-W(5)-O(8)	163.1(3)
O(34)#1-Co(1)-O(10)	112.5(3)	O(18)-W(5)-O(8)	90.8(3)
O(34)#1-Co(2)-O(26)	93.4(3)	O(22)-W(5)-O(8)	85.8(3)
O(34)#1-Co(2)-O(29)	94.1(3)	O(20)-W(5)-O(10)	165.7(3)
O(26)-Co(2)-O(29)	89.7(3)	O(21)-W(5)-O(10)	89.0(3)
O(34)#1-Co(2)-O(21)#1	79.2(3)	O(18)-W(5)-O(10)	88.8(3)
O(26)-Co(2)-O(21)#1	172.4(3)	O(22)-W(5)-O(10)	74.6(3)
O(29)-Co(2)-O(21)#1	92.4(3)	O(8)-W(5)-O(10)	74.1(3)
O(34)#1-Co(2)-O(17)#1	78.4(3)	O(24)-W(6)-O(25)	102.3(4)
O(26)-Co(2)-O(17)#1	91.3(3)	O(24)-W(6)-O(23)	101.9(4)
O(29)-Co(2)-O(17)#1	172.4(3)	O(25)-W(6)-O(23)	89.2(3)
O(21)#1-Co(2)-O(17)#1	85.7(3)	O(24)-W(6)-O(22)	96.9(3)
O(34)#1-Co(2)-O(1W)	174.0(3)	O(25)-W(6)-O(22)	160.8(3)
O(26)-Co(2)-O(1W)	91.8(3)	O(23)-W(6)-O(22)	87.6(3)
O(29)-Co(2)-O(1W)	82.8(3)	O(24)-W(6)-O(9)	95.8(3)
O(21)#1-Co(2)-O(1W)	95.7(3)	O(25)-W(6)-O(9)	90.5(3)
O(17)#1-Co(2)-O(1W)	104.6(3)	O(23)-W(6)-O(9)	161.9(3)
O(23)-Co(3)-O(32)#1	97.1(3)	O(22)-W(6)-O(9)	86.8(3)
O(23)-Co(3)-O(34)#1	94.7(3)	O(24)-W(6)-O(10)	167.6(3)
O(32)#1-Co(3)-O(34)#1	167.0(3)	O(25)-W(6)-O(10)	86.7(3)
O(23)-Co(3)-O(34)	165.8(3)	O(23)-W(6)-O(10)	86.5(3)
O(32)#1-Co(3)-O(34)	91.9(3)	O(22)-W(6)-O(10)	74.2(3)
O(34)#1-Co(3)-O(34)	77.6(3)	O(9)-W(6)-O(10)	75.4(3)
O(23)-Co(3)-O(17)#1	97.3(3)	O(27)-W(7)-O(26)	103.6(4)
O(32)#1-Co(3)-O(17)#1	89.4(3)	O(27)-W(7)-O(25)	100.1(4)
O(34)#1-Co(3)-O(17)#1	83.7(3)	O(26)-W(7)-O(25)	94.4(4)
O(34)-Co(3)-O(17)#1	93.8(3)	O(27)-W(7)-O(28)	97.3(4)
O(23)-Co(3)-O(21)	86.5(3)	O(26)-W(7)-O(28)	92.2(4)
O(32)#1-Co(3)-O(21)	93.4(3)	O(25)-W(7)-O(28)	159.4(3)

O(34)#1-Co(3)-O(21)	92.7(3)	O(27)-W(7)-O(15)	90.1(4)
O(34)-Co(3)-O(21)	81.9(3)	O(26)-W(7)-O(15)	165.9(3)
O(17)#1-Co(3)-O(21)	175.0(3)	O(25)-W(7)-O(15)	86.3(3)
W(9)-O(2)-W(1)	112.3(4)	O(28)-W(7)-O(15)	82.7(3)
W(4)-O(3)-W(1)	113.4(4)	O(27)-W(7)-O(13)	161.4(3)
W(1)-O(4)-W(3)	155.6(5)	O(26)-W(7)-O(13)	93.0(3)
Co(1)-O(5)-W(9)	116.8(3)	O(25)-W(7)-O(13)	86.7(3)
Co(1)-O(5)-W(4)	120.3(3)	O(28)-W(7)-O(13)	73.5(3)
W(9)-O(5)-W(4)	97.2(3)	O(15)-W(7)-O(13)	73.0(3)
Co(1)-O(5)-W(1)	121.3(3)	O(30)-W(8)-O(29)	102.4(4)
W(9)-O(5)-W(1)	97.7(3)	O(30)-W(8)-O(28)	98.2(4)
W(4)-O(5)-W(1)	98.4(3)	O(29)-W(8)-O(28)	95.2(4)
W(1)-O(6)-W(2)	147.4(4)	O(30)-W(8)-O(31)	98.8(4)
W(2)-O(8)-W(5)	113.2(4)	O(29)-W(8)-O(31)	92.4(3)
W(2)-O(9)-W(6)	112.5(4)	O(28)-W(8)-O(31)	159.4(3)
Co(1)-O(10)-W(5)	117.6(3)	O(30)-W(8)-O(14)	90.5(4)
Co(1)-O(10)-W(6)	118.2(4)	O(29)-W(8)-O(14)	167.1(3)
W(5)-O(10)-W(6)	98.5(3)	O(28)-W(8)-O(14)	83.9(3)
Co(1)-O(10)-W(2)	121.7(4)	O(31)-W(8)-O(14)	84.4(3)
W(5)-O(10)-W(2)	98.7(3)	O(30)-W(8)-O(13)	163.0(3)
W(6)-O(10)-W(2)	97.6(3)	O(29)-W(8)-O(13)	93.8(3)
W(2)-O(11)-W(3)	157.9(5)	O(28)-W(8)-O(13)	74.9(3)
Co(1)-O(13)-W(8)	119.5(4)	O(31)-W(8)-O(13)	85.5(3)
Co(1)-O(13)-W(7)	117.8(4)	O(14)-W(8)-O(13)	73.4(3)
W(8)-O(13)-W(7)	97.5(3)	O(33)-W(9)-O(31)	100.9(4)
Co(1)-O(13)-W(3)	120.9(4)	O(33)-W(9)-O(32)	102.0(4)
W(8)-O(13)-W(3)	98.0(3)	O(31)-W(9)-O(32)	91.0(3)
W(7)-O(13)-W(3)	98.5(3)	O(33)-W(9)-O(2)	95.8(4)
W(3)-O(14)-W(8)	112.7(4)	O(31)-W(9)-O(2)	91.5(3)
W(3)-O(15)-W(7)	113.1(4)	O(32)-W(9)-O(2)	161.2(3)
W(4)-O(17)-W(10)#1	137.6(4)	O(33)-W(9)-O(19)	96.9(3)
W(4)-O(17)-Co(3)#1	137.6(4)	O(31)-W(9)-O(19)	162.2(3)
W(10)#1-O(17)- Co(3)#1	0.00(5)	O(32)-W(9)-O(19)	85.9(3)
W(4)-O(17)-Co(2)#1	123.9(4)	O(2)-W(9)-O(19)	86.1(3)

W(10)#1-O(17)- Co(2)#1	96.1(3)	O(33)-W(9)-O(5)	167.4(3)
Co(3)#1-O(17)-Co(2)#1	96.1(3)	O(31)-W(9)-O(5)	88.2(3)
W(5)-O(18)-W(4)	155.9(4)	O(32)-W(9)-O(5)	86.3(3)
W(4)-O(19)-W(9)	112.4(4)	O(2)-W(9)-O(5)	75.2(3)
W(4)-O(19)-Na(2)#13	128.3(4)	O(19)-W(9)-O(5)	74.1(3)
W(9)-O(19)-Na(2)#13	117.2(4)	Co(3)-O(21)-Co(2)#1	96.2(3)
W(5)-O(21)-Co(3)	138.3(4)		
Symmetry transformations used to generate equivalent atoms: #1 -x+1,-y+1,-z #2 x+1,y,z #3 x+1/2,-y+1/2,z-1/2 #4 -x+3/2,y+1/2,-z+1/2 #5 -x+1,-y+1,-z+1 #6 x-1/2,-y+1/2,z+1/2 #7 x,y,z+1 #8 x+1/2,-y+1/2,z+1/2 #9 x-1/2,-y+1/2,z-1/2 #10 -x+3/2,y-1/2,-z+1/2 #11 -x+1/2,y-1/2,-z+1/2 #12 x,y-1,z #13 x,y,z-1 #14 x-1,y,z #15 -x+1/2,y+1/2,-z+1/2 #16 x,y+1,z			

BVS calculation (Table 6-3) of the cobalt atoms of the complex 1 indicates that two tetrahedral (Co1) and two octahedral (Co2) cobalt atoms are in their +2 oxidation states. However, the oxidation states of Co3 and W10 atoms on the belt position are +2.571 and +4.922, which are deviated from the normal +2 and +6 ones, respectively. This offsets indicate that the two sites, Co3 and W10, are disordered in the crystal structure.

Table 6-3. The Bond valence sums of cobalt atoms and belt tungsten atom.

	$\Sigma(\text{Co-O})$	$\Sigma(\text{W-O})$
Co1	2.134	
Co2	1.770	
Co3	2.571	
W10		4.922

In order to reveal the surface chemical compositions and the valence states of cobalt and tungsten species, X-ray photoelectron spectra on the Co2p and W4f regions in **1** were collected (Figure 6-3).

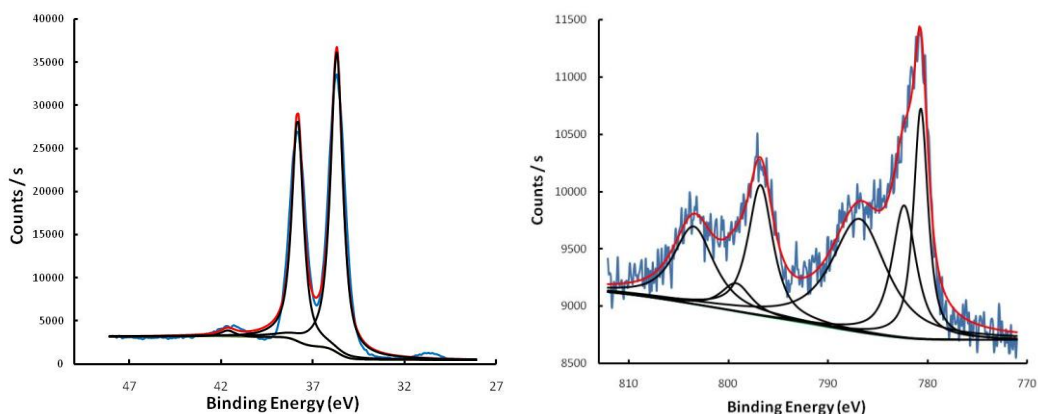


Figure 6-3. XPS diagram of **1** for W4f (Left) and Co3p (Right). Blue line represents raw data, red line represents simulated data.

The ratio of Co: W ratio is $\sim 5.06: 19$, which is in good consistence with the chemical formula of **1**. In addition, the high resolution spectra of Co 2p and W 4f were fitted with the XPSPEAK41 software and Shirley-type background and the fitted curves are well in agreement with the experimental results. The binding energy peaks for Co 2p can be deconvoluted into at least 3 sets of doublet peaks (Figure 6-3, Right), corresponding to the Co $2p_{1/2}$ and Co $2p_{3/2}$ peaks in three types of cobalt atoms with different chemical environments. The binding energy peaks demonstrate cobalt atoms are in +2 oxidation state. For tungsten atoms (Figure 6-3, Left), the binding energy peaks at 35.7 and 37.8 eV are attributed to W $4f_{7/2}$ and W $4f_{5/2}$, respectively, indicating they are in +6 oxidation state.

Figure 6-4 shows the thermal stability and decomposition characteristics of **1** assessed by thermogravimetric analysis (TGA). The TGA curve shows a total weight loss

of ~14% between 30 and 300 °C, which is associated with the loss of 46 water molecules (water molecules of crystallization and terminally bound aqua ligands on the Co centers).

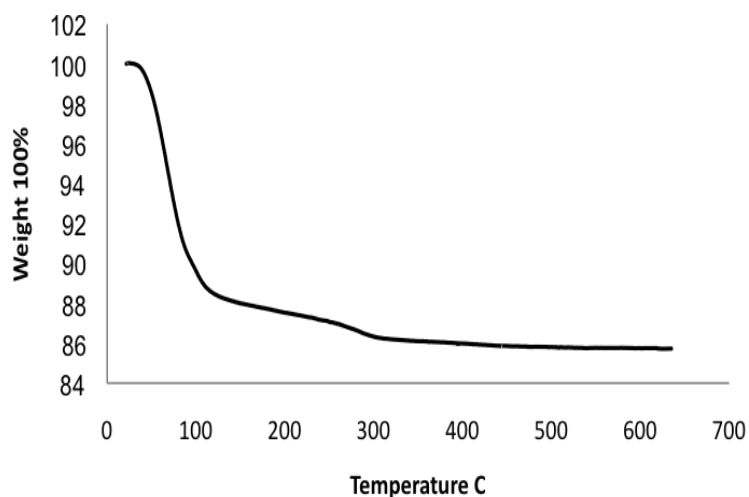


Figure 6-4. Thermogravimetric Analysis (TGA) of crystalline **1**. The total weight loss observed (14%) is attributed to hydration water, the calculation shows that there are approximately 46 hydration water molecules.

The UV-vis (Figure 6-5) of **1** in borate buffer solution shows strong absorption in the range of 540 to 680 nm with the maximum absorption at 609 nm. The calculated extinction coefficient at λ_{\max} is $\epsilon_{609} = 622 \text{ M}^{-1} \text{ cm}^{-1}$.

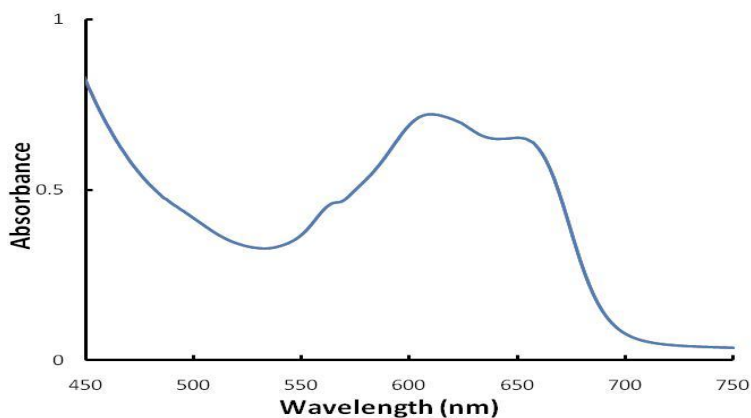


Figure 6-5. UV-Visible spectroscopy of 1 mM **1** in borate buffer (0.2M, pH = 9.0). The calculated extinction coefficient at λ_{\max} (609 nm) is $\epsilon_{609} = 622 \text{ M}^{-1} \text{ cm}^{-1}$.

FT-IR spectrum shows the characteristic vibration modes, such as terminal W-O stretching (939 cm^{-1}) and W-O-W bending (882 and 767 cm^{-1}) bands.

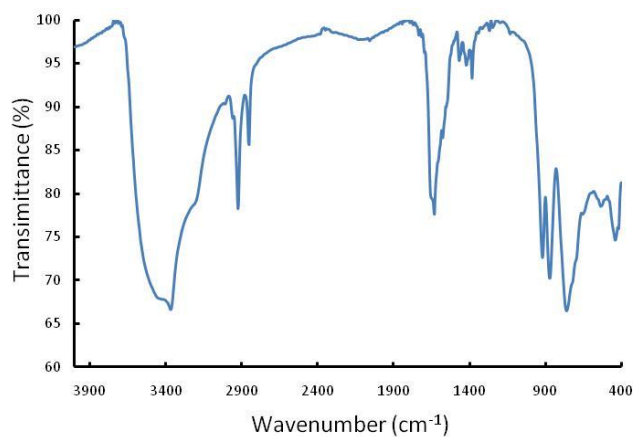


Figure 6-6. FT-IR spectrum of **1**. The FT-IR spectroscopy were performed using 1 wt% sample in KBr pellet.

The redox properties of **Co5** was assessed by cyclic voltammetry (CV) (Figure 6-7), which shows a small quasi-reversible peak at $E_a \approx 0.85\text{ mV}$ and $E_c \approx 0.75\text{ V}$ that are associated with oxidation/reduction of Co atoms in **1**. At potentials $> 1.0\text{ V}$, the anodic current significantly increases indicating the electrocatalytic water oxidation.

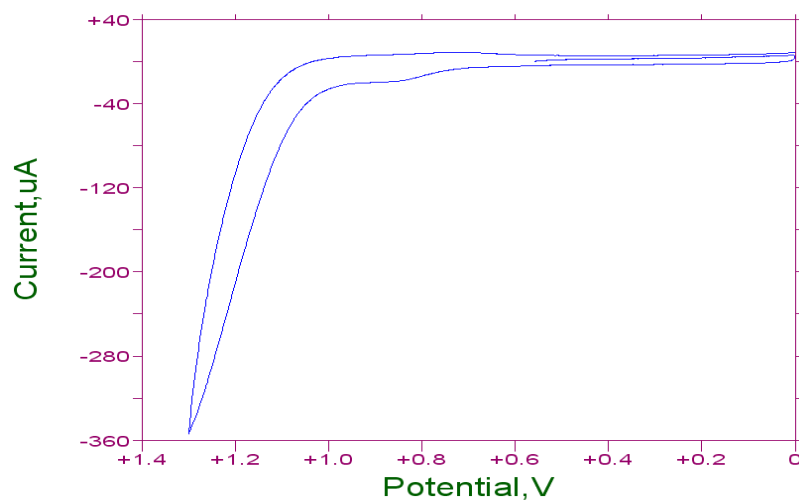
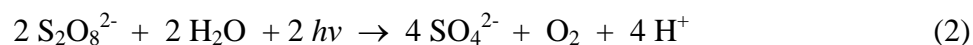
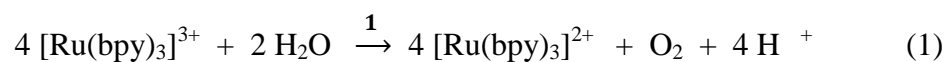


Figure 6-7. Cyclic voltammetry spectrum of **1** (0.16 mM) in sodium borate buffer (20 mM, pH=9).

The catalytic efficiency of **Co5** and other catalysts for water oxidation can be compared from the kinetics for the disappearance of $[\text{Ru}(\text{bpy})_3]^{3+}$ in the stoichiometric dark water oxidation system (Figure 6-8). The thermal oxidation of water using $[\text{Ru}(\text{bpy})_3]^{3+}$ ($\epsilon_{670} = 420 \text{ M}^{-1}\text{cm}^{-1}$) is monitored using stopped-flow technique by following the kinetics of decay of the oxidized dye to $[\text{Ru}(\text{bpy})_3]^{2+}$ ($\epsilon_{670} = 5 \text{ M}^{-1}\text{cm}^{-1}$) in 40 mM borate buffer at pH = 9. The solutions containing $[\text{Ru}(\text{bpy})_3]^{3+}$ and the catalysts, respectively, were rapidly mixed in the stopped-flow machine. Typically there are two competing pathways for $[\text{Ru}(\text{bpy})_3]^{3+}$ consumption: catalytic water oxidation (Eq. 1) and the self-decomposition reaction.



The degradation rate of $[\text{Ru}(\text{bpy})_3]^{3+}$ to $[\text{Ru}(\text{bpy})_3]^{2+}$ suggests that **1**, is like $\text{Na}_{10}[\text{Co}_4(\text{H}_2\text{O})_2(\text{PW}_9\text{O}_{34})_2]$ (**Co4**) that are active water oxidation catalysts recently reported, but faster than the later (Figure 6-8).

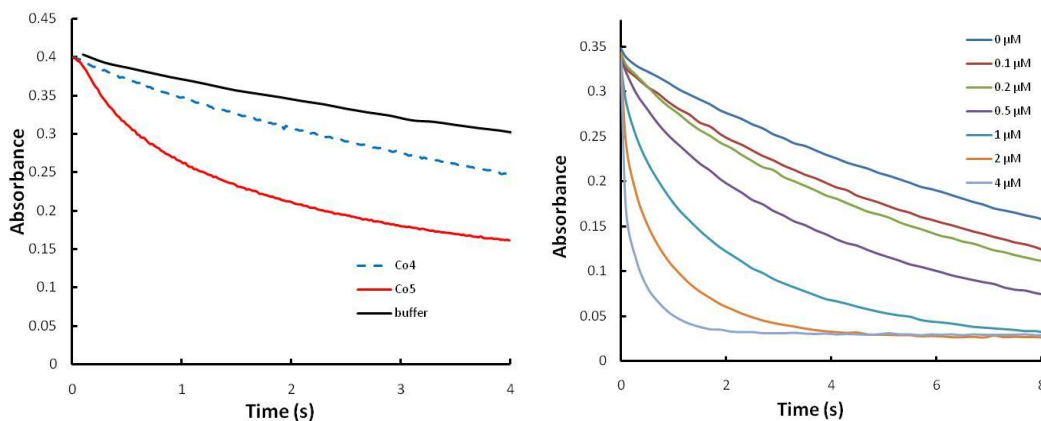


Figure 6-8. Kinetics of $[\text{Ru}(\text{bpy})_3]^{3+}$ reduction to $[\text{Ru}(\text{bpy})_3]^{2+}$ over different catalysts (Left), and different concentrations of **1**. The absorbance was measured at 670 nm. Conditions: Left: **Buffer** (black solid line), **Co4** (blue dot line; 0.5 μM (final)), **1** (red solid line; 0.5 μM (final)); Right: **1** (0.1 μM ~ 4 μM); 1 mM $[\text{Ru}(\text{bpy})_3]^{3+}$ (final), 40 mM sodium borate buffer (final), pH 9.0, 298 K

The $[\text{Ru}(\text{bpy})_3]^{3+}$ with a half-life of ~ 8 s (no catalyst) in the 40 mM borate buffer solution at pH 9 is significantly reduced to 2.5 s and 6 s on addition of **1** and **Co4** at the concentration of 0.5 μM , respectively, which strongly suggest that Co5 is much faster. These kinetics traces of $[\text{Ru}(\text{bpy})_3]^{3+}$ degraded to $[\text{Ru}(\text{bpy})_3]^{2+}$ and other decomposed side products, which was known but hard to be identified, indicate that all these POMs are efficient catalysts for degradation of $[\text{Ru}(\text{bpy})_3]^{3+}$ but do not ensure that they are also have a high selectivity to produce oxygen from water because the stopped-flow does not allow tracking the O_2 formation.

Efficiency of water splitting into oxygen catalyzed by these polyanions under visible-light driven condition using $[\text{Ru}(\text{bpy})_3]^{2+}$ as a photosensitizer, persulfate as a sacrificial electron acceptor, and borate solution (40 mM, pH 9.0) as buffer was further

explored in detail, which can be quantified by the O₂ production using GC. The evolution of dioxygen from water is observed in this system (Figures 6-9 and 6-10).

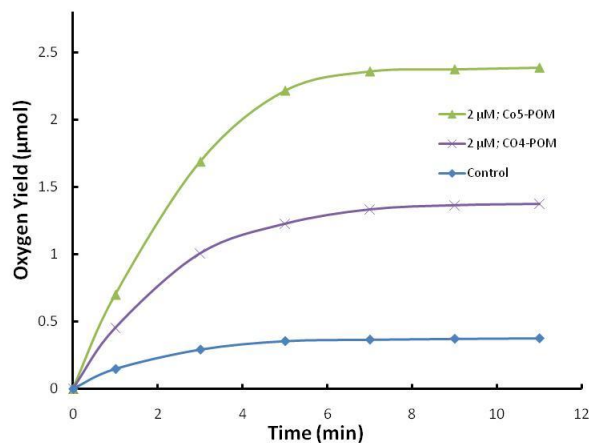


Figure 6-9. Kinetics of O₂ evolution over different POM catalysts in the photocatalytic system. **1** (green triangles), **Co4** (Na₁₀[Co₄(H₂O)₂(PW₉O₃₄)₂], green crosses), and buffer control (blue squares). Conditions: LED-lamp, 455 nm, 17 mW light beam with a diameter of ~0.4 cm focused on the reaction solution, 1.0 mM [Ru(bpy)₃]²⁺, 5.0 mM Na₂S₂O₈, 40 mM sodium borate buffer (initial pH 9.0), total reaction volume 2.0 mL, vigorous stirring (4 × 10³ RPM). Concentrations of catalyst: 2 μM.

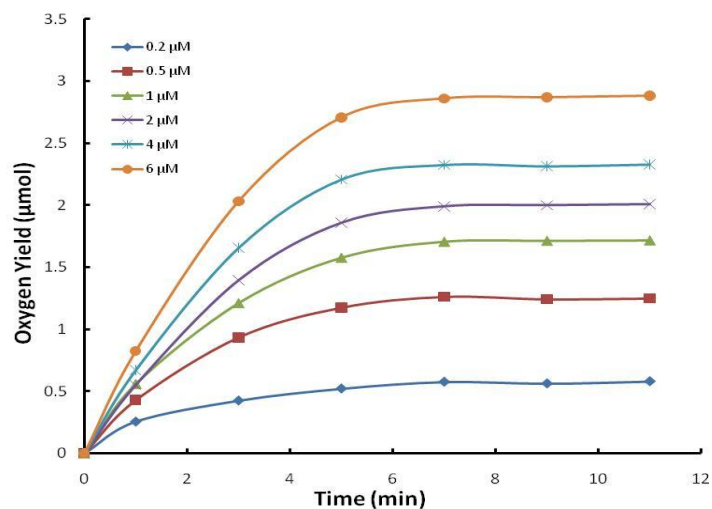


Figure 6-10. Kinetics of O₂ formation at different concentrations of **1** (0.2 ~ 6.0 μM). Condition: see Figure 6-9.

High turnover number (TON \approx 1500) and turnover frequency (TOF, up to 10.65 s⁻¹) were achieved at 0.2 μ M of **1** (Table 6-4). The quantum efficiency of O₂ formation, which is defined as the number of O₂ molecules formed per two absorbed photons and could be calculated using Eq. 3, showed to be ~55% catalyzed by **1** at the concentration of 6 μ M:

$$\Phi = N(O_2)/[N(h\nu)/2] \quad (3)$$

Table 6-4. Turnover numbers (TON), chemical yields, and initial turnover frequency (TOF) for homogeneous visible-light-driven water oxidation catalyzed by different POM catalysts^a.

<i>Catalyst</i>	<i>TON</i> ^b	<i>Chemical Yield</i> ^c	<i>Quantum Yield</i> ^d	<i>Initial TOF</i> ^e
1 at 0.2 μ M	1500	0.18	0.17	10.65
1 at 2 μ M	498	0.46	0.37	2.30
1 at 6 μ M	240	0.65	0.55	1.15
1 at 6 μ M ^f	380	0.45	0.55	1.36
Co4 at 2 μ M	230	0.28	0.20	1.21

^a For experimental conditions, see Figure 6-9 caption. TON and chemical yields are the results at 11 minutes, the control was already subtracted. ^b (O₂ yield at 11 minutes) / (catalyst concentration) = [O₂]_f/[catalyst]; ^c $\Phi_{CY} = 2[O_2]_f / [Na_2S_2O_8]_0$ (the initial concentration of persulfate); ^d $\Phi_{QY}(0) = N(O_2)/[N(h\nu)/2] = 2 (\Delta[O_2]/\Delta(h\nu))_0$, (initial O₂ formation rate) / (photon flux); ^e Initial TOF (s⁻¹) = TON (at 60 seconds) / Reaction time (60 seconds). ^f using 10 mM Na₂S₂O₈.

The control experiment without catalyst shows that borate buffer is an innocent reaction media, from which O₂ are also evolved in a yield of 7%. However, this amount of oxygen is negligible in comparison with that of reaction catalyzed by **1**, the oxygen yield of which is around 46% at 2 μ M and 65% at 6 μ M of **1**. A higher chemical yield

indicates a faster conversion and a higher selectivity of reducing $[\text{Ru}(\text{bpy})_3]^{3+}$ to $[\text{Ru}(\text{bpy})_3]^{2+}$ in the presence of the catalyst.

As shown in Table 6-4 and Figure 6-11, complex **Co4** (O_2 yield $\approx 28\%$, TON ≈ 230 , and TOF ≈ 1.21) and **1** (O_2 yield $\approx 46\%$, TON ≈ 498 , and TOF ≈ 2.3) exhibited reasonable catalytic activities under visible light driven system. It can be easily concluded that catalyst **1** shows much more efficient photocatalytic activity by giving almost 1.7 times more oxygen yield and 1.9 times faster initial rate for oxygen evolution than that of **Co4**. Furthermore, when the concentration of **1** is lowered to $0.2 \mu\text{M}$, the initial TOF of **1**-catalyzed oxidation of water can reach as high as 10.65 s^{-1} , which is 3 fold faster than that of **Co4** under the same other experimental conditions. In addition, concentration-dependence of sodium persulfate was also conducted (Figure 6-11 and Table 6-4). The TON and TOF with double-fold concentration of sodium persulfate (TON ≈ 380 , and TOF ≈ 1.36) increased by 0.6 and 0.2 fold, respectively, than that of typical reaction in the presence of $6 \mu\text{M}$ catalyst **1**, even though the chemical yield of oxygen shows 44% drop.

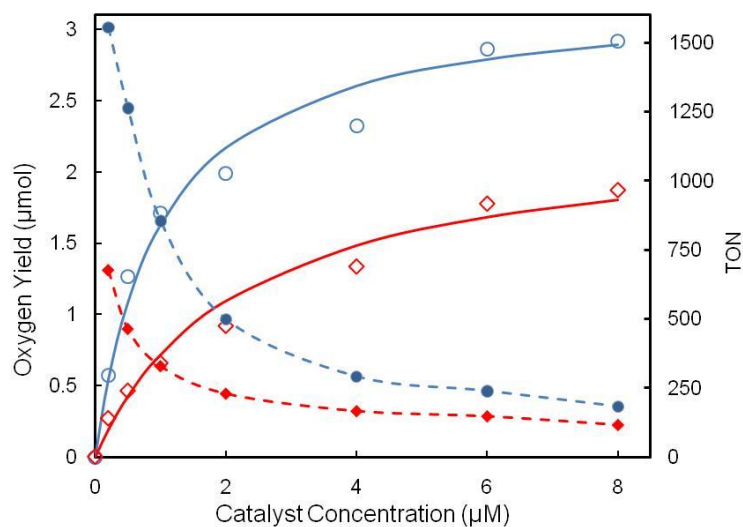


Figure 6-11. O₂ yield and turn-over number vs. concentration of **1** at 11 minutes of illumination. Red line: Co4; blue line: **1**. Condition: see Figure 6-1.

The poisoning experiment is also done by adding different amounts of 2,2'-bipyridine to the reaction system to form [Co(bpy)₃]²⁺, which is no active for water oxidation (Figures 6-12). As can be seen, catalyst **1** still shows activity even though 6-fold 2,2'-bipyridine per cobalt was added into the reaction solution, indicating that **1** is stable under catalytic turnover conditions.

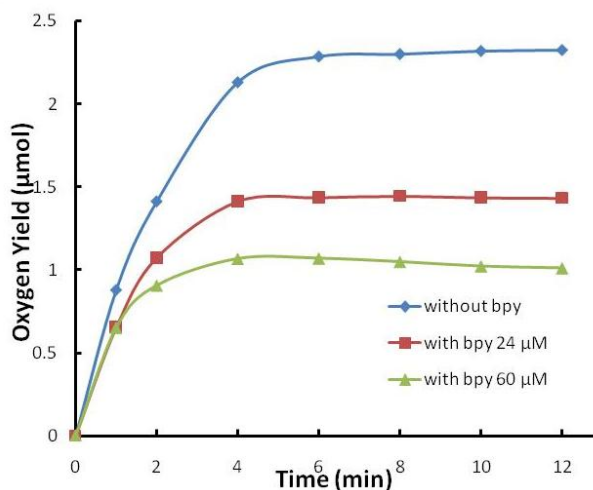


Figure 6-12. Kinetics of O₂ formation in the photo-catalytic system. Freshly-prepared solution **1** in the presence of 2,2'-bipyridine. Condition: see Figure 6-1. Blue squares: 2 μM **1**; Red squares: 2 μM **1** + 24 μM bpy; Green triangles: 2 μM **1** + 60 μM bpy.

To further test the stability of **1**, the FT-IR spectra of the reaction mixture including **1** before and after the reaction have been checked (Figure 6-13). As shown in Figure 6-13, there is no significant difference for the FT-IR spectra before and after the photo-driven water oxidation process. All these spectra show the characteristic terminal W-O stretching (939 cm⁻¹), and W-O-W bending (882 and 767 cm⁻¹) bands, demonstrating the stability of **1** under turnover conditions.

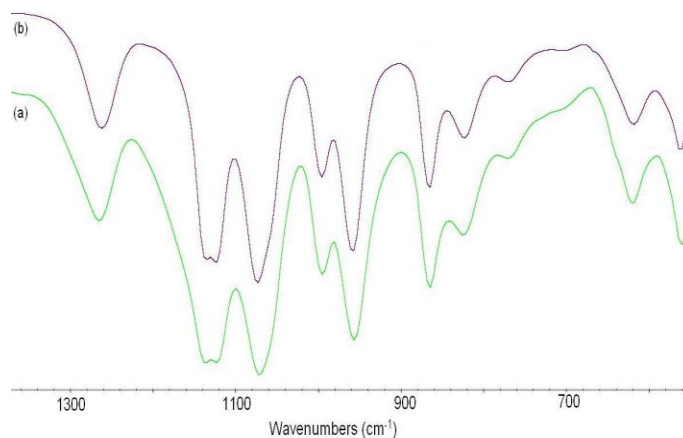


Figure 6-13. FT-IR spectra for **1** under photo driven water oxidation before (a) the dark-yellow precipitate obtained from mixing two concentrated solutions of **Na10-1** and $[\text{Ru}(\text{bpy})_3]^{2+}$, and after reaction (b) the light-yellow precipitate re-isolated from a “post-chemical reaction” solution. All FT-IR spectroscopy were performed using 1 wt% sample in KBr pellet.

Combination of spectroscopic, electrochemical, and kinetics studies indicates that **1** is extremely stable under both thermal and photo-driven catalytic reaction conditions. These results combining both thermal and light-driven reaction data, collectively suggest that **1** is unambiguously an efficient WOC catalyst because of its extraordinary high O_2 yield under the identical experimental condition, which reversely indicates **1** has much higher selectivity of water oxidation to other side reaction such as bpy ligand oxidation than that of **Co4**.

Conclusion

To our best knowledge, the present study clearly documents a new molecular water oxidation catalyst of high efficiency and stability based on abundant transition

metals for photo-driven water oxidation. Comparing with the known active POMs, **Co₄**, **1** with distinct molecular structure from the others demonstrates extraordinary catalytic activity for water oxidation to produce oxygen. Considering that there is thousands of molecular POMs reported to date, the current findings obviously indicate that by selectively assembling different elements, the catalytic activity of POMs for water oxidation can be well tuned and promisingly refined to approach to the final goal for practical water splitting applications in artificial photosynthesis. These findings further indicate that POMs can be tuned systematically and are highly attractive candidates as catalysts for multi-electron transfer processes in the context of artificial photosynthesis studies to produce renewable energy.

References

- (1) Kanan, M. W.; Surendranath, Y.; Nocera, D. G. *Chem. Soc. Rev.* **2009**, *38*, 109.
- (2) Lutterman, D. A.; Surendranath, Y.; Nocera, D. G. *J. Am. Chem. Soc.* **2009**, *131*, 3838.
- (3) Kanan, M. W.; Nocera, D. G. *Science* **2008**, *321*, 1072.
- (4) Lewis, N. S.; Nocera, D. G. *Proc. Natl. Acad. Sci.* **2006**, *103*(43), 15729.
- (5) Cook, T. R.; Dogutan, D. K.; Reece, S. Y.; Surendranath, Y.; Teets, T. S.; Nocera, D. G. *Chem. Rev.* **2010**, *110*, 6474.
- (6) Geletii, Y. V.; Yin, Q.; Hou, Y.; Huang, Z.; Ma, H.; Song, J.; Besson, C.; Luo, Z.; Cao, R.; OHalloran, K. P.; Zhu, G.; Zhao, C.; Vickers, J.; Ding, Y.; Mohebbi, S.; Kuznetsov, A. E.; Musaev, D. G.; Lian, T.; Hill, C. L. *Isr. J. Chem.* **2011**, *51*, 238.

- (7) Fujishima, A.; Honda, K. *Nature* **1972**, 238, 37.
- (8) Ling, Y.; Wang, G.; Wheeler, D. A.; Zhang, J. Z.; Li, Y. *Nano. Lett.* April 8, **2011**, pp. A.
- (9) Zhong, D. K.; Sun, J.; Inumaru, H.; Gamelin, D. R. *J. Am. Chem. Soc.* **2009**, 131, 6086.
- (10) Dincă, M.; Surendranath, Y.; Nocera, D. G. *Proc. Natl. Acad. Sci.* **2010**, 107, 10337.
- (11) Concepcion, J. J.; Jurss, J. W.; Templeton, J. L.; Meyer, T. J. *Proc. Natl. Acad. Sci.* **2008**, 105, 17632.
- (12) Concepcion, J. J.; Jurss, J. W.; Templeton, J. L.; Meyer, T. J. *J. Am. Chem. Soc.* **2008**, 130, 16462.
- (13) Liu, F.; Concepcion, J. J.; Jurss, J. W.; Cardolaccia, T.; Templeton, J. L.; Meyer, T. J. *Inorg. Chem.* **2008**, 47, 1727.
- (14) Duan, L.; Fischer, A.; Xu, Y.; Sun, L. *J. Am. Chem. Soc.* **2009**, 131, 10397.
- (15) Sun, C.-Y.; Liu, S.-X.; Liang, D.-D.; Shao, K.-Z.; Ren, Y.-H.; Su, Z.-M. *J. Am. Chem. Soc.* **2009**, 131, 1883.
- (16) Xu, Y.; Åkermark, T.; Gyollai, V.; Zou, D.; Eriksson, L.; Duan, L.; Zhang, R.; Åkermark, B.; Sun, L. *Inorg. Chem.* **2009**, 48, 2717.
- (17) Blakemore, J. D.; Schley, N. D.; Balcells, D.; Hull, J. F.; Olack, G. W.; Incarvito, C. D.; Eisenstein, O.; Brudvig, G. W.; Crabtree, R. H. *J. Am. Chem. Soc.* **2010**, 132, 16017.

- (18) Hull, J. F.; Balcells, D.; Blakemore, J. D.; Incarvito, C. D.; Eisenstein, O.; Brudvig, G. W.; Crabtree, R. H. *J. Am. Chem. Soc.* **2009**, *131*, 8730.
- (19) Limburg, J.; Vrettos, J. S.; Chen, H.; Paula, J. C. d.; Crabtree, R. H.; Brudvig, G. W. *J. Am. Chem. Soc.* **2001**, *123*, 423.
- (20) Limburg, J.; Vrettos, J. S.; Liable-Sands, L. M.; Rheingold, A. L.; Crabtree, R. H.; Brudvig, G. W. *Science* **1999**, *283*, 1524.
- (21) Tagore, R.; Chen, H.; Zhang, H.; Crabtree, R. H.; Brudvig, G. W. In *Inorg. Chimi. Acta* **2007**, *360*, 2983.
- (22) Tagore, R.; Crabtree, R. H.; Brudvig, G. W. *Inorg. Chem.* **2008**, *47*, 1815.
- (23) Kurz, P.; Berggren, G.; Anderlund, M. F.; Styring, S. *Dalton Trans.* **2007**, 4258.
- (24) Wasylenko, D. J.; Ganesamoorthy, C.; Borau-Garcia, J.; Berlinguette, C. *P. Chem. Commun.* **2011**, *47*, 4249.
- (25) Dogutan, D. K.; McGuire, R.; Nocera, D. G. *J. Am. Chem. Soc.* **2011**, *133*, 9178.
- (26) Lee, C. H.; Dogutan, D. K.; Nocera, D. G. *J. Am. Chem. Soc.* **2011**, *133*, 8775.
- (27) Hill, C. L. *Chem. Rev.* **1998**, *98*, 1.
- (28) Hill, C. L. *Chem. Rev.* **1998**, *98*, 1.
- (29) *Special Thematic Issue on Polyoxometalates*; Hill, C. L., Ed., 1998; Vol. 98, No. 1.
- (30) Besson, C.; Huang, Z.; Geletii, Y. V.; Lense, S.; Hardcastle, K. I.; Musaev, D. G.; Lian, T.; Proust, A.; Hill, C. L. *Chem. Commun.* **2010**, 2784.

- (31) Geletii, Y. V.; Botar, B.; Kögerler, P.; Hillesheim, D. A.; Musaev, D. G.; Hill, C. L. *Angew. Chem. Int. Ed.* **2008**, *47*, 3896.
- (32) Geletii, Y. V.; Huang, Z.; Hou, Y.; Musaev, D. G.; Lian, T.; Hill, C. L. *J. Am. Chem. Soc.* **2009**, *131*, 7522.
- (33) Toma, F. M.; Sartorel, A.; Iurlo, M.; Carraro, M.; Parisse, P.; Maccato, C.; Rapino, S.; Gonzalez, B. R.; Amenitsch, H.; Ros, T. D.; Casalis, L.; Goldoni, A.; Marcaccio, M.; Scorrano, G.; Scoles, G.; Paolucci, F.; Prato, M.; Bonchio, M. *Nature Chem.* **2010**, *2*, 826.
- (34) Puntoriero, F.; Ganga, G. L.; Sartorel, A.; Carraro, M.; Scorrano, G.; Bonchio, M.; Campagna, S. *Chem. Commun.* **2010**, *46*, 4725.
- (35) Orlandi, M.; Argazzi, R.; Sartorel, A.; Carraro, M.; Scorrano, G.; Bonchio, M.; Scandola, F. *Chem. Commun.* **2010**, *46*, 3152.
- (36) Sartorel, A.; Miro, P.; Salvadori, E.; Romain, S.; Carraro, M.; Scorrano, G.; Valentin, M. D.; Llobet, A.; Bo, C.; Bonchio, M. *J. Am. Chem. Soc.* **2009**, *131*, 16051.
- (37) Sartorel, A.; Carraro, M.; Scorrano, G.; Zorzi, R. D.; Geremia, S.; McDaniel, N. D.; Bernhard, S.; Bonchio, M. *J. Am. Chem. Soc.* **2008**, *130*, 5006.
- (38) Huang, Z.; Luo, Z.; Geletii, Y. V.; Vickers, J.; Yin, Q.; Wu, D.; Hou, Y.; Ding, Y.; Song, J.; Musaev, D. G.; Hill, C. L.; Lian, T. *J. Am. Chem. Soc.* **2011**, *133*, 2068.
- (39) Yin, Q.; Tan, J. M.; Besson, C.; Geletii, Y. V.; Musaev, D. G.; Kuznetsov, A. E.; Luo, Z.; Hardcastle, K. I.; Hill, C. L. *Science* **2010**, *328*, 342.

- (40) Tourné C. M.; Tourné G. F.; Zonnevijlle, F. *J. Chem. Soc. Dalton Trans.* **1991**, *1*, 143.
- (41) Neumann, R.; Dahan, M. *Nature* **1997**, *388*, 353.
- (42) Morris, A. M.; Anderson, O. P.; Finke, R. G. *Inorg. Chem.* **2009**, *48*, 4411.